12

AD

PERMANENT DEFORMATION OF FLEXIBLE PAVEMENTS

Final Technical Report

by

S.F. Brown, C.A. Bell and B.V. Brodrick

March 1977

EUROPEAN RESEARCH OFFICE

United States Army

London England

GRANT NUMBER DA-ERO-75-G-023

University of Nottingham, England

(6) PERMANENT DEFORMATION OF FLEXIBLE PAVEMENTS.

(10) by S.F. Brown, C.A. Bell B.V. Brodrick

University of Nottingham, England

(7) Final Technical Report Sep 74 - Mar 77,

11 Mar 1977

1. 13 1p.

DMIC (11)

European Research Office

United States Army

London England

(15) GRANT NUMBER DA-ERO-75-G-023

CONTENTS

CHAPTER ONE

INTRODUCTION

This report presents details of the second and third years' work in a three-year project concerned with the development of predictive design procedures for the permanent deformation which develops in flexible pavements. The first year's work was described in an earlier report (1) to which reference should be made for the detailed background to the project.

During the course of this work, three semi-full scale asphalt pavements have been tested in a newly developed pavement test facility. These pavements consisted of dense bitumen macadam placed directly over a silty clay subgrade. The experimental work used extensive in situ instrumentation to determine stresses, elastic strains and permanent strains in the structure. A large testing programme was carried out on samples of the constituent materials to evaluate their stress-strain relationships. The experimental work was backed up by, and coordinated with, theoretical developments aimed at producing computer orientated calculation procedures to predict the permanent deformation response of each pavement.

This work has taken place during a period when there has been considerable interest, internationally, in the problem of pavement deformation. This has followed an earlier period of research over, perhaps, 20 years during which the major interest was in developing design methods to prevent fatigue cracking and this has been largely successful (2).

During the course of the work described herein, the U.S. Transportation Research Board held a symposium on the subject to which

the Principal Investigator contributed (3) and which brought together a number of papers of direct relevance to the research. There has been a measure of cooperation with the related work at Trinity College, Dublin and the Shell Laboratories in Amsterdam which has proved useful and interesting.

The forthcoming 4th International Conference on the Structural Design of Asphalt Pavements (4) to be held in August 1977 at Ann Arbor, Michigan includes a session devoted entirely to permanent deformation design problems. The papers to be presented are from several different countries and include one written on some aspects of the work in this report by Brown and Bell (5). The Authors have also been invited to participate in several other informal meetings during the course of the past three years. The work on in situ instrumentation is to be presented at a conference in England during September 1977 (6) and there are plans to publish details of the pavement test facility also.

Continuation of the work herein is assured over the period to 1980 under a new U.S. Army research contract and the first year will be devoted to pavements with thin asphalt surfacings over crushed rock bases. A feature of this work will be the inclusion of man-made fabric below the base to assess its potential for inclusion in permanent road construction. Additional support for this work is being provided by ICI Fibres Ltd.

CHAPTER TWO

PAVEMENT TEST FACILITY

2.1 INTRODUCTION

This facility reciprocates a loaded rolling wheel over a flexible pavement structure to simulate the effect of moving vehicles. The wheel is attached to a loading carriage guided between two 'I' section reaction beams in the direction of the principal linear motion, and the complete assembly can be moved at right angles to this motion to reproduce the lateral wheel distribution likely to occur in practice.

A total longitudinal travel of 6.7 m for the wheel includes 2.5 m for acceleration, 1.9 m at a constant speed up to 14.5 km/h and the remainder deceleration before reversal. Higher speeds are obtainable with some loss of velocity control and a tendency to approach the overtravel safety cut-outs. The level of load required was 10 kN and the system is capable of exerting 20 kN but this may result in damage to the pneumatic tyre. A heavy duty forklift truck tyre was chosen and this was modified to present a smooth, consistent contact area to the pavement surface. Its overall diameter was 560 mm and at a 10 kN load presented an elliptical contact area of approximately 180 mm major diameter x 130 mm minor diameter. The equipment was located in a 10 x 4.5 m laboratory, with a false insulated ceiling in order to maintain the pavement temperature at 30°C. Controlled lateral movement was limited to 0.46 m about the pavement centre but this can be increased to 1.22 m by mechanically disconnecting the power traverse.

The first pavement was installed in a 4.9 x 2.4 x 1.5 m deep pit lined with concrete and waterproofed with a liquid sealant and overlapping strips of "Bituthene". The subgrade soil was placed in the

manner described in the first report (1) to within 150 mm of the floor level. The first pavement, which consisted of 150 mm of dense bitumen macadam (DBM) was then laid prior to assembly of the test facility. After completion of testing, the pit was symmetrically extended to a length of 7.2 m for the second and third pavements. A 75 mm layer of lean concrete was placed at each end as shown in Fig. 2.1. This presented some scope for comparing the behaviour of the bitumen layer over both a rigid and a flexible support. Pavement 2 consisted of 150 mm of DBM over both the soil and the lean concrete while pavement 3 incorporated a 230 mm layer of DBM over the subgrade with 150 mm over the lean concrete. The asphalt mix was intended to be identical to pavement 1 and was placed in 76 mm lifts. Instrument installation is described in Chapters 3 and 4.

Improvements were made to the loading facility without interrupting the test programme and the final version is described in the following sections. Preliminary details were given in the first report (1), but in view of the fact that certain critical design details have since been isolated, a complete description is now presented.

2.2 REACTION BEAMS

Initially, two transverse rails were bolted to the floor, one at each end of the room, to provide support and a running surface for two heavy "bogies". Two 'I' section beams (203 mm x 203 mm) were then fixed to identical section cantilevers attached to the bogies as shown in Fig. 2.2. These were shimmed and adjusted until they were parallel with the floor level and the longitudinal centre line of the pavement. The loading carriage was fitted just prior to this stage in order to ensure free running within the beams. The main reaction members,

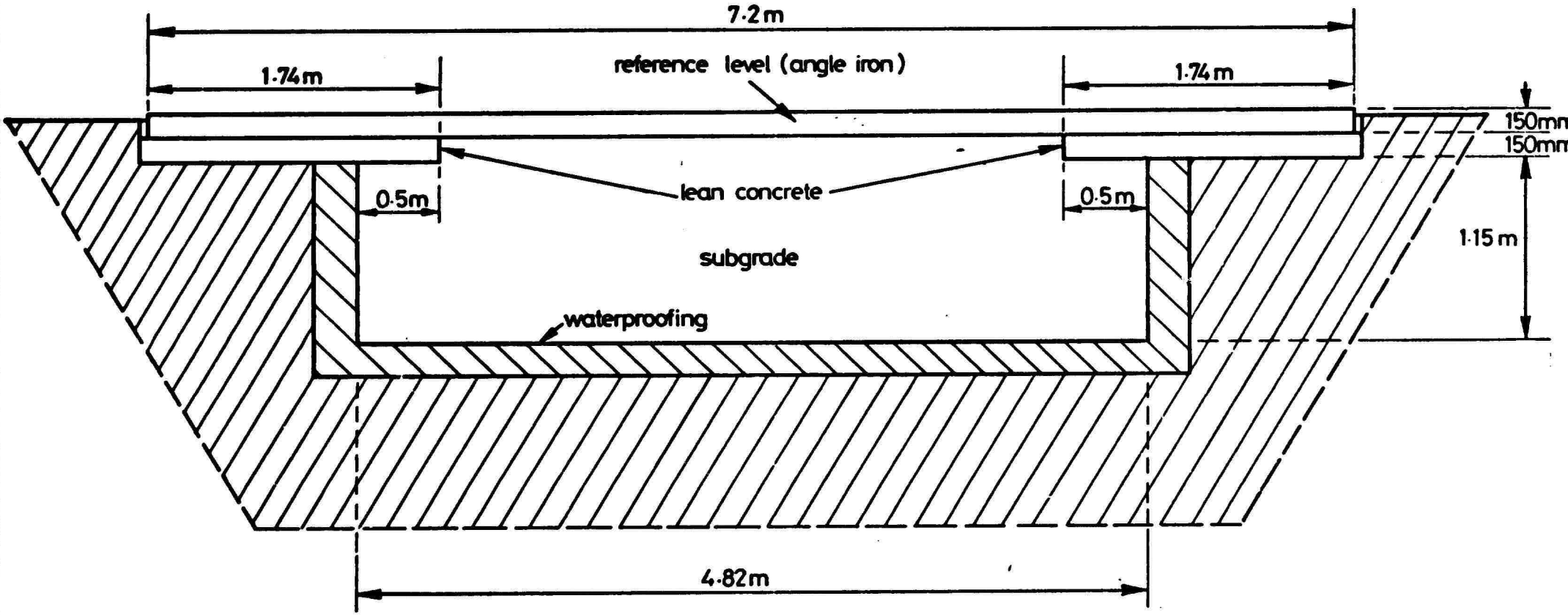

Note : pavement surface is at reference level

FIG. 2.1 SIDE VIEW OF EXTENDED PIT

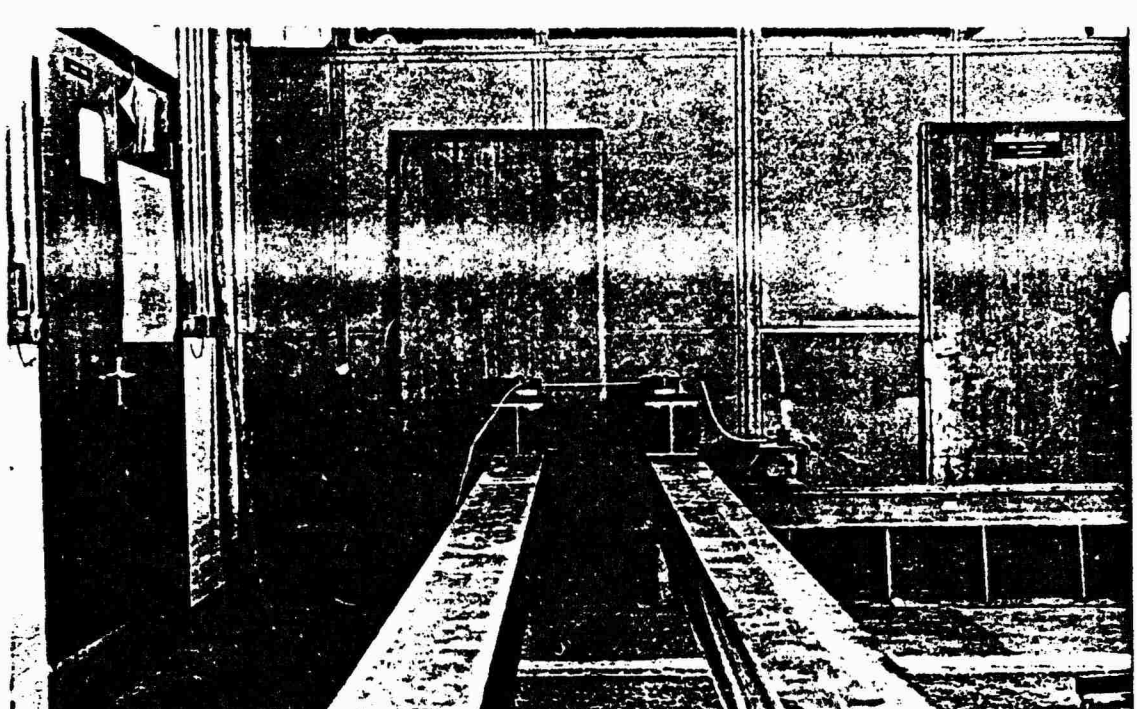

FIG. 2.2 MAIN REACTION BEAMS

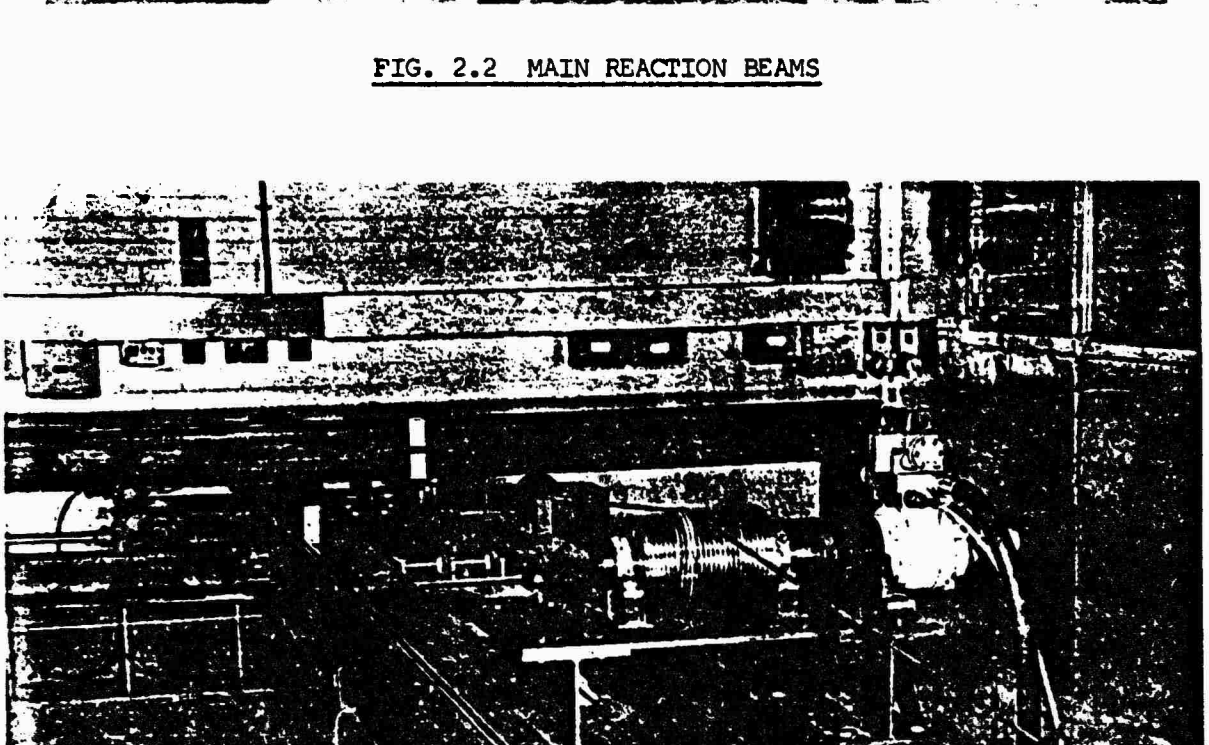

FIG. 2.3 HYDRAULIC DRIVE ARRANGEMENT

consisting of two portal frames, were then positioned over the pavement and towards each end, and their height was adjusted to make contact with traversing wheels on the main beams as can be seen in Fig. 2.3. This arrangement provided the necessary reaction for any lateral position of the loading carriage and the main beams. Fig. 2.3 shows the sections which were bolted centrally on the beams and "tied" together with a substantial metal plate so as to support the driving system.

2.3 THE LOADING CARRIAGE

A strong rectangular aluminium chassis was constructed to mount the guide bearings and wheel loading assembly (Figs 2.4 and 2.5). Four pairs of bearings were positioned at the four corners to accommodate the vertical forces between the carriage and the lower flanges of the reaction beams. The eight lower bearings transmitted the thrust when operational while the other bearings took the weight of the carriage when the wheel was clear of the pavement. A further four horizontal bearings maintained the horizontal alignment of the carriage between the beam webs. Slight clearance was necessary to eliminate "wedging". The carriage chassis housed a dual triangular lever arrangement operated by twin rams and pivoted on phosphor bronze bushes about a steel shaft. Another shaft at the mid-point and between the levers supported the wheel and associated bearings. Thus, operation of the rams caused a downward thrust on the wheel when the carriage was restrained by the reaction beams (Fig. 2.5a).

A self-contained hydraulic system was fitted to the chassis to provide power for the rams, details being presented in Fig. 2.5b. An oil reservoir was connected to a gear pump which supplied oil under

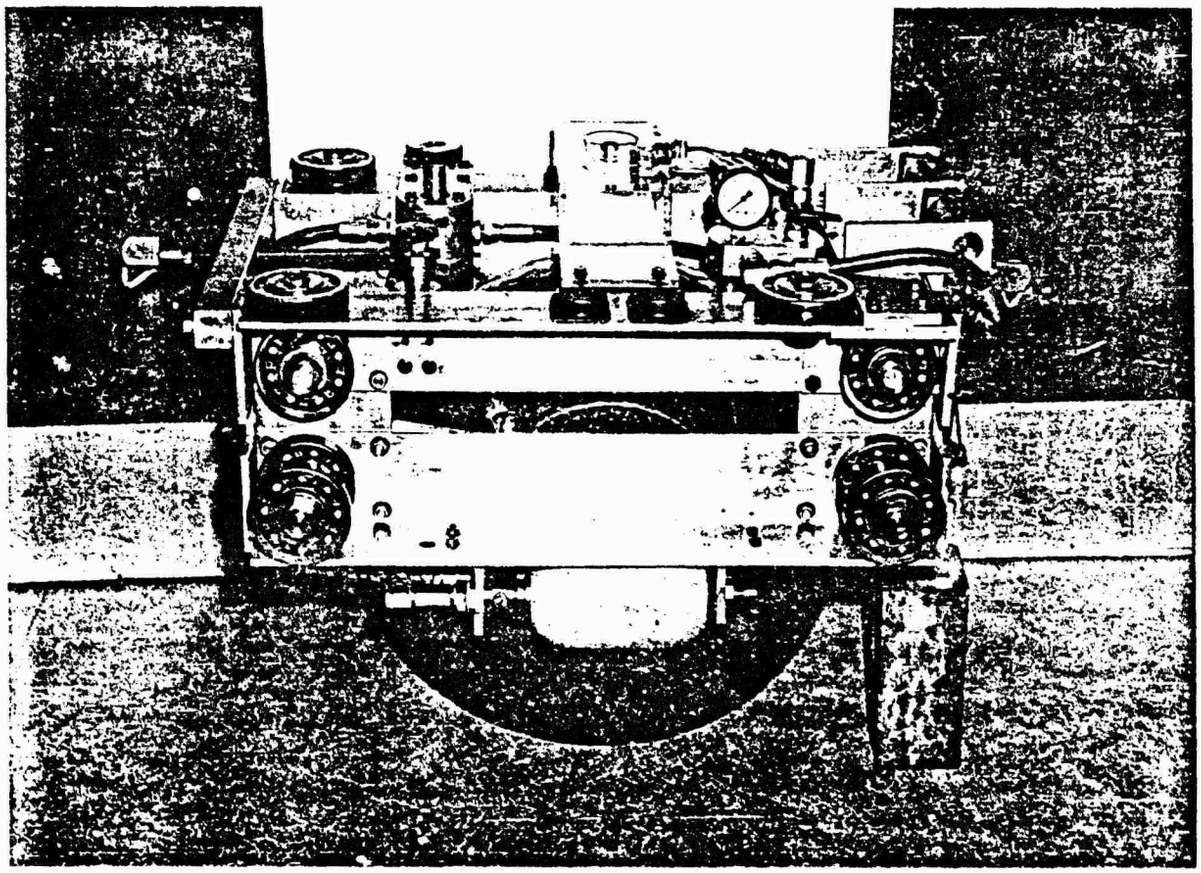

FIG. 2.4 CARRIAGE

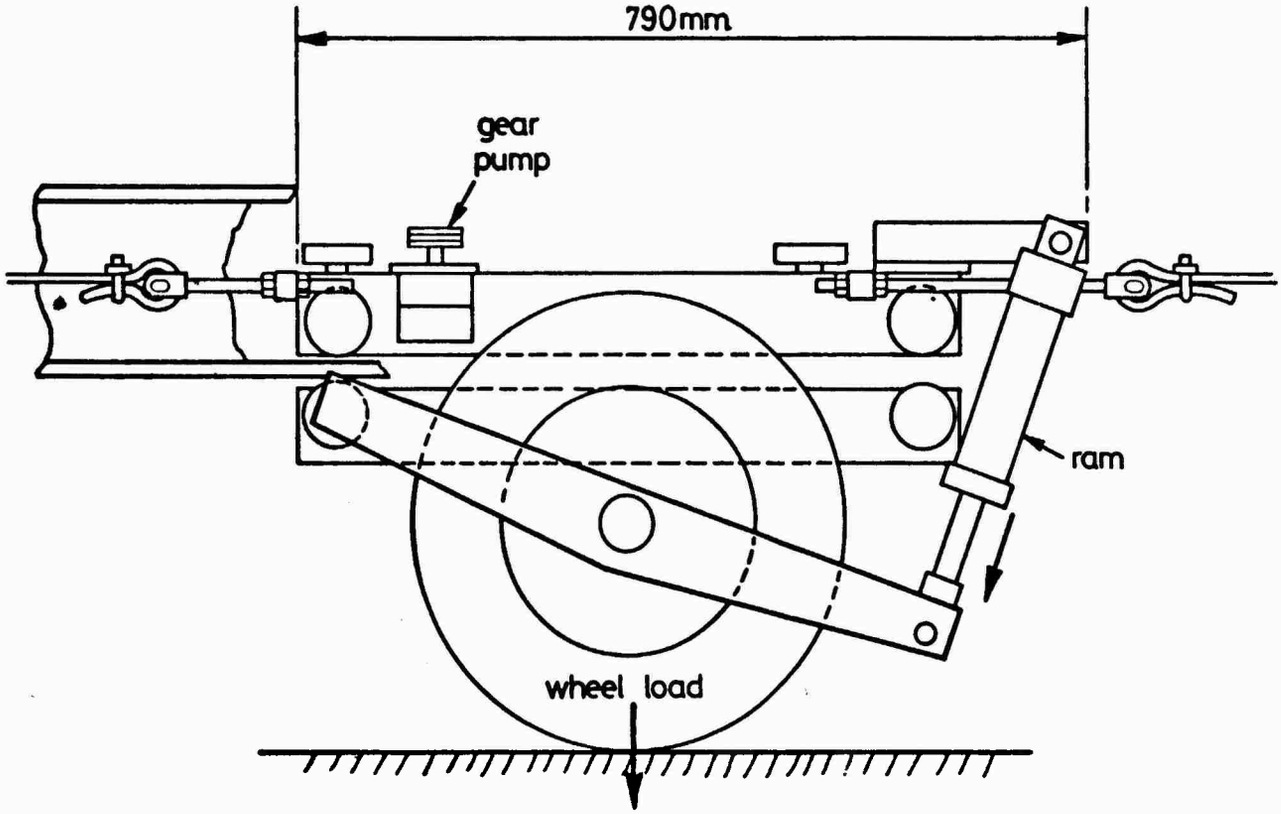

(a) LOADING SYSTEM

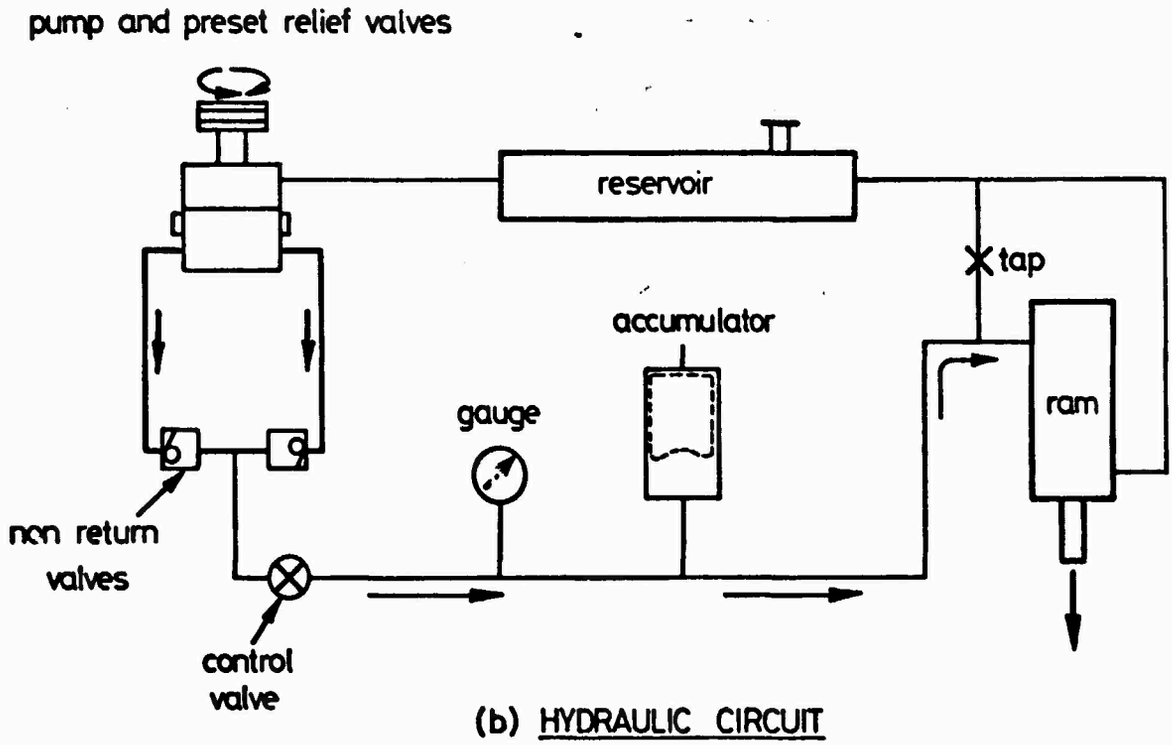

(b) HYDRAULIC CIRCUIT

FIG. 2.5 LOADING CARRIAGE

pressure through non-return valves and a control valve, to an accumulator. A pressurised nitrogen bag within the accumulator absorbed low frequency pressure surges and assisted in maintaining the required constant pressure in the rams. The relief valves in the gear pump were set at a slightly higher pressure and the correct pressure was set by the control valve. Final adjustment of the load was determined by the readings from strain gauges attached to the reaction beams. These were calibrated beforehand as described in Section 2.6.

The gear pump only required intermittent operation to prevent loss of pressure. This was accomplished by attaching a wheel to the pump drive shaft which, when the carriage was moving, revolved on contact with a short length of hard wood fitted to the reaction beams. Since the hydraulic system could not respond to rapid back pressure fluctuations, constant load application was best obtained when the pavement surface had a good level finish.

2.4 CABLE DRIVE SYSTEM

A grooved drum was mounted in bearings on the central plate above the reaction beams as can be seen in Fig. 2.3. A wire cable was clamped to a threaded tensioning rod on the carriage, passed around a pulley at one end of the reaction beams and wrapped at least four times around the drum. It was then taken around a pulley at the opposite end of the beams and connected to another tensioning rod on the carriage. Thus with the cable taut, rotation of the drum caused the carriage to move between the beams. Additional grooved pulleys were added to take the cable under the lateral reaction members as shown in Fig. 2.6 though not fitted when the photograph of Fig. 2.3 was taken.

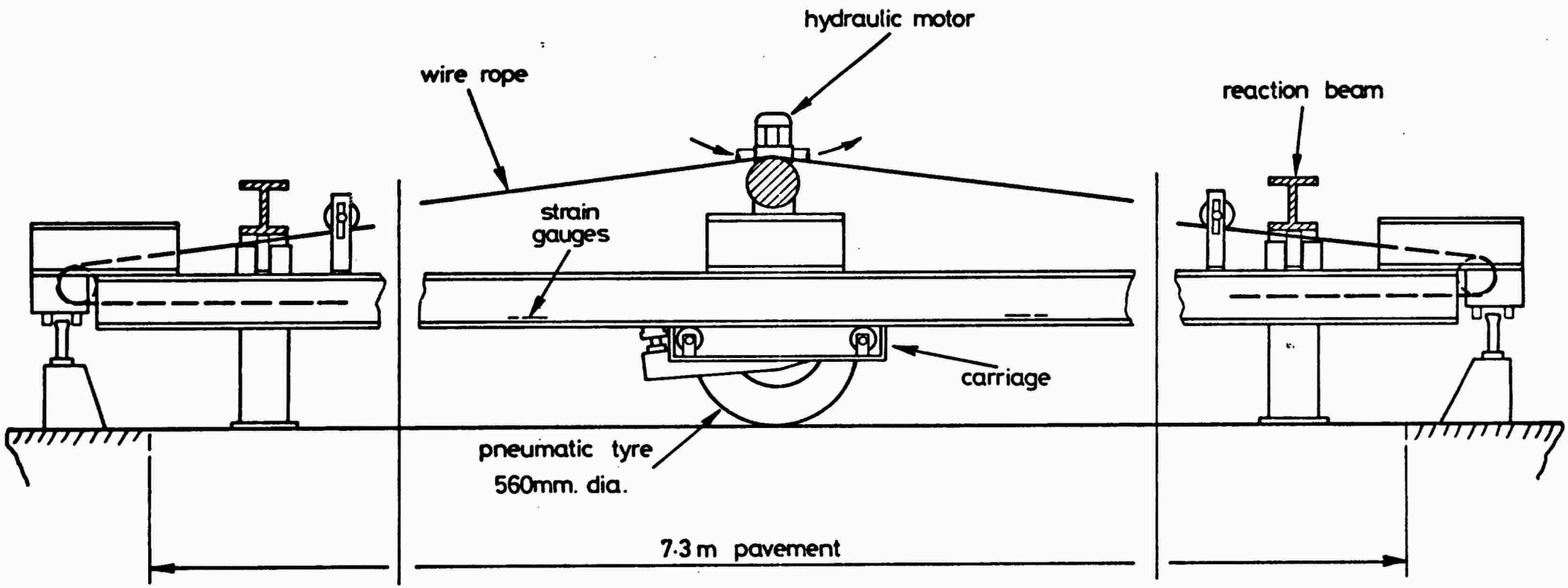

FIG. 2.6 SIDE VIEW OF PAVEMENT TESTING FACILITY

The sizes of the drum and cable were one of the critical design areas as the drive system torque characteristics favoured a small drum and this conflicted with the safe bending radius of a sufficiently strong cable. However, a compromise was reached which permitted the use of an 8 mm cable around a 180 mm drum. Regular inspections of the cable will reveal any strand fractures due to the fatigue action of wrapping and unwrapping around the drum, and a cage is fitted over the drive system as an essential precaution. It has been noted that a cable change is only required after the completion of each test, i.e. in excess of 120,000 operations. The ideal drum diameter would have been 100 mm as this operated at a rotational speed compatible with the maximum torque available and the inertial effects were less. Thus, with the larger drum more power was necessary but it was felt that the vast improvement in cable life was adequate compensation.

2.5 HYDRAULIC DRIVE SYSTEM

The basic components of this system are a hydraulic power pack (oil pump), a hydraulic motor and a servo valve. The pump supplies oil under pressure to a distribution block connecting the servo valve to the motor, and it is the precise action of this valve which controls the direction and rotational speed of the motor shaft. The motor, block and servo valve are shown in Fig. 2.3. A flexible coupling links the motor shaft to the grooved drum to reduce any slight misalignment and vibration effects, which could otherwise be transmitted to the motor housing carrying the servo valve and tachogenerator.

Opening the valve causes oil to impinge on the vanes of a rotor which is part of the motor shaft, hence causing rotation of the drum. Redirecting the oil through an alternative orifice leading to the

other sides of the vanes reverses the shaft rotation. This rotation is converted to linear motion through the cable drive permitting acceleration, constant speed, deceleration and reversal of the carriage. Response is very precise due to the proximity of the servo valve to the motor and the low inertia of the rotating parts. The distribution block separating these components contains relief valves related to the direction of oil flow, and these operate if an excessive pressure surge occurs within the system.

The servo valve consists of a sliding spool linking a pressure port and a return port to the control ports of the distribution block and motor. Substantial hydraulic power can be precisely controlled by small variations in pressure differentials on the spool ends as a result of electrical signals. The generation and control of these signals is discussed in Section 2.7 and Appendix 1. Distribution of pressure within the motor results in a uniform torque output and the vane arrangement remains hydraulically balanced. Torque and speed are proportional to pressure and flow and the system is characterised by low friction, low inertia properties, high starting torque and the ability to withstand rapid reversals.

The oil is supplied by a 40 h.p. (30 kW) pump capable of operating at 14,000 kN/m^2 at a delivery rate of 155 litres/min. This is adequately driven from a 440 volt, 100 A three phase supply. Filtration is at a level (passing 10 microns) which protects the servo valve and motor although extra filter elements are integral components of the valve. The oil is cooled by an air blasting system because of a prohibition on the use of mains water as a coolant.

2.6 FEEDBACK TRANSDUCERS

It is essential that the carriage speed, carriage position and wheel load are accurately maintained in order to control the rig performance.

Wheel load is determined from eight strain gauges attached to the bottom flange of one of the reaction beams and they monitor the thrust from the carriage reaction bearings. The gauges are positioned 610 mm either side of the beam centre in two groups of four, and subdivided into lateral and longitudinal pairs. By series connecting two unidirectional gauges, one from each group, in the same arm of a Wheatstone bridge circuit, a constant output can be obtained proportional to the wheel load. This arrangement worked satisfactorily except when the carriage approached the ends of its travel. In addition, peaks were noticed when the carriage bearings were symmetrically situated about a group of gauges. Calibration was carried out with a load cell jacked against a frame attached to two round bars which simulated the transmission of load from the carriage bearings.

Although the arrangement for load measurement and control was not a direct feedback system, manual adjustment to the ram pressures on the carriage, when it was stationery, were made if significant load changes were observed.

The carriage position is monitored by an LVDT displacement transducer which responds to a mechanical reduction of the total linear movement. This is derived from a threaded shaft axially attached to a sprocket driven by a chain connected to the carriage (Figs 2.7 and 2.8). The shaft is screwed into a cylindrical block which is prevented from turning by a keyway but can slide in a housing when the shaft turns. The LVDT core is attached to the block and runs

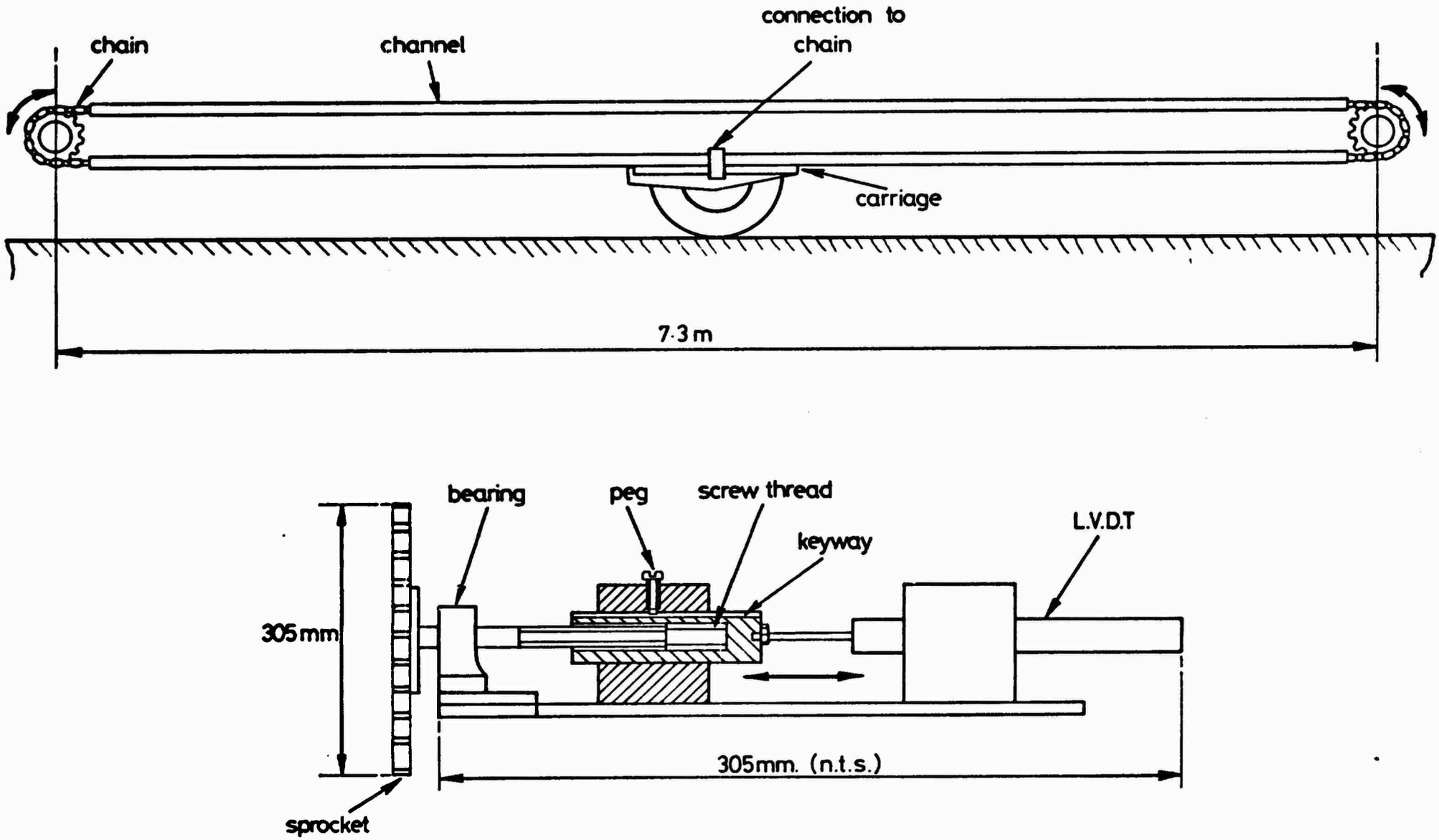

FIG. 2.7 CARRIAGE POSITION TRANSDUCER

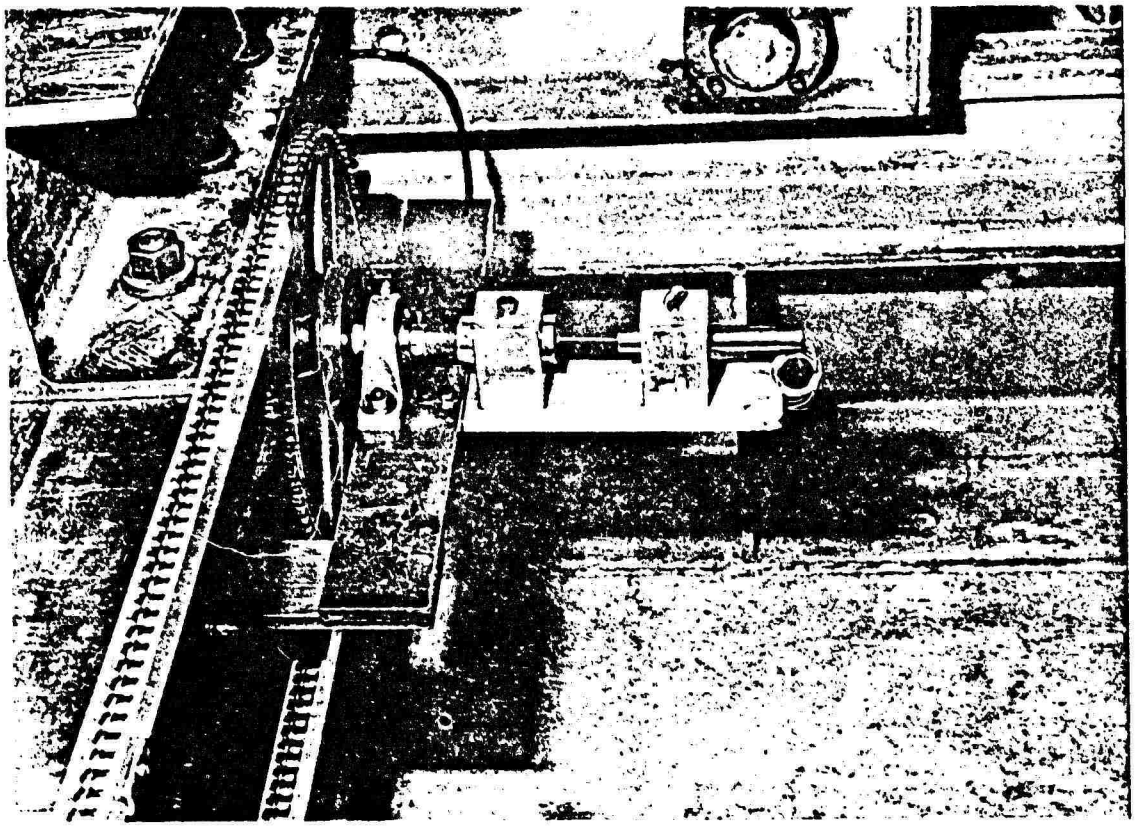

FIG. 2.8 CARRIAGE POSITION FEEDBACK TRANSDUCER

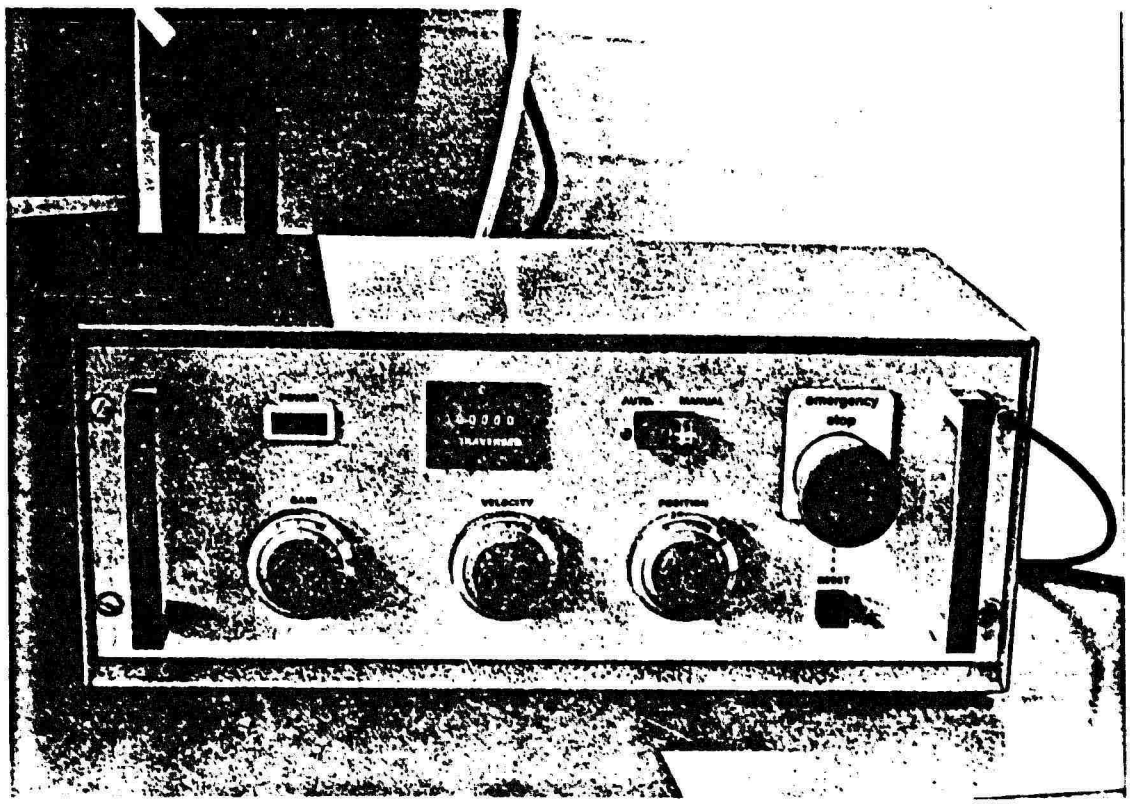

FIG. 2.9 CARRIAGE RESPONSE CONTROL UNIT

through a fixed LVDT body when the sprocket rotates, resulting in an electrical output proportional to the carriage position. The sprocket bearing mountings are adjustable so as to allow for tensioning of the chain which runs in lubricated supporting channels.

The carriage velocity is monitored by a tachometer generator connected to the shaft of the hydraulic motor. It consists of windings on a rotor moving within the field of a permanent magnet attached to an outside casing, and a generated d.c. voltage is picked off by brushes in contact with silver commutator segments connected to the windings. The voltage is relatively high (40 v/100 revs) in order to swamp the electrical noise inherent with this type of device.

2.7 ELECTRONIC CONTROL SYSTEM

This unit, shown in Fig. 2.9, consists of a velocity setting in the automatic mode and a positional control in the manual mode. A gain control operates in both modes to provide a smooth response at the drive, i.e. at low gain the carriage movement is sluggish while at high gain it overshoots. A counter monitors the number of wheel passes and an emergency stop cuts out the pump motor. Facilities are provided on the rear of the unit for monitoring the carriage velocity and position, and the signal to the servo valve. These are displayed on an oscilloscope to determine the system performance particularly in terms of the carriage speed with respect to its position about the centre of the pavement. This indicated a reduction in the length of the constant speed section at higher velocities since an increased distance is required for acceleration. Although the carriage can accelerate to 24 km/hr it was more practical to operate just below 16 km/hr as this was the stage at which speed control tolerances just exceeded $\pm$ 1 km/hr.

Several safety circuits are incorporated which cut out the power to the hydraulic pump. These operate in the event of carriage over-travel, cable failure, excessive speed at each end of the travel, accidental engagement of both manual and automatic control modes and loss of supply to the electronics system. Large springs are welded to the ends of the reaction beams to prevent damage to the carriage in the event of overshoot and possibly to rebound it back into the operating range. A reset facility is provided on the control unit and is operational only when the safety circuits are cleared.

At the pump operating pressure of 7,000 kN/m^2 the carriage is capable of attaining any constant speed within the practical range in the first pass, and can be rapidly and smoothly stopped at any position. A more detailed description of the electronic control system is contained in Appendix 1.

2.8 THE TRAVERSING FACILITY

The transverse motion of the loading facility is mechanically actuated by long stroke hydraulic rams connected to the bogies at each end of the reaction beams. Its position is monitored by an LVDT operating on the same principle as the carriage position transducer. In this case a chain is fixed to the end wall and drives a sprocket fitted to the moving assembly. Figs 2.10 and 2.11 show the general arrangement of the traversing facility and its associated control unit. A pump motor develops oil pressure and flow to operate the rams and two solenoid valves direct the oil to the appropriate ports on the rams consistent with their required directional response. Compensation for any unequal rate of bogie travel is achieved by throttling the oil flow to the fastest ram.

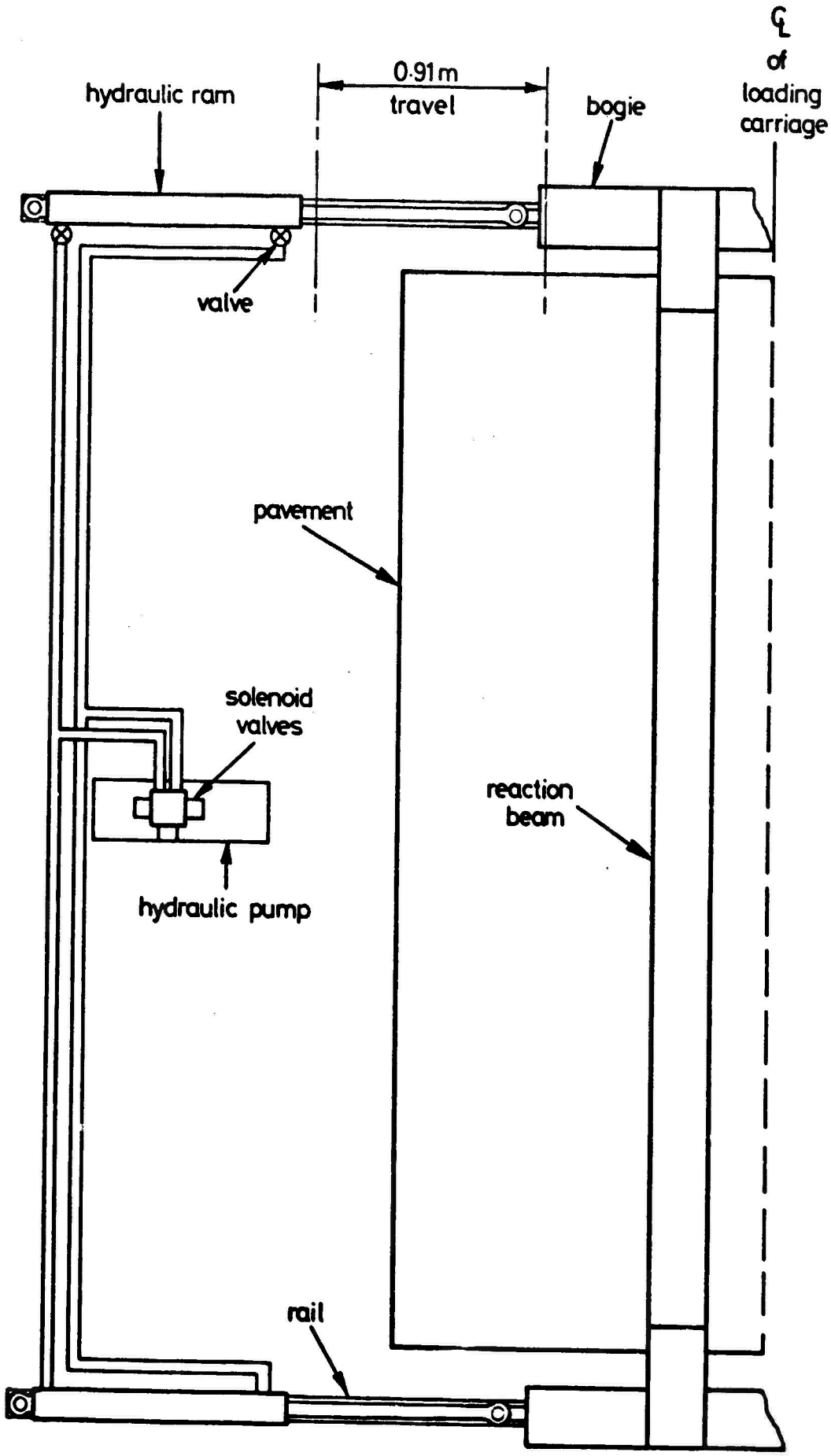

FIG. 2.10 TRAVERSING FACILITY

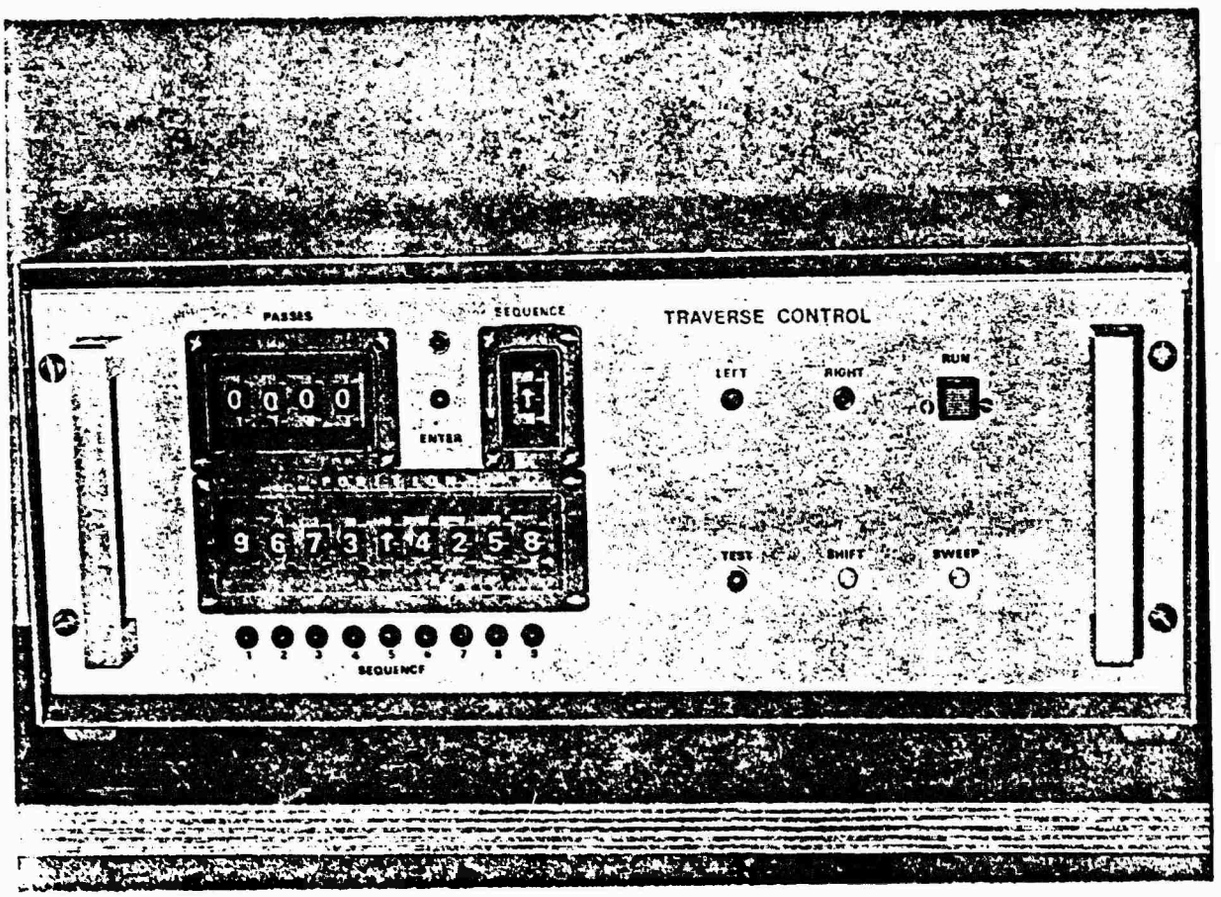

FIG. 2.11 TRAVERSING CONTROL UNIT

The control unit can be programmed to transmit electrical signals via relays to switch the pump off, in order to traverse the loading facility after completion of a specific number of passes at any one of nine lateral positions. Switches on the unit permit the nine positions to be preset so that up to 9,999 passes can be obtained for each. Furthermore, the order in which each of the nine positions is selected can also be preset. This is done in a semi-random manner.

The nine lateral positions can be set at various spacings and a 75 mm separation was chosen in order to ensure overlap of the tyre contact area between adjacent positions. When each position has been loaded, the carriage must be stopped if a programming change is required otherwise the programme will be repeated. An operational disadvantage is that up to 5 passes will be completed during the course of moving from one position to the next. This effect becomes significant in the early part of a test when the number of passes for the outside positions is less than about 30. If a low number of passes is required the traverse hydraulics can be operated by a manual switch and movement of the loading carriage restricted to a short section at one end of its run away from the test zone. It is not possible to operate the traversing movement with the wheel stationary as damage to the tyre will result. Full details of the electronic controls are given in Appendix 2.

CHAPTER THREE

PAVEMENT INSTRUMENTATION

3.1 INTRODUCTION

An understanding of the problems associated with the use of pavement instrumentation has indicated the need for specialist instruments, calibration and installation techniques. This has arisen from the local redistribution of stress and strain fields caused by the introduction of the instrument into the material within which measurements are made. Thus the reading obtained based on a simple calibration does not necessarily represent the true stress or strain level, i.e. the value which would be present if the instrument were not.

A state-of-the-art on field instrumentation has been presented by Brown (7) and descriptions of the particular instruments used in this project were given in the first report (1). Further details on their operating principles have been described by Brown and Brodrick (8).

Measurements of permanent and elastic strains were made with Bison Instruments strain coils, Nottingham strain coils, conventional strain gauges and Nottingham strain cells, while stresses were measured with Nottingham pressure cells. A summary of the application of these instruments is given in Table 3.1.

In addition, the elastic surface deflection of the pavement was determined by use of an accelerometer, temperature was monitored by thermocouples and a profilometer recorded the transverse surface profile.

Table 3.1 Application of Pavement Instruments

Instrument	Measurement	Material	Registration
Strain coils	permanent strains elastic strains	bituminous layer and subgrade	1.0
Strain gauge carrier blocks	elastic strains	bituminous layer	In situ calibration in material specimens
Strain cells	permanent strains elastic strains	subgrade	0.87 0.82
Pressure cells	stresses	bituminous layer and subgrade	0.94 0.92
Accelerometers (a) Servo type (b) Piezo-electric type	elastic vertical deflection	pavement surface	Manufacturer's calibration Bench calibration
Thermocouples	temperature	bituminous layer and subgrade	direct reading

3.2 STRAIN MEASUREMENTS

The major objective of the experiments was to determine the variation of permanent strain with depth through the bituminous layer and into the subgrade. This was accomplished by using continuous vertical stacks of strain coils and monitoring the contribution of each pair to the overall pavement deformation. In practice, there must be some material disturbance during installation and a degree of interaction between the instrument and the material because of their differing moduli of elasticity. Other factors to be considered were the proximity effects of "out of circuit" coils, the metallic components of the rolling wheel and survival during paving operations. Careful calibration tests were, therefore, considered necessary.

In order to provide additional elastic strain measurements, vertical strain gauges were attached to asphalt carrier blocks in the bituminous layer and two Nottingham strain cells were used in the subgrade.

Longitudinal and transverse horizontal strains were measured at the asphalt/subgrade interface with a coplanar arrangement of strain coils, and with strain gauges on carrier blocks. Horizontal elastic strains were also measured by strain gauged carriers within the bituminous layer at positions above the interface carrier.

Appropriate calibration tests were carried out to overcome some of the difficulties mentioned above. These involved a comparison of bench calibrations with those carried out in samples of the test materials. Notice was also taken of experience reported by other research workers in the literature (9,10). A detailed description of calibration techniques has been given by Brown and Brodrick (8) and by Brown et al (1) in the first report. The procedure, therefore, presented in summary is as follows.

The initial bench calibration was based on the coils or cell output with reference to the incremental steps of a micrometer or pressure. Then the instrument was placed in a large specimen (230 mm dia.) of the pavement material and loaded in a triaxial cell over a stress range compatible with the expected strain levels. This involved a static and dynamic testing procedure so far as the vertical stress was concerned, while various levels of static confining stress were applied. The coil outputs were plotted against readings from strain collars attached to the sides of the specimen and the slope of the graph was divided by that of the bench calibration. This factor was termed cell registration and was derived from several tests to assess the scatter generally resulting from installation effects. These tests were only carried out in the subgrade material, and at low strains revealed a frictional effect for the strain cell. However, excellent linear response was obtained for the coils. The strain cell under-registered by about 15%, probably due to its inherent mechanical resistance over the gauge length. An apparently high over-registration was obtained for the free moving coils.

As a result of these tests the strain cells were installed in subgrade locations where high elastic strains were expected. However, it was felt that coil calibrations were possibly affected by the metallic components of the triaxial cell and interference from the strain collar LVDTs, which spanned their gauge length. Furthermore, the coils were installed at convenient layers as the specimen was completed and it was hoped that this technique could be repeated in the pavement experiment. Unfortunately, the subgrade layers were subsequently compacted in such a way that considerable material movement occurred and the cored hole installation method adopted for the strain cell (1) was also applied to the strain coils.

Bench calibrations were repeated with subgrade and asphalt blocks between the coils in order to eliminate the triaxial cell and strain collar interference effects. This arrangement indicated a registration of 1. Modifications to this figure for permanent strain due to installation effects could be assessed by correlation with the rut depths measurements and the distances between the coils on removal. Paterson (9) also obtained a registration of unity in a specimen of asphaltic concrete using 50 mm coils and it was considered that the 25 mm coils would have a comparable response.

A direct calibration of the strain gauge carrier blocks was obtained by installing a vertical element in a dense bitumen macadam specimen. This element was effectively a 25 mm cube and the specimen dimensions were 100 mm dia. x 150 mm deep. The element consisted of two sandsheet blocks sandwiching a vertical strain gauge (attached to one block) and any air voids between the blocks were filled with a flexible adhesive. A gauge length of 10 mm was chosen for the vertical gauge which was attached to an exposed section of fine material. This principle was also applied, at a later stage, for the 20 mm horizontal gauges during preparation for installation. The carrier was then placed at mid height in the DBM specimen which had been compacted in layers in a split mould. Two displacement transducers were attached to the specimen to monitor vertical deformations at diametrically opposed locations, and the assembly was positioned in a compression testing machine. The specimen was loaded incrementally to attain a 0.5% strain reading at 30^{o}C and then taken to failure to assess the gauge properties under extreme conditions. This revealed an initial linear response which changed to a curve of decreasing slope as shown in Fig. 3.1 as failure was

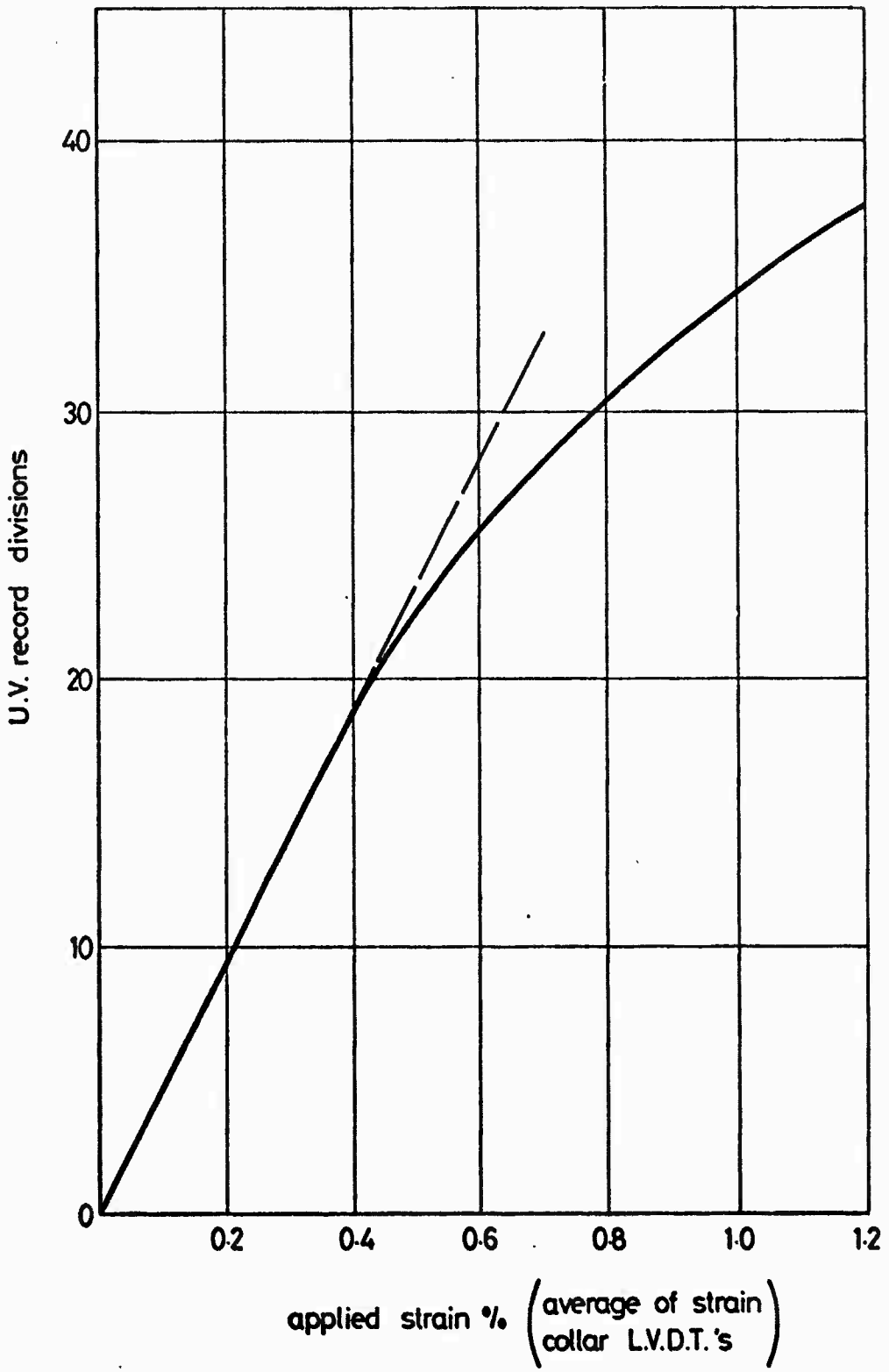

FIG. 3.1 CALIBRATION OF STRAIN GAUGE CARRIER BLOCK IN DBM SPECIMEN

approached. The slope of the linear portion was taken as the calibration for elastic readings below 0.5% strain. The non-linear response was possibly due to exceeding the elastic limit of the gauge (approx. 3% strain), as it would have been substantially strained during compaction. Alternatively, there may have been slippage between the carrier block and the parent material.

3.3 SURFACE DEFLECTION AND DEFORMATION MEASUREMENT

Two types of accelerometer were used, a servo device with a linear output down to d.c. and a piezo-electric device operational between 2 Hz and 7 kHz. These instruments are shown in Fig. 3.2. The manufacturer's calibration was accepted for the former and its output after electronic double integration was substituted into a formula (11) to determine the total transient deflection of the pavement. A similar circuit was connected to the piezo-electric accelerometer and this was calibrated on a vibrator.

The profilometer, shown on Fig. 3.3, consisted of a displacement transducer attached to a sliding block which ran on a stiff guide rail. A dual wheel arrangement was fixed to the sliding shaft of the transducer and this followed the height variations in the pavement surface when traversed. The total movement of the transducer was calibrated in increments against a micrometer and checked with slip gauges between tests. These gauges are precision blocks and were placed under the wheels when the profilometer was positioned above an external reference point.

3.4 STRESS MEASUREMENTS

Vertical and horizontal stresses were measured with Nottingham

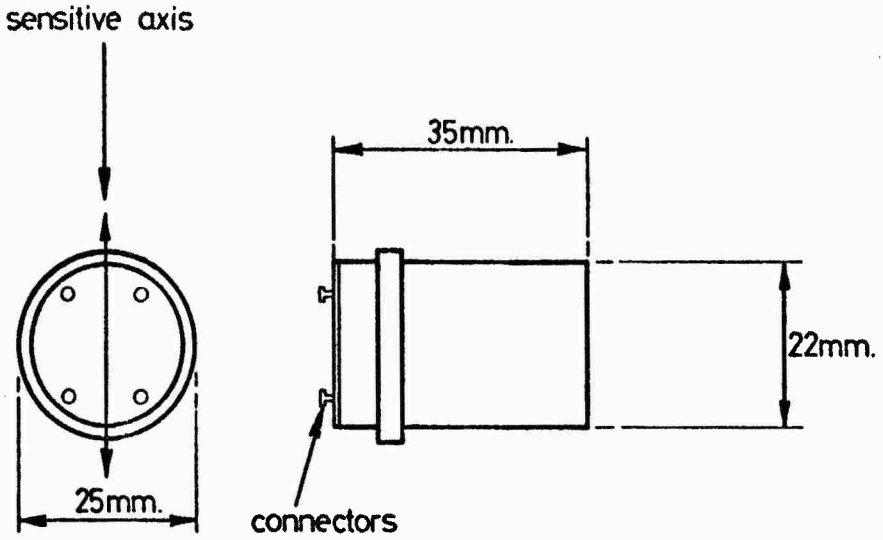

(a) SERVO ACCELEROMETER

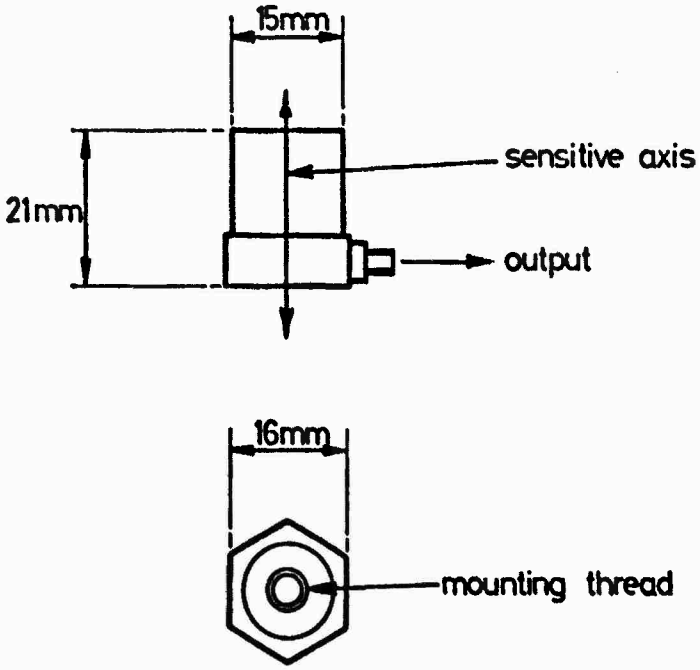

(b) PIEZO ELECTRIC ACCELEROMETER

FIG. 3.2 DETAILS OF ACCELEROMETERS

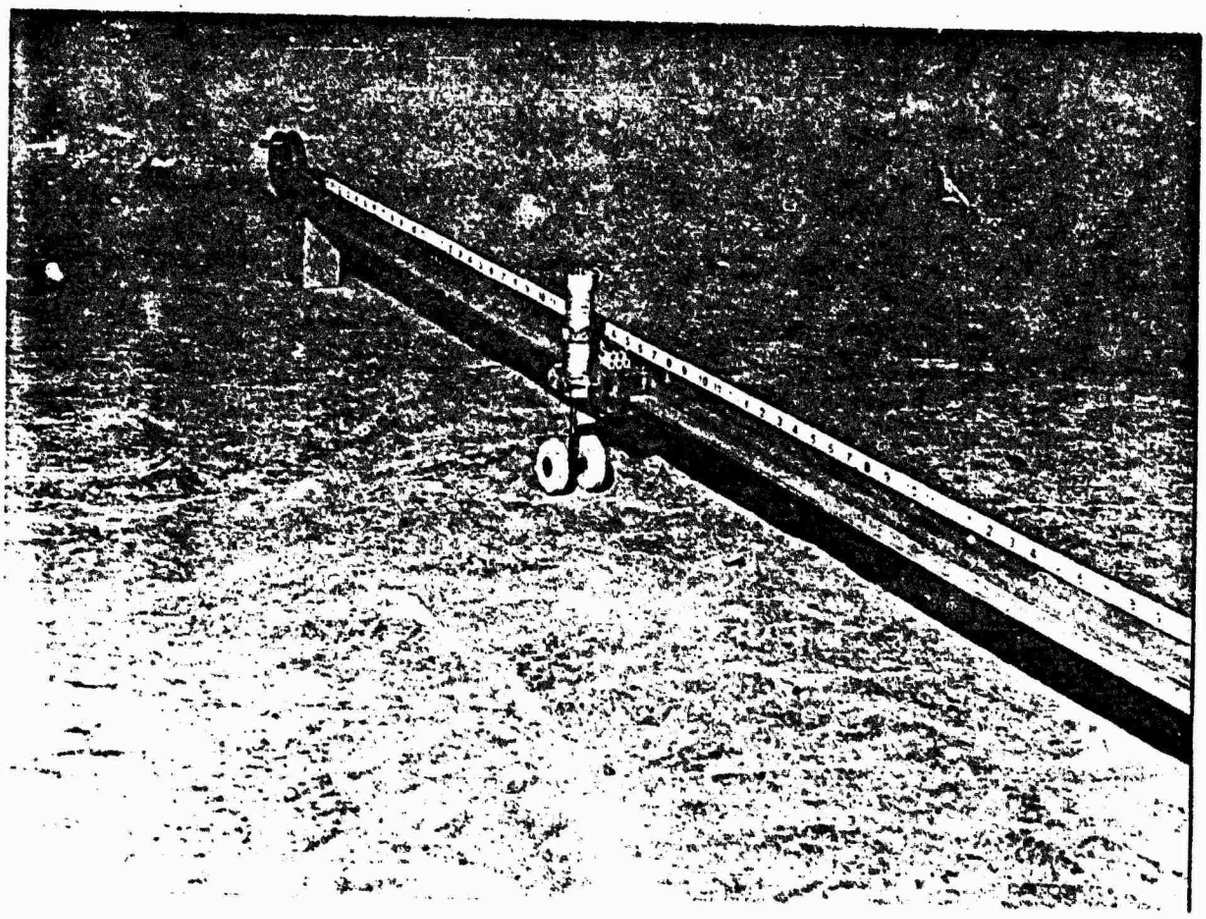

FIG. 3.3 PROFILOMETER

pressure cells. Many investigations have been carried out on the design and behaviour of these instruments over the last decade, culminating in a satisfactory understanding of their performance in a soil mass (8). The same philosophy of calibration and replicate installation was applied as described for the strain coils.

The bench calibration was carried out by applying oil pressure to rubber membranes in contact with the cell diaphragm and lid as described by Brown and Brodrick (8). Calibration in the soil was carried out by installing the cell centrally in a specimen which, as with the strain coils, was incrementally loaded and true stress was determined by dividing an external axial load cell reading by the specimen cross sectional area. Average static and dynamic cell registrations were 0.97 and 0.92 respectively and the latter was chosen to calculate the true subgrade stress in the pavement.

A further exercise had to be carried out as a result of using the cells in the bituminous layer in pavement 3. Theoretical prediction of registration (Fig. 3.4) (12), for the titanium pressure cell in soils indicated consistent results at low values of Young's modulus (< 30 MN/m^2). The registration decreases as soil stiffness (modulus) increases and considerable under-registration (0.4) occurs at a soil modulus of 1,300 MN/m^2, which is equivalent to the highest dynamic stiffness measured for the bituminous layer in pavement 3. The lowest stiffness was 300 MN/m^2 and a cell operating in this region would have a theoretical registration of 0.75. However, the characteristics of the two materials differ, and it was felt that less variation in cell performance may occur in bituminous material. A further reason for questioning the theoretical prediction was the presence of a fine mix placed around the cell principally to protect

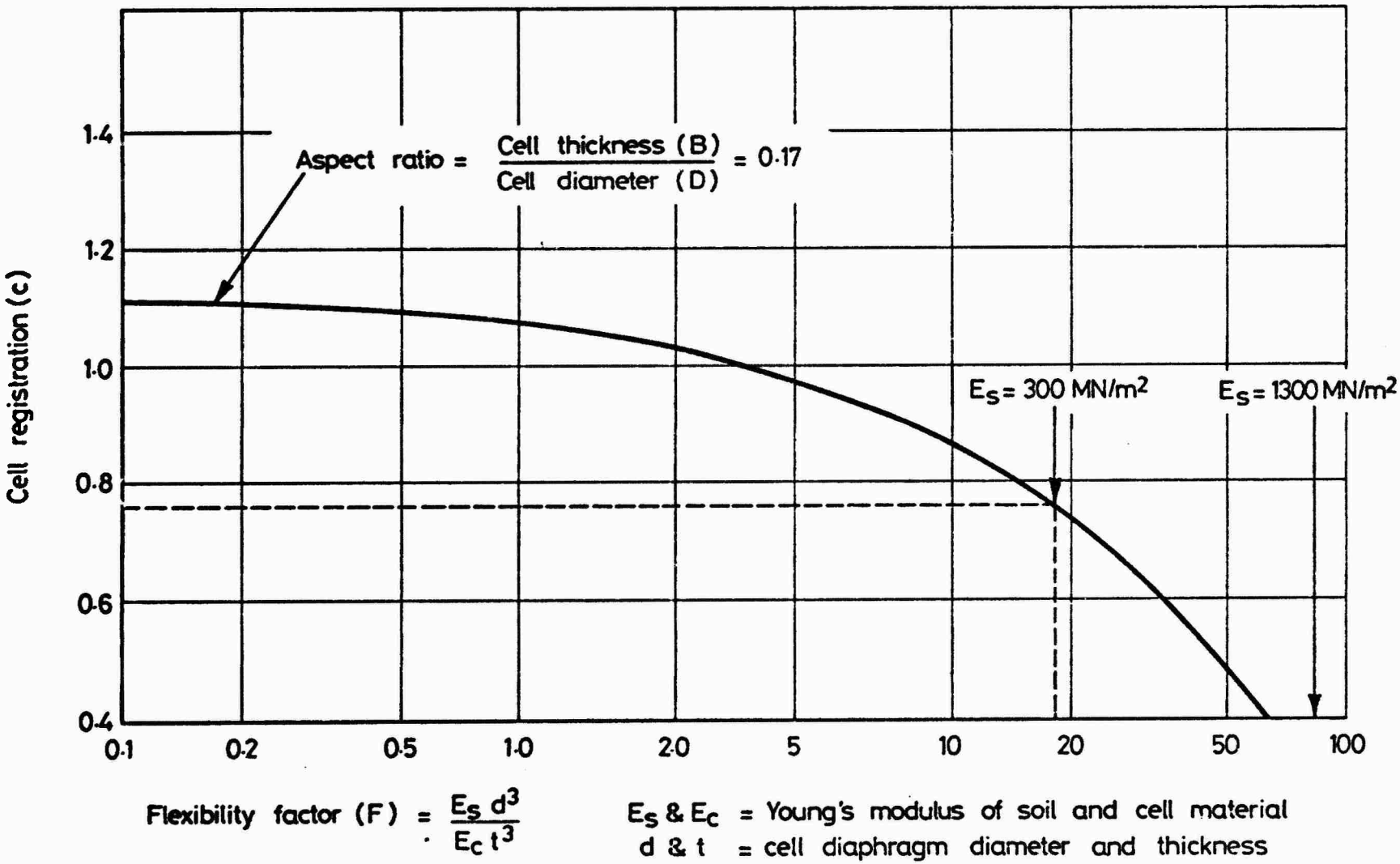

FIG. 3.4 THEORETICAL PREDICTION OF TITANIUM P. CELL REGISTRATION (After Tory and Sparrow (12))

the diaphragm, from point loads. A cell redesign was not possible within the testing schedule and an attempt was made to calibrate the instrument in a 150 mm diameter DBM specimen using the installation technique employed in the pavement. This followed the procedure outlined for the subgrade but with emphasis on reproducing the test temperature and rate of loading. As a result, a registration of 0.94 was established but it must be stated that the cells were not prepared for surviving high temperatures. Further research has since been initiated to calibrate the cell in a DBM specimen and investigate the effect of variations in stiffness in order to produce a cell registration prediction curve.

3.5 TEMPERATURE MEASUREMENT

Copper-constantan thermocouples were used for temperature measurements. They were connected to a continuously sampling single point chart recorder. A calibrated measuring circuit and reference cold junction were integral units of the instrument and calibration was unnecessary. However, a spare thermocouple was immersed in a constant temperature water bath at 30°C to provide a reference "print out".

3.6 READOUT FACILITIES

The change in spacing of the strain coils, related to permanent strain, was determined from the reading on the amplitude dial of the Bison balancing instrument. Elastic strains were monitored on an Ultra Violet recorder connected to an output facility on the instrument. A sequential selector switch coupled pairs of coils and the sensitivity switch was slowly increased from a minimum during balancing to avoid

damage to the galvanometers. It was important to maintain circuit conditions consistent with the calibration arrangement as experience revealed an output offset effect arising from cable screen interconnections with other instruments through common impedance matching circuitry.

Elastic readings from the strain cells, stresses from the pressure cells and the wheel load were also obtained on the U.V. recorder. Simulated strain and stress inputs were available for the coils, pressure cell and wheel load instrumentation. These were in the form of step inputs on the record, produced by depressing a calibration switch, and were related to strain, stress and load values determined during calibration. Thus quantitative analysis was accomplished by multiplying the ratio of the test reading to the step input by the corresponding strain, stress or load value. Permanent strain from the strain cells was in the form of a d.c. voltage and indicated on a digital voltmeter. A separate U.V. recorder was connected to all the strain gauge outputs and only elastic measurements were made as it was difficult to isolate permanent strain output from their inherent electrical drift. All the instruments with strain gauge sensing elements and the d.c. strain cell were supplied by D.C. stabilised power packs.

The accelerometer output in terms of acceleration, velocity and displacement was obtained directly from the transducer or from tappings at each stage of the electronic double integration. It was displayed on a storage oscilloscope. This device was also used for examining the response of those instruments which developed sufficient dynamic output.

The profilometer output was monitored on a digital voltmeter and

a reference point was established which produced a check reading before rut measurement commenced.

3.7 GENERAL COMMENTS ON INSTRUMENT PERFORMANCE

Observations on instrument performance were made during calibration, installation, testing and their removal from the pavement.

With the exception of the strain coils all the instruments exhibited a linear bench calibration response and therefore their sensitivity could be easily expressed. The inherent non-linear response of the coils required a graphical interpretation for large displacements, i.e. the permanent strain readings as each test progressed. A linear response can be assumed for small strains about the installation gauge length but, as a result of the overall non-linearity, the sensitivity of this response changes with the reading (amplitude dial) related to the coil spacing. Thus a graph of the range of readings expected during the test is plotted against sensitivity and applied to the analysis of the U.V. record trace. A combination of the sensitivity control and calibration dial setting also provided a reference strain pulse on the record.

The instruments calibrated in the subgrade generally appeared to be unaffected by variations in confining stress, or variations in material stiffness within the limits of the test conditions, except for slight decreases in cell registration of the pressure cells and strain cells under dynamic conditions.

There was a tendency to improve installation technique and preparation of the instruments as each pavement was laid and in general problems only arose with the strain gauges, Nottingham strain coils and with the complexity of the accelerometer equipment.

Temperature measurements were completely successful and this was attributed to the choice of a robust cable.

Each bituminous layer was removed on completion of the loading programme by sawing the central area containing the instruments into sections and also areas at each end over the lean concrete. The remainder was broken and discarded to facilitate examination and removal of the chosen sections. A small demolition hammer was used to work away the asphalt around the instruments permitting physical measurements of the coil separations and orientation. A more detailed account of the instrumentation performance is contained in Chapter 5.

CHAPTER FOUR

THE PAVEMENT EXPERIMENTS

4.1 INTRODUCTION

The three pavements were subjected to a loading programme which was intended initially to involve a 10 kN wheel load at a speed of 16 km/hr. However, during commissioning of the loading facility, which included the tests on pavement 1, small bore pipes on the loading arrangement limited the response of the rams. This resulted in a higher average load setting of 15 kN and was set manually by pumping up the carriage hydraulic circuit prior to each lateral movement. Subsequent modifications reduced the load setting to 11 kN for pavements 2 and 3. All three levels of load were generally satisfactorily maintained during the tests. Speed control was found to be more accurate at 14 km/hr and was set at this level for all three tests.

Two types of test were conducted on each pavement. The first and main test was a multi-track test, in which a "normal distribution" of wheel loads was applied in the centre of the pavement. The second was a single track test, carried out on a separate part of the pavement and consisted of the same number of passes that had been applied on the central track of the multi-track test.

The three pavements were tested at 30°C and were all 2-layer structures, consisting of a silty clay subgrade of Keuper marl and a dense bitumen macadam (DBM) surfacing. The DBM was nominally the same road base mix in all cases, and was nominally 150 mm thick for pavements 1 and 2, and 230 mm for pavement 3. A 150 mm layer of lean concrete was installed for pavements 2 and 3, at each end. The

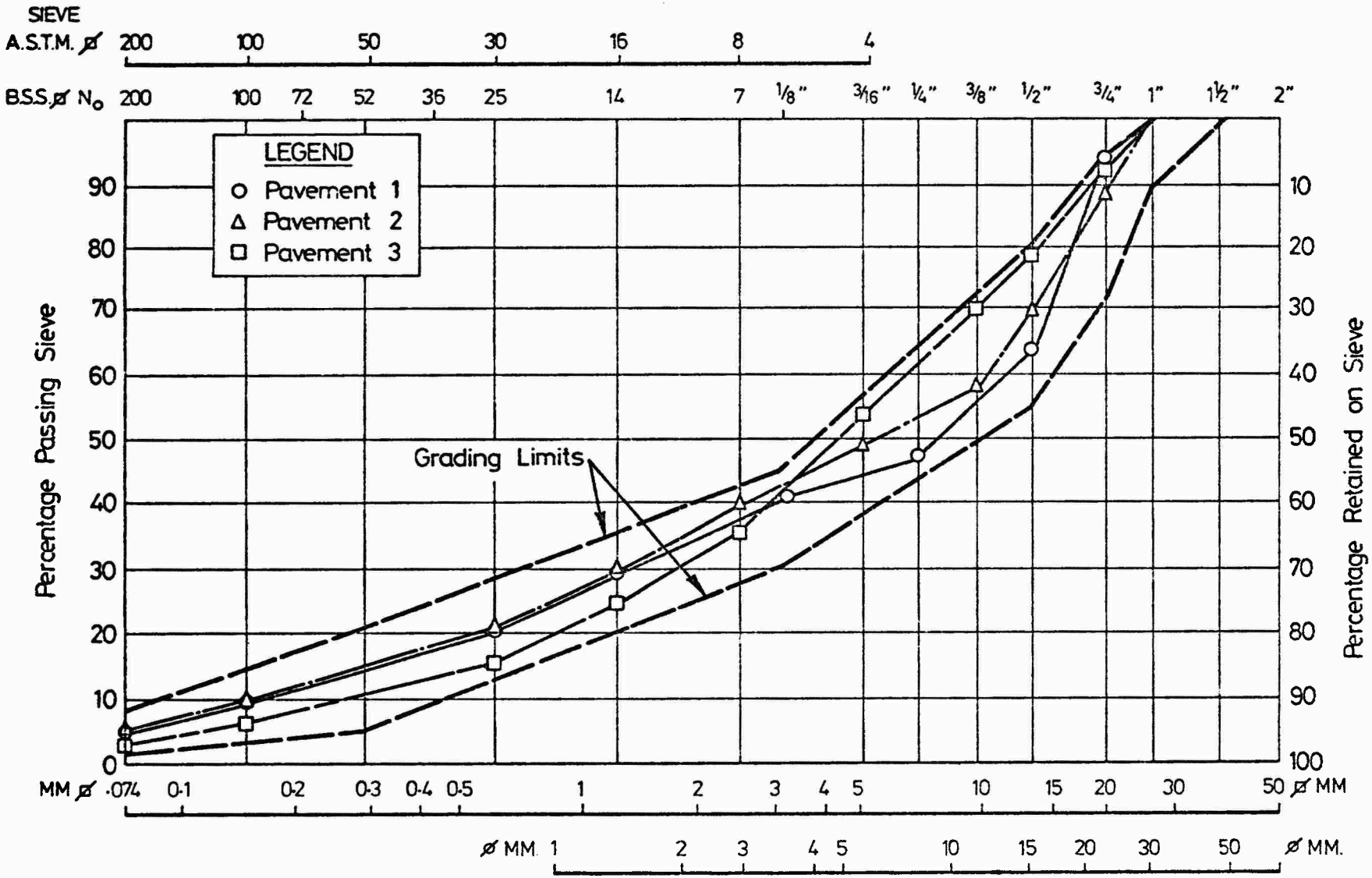

FIG. 4.1 GRADING CURVES FOR DBM FROM ALL THREE PAVEMENTS

contact pressure for each pavement was determined from measurements of the contact area and the load. For pavement 1 an average value of 660 kN/m^2 was evaluated, and for pavements 2 and 3 a value of 550 kN/m^2.

The principal measurements that were taken included the rut profiles, and the distribution of permanent strain with depth. The instruments used for these and additional measurements have been described in Chapter 3.

4.2 PAVEMENT MATERIALS

4.2.1 Dense Bitumen Macadam

This was a road base mix complying the the Specification for Road and Bridge Works (13) using a crushed rock aggregate, specific gravity 2.79, with a maximum size of 25 mm. Grading curves for the three pavements are shown in Fig. 4.1, which also shows the specified grading limits. The curves are based on average values from several samples of aggregate obtained after cores of the material had been tested. Thus, the curves are not a true representation for the larger particles, a considerable number of which were reduced in size due to sawing of the core. The binder was 100 pen bitumen with a specific gravity of 1.02. Table 4.1 shows the average binder contents and void contents measured from a number of cores, for each pavement.

Table 4.1

Pavement	Binder Content (%)	Void Content (%)
1	4.7	5.2
2	4.9	9.7
3	5.0	8.3

4.2.2 Keuper Marl

This material is a silty clay with low to medium plasticity. Some basic properties are shown in Table 4.2. Fig. 4.2 shows the results of a British Standard Compaction test, with the dry densities and moisture contents of cores taken before and after the experiments on pavements 1 and 2 superimposed. It was found that the clay lost moisture during a test and became more dense due to trafficking (zones 2 and 4). It was also found necessary to remove the surface of the clay following excavation of the DBM, due to saturation of the surface following sawing operations and for excavation of the instruments. This necessitated the addition of 150 mm of new material for pavement 2 (zone 3), but no replacement material was required for pavement 3, due to the thicker DBM layer.

Table 4.2 Results of Preliminary Tests on Keuper Marl

Liquid Limit	30%
Plastic Limit	16%
Plastic Index	14%
CBR	5%
Sieve Analysis:	
Percentage by weight retained on No. 200 sieve	52%
BS Compaction Test:	
Maximum Dry Density	1880 kg/m^3
Optimum Moisture Content	15.2%

4.2.3 Lean Concrete

This also complied to the Specification for Road and Bridge Works (13). An aggregate to cement ratio of 15:1 was used, with 40% of the aggregate passing a 5 mm sieve, and a nominal maximum size of 19 mm. A water/cement ratio of 1 ensured good workability. The mix was compacted with a small vibrating roller, and by vibrating plates. Cubes of the mix were used for control tests, the cube strengths at 7 and 28 days being greater than the minima recommended (13). Beams of the material were tested non-destructively to obtain values for the dynamic Young's modulus, and Poisson's ratio. The 28 day values were 29,600 MN/m^2 and 0.24 respectively.

4.3 INSTRUMENTATION LAYOUT

The instrumentation arrangements for each pavement can be seen in Figs 4.3 to 4.5. Strain measurements were concentrated on the longitudinal centre line of the pavements and the subgrade cells were centrally placed under the outermost lateral wheel positions (1 and 9). Five pressure cells were installed in the bituminous layer of pavement 3 on its longitudinal centre line.

Only one stack of 25 mm strain coils was installed in pavement 1 as it was necessary to prove the potential of this grouping and at that stage their availability was limited. As a result, it was concluded that the stack arrangement was satisfactory if the gauge lengths were increased from 25 mm to 38 mm and DBM carrier blocks used in place of the sandsheet ones. The lift thickness of the bituminous layer was increased from 50 mm to 76 mm to accommodate this change for pavements 2 and 3. Two stacks were then introduced for comparative purposes and to compensate for a limited number of circuit failures.

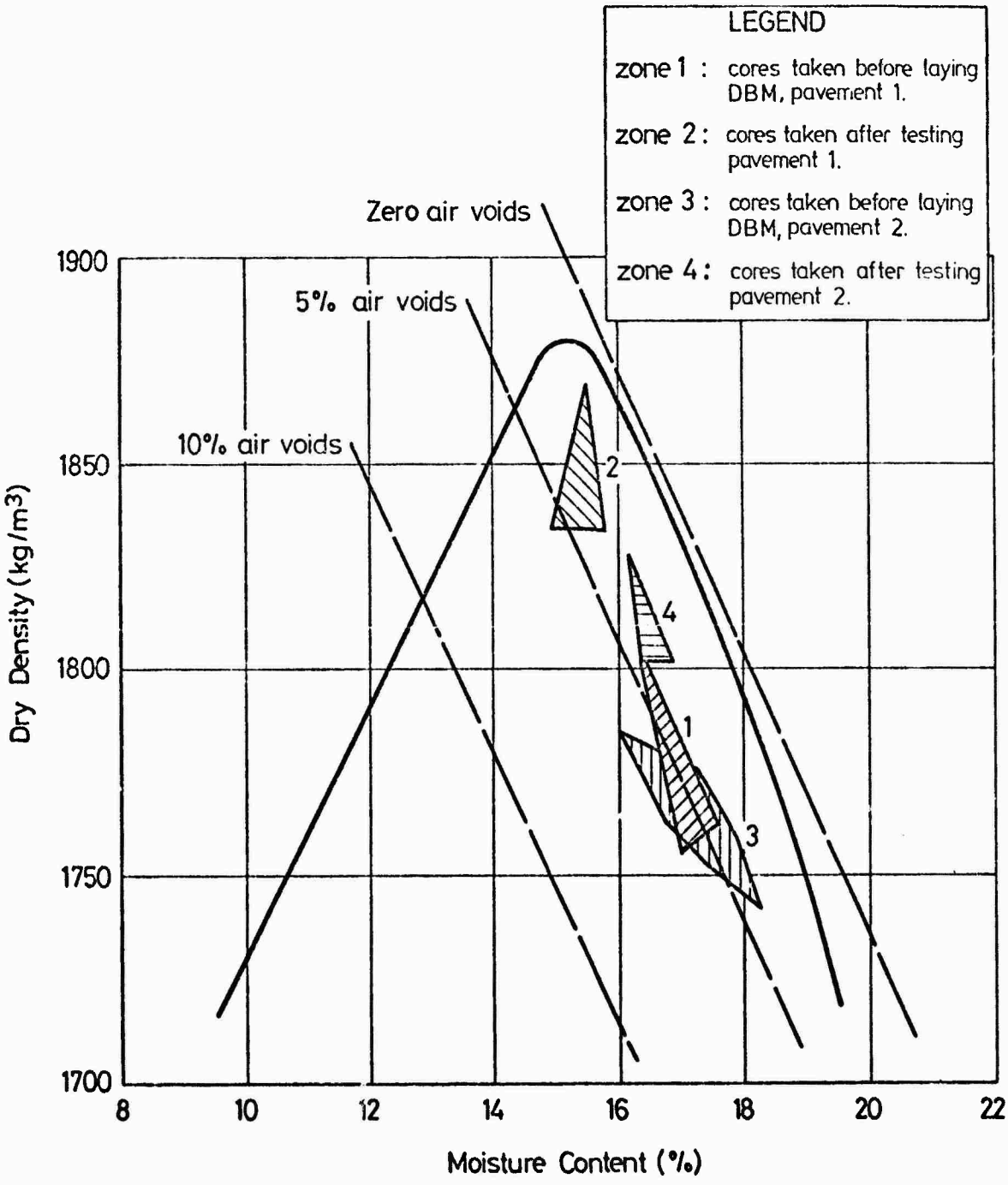

FIG. 4.2 DRY DENSITY VERSUS MOISTURE CONTENT RELATIONSHIP FOR KEUPER MARL, WITH RESULTS FROM CORES

LEGEND

1 25mm strain coils
2 50mm strain coils
3 strain cells
4 vert. carrier blocks
5 horiz. carrier blocks
6 pressure cells
7 thermocouples

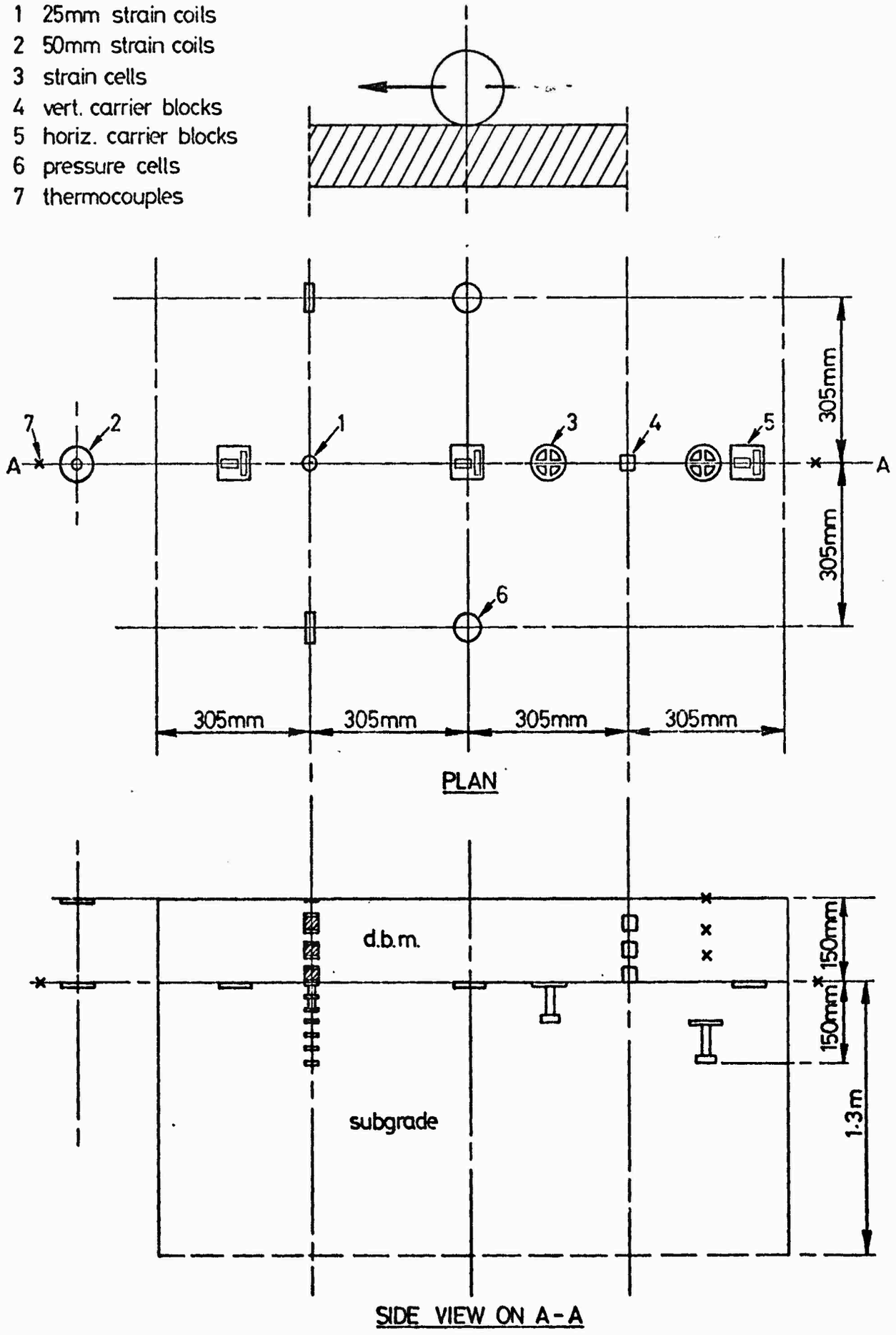

FIG. 4.3 INSTRUMENT LAYOUT, PAVEMENT NO. 1

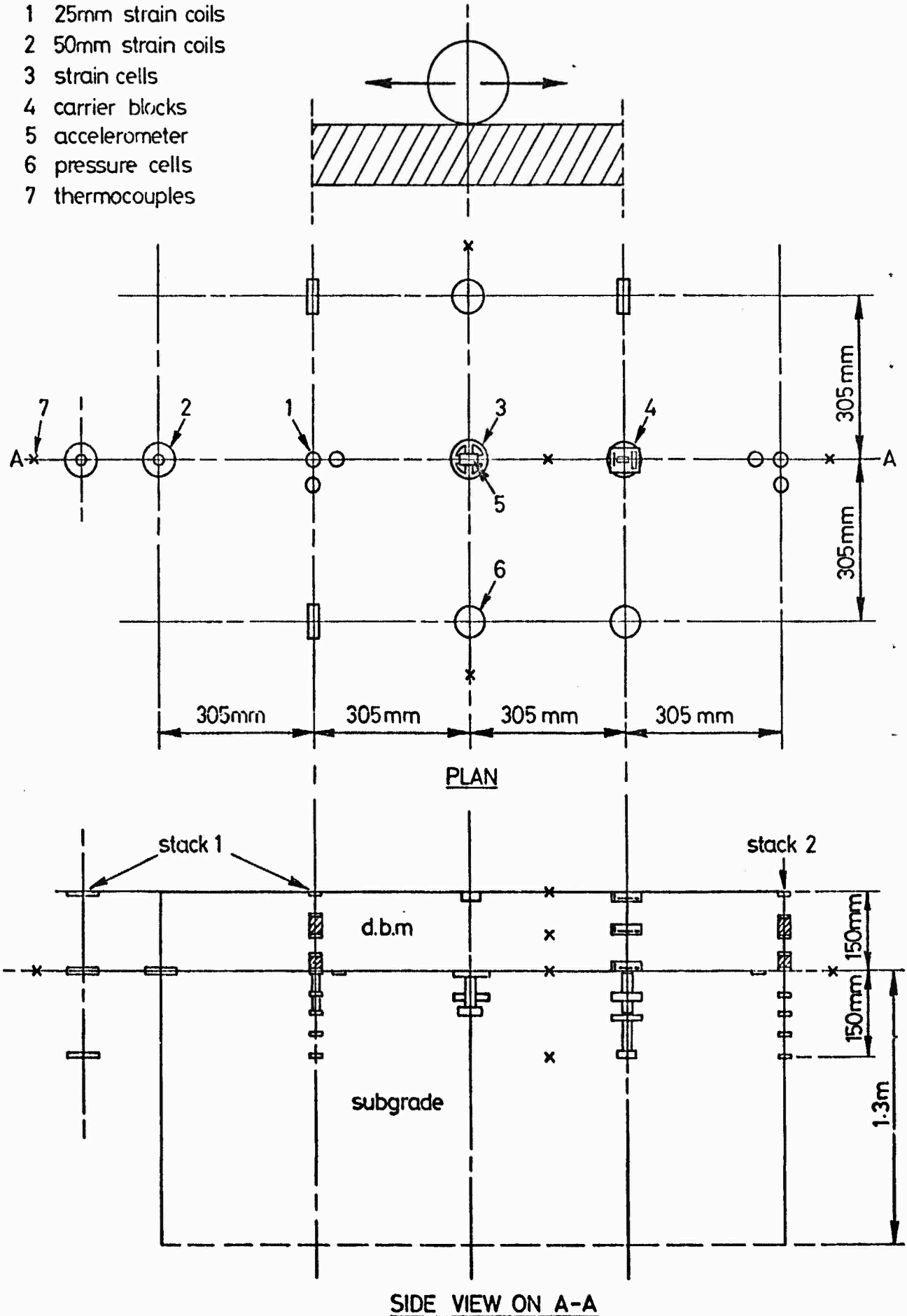

FIG. 4.4 INSTRUMENT LAYOUT, PAVEMENT NO. 2

LEGEND

1 25mm strain coils
2 50mm strain coils
3 strain cells
4 carrier blocks
5 accelerometer
6 pressure cells
7 thermocouples

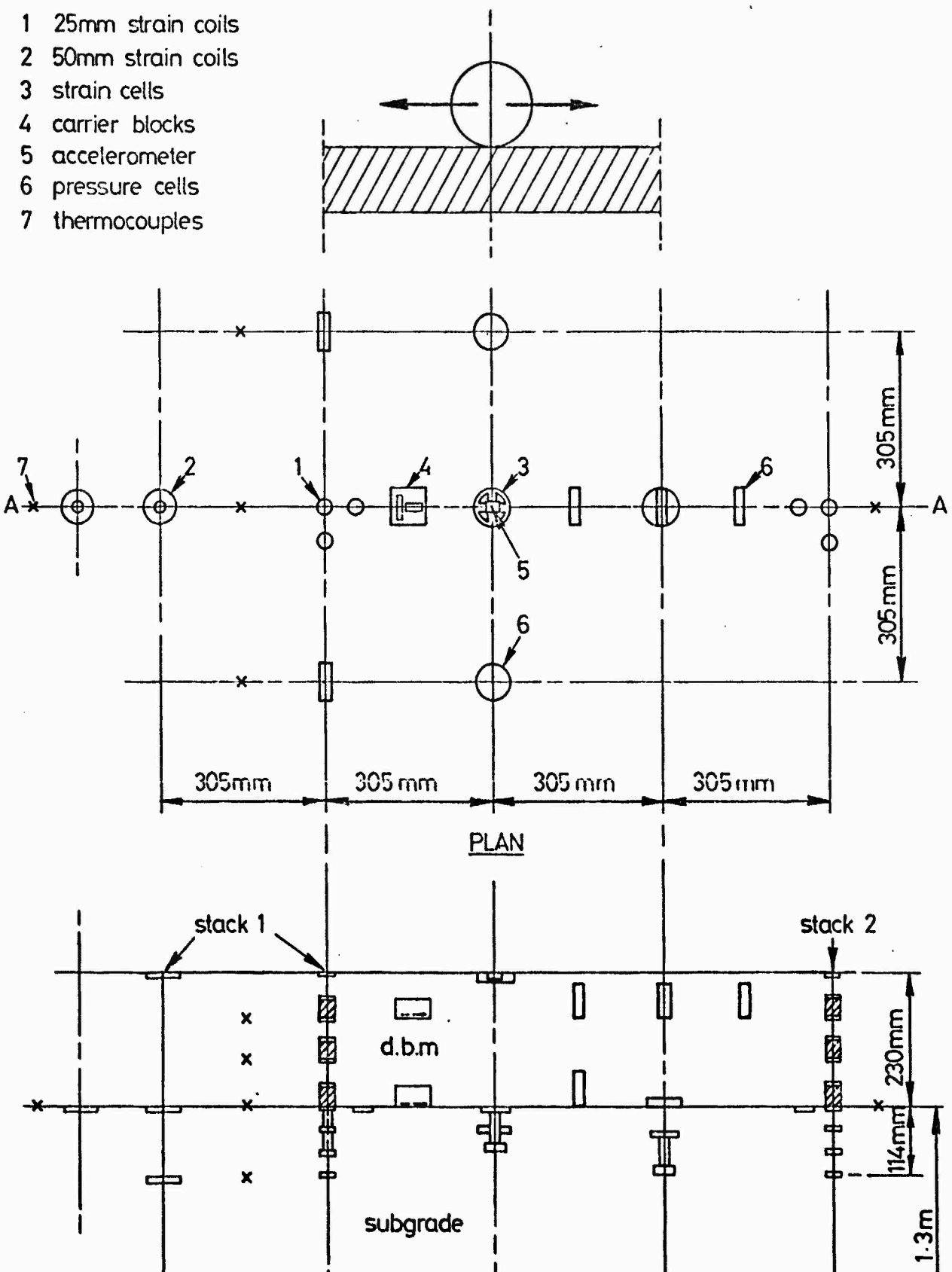

PLAN

SIDE VIEW ON A-A

FIG. 4.5 INSTRUMENT LAYOUT, PAVEMENT NO. 3

Horizontal permanent and elastic strains were measured at the interface with the 25 mm and 50 mm coils for pavements 2 and 3. The overall deformation behaviour of the bituminous layer and subgrade (to a depth considered significant) was measured with the 50 mm coils and the accumulated readings from the 25 mm stacks. Thus it was possible to measure total permanent and elastic strains with depth at three separate positions with the coils for pavements 2 and 3.

Vertical and horizontal elastic strains were measured with strain gauges on carrier blocks at the interface and within the bituminous layer for all three pavements. The arrangement of these carriers varied slightly for each pavement, and the continuous monitoring of more than six outputs was the practical limit on the U.V. recorder. As a result, only two carriers were installed in the first and third lifts of pavement 3.

Minor changes were made to the position of the soil strain cells in order to maintain their separation from the other instruments and to effectively cover the same depths as the subgrade coils. The gauge length of the strain cells was 76 mm and this covered the total depth of the subgrade installation for pavements 1 and 2, while for pavement 3 they overlapped to correspond with the smaller 114 mm depth of coils.

Two pairs of pressure cells were installed in pavement 1 to determine vertical stress at the interface and horizontal stress in the subgrade. This arrangement was improved for pavement 2 by the addition of two extra pressure cells. The cells were repositioned to measure stresses in the vertical and horizontal directions at the same level. In the case of pavement 3, four cells were installed in the subgrade, and six in the bituminous layer, with particular emphasis on

measurements near the top of the layer. The theoretical calculations for permanent deformation in pavements 1 and 2 indicated the need for stress measurements in the DBM as a check on the calculated values. Although the earth pressure cells were not designed for use in this material, it was considered that some should be installed and appropriate calibration tests were performed.

The servo and piezo-electric accelerometers were installed in pavements 2 and 3 respectively. They were positioned as near to the surface as practicable at the pavement centre in order to determine elastic deflection of the pavement surface.

Temperature distribution through the bituminous layer was measured with thermocouples in pavement 1. An additional thermocouple was installed in pavement 2 in order to extend the depth of measurement to the lowest instrument in the subgrade. There was a tendency for the surface thermocouple to be worked out of the pavement by the action of the wheel and consequently it was not installed in pavement 3. Air temperature was monitored for all three pavements by a thermometer.

4.4 INSTALLATION OF INSTRUMENTS

4.4.1 General

The consistent features of all three pavements were strain coils arranged in columns with strain gauges and strain cells at complementary levels. A basic initial pressure cell layout was adopted and additional pressure cells installed to improve the effectiveness of stress measurement as the tests progressed. It was necessary to restrict the instruments to a 1.4 m x 0.6 m x 0.3 m deep central section, to prevent interaction of the wheel loading effects with the restraining influence

of the pavement boundaries. Furthermore, a compromise had to be considered in terms of adequate instrumentation without creating excessive interference with the true pavement performance.

Installation of each instrument is described in the following sections but certain common principles and techniques are of general application. These include a basic minimum centre to centre separation of 300 mm for the pressure cells and strain cells and a recommendation of at least three replicate measurements of each parameter. An exception to the former was the pressure cell arrangement in the bituminous layer of pavement 3 as shown in Fig. 4.5. In this case, an absolute minimum separation of 150 mm was adopted to allow positioning of the cells along the centre line, at an instrument free location, in order to measure a specific parameter. In addition, these instruments were isolated from the 25 mm strain coils by at least three times the coil gauge length in order to eliminate disturbance to the electro magnetic coupling of the coils. Further similar interference due to the proximity of the strain gauges was considered to be minimal as their mass was negligible and the effect of adjacent "out of circuit" coils was cancelled out during calibration. Measurements from the pavement 1 tests indicated an insignificant response from the coils set at approximately 150 mm into the subgrade. As a result the maximum installation depth in the subgrade was 150 mm for pavement 2, and 114 mm for pavement 3 due to the increased thickness of the bituminous layer.

Cable trenches had to be excavated for all the instruments and special tools were evolved for this purpose and for installation as shown in Fig. 4.6. Usually, a slot was cut into the subgrade to accommodate the instrument cable and this led to one of four channels

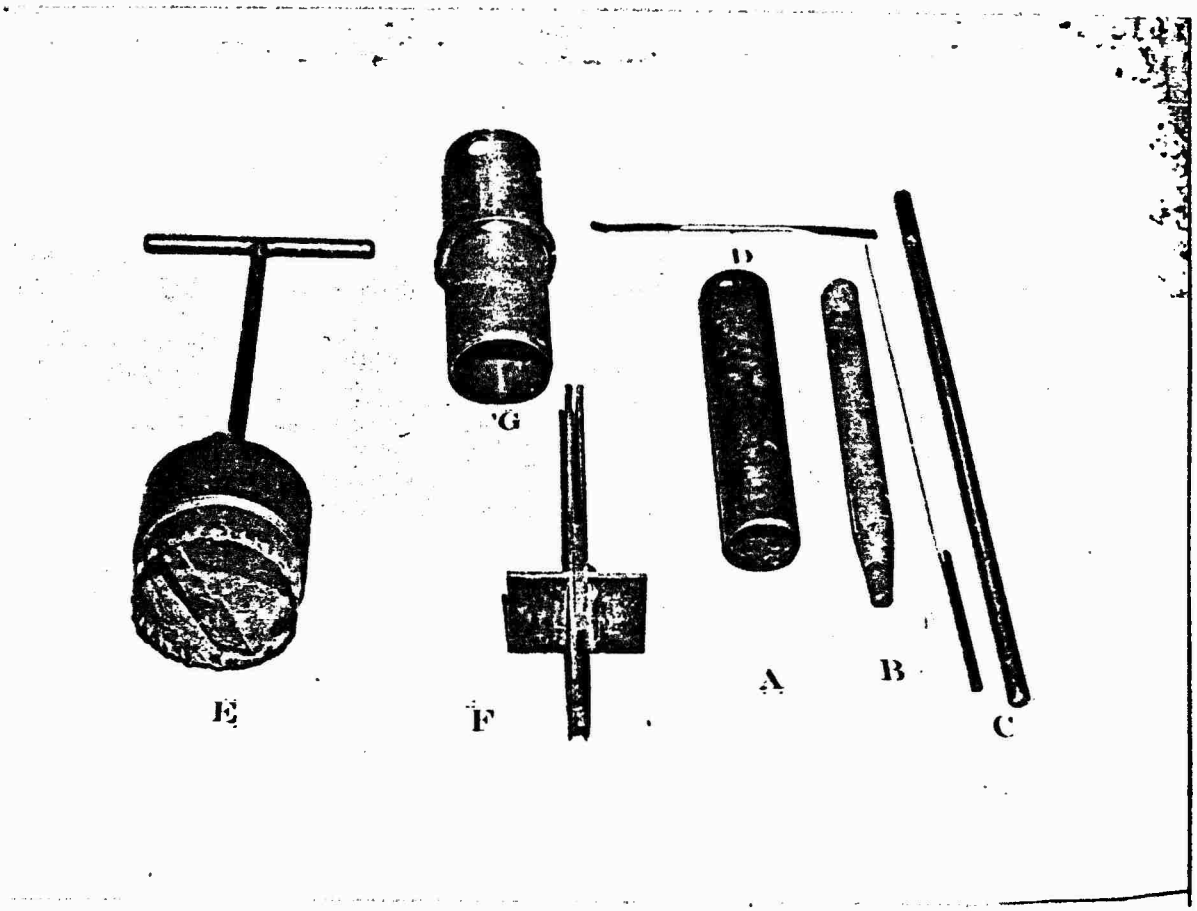

FIG. 4.6 INSTALLATION EQUIPMENT

at the surface. These channels converge into a main trench extending from the pavement edge where a single outlet was linked to the readout facilities. The trenches were filled with fine subgrade material after installation was completed, and careful hand compaction was carried out to reduce the risk of sharp particles damaging the cables. When the instruments were installed at each lift of the bituminous layer during construction, their associated cables were covered with fine, hand compacted, hot DBM. Several instruments were also installed at the surface and square section bars were rolled into the hot pavement mix to form cable trenches. These were removed after the pavement had cooled and the cables of the subsequently located surface instruments were covered with a hot sandsheet mix. A general practice of initially rolling without vibration was adopted to partially compact the bituminous layer at each lift in order to settle the material around the cable and instrument. The vibrator was then switched on and paving operations completed. All the subgrade instruments were checked after installation and the instruments in the bituminous layer were monitored for any indications of failure before rolling operations commenced.

4.4.2 Strain Coil Installation

Nottingham strain coils and Bison strain coils were installed in pavement 1. The former were used in the subgrade and cable failures were observed at the coil cable entry junction and at the connections with the extension wiring. It was noted that the high temperature, twisted p.t.f.e. extension cable intended for exclusive use in the bituminous layer withstood the rigours of direct contact with the coated aggregate during rolling. This cable was subsequently used for

all the coils in pavements 2 and 3 and the Nottingham coils were replaced with Bison coils. Furthermore, the extension connections and cable entries were coated with an adhesive and an additional p.v.c. sheath covered the installed length of cable. The abrasive qualities of the DBM mix also tended to remove the peripheral coil insulation and this had to be repaired between tests. These measures were intended to ensure survival of the coils, despite certain adverse reactions of the p.v.c. and adhesive at elevated temperatures, and provided a protective interface which remained effective after cooling.

All the subgrade instruments were installed on the completion and levelling of this layer. Longitudinal and lateral centre lines were marked as datums for relating the positions of the instruments and three plumb lines were suspended from the false ceiling above the coil locations. The suspension points for these lines were maintained throughout the tests and permitted subsequent measurements of any horizontal movement of the coils.

A 38 mm core cutter was used to extract material to the depth of the lowest 25 mm coil and provide a working clearance around the instruments. Then a 6 mm triangular slot was cut to the base of the hole and connected into the nearest cable trench. The base of the hole was carefully levelled with a light rubber tipped wooden tamper and checked with a circular spirit level. Advantage was taken of a pointer on the plumb weight to locate the central hole of the coil. The coil was positioned by slight pressure and movement to bed it down satisfactorily. This was checked by removing the coil and examining its imprint. Soil retained from the core and slot at this level was "broken up", placed around the coil and used to anchor the cable.

The plastic nature of the moist soil aided the initial firm positioning of the instrument and thus prevented any possible lift of the coil at the first stages of tamping. A small diameter steel rod was used to tamp the fine material around the coil periphery and in the slot, and three layers were added using the light tamper before the next coil was installed. Each coil was checked for parallel alignment with the circular spirit level. The sides of the slot, hole and the surface of each layer were scarified with a spatula in order to encourage "interlock" with the backfill. In general, only the material from the core and slot which had occupied the relevant space was used for backfilling. A guide to the required compactive effort could be detected from the rebound "feel" of the light tamper during installation by comparing it to the same action applied to the subgrade surface.

An accurate gauge length for each pair of coils was attained by adjusting their separation during installation and achieving balance on the Bison instrument at the required preset spacing reading. This procedure was repeated for all the subgrade coils and the final sensor was paired with the lower coil attached to a bituminous carrier block on the subgrade surface. The positions of the interface horizontal coils were accurately marked out with reference to the plumb line and they were firmly installed in shallow matching recesses.

There was always a tendency to need slightly more than the cored material for backfilling due to the concentrated effect of tamping over a small area. The confined working space resulted in installation difficulties with the first coil but it was felt that a larger excavation would disturb the soil to an unnecessary extent. All the vertical coils were aligned to make contact with the edge of the hole,

opposite the cable slot, and they were partially worked into the parent material. This was intended to improve the bond with the undisturbed material and could have been further developed by extending undersized slots into this material to accommodate the strain coils. Similar techniques were used to install the 50 mm coil at the base of a cored clearance hole and the associated interface coils for vertical and horizontal measurements.

The 25 mm coils in the bituminous layer were attached by means of a flexible adhesive to sandsheet or DBM carrier blocks (Fig. 4.7). Sandsheet blocks were used in pavement 1 and DBM blocks extracted from previous pavements were used in pavements 2 and 3. This change was made in order to match the deformation characteristics of the carriers with the bituminous layer. A gauge length was chosen which was equal to half the thickness of each lift and this dictated the number of installed coils. As an example, pavement 2 was laid in two 76 mm lifts and contained coils at nominally 38 mm centres (Fig. 4.4). The strain coil carrier blocks were positioned under the plumb lines and checked for parallel alignment with the circular spirit level. They were held in place with a small amount of sandsheet and a related quantity of the hot pavement mix from which large aggregate was removed. The surface coils, including the 50 mm coils, were installed after paving in recesses formed by metal discs rolled into the top of the final lift. These discs were placed between the dead weight rolling and vibrating rolling stages in order to avoid significant reorientation. They were also oversize to allow sufficient freedom for accurate installation of the coils which were attached to the base of the recess with adhesive. The specially prepared hot sandsheet mix was compacted over and around the coils in order to complete their installation.

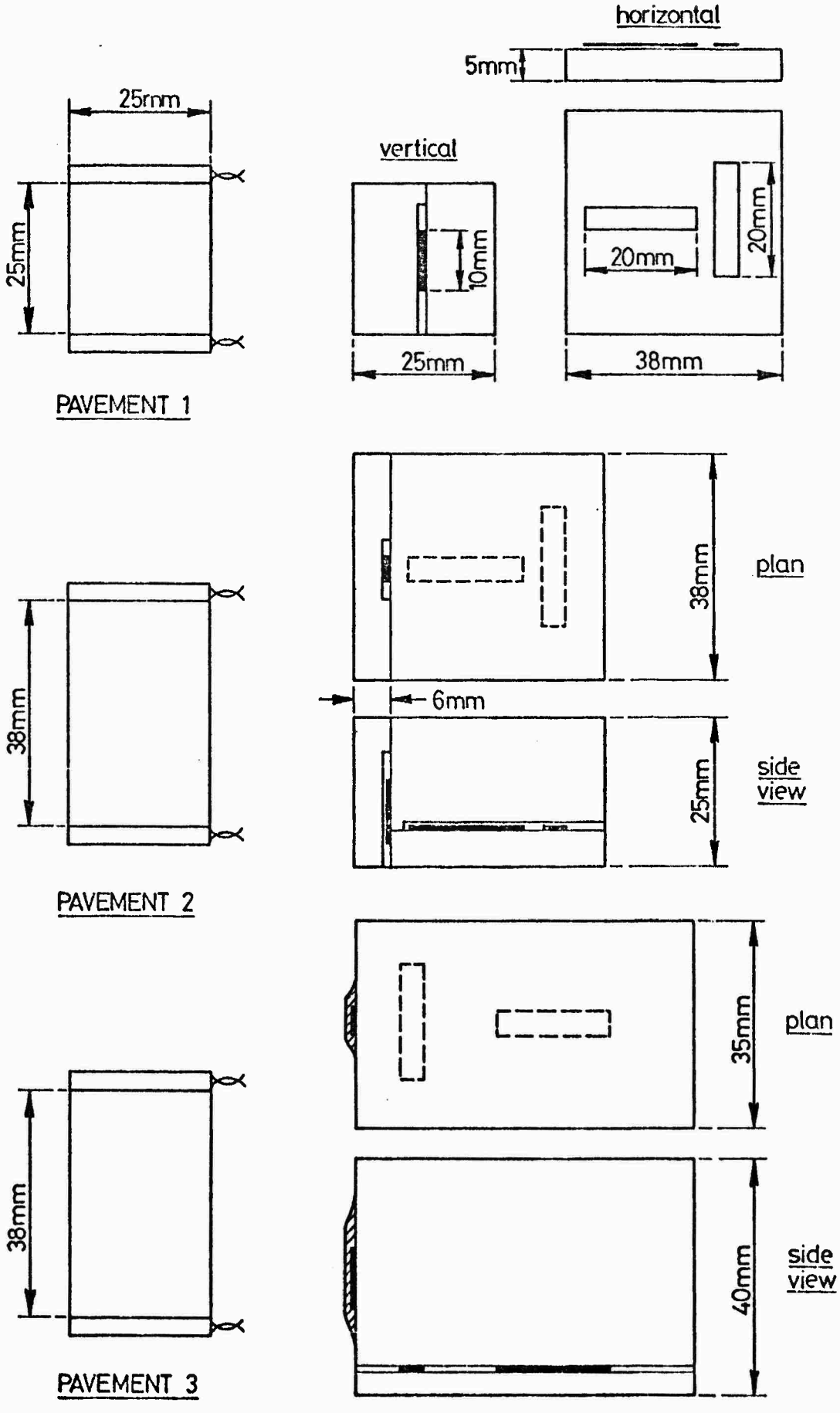

FIG. 4.7 DETAILS OF BITUMINOUS CARRIER BLOCKS

The gauge length of the coils on the DBM carrier blocks was quite accurately maintained during rolling operations, but variations in layer thickness and the apparent weakness of the sandsheet carriers in pavement 1 caused an excessive reduction of the spacing of some of the coils. This indicated the need for a gauge length in the middle range (range 2) of the Bison instrument in order to prevent a loss of balancing capability in the later stages of the test.

4.4.3 Strain Gauge Installation

The interface strain gauges in pavement 1 were attached to thin rectangular blocks of sandsheet. The vertical gauges for this pavement and the gauges for the other two pavements were attached to DBM carrier blocks. Bostik No. 6 waterproofing sealant and Bostik No. 2 adhesive were used to coat the gauges and join the blocks for the sandwiched gauges. These grades of Bostik are flexible and capable of filling in any voids resulting from sawing the blocks to the correct dimensions. Details of these dimensions are given in Fig. 4.7. As an alternative, a rectangular metal block was rolled into the surface of pavement 2 and removed after cooling. Strain gauges were attached to one side and the base of the recess and waterproofed as previously described. The recess was then hand-filled with a reheated selection of the original mix which was very carefully compacted over the gauges. A similar technique to that used for the installation of the strain coil carriers was adopted for the strain gauge carrier blocks. An immediate layer of hot sandsheet around the base of the carrier located its position and a mound of the pavement mix (DBM), again free from larger aggregate, acted as a protective interface. This also ensured that the block was keyed into the

surrounding material as paving operations continued. The bonding process was effected by the heat of the mass of pavement mix and the rolling operations. It was important to firmly compact the interface material and to install the blocks rapidly in order to allow paving to be completed at reasonable temperature levels (> 140°C). Horizontal and vertical alignment of the gauges was successfully maintained with the DBM carriers. This was not the case with the sandsheet carriers which were more susceptible to deformation when hot and this resulted in significant distortion of the gauges.

A 100 mm sample was cored from the bituminous layer and sawn in half to present a flat surface for the attachment of dummy gauges. The ungauged half was recessed in order to clear the gauges and connections and the two sections were joined with an outer binding of adhesive tape. This was to avoid the collapse of the sample, which was now a clearance fit in the cored hole, and would otherwise be unsupported at the test temperature of 30°C.

4.4.4 Strain Cell Installation

The core cutter for this operation shown in Fig. 4.6g consisted of a sharpened tube with an upper shoulder at an increased diameter. It was driven into the soil to form a stepped hole which located the cell base and upper wheel. The cutter ensured a clearance around the cell and the step set the instrument at the upper end of its working range. An angled slot was cut to accommodate the cable and the base of the hole was levelled using the light tamper. The cell was positioned with its upper wheel removed, and a greased rubber sleeve was slipped over the tubular guide stem in order to act as a shear break and seal the upper moving components. Then the sides of

the hole were scarified and extracted material was broken and tamped around the cell and cable in layers with the small diameter rod. The wheel was screwed into position and fine subgrade material was compacted between the spokes. Any voids beneath these spokes were exposed by turning the wheel and were subsequently filled. The installation of the cell at the lower level in the subgrade was more difficult and a large diameter upper recess was formed to allow insertion of the core cutter.

4.4.5 Pressure Cell Installation

The horizontal subgrade cells (for measurement of vertical stress) were positioned with their diaphragms facing upwards at the required depth in a clearance hole. A cylinder with crossed blades (Fig. 4.6e) and a serrated rim was used to extract the material and was designed to form a cavity of the correct dimensions. A cable slot was cut and the base of the cavity was recessed, partly by tamping and then using the cell as a cutting instrument. The latter was accomplished by pressing on the cell and moving it in a circular manner to bed it well in. Removal of the cell and filling in voids was necessary if any stones had been dragged through the material as a result of this activity. Positioning was checked by measurement and a spirit level before backfilling around the cell and compacting fine extracted material in layers above it. Any stones in the thin layer (> 1 mm) in contact with the diaphragm were removed.

Two methods were employed to install the vertical cells (for horizontal measurement). The first involved the use of the cutting tool, shown in Fig. 4.6f, which consisted of two semi-circular steel blades, spaced by pins, and it was designed to produce a vertical slot

in the subgrade. The gap between the blades permitted extraction of the soil during cutting and an integral upper plate determined the depth and vertical alignment of the slot. This slot was slightly undersized with respect to the dimensions of the pressure cell and it was necessary to tap the instrument into position as a result of this. The diaphragm side of the slot was cleared of any visible stones, a 45^{o} cable entry was cut and the cell was installed. Extracted material was compacted over the exposed upper edges of the instrument and the local surface area around the cell was tamped with a 125 mm diameter ram weighing approximately 10 kg. This was carried out with the pressure cell operative and resulted in an electrical output which indicated satisfactory material contact with the diaphragm.

This method was adopted for only one cell in pavement 3 as an attempt to establish a reproduceable technique requiring the minimum of soil disturbance. The second method was common to all three pavements. This involved the cutting of a similar vertical slot and then removing a wedge of material on the proposed diaphragm side. The cell was positioned and located by the semi-circular base of the slot and layers of fine extracted material compacted over the exposed surfaces of the cell. It was felt that this method ensured a more positive soil contact with the cell diaphragm and it was easier to fill any voids in the lid side of the slot.

The pavement 3 horizontal and vertical pressure cells in the bituminous layer were positioned with a hot, hand-compacted, sandsheet mix. It was possible to cover the diaphragms evenly with this material, even in the case of the vertical cells by forming a mound over the instrument. However, this was kept to a minimum and a quantity of the actual pavement mix was immediately compacted with a ram over the

sandsheet in order to integrate the two materials. This operation required a more sensitive approach for the vertical cells to reduce the possibility of misalignment. Again, paving operations were commenced as soon as the installations were complete in order to establish a satisfactory bond with the interface materials.

4.4.6 Accelerometer Installation

A cylindrical steel block machined to provide a substantial clearance fit for the accelerometer (Fig. 3.2a) was rolled into the surface as the pavement neared completion. This tended to be displaced in the direction of rolling for the first pass, but recovered sufficiently on the return pass to allow the accurate positioning of the accelerometer. The main difficulty was establishing the precise orientation of the direction of sensitivity of the instrument. This was indicated by an arrow on the servo accelerometer and its alignment was adjusted by carefully settling the instrument in a hot sandsheet mix. The piezo-electric accelerometer (Fig. 3.2b) was placed in a vertical clearance hole formed by a suitable blank and its position checked with a spirit level.

4.5 PAVEMENT LOADING PROCEDURE

Certain basic dimensional references were established for the three pavements and these are shown in Fig. 4.8. These included a longitudinal centre line about which the loaded wheel traversed, and two remote base lines either side of the pavement and parallel to the centre line. The latter were necessary for zeroing a surveyor's level and checking the output from the profilometer. The profilometer and supports were also mounted on these base lines and the surveyor's level

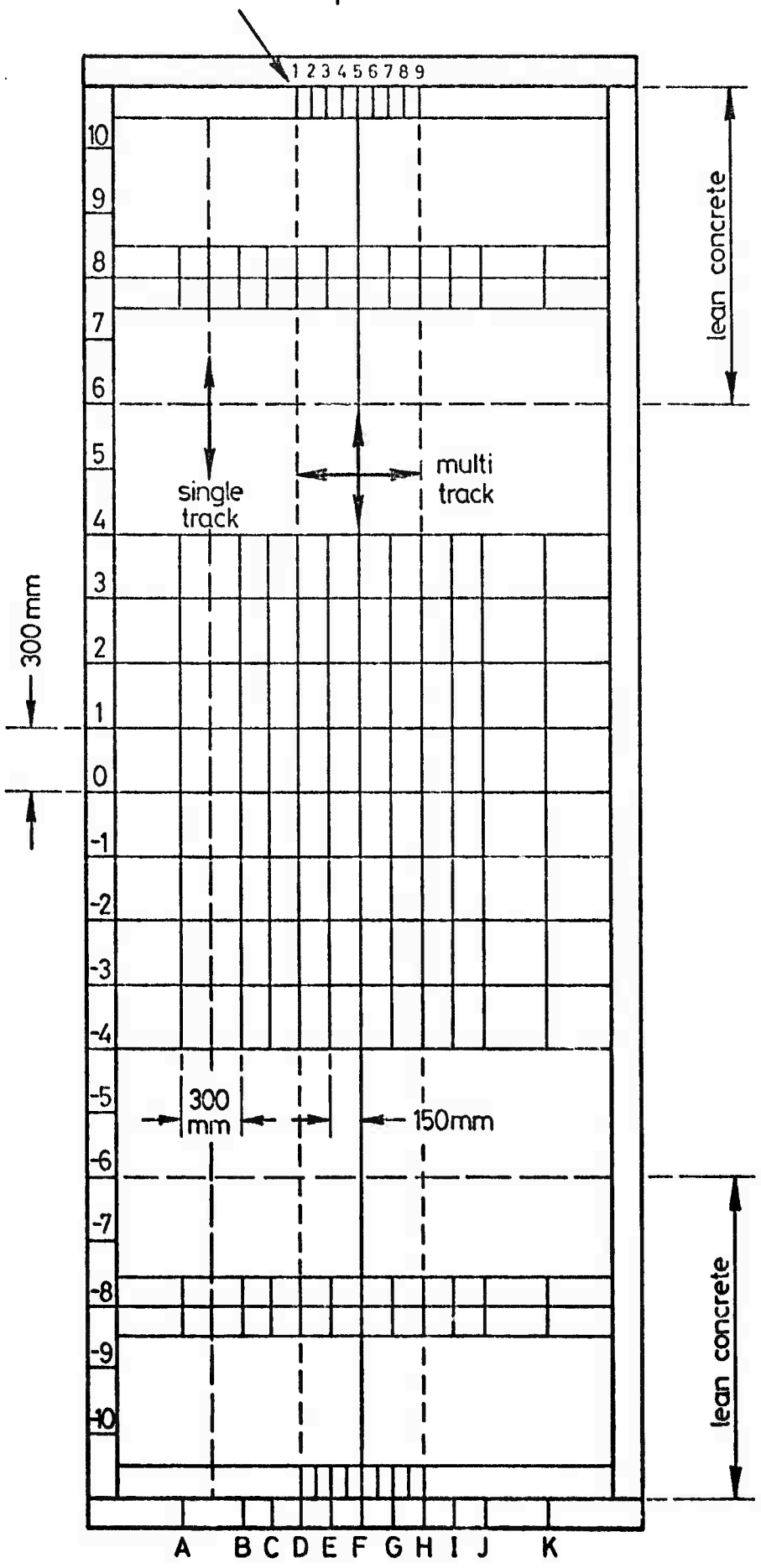

FIG. 4.8 PAVEMENT GRID

readings were omitted when the accuracy of the profilometer had been confirmed. A lateral centre line was also marked and the positions of the pavement instruments were known in relation to its intersection with the longitudinal centre line, i.e. the pavement centre. A comprehensive grid was then marked out with white road paint, and was composed of 150 mm lateral divisions and 300 mm longitudinal divisions.

The unloaded wheel was then set to run along the major centre line in order to eliminate any longitudinal misalignment resulting from unequal settings of the traversing rams. Traversing was arranged to cover 300 mm either side of this centre in 75 mm steps. This resulted in nine lateral wheel positions and provided overlap of the tyre, between adjacent positions, since it had an approximately elliptical contact area of 180 mm length in the direction of travel and 130 mm width. The extreme outer positions (1 and 9) were each 850 mm from the pavement edge and profilometer readings were taken beyond these lateral limits to determine the extent (at the surface) of the subsequent influence of the loaded wheel.

The lateral distribution of passes was in the form of a histogram which approximated to a normal distribution. The lowest practical total number of passes across the pavement was 100 and this was sub-divided into nine discrete numbers which formed the basis of all subsequent totals as shown in Table 4.1. These totals were increased on a logarithmic scale until a final figure of 100,000 passes was accumulated. This enabled surface profile measurements to be made at intervals compatible with the deformation response of the pavement. In the case of pavement 1, the traversing system was not complete and the loading facility was moved manually from position 9 to position 1 via each position in order. The number of passes applied was as

Table 4.1 Distribution of Wheel Passes

Lateral total	Position								
	1	2	3	4	5	6	7	8	9
100	3	6	12	18	22	18	12	6	3
200	3	6	12	18	22	18	12	6	3
500	9	18	36	54	66	54	36	18	9
1000	15	30	60	90	110	90	60	30	15
2000	30	60	120	180	220	180	120	60	30
5000	90	180	360	540	660	540	360	180	90
10000	150	300	600	900	1100	900	600	300	150
20000	300	600	1200	1800	2200	1800	1200	600	300
50000	900	1800	3600	5400	6600	5400	3600	1800	900
70000	600	1200	2400	3600	4400	3400	2400	1200	600
100000	900	1800	3600	5400	6600	5400	3600	1800	900
Accumulated total =	3000	6000	12000	18000	22000	18000	12000	8000	3000

These passes were applied in the following order for pavements 2 and 3:

Sequence	9	6	7	3	1	4	2	5	8

All lateral totals were accumulated as multiples of the distribution required for 1000 passes during automatic traversing, i.e.

1000 - 2000	30	60	120	180	220	180	120	60	30

tabulated until 10,000 were completed and then the remaining passes were accumulated in totals of 5,000 across the pavement.

Pavements 2 and 3 were loaded in a more random manner with the aid of the traversing facility in order to be more compatible with the real road situation. The sequence of lateral positions taken up by the wheel is shown in Table 4.1. The lower number of passes was accomplished using the manual switch as described in Chapter 2, and automatic operation commenced upon completion of 1000 passes. A total of 1000 passes across the pavement was chosen as the basis for the accumulation of the remaining passes. Thus the loading facility had to traverse 30 times, on completion of 20,000 passes, in order to reach 50,000. This ensured a maximum of 220 passes on the centre line of the pavement, and appeared to avoid a ridging effect noted for pavement 1, due to the length of time the loaded wheel remained in the central position at the later stages of the test.

The wheel was unloaded and positioned away from the test area on completion of each stage of the programme. This was necessary to allow freedom of movement for the profilometer during measurements at the positions indicated in Fig. 4.8. On completion of the multi-track test a single track test was performed on an untrafficked area of the pavement. The numbers of passes were equal to the total designated for the central position, 5, in the multi-track test, and resulted in a final figure of 22,000.

4.6 READOUT PROCEDURE

The outputs from the pavement instruments were zeroed and readings of lateral and longitudinal profile were made before the pavement was loaded and when temperature equilibrium at 30°C was reached. Measurements

of permanent strain and pavement profile were then taken at the intervals defined by each stage of the accumulation of passes. The pavement was also examined for possible cracks in the surface. Stress and elastic strain readings were taken on the U.V. recorders for the on and off axis lateral positions of the wheel. This information was more readily obtained for pavement 3 due to the introduction of an improved switching arrangement for the strain coils and pressure cells. However, the necessity to balance each selected pair of strain coils, arising from their differences in separation during installation, meant that several decades of wheel passes occurred as each stack of coils was monitored. Thus in the initial stages, when data acquisition time was minimal, the more responsive coils in the subgrade and the horizontal coils at the interface were chosen, with an additional selection of coils in the bituminous layer when time allowed. On completion of 5,000 passes sufficient time was available to monitor all the instruments in order to establish the pattern of stresses and elastic strains throughout the pavement. By this stage the 20 or 30 passes needed to complete readings had become a relatively small proportion of the total.

CHAPTER FIVE

PAVEMENT PERFORMANCE

5.1 INTRODUCTION

This chapter is concerned with pavement performance during the multitrack tests based on the measurements made with the instrumentation installed in both the bituminous layer and the subgrade. The readings are presented in graphical form for each pavement and wherever possible a uniform system of scales is adopted to facilitate comparisons.

An assessment of the theoretical predictions related to these measured values is presented in Chapter 8. This assessment depends upon the ability of the instruments to accurately record the pavement behaviour and the precision of the loading details. It is, therefore, necessary to critically examine the performance of the instruments and the reliability of their measurements.

The magnitude of loading, tyre pressure and wheel speed were generally satisfactorily controlled during the tests. The measurements which were made on each pavement included surface profiles, permanent strain, elastic strain and transient stress. Each of these is discussed and specific comments are made on the various instruments.

The results common to all three pavements are those representing permanent deformation and strain. The permanent deformation measurements with the strain coils were reasonably easy to correlate with the measured surface rut as the instruments were arranged in vertical stacks. However, the variation of permanent strains within the structure and the accuracy of the elastic strains must be assessed from the variations between instruments and the effects of the installation on the response of the local material. Furthermore, the elastic

strains can be related to the measured stresses in order to compare the resulting elastic moduli with the values determined from sample testing (Section 8.5).

5.2 PERMANENT DEFORMATION

The increase in maximum permanent deformation at the surface (rut depth) of each pavement during the course of testing is shown in Figs 5.1 to 5.3. The deformation of pavement 2 was much larger than for either of the others in view of the poor compaction achieved in the DBM (Section 4.2). In all cases the average accumulated readings of the strain coils were lower than the surface measurements indicating a possible further contribution of the deformation at a greater depth in the subgrade. Alternatively, some coil misalignment and reorientation may have reduced the sensitivity of these instruments. High values were obtained for stack 1 of pavement 3 (Fig. 5.3), but the average result compares more favourably with the development of the rut than in the other structures. This may be a result of the thicker bituminous layer for pavement 3 which would tend to limit the depth of significant deformation in the subgrade.

The contributions to the rut from the subgrade and bituminous layer for each pavement are summarised in Table 5.1 . Missing data is attributed to the loss of certain critical strain coils, and although re-pairing of coils above and below the affected ones was carried out, there was some uncertainty concerning the original gauge lengths. However, the information is complete for pavement 3 and in general these results are a reasonable guide to the response of the layers at 20,000 and 100,000 passes. It appears that the contribution to the total deformation by the subgrade in pavement 2 approaches 80 per cent

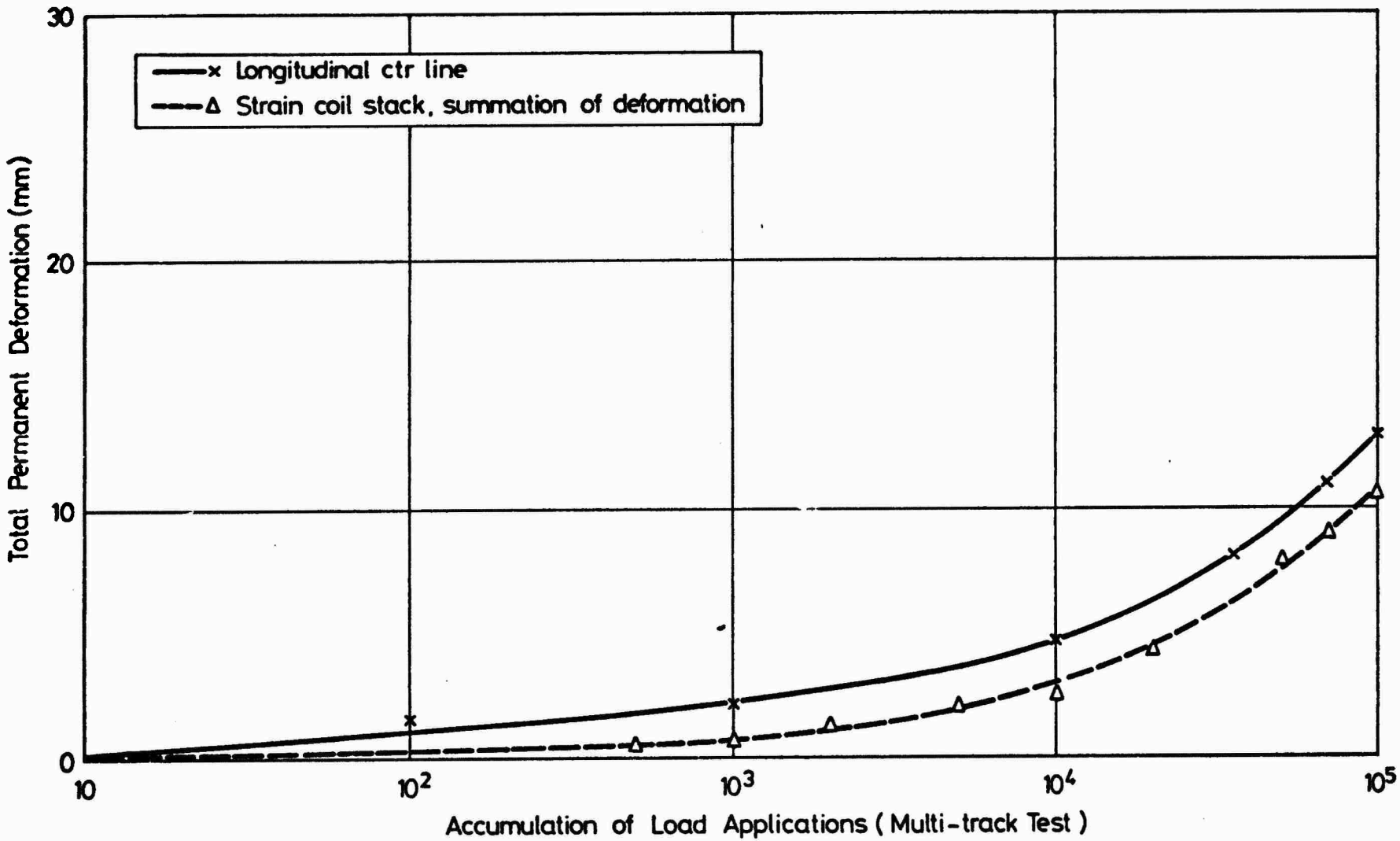

FIG. 5.1 ACCUMULATION OF PERMANENT DEFORMATION, PAVEMENT NO. 1

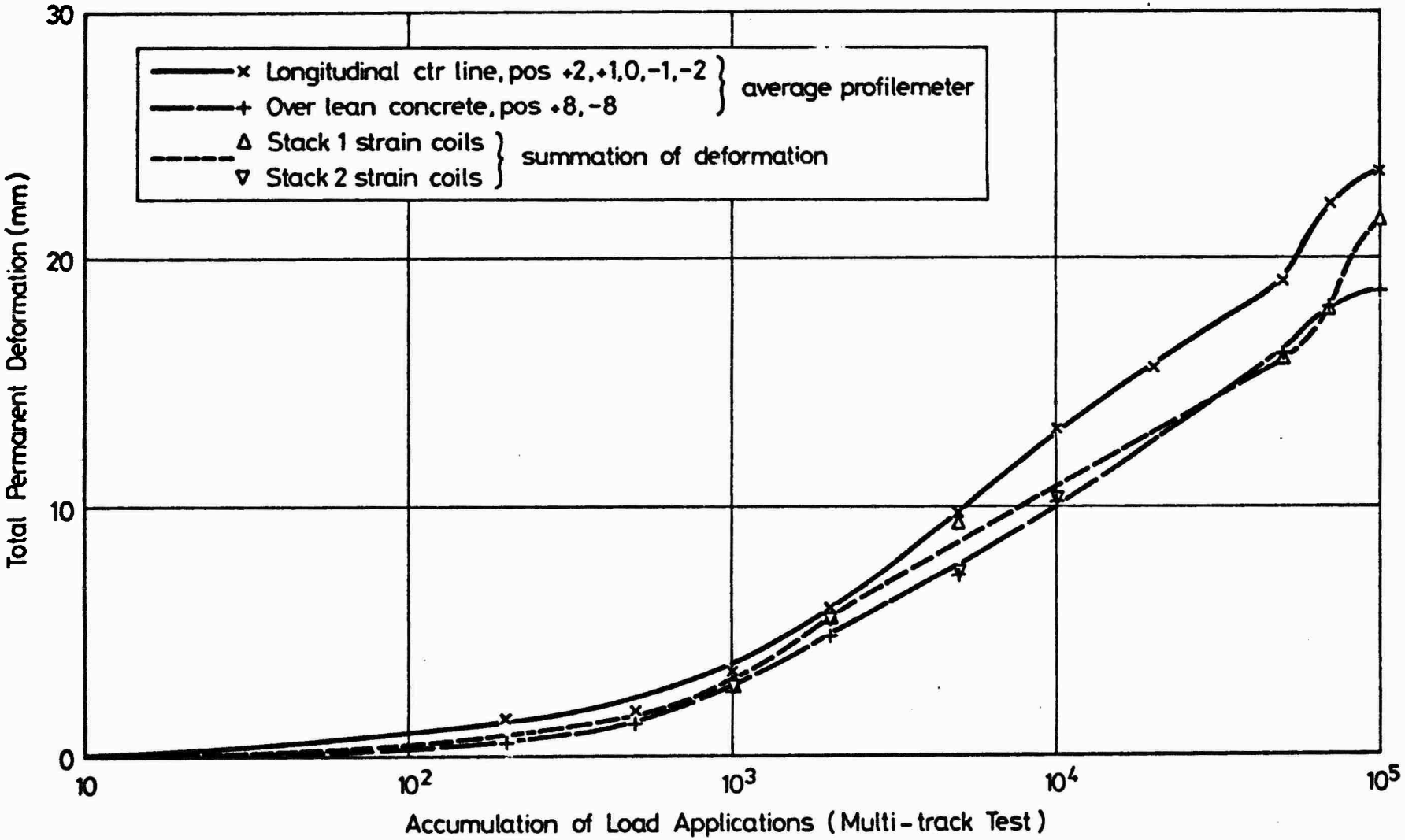

FIG. 5.2 ACCUMULATION OF PERMANENT DEFORMATION, PAVEMENT NO. 2

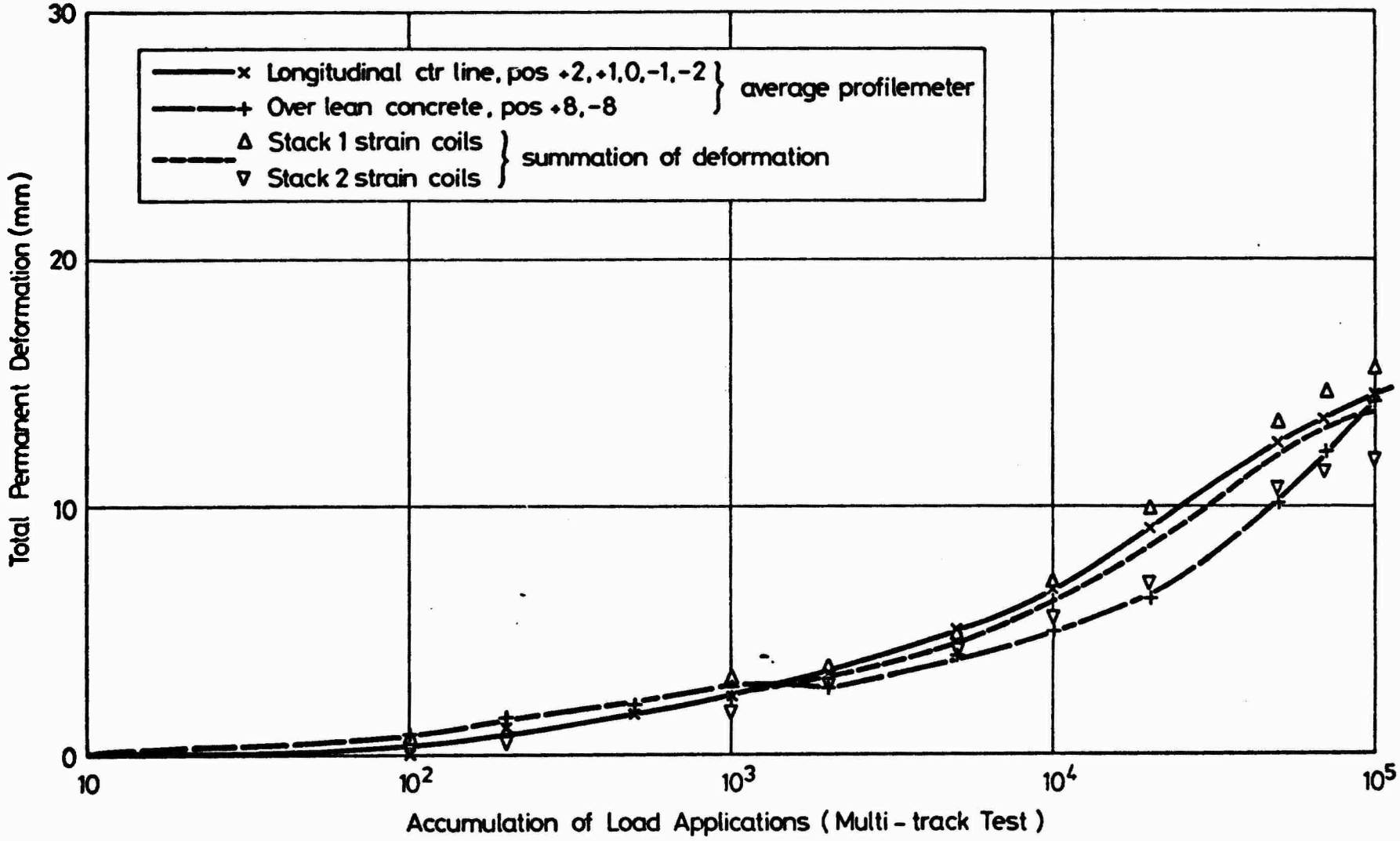

FIG. 5.3 ACCUMULATION OF PERMANENT DEFORMATION, PAVEMENT NO. 3

Table 5.1 Comparison of in situ deformations from strain coils and rut depths

Pavement No.	Stack No.	No. of wheel passes	Permanent deformation (mm)			
			Subgrade	DBM	Subgrade + DBM	Rut Depth
1	1	20,000	1.3	2.7	4.0	6.2
	50 mm coils		-	3.6	-	
	1	100,000	-	6.3	-	12.4
	50 mm coils		-	7.4	-	
2	1	20,000	5.0	6.7	11.7	15.6
	2		6.2	-	-	
	1	100,000	9.9	11.4	21.3	23.4
	2		-	-	-	
3	1	20,000	1.7	8.2	9.9	9.2
	2		0.7	6.5	7.2	
	1	100,000	2.2	13.3	15.5	14.6
	2		0.9	11.0	11.9	

of that contributed by the bituminous layer. Furthermore, the greater rut depth indicates a relatively weak structure with high stresses transmitted to the subgrade. Although the total rut depths for pavements 1 and 3 are similar, the proportional contribution from each layer is different; the deformation in the bituminous layer for pavement 3 is more significant because of its greater thickness, since the average strains for the two cases were similar.

It is possible to consider the accuracy of the strain coils from the thickness measurements made on the DBM after sawing and removal of slabs. This data is summarised in Table 5.2. The error for stack 1 in pavement 1 is difficult to explain, but as the rut depths calculated from these coils (Fig. 5.1) are of the right order, it is possible that a d.c. offset occurred as a result of an electrical earth loop in the circuitry. It can be seen that the 50 mm coils recorded the exact final thickness and the deformation measured by these coils should, therefore, be precise. The difference between the coils and the measurement for stack 1, pavement 2, was due to a 6 mm penetration of the bottom coil into the subgrade, probably during compaction, but the measurements from all but this pair of coils are considered reliable. Thickness measurements were more difficult to obtain for pavement 3 as the saw cut in the DBM was limited to 150 mm and the remainder had to be broken with a demolition hammer. However, measurements were made with large calipers beyond the damaged edges. The discrepancies in this case may be due to the remoteness of these measurements from the exact location of the coils, and the positioning of the top coils for each stack in a recess below the pavement surface. Fortunately, in pavement 3 it was possible to remove four of the carrier blocks virtually intact as shown in Fig. 5.4 and further checks on the coil

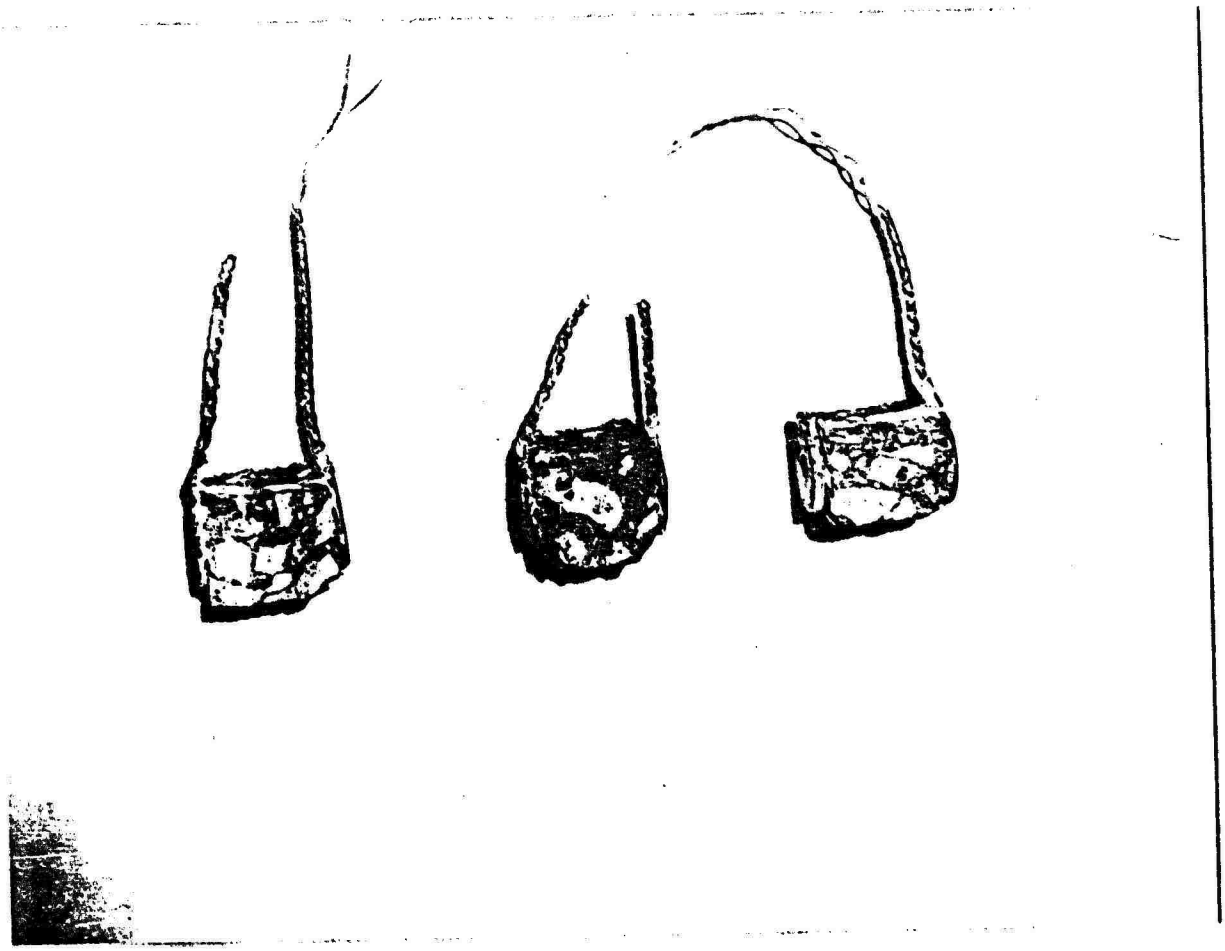

FIG. 5.4 EXCAVATED CARRIER BLOCKS

Table 5.2 Thickness measurements

Pavement No.	Thickness of bituminous layer (mm)			
	From excavated slabs at the rut centre		From final strain coil readings	
			Stack 1	Stack 2
1	136		151	136 (50mm coils)
2	121		127	-
3	226		215	220
	From recovered carriers			
	Stack 1	Stack 2		
3	-	39.9	-	top pair 40.1
	-	41.0	-	centre pair 41.3
	40.3	42.3	bottom pair 40.3	bottom pair 42.8

readings are hence added to Table 5.2. These compared favourably and revealed a maximum error of 0.5 mm. Similar checks were not possible for the subgrade coils since the surrounding material was disturbed on removal of the bituminous slabs. The preceding observations generally show that the strain coils performed satisfactory so far as permanent strain was concerned.

No information was obtained from the 50 mm strain coils in pavements 2 and 3 since the interface coil was damaged in the former and the surface coil remained just out of balance in the latter (due to the overall layer thickness being slightly excessive at the installation point). The failure of two subgrade coils in pavement 1 required the linking of adjacent coils over a greater gauge length. A similar course of action was necessary for pavement 2 when one pair of coils in

stack 2 went out of balance. Subsequent investigation showed that they had become mutually reorientated. One coil became inoperative in stack 1 and another pair in this stack was out of range after compaction. In essence, there were only two outright failures among all the Bison coils which were used, although it is recognised that their loss reduced the effectiveness of the overall strain measuring capability.

5.3 PERMANENT STRAIN PROFILES

Figs 5.5 to 5.9 show the distribution with depth of vertical strain developed from the output of the 25 mm strain coils and also include the locations of the ineffective coils. The results from pavement 3 (Figs 5.8 and 5.9) plainly illustrate a distortion of the vertical strain profile in the bituminous layer related to the position of the carrier blocks. As these carriers were intact on removal at the end of the test, it was possible that they were incompatible with the main DBM mix. Thus they may have restrained the free movement of the material over their length and higher strains would have been attracted to the intervening material. As the overall measurements, discussed in the previous section, appeared to be of the right order, a line was projected through the measured strains based on the average between a pair of coils spanning a carrier and the adjacent pair across the intervening material.

The carrier blocks in pavement 2 appeared to bond satisfactorily with the surrounding material but there was some evidence of restraint (Figs 5.6 and 5.7). This was somewhat disguised for stack 1 as it was necessary to take readings across the out of balance coils and these would probably have indicated higher strains compared to the coils across the carrier. An estimation of the profile is shown by the dotted line.

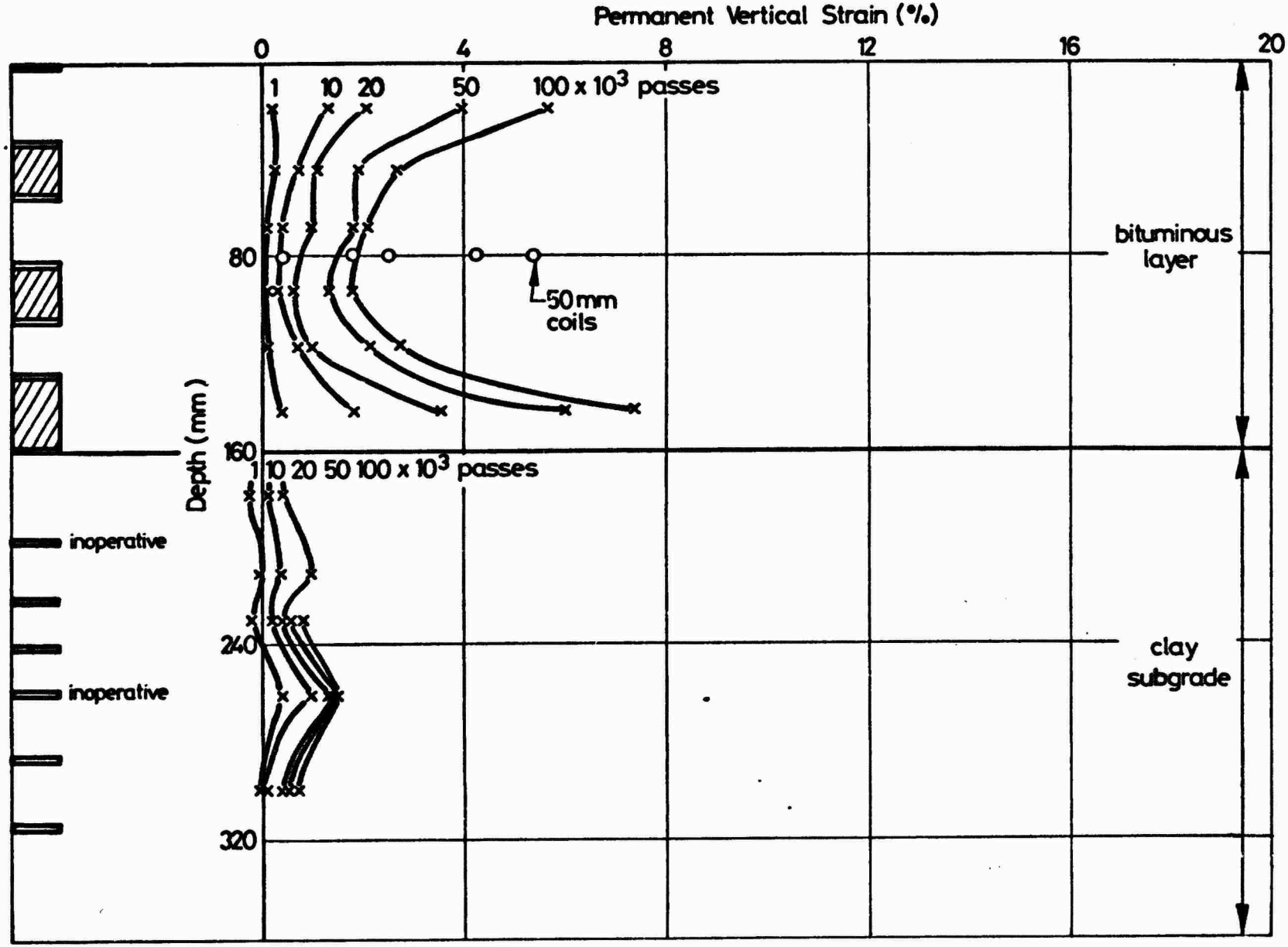

FIG. 5.5 VARIATION OF PERMANENT VERTICAL STRAIN WITH DEPTH, PAVEMENT NO. 1

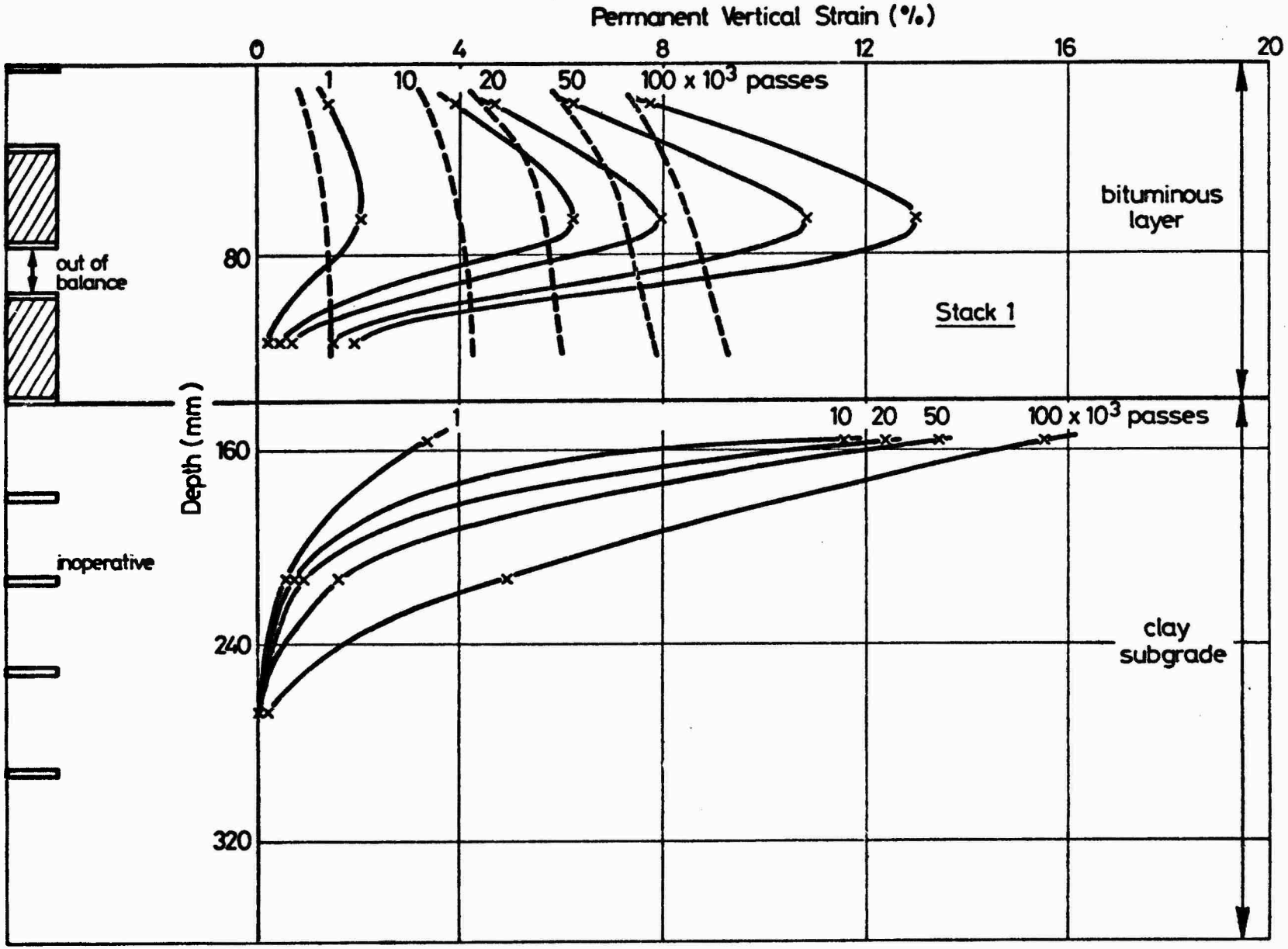

FIG. 5.6 VARIATION OF PERMANENT VERTICAL STRAIN WITH DEPTH, PAVEMENT NO. 2

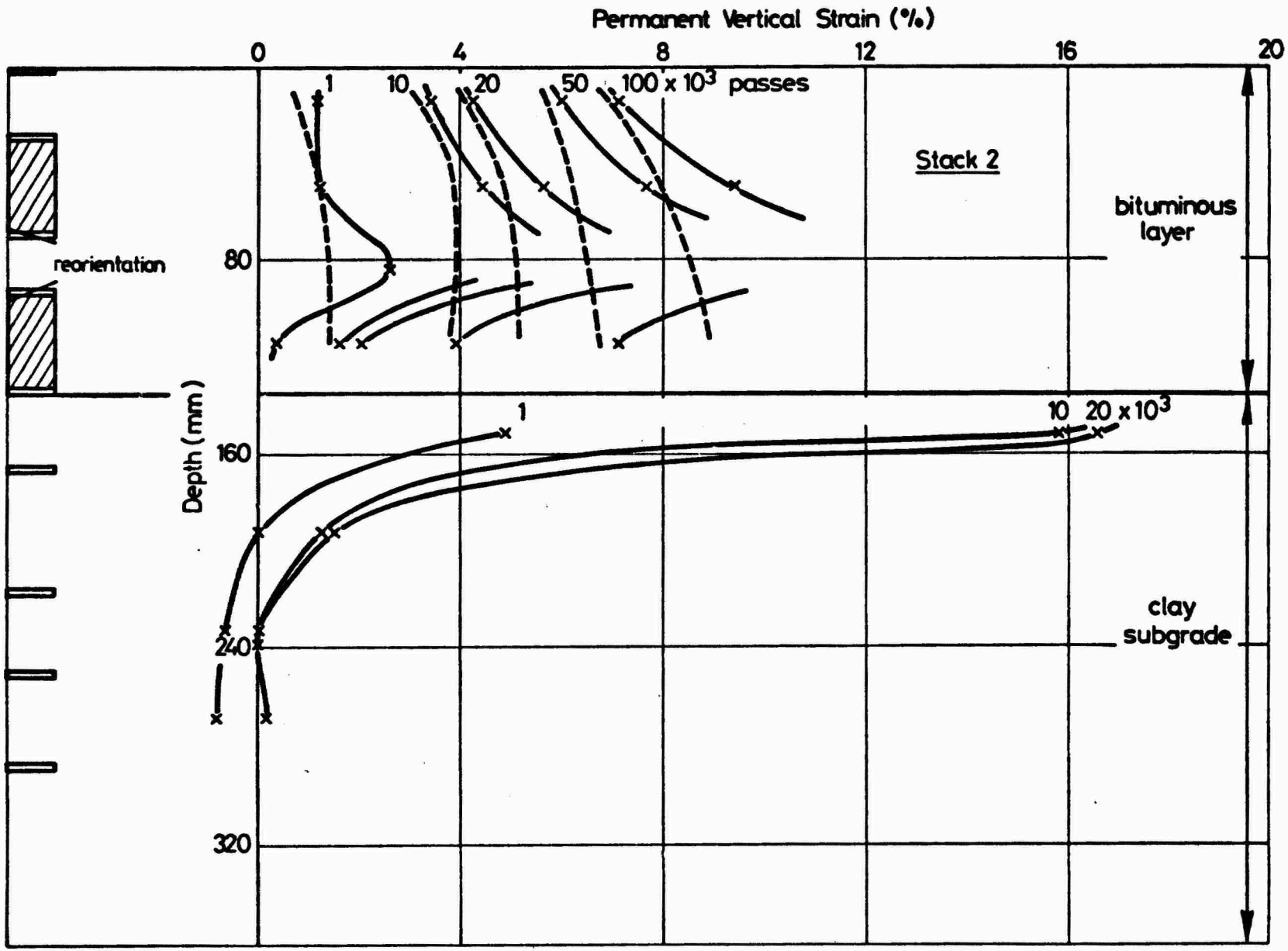

FIG. 5.7 VARIATION OF PERMANENT VERTICAL STRAIN WITH DEPTH, PAVEMENT NO. 2

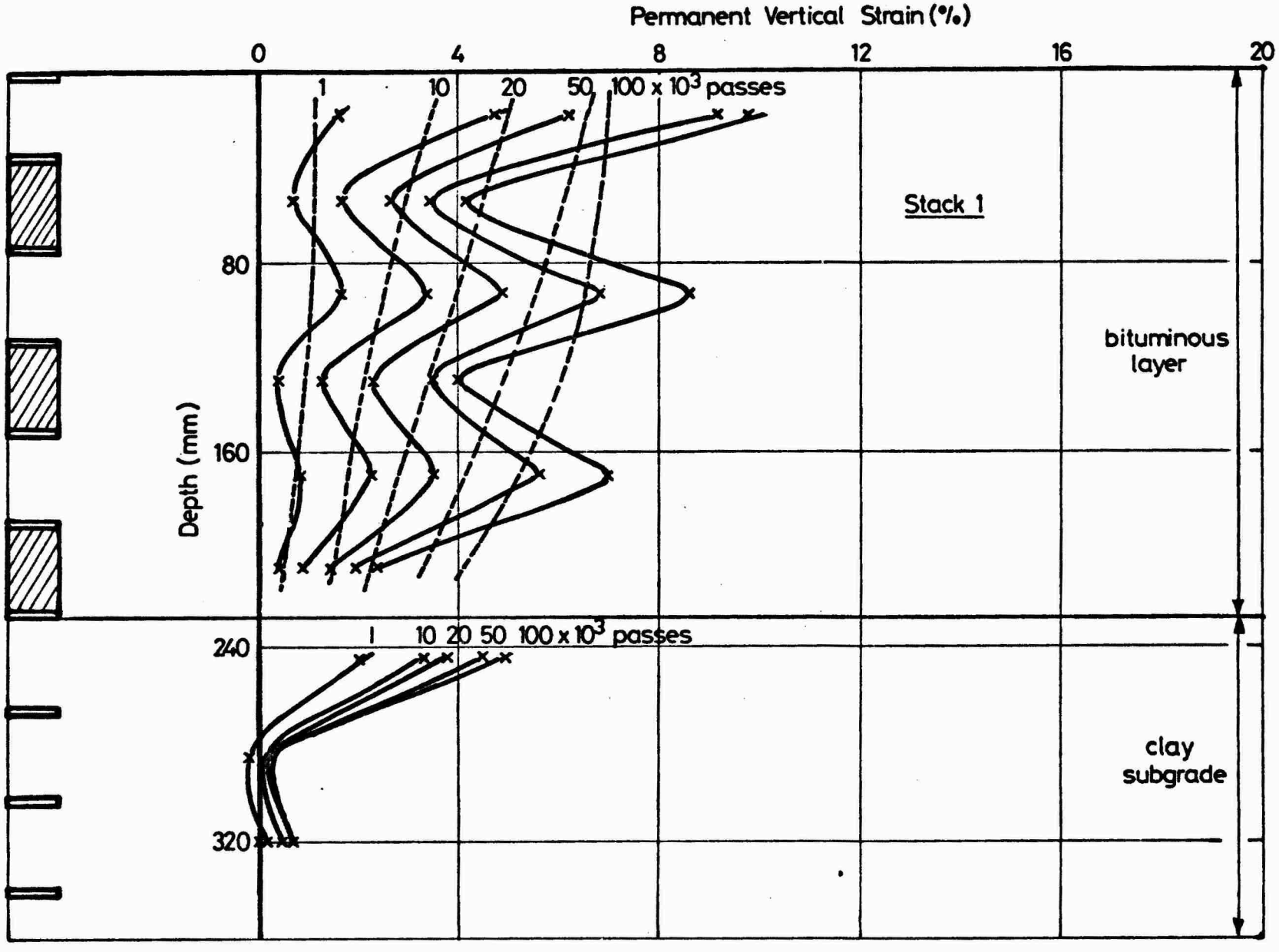

FIG. 5.8 VARIATION OF PERMANENT VERTICAL STRAIN WITH DEPTH, PAVEMENT NO. 3

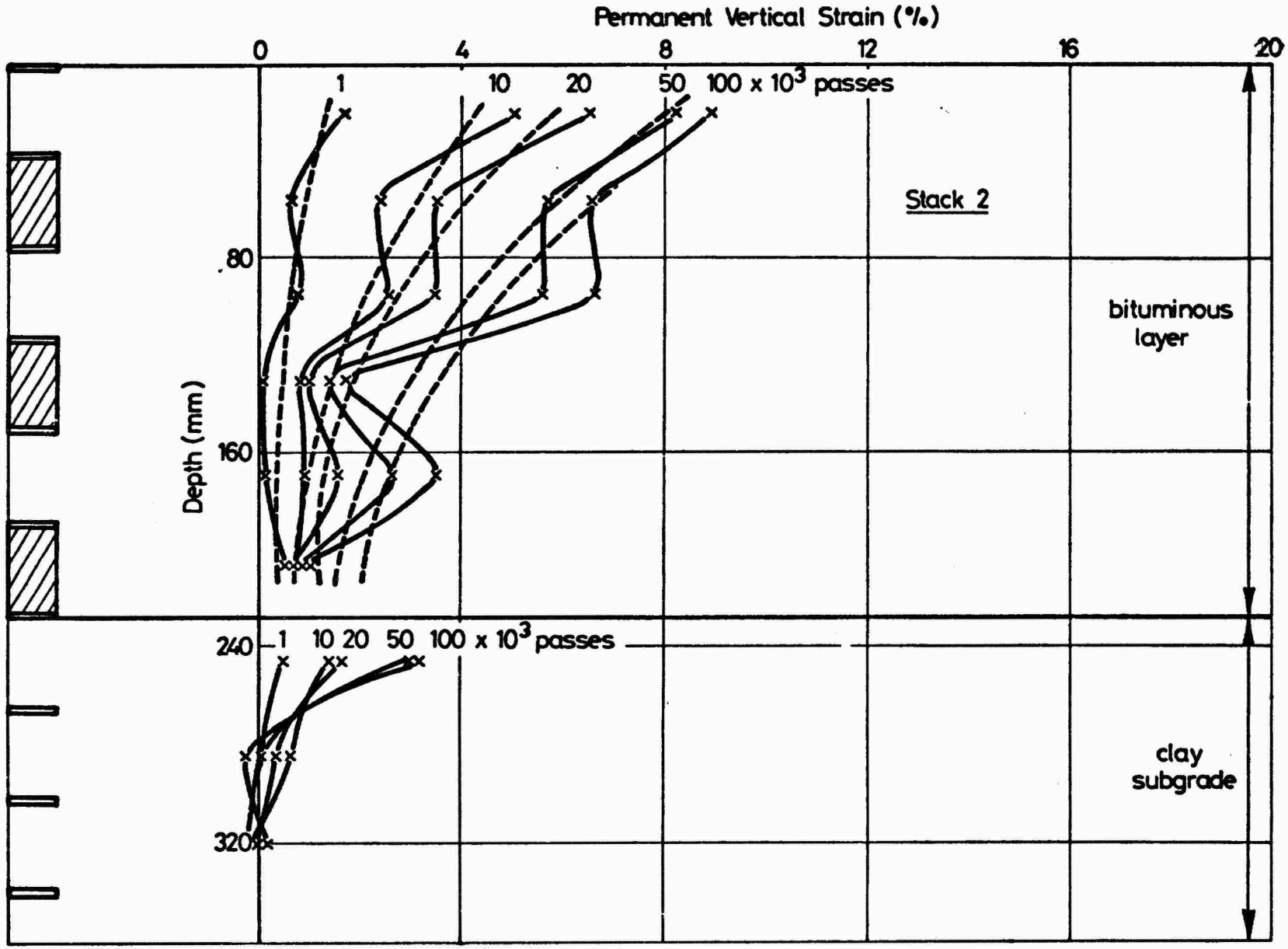

FIG. 5.9 VARIATION OF PERMANENT VERTICAL STRAIN WITH DEPTH, PAVEMENT NO. 3

The vertical strain profile in the bituminous layer of pavement 1 (Fig. 5.5) indicated that the sandsheet carrier blocks may have been more successful in bonding to the main mix in this case. The readings from the 50 mm coils have been included in the figure and appear to be somewhat higher than the average level of the strains from the 25 mm coils.

It is clear from these results that the successful use of carrier blocks in bituminous layers depends on satisfactory matching of the materials. It is probably more effective to avoid the use of carriers, in order to eliminate pockets of the main mix within the stack.

The permanent strain distribution in the subgrade is also shown in Figs 5.5 to 5.9. Maximum values occurred near the interface for pavements 2 and 3 but not for pavement 1. In pavement 1 failure of the upper pair of Nottingham strain coils limited the extent of the readings in this critical zone. It seems likely that the strain levels should be greater near the interface and the main uncertainty is the depth to which they are significant.

Exceptionally high values of strain were obtained ror pavement 2, particularly in the subgrade, and stack 2 indicated nearly 17% strain at 20,000 passes. Readings were discontinued for this stack as the upper coils approached the out of balance condition due to their increased proximity. The bottom pair of subgrade coils for all pavements indicated significant permanent deformation and this was at a maximum for pavement 1. This supports the view that the general underestimation of the rut depth from the coils was to some extent caused by the amount of deformation taking place below the lowest pair of coils. A degree of tensile strain was noted in the early stages of the tests and at 100,000 passes for stack 2 of pavement 3. Some redistribution of

material movement or stress conditions may occur at the start of the test as the pavement settles and could result in this effect. However, the reasons for a tensile reading at 100,000 passes are not immediately apparent. Since both stacks in pavement 3 show the same general effect it would appear to be genuine.

In general, the measurements of overall permanent deformation from the coils are reasonably accurate and therefore the strain profiles will represent a distribution compatible with the average strain. The profiles developed from the instruments were not conclusively defined, although it was felt that the subgrade readings from pavements 2 and 3, the average profiles for pavement 3 and the readings for pavement 1 in the bituminous layer were a reasonable representation. A considerable aid to checking the validity of these profiles would be provided by similar information on the stress conditions, vertically and radially. However, stress measurements in the DTM were only attempted for pavement 3 and these are discussed in Section 5.6.

5.4 HORIZONTAL PERMANENT STRAIN

Figs 5.10 and 5.11 show the variations of permanent horizontal strain with load applications. The term "longitudinal radial" refers to the strains in the direction of the wheel, and "lateral radial" strains are at right angles to these. As expected, the lateral permanent strains are higher than the longitudinal strains in all cases. However, the longitudinal strains would be expected to be minimal due to the strain reversal as the wheel passes over the point of measurement. The lateral strains for stack 2, pavement 2, indicate an approach to pavement failure at the location of these coils. Consequently, the undersides of the slabs were carefully examined for

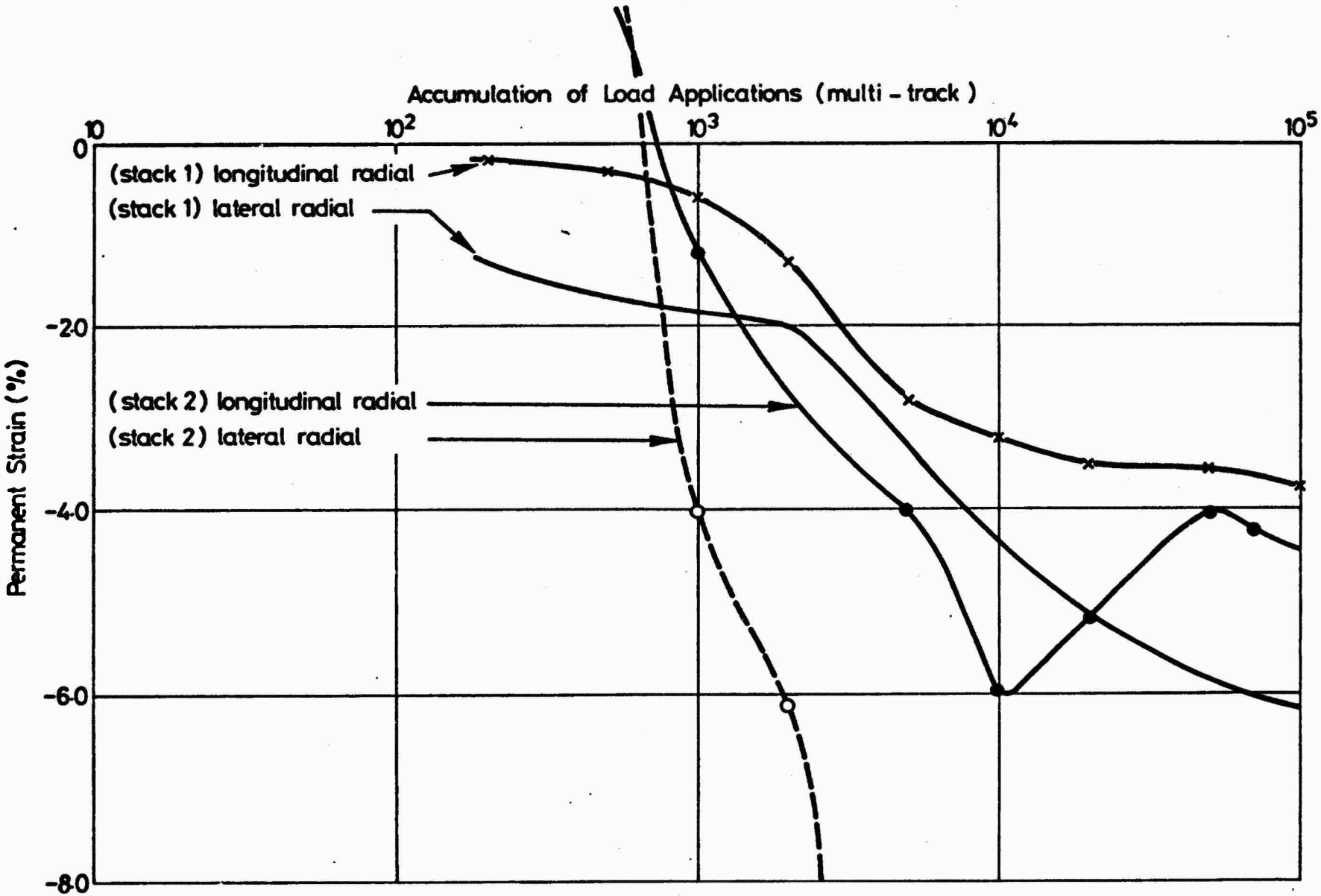

FIG. 5.10 PERMANENT HORIZONTAL STRAINS AT THE INTERFACE, PAVEMENT NO. 2

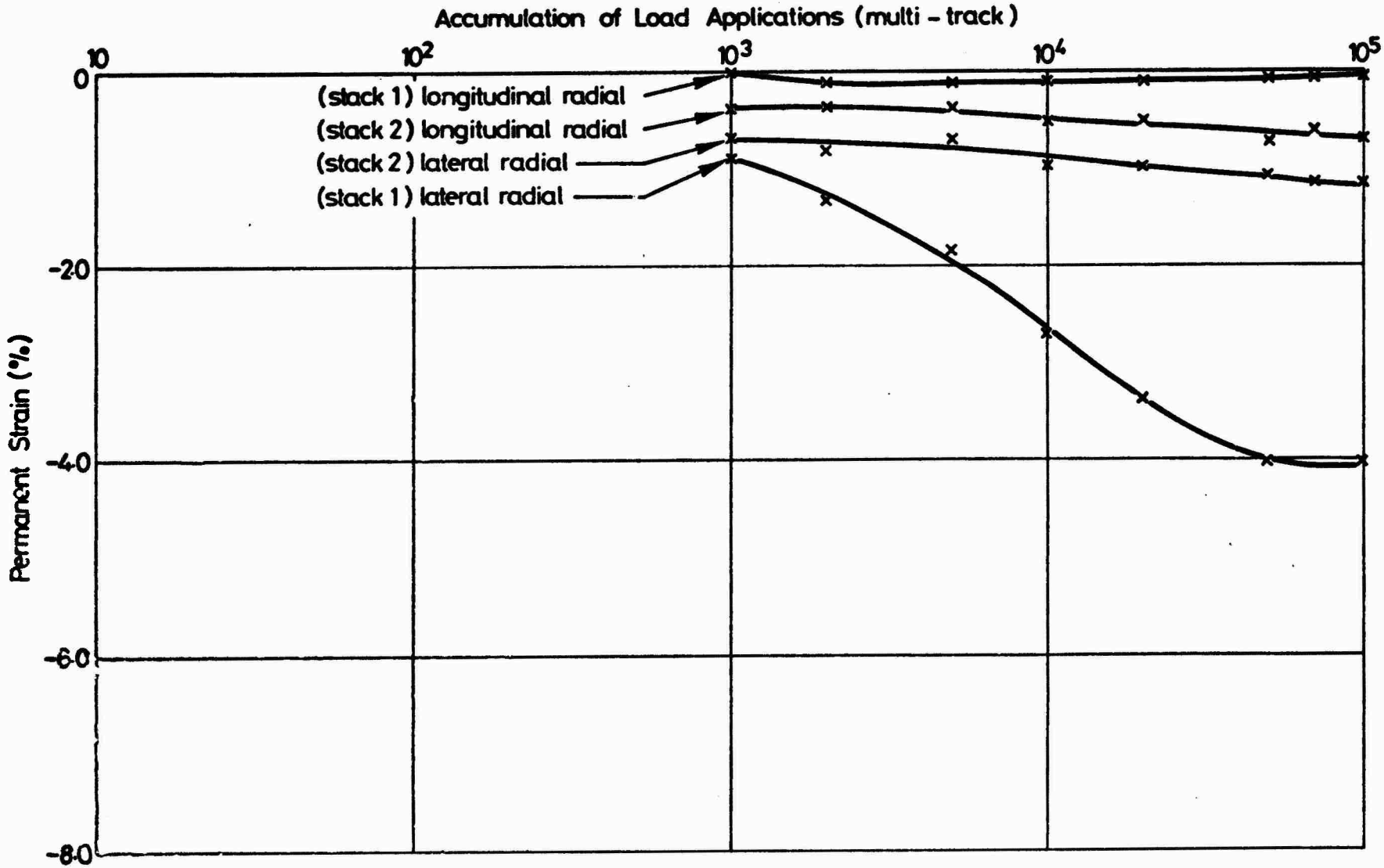

FIG. 5.11 PERMANENT HORIZONTAL STRAINS AT THE INTERFACE, PAVEMENT NO. 3

cracks after removal, but none were obvious in the rough texture of the exposed surface.

5.5 ELASTIC STRAINS

The elastic strain profiles, with depth, shown in Figs 5.12 to 5.14, were developed from the average of several readings taken after about 50,000 passes for pavements 1 and 2 and from all the readings for pavement 3. This was to avoid establishing the profiles from single point readings at some selected stage of the tests since Figs 5.15 and 5.16 show that the strains changed somewhat as the tests proceeded. This procedure appeared to be generally justified with the possible exception of the vertical subgrade strain in pavement 2. In essence, these profiles can be considered to be representative of the elastic strains during the second half of the test.

The results for pavement 3 (Fig. 5.14) revealed a similar pattern to the permanent strain profiles (Figs 5.8 and 5.9) and the averages of stacks 1 and 2 in the bituminous layer produced identical curves. The subgrade measurements for this pavement did not indicate the apparent restraint observed for the permanent strains for the centre pair of coils. Higher elastic strains were characteristic of pavements 1 and 2 as a result of the thinner bituminous layers. There appears to be no obvious correlation between the elastic and permanent strains in the bituminous layers of pavements 1 and 2. A carrier block effect was apparent for pavement 1 resulting in a considerable distortion of the elastic strain profile though this was not observed for the permanent strains (Fig. 5.5). It was noticeable that the elastic strains in the subgrade were significant for all the coils in each pavement suggesting the development of significant strains to greater depths than the instruments.

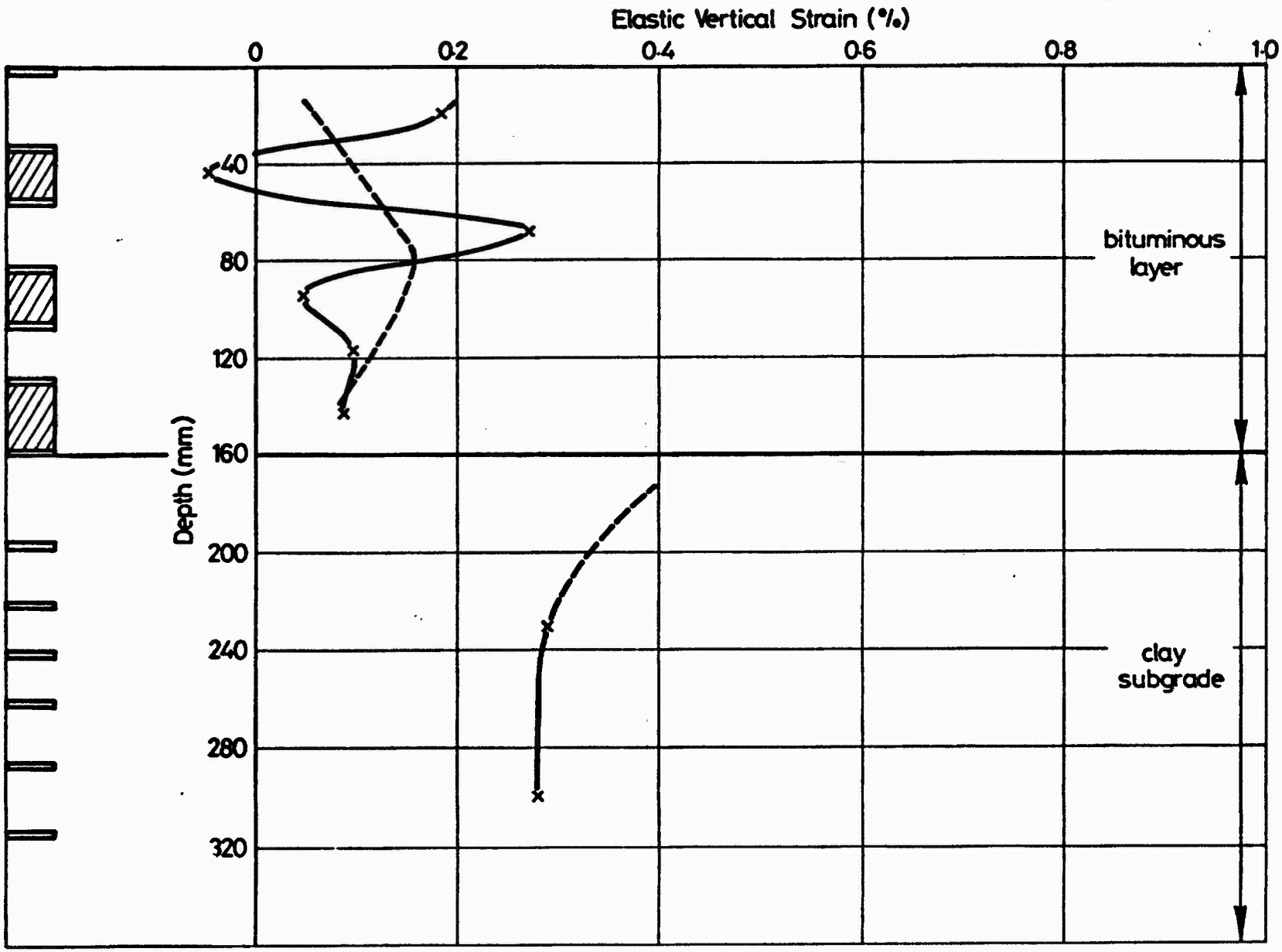

FIG. 5.12 VARIATION OF ELASTIC VERTICAL STRAIN WITH DEPTH, PAVEMENT NO. 1

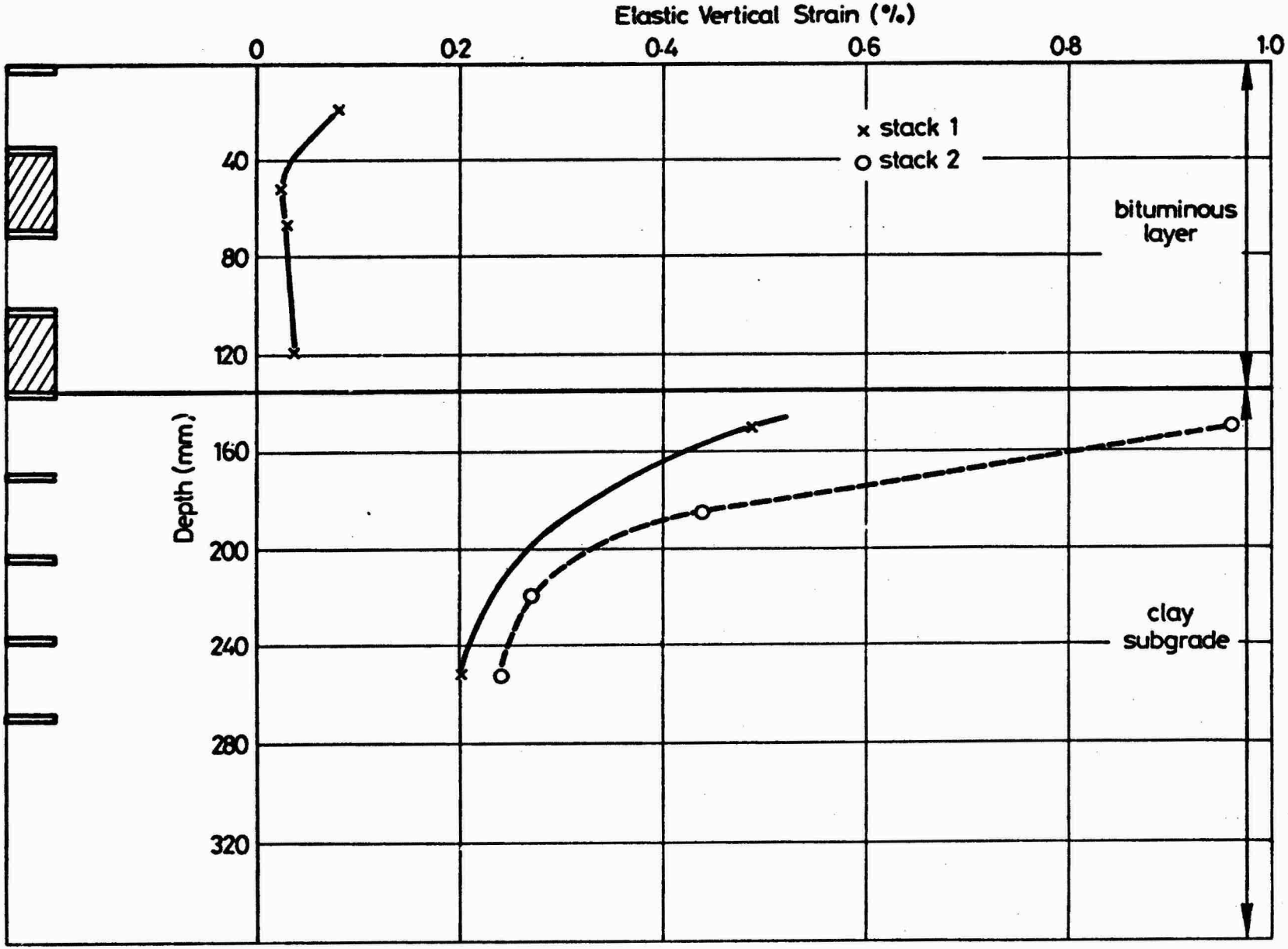

FIG. 5.13 VARIATION OF ELASTIC VERTICAL STRAIN WITH DEPTH, PAVEMENT NO. 2

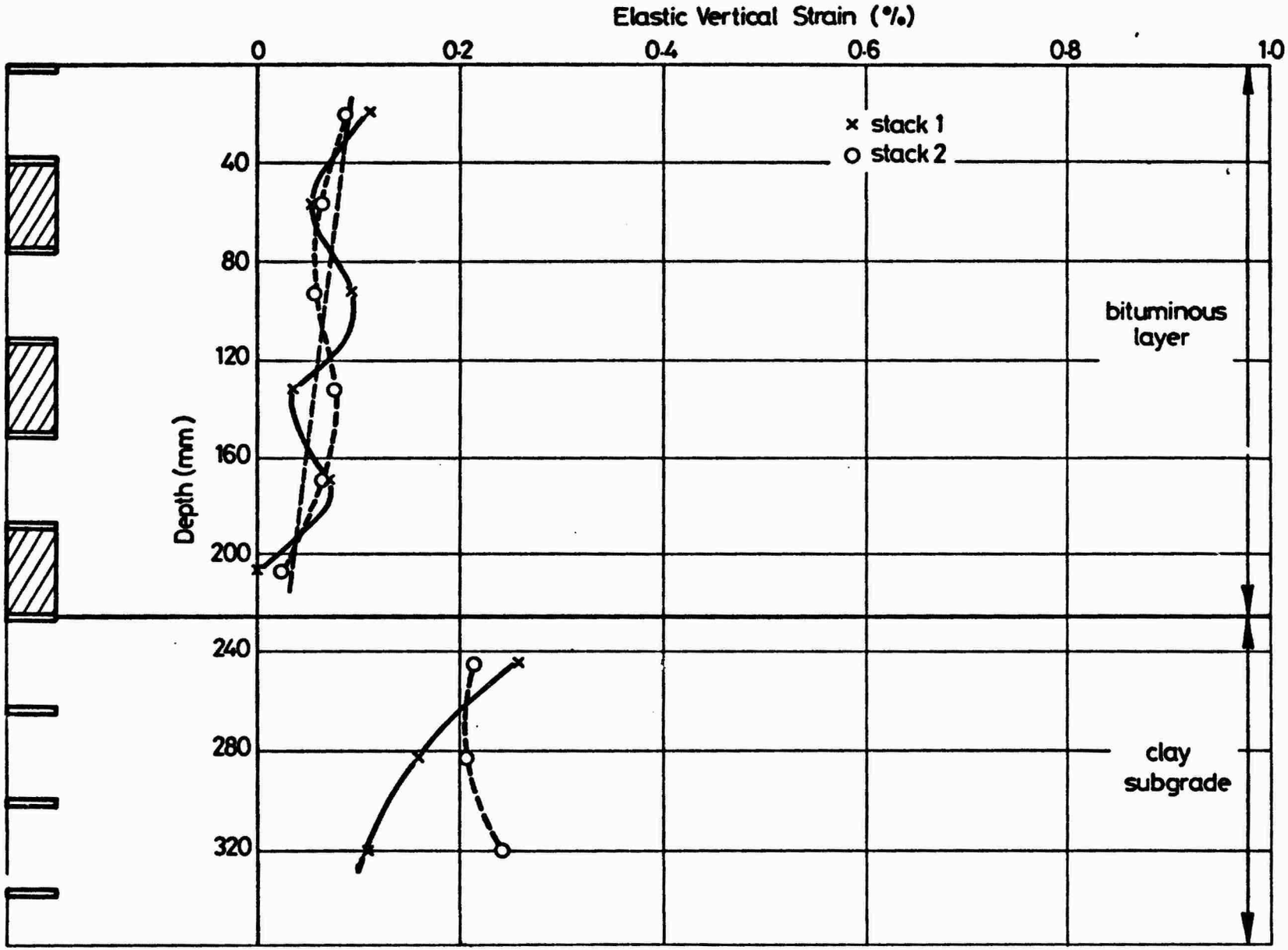

FIG. 5.14 VARIATION OF ELASTIC VERTICAL STRAIN WITH DEPTH, PAVEMENT NO. 3

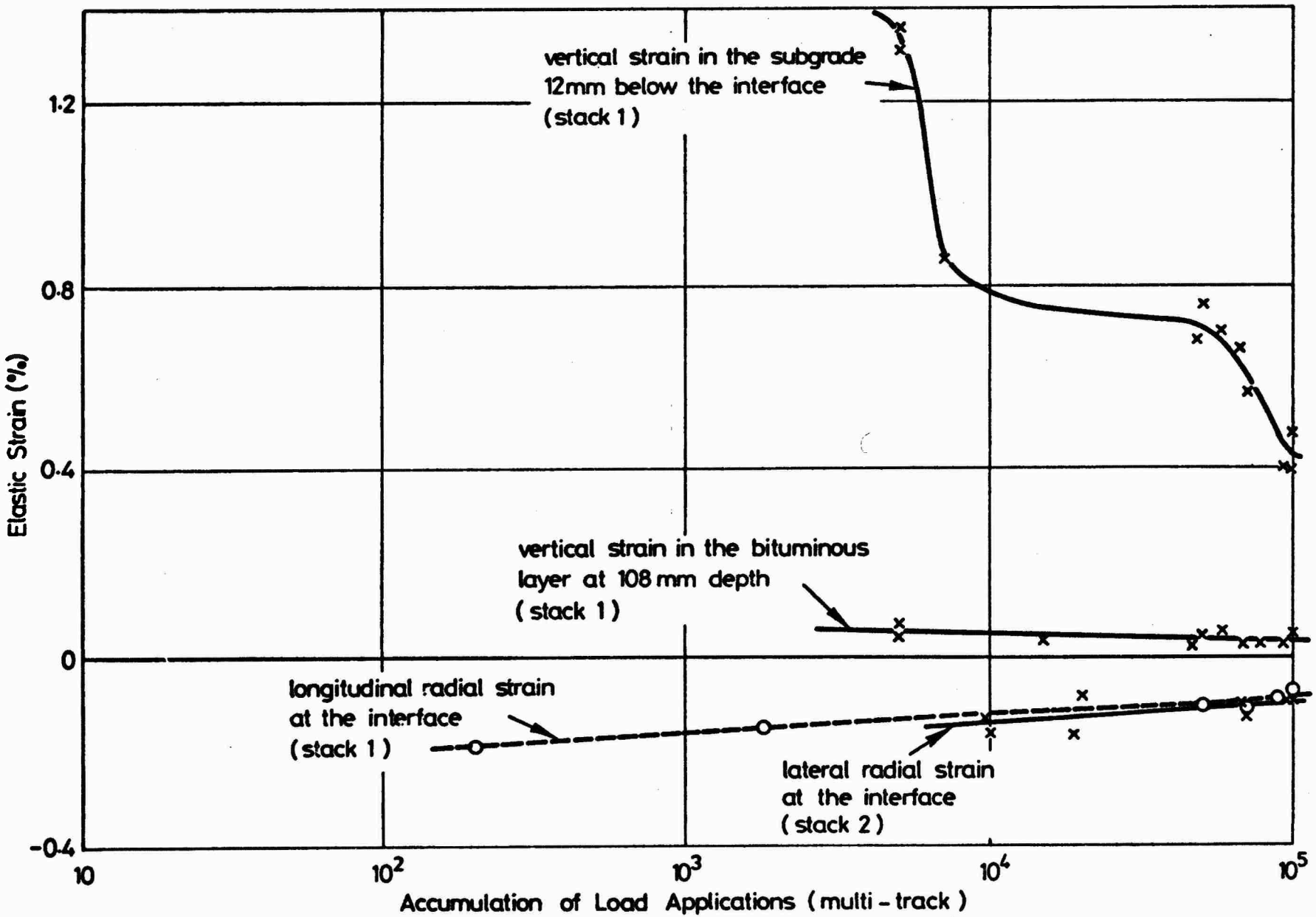

FIG. 5.15 VARIABILITY OF ELASTIC STRAIN MEASUREMENTS, PAVEMENT NO. 2

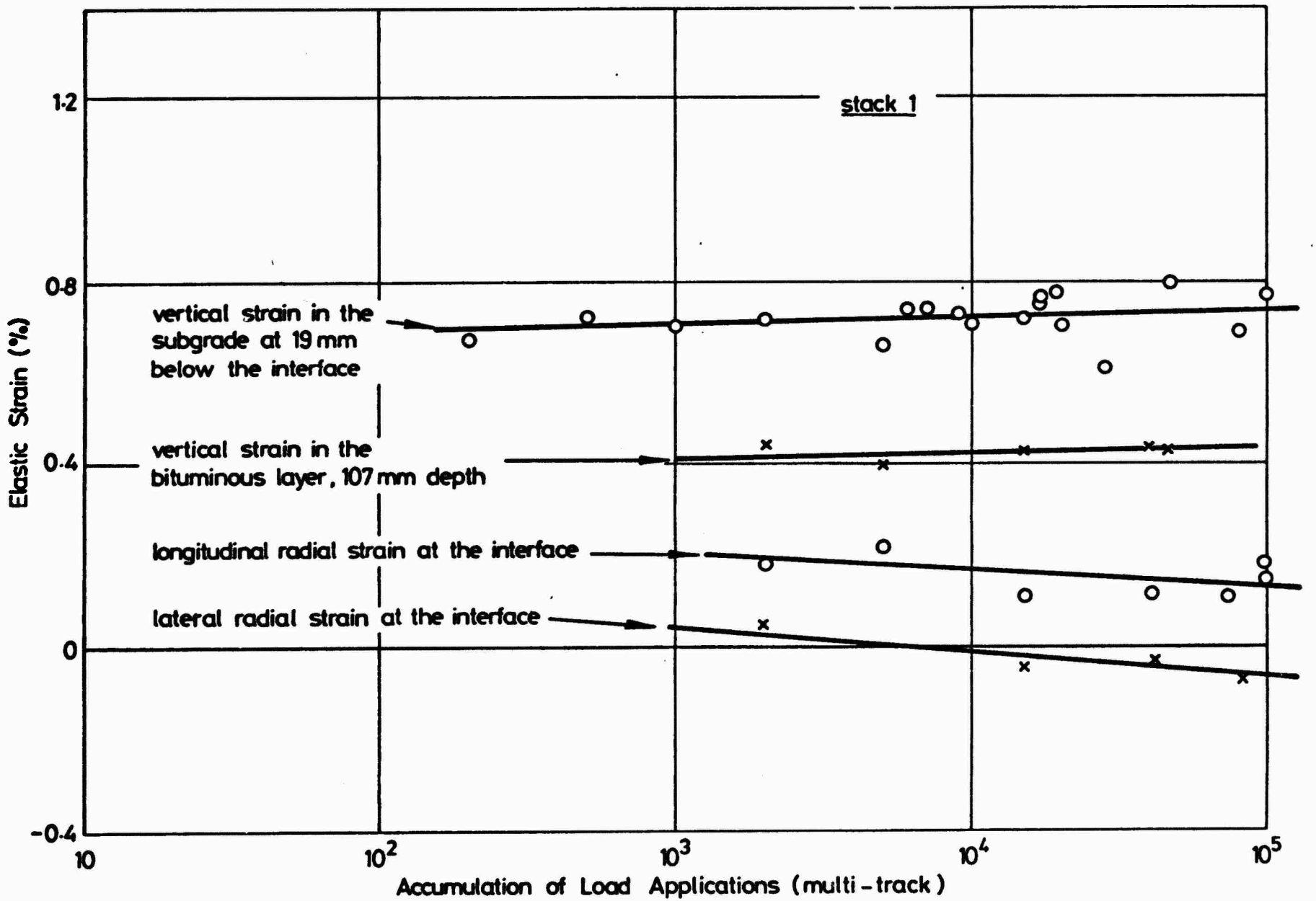

FIG. 5.16 VARIABILITY OF ELASTIC STRAIN MEASUREMENTS, PAVEMENT NO. 3

An assessment of the lateral profile of the elastic strains is summarised in Figs 5.17 and 5.18, and again these have been developed from averages of several strain readings measured during the second half of each test. The measurements were taken as the loaded wheel passed at various distances from the position of the coils. The profiles are not exactly symmetrical and this could reflect a variation in the materials or be a result of less reliable mean values either side of the centre since fewer readings were taken in the shorter time available at these locations because of the normal lateral distribution of wheel passes.

Results from the Nottingham strain cells have not been included as the d.c. instrument produced erratic readings and the a.c. cell appeared to over-register. However, the lateral strain profile from the latter cell was similar in appearance to that produced by the coils.

Elastic strains determined from the strain gauge readings are included in Figs 5.19 to 5.21. The vertical strain results for pavement 1 are similar in magnitude to the average obtained from the strain coils for this pavement. The top vertical strain gauge in the bituminous layer exhibited a "tension-compression" output while the middle gauge gave a lower compressive output and the bottom gauge showed a larger compressive strain. The pattern of the compressive strains in pavement 1 was similar to the results obtained for the permanent strains with depth (Fig. 5.5). As with previous measurements at the interface, the lateral radial strain level exceeded the longitudinal strains. There was no significant trend with increasing load applications and variations were probably influenced by the less efficient wheel load setting arrangement for the pavement 1 test.

The results for pavements 2 and 3 (Figs 5.20 and 5.21) were very

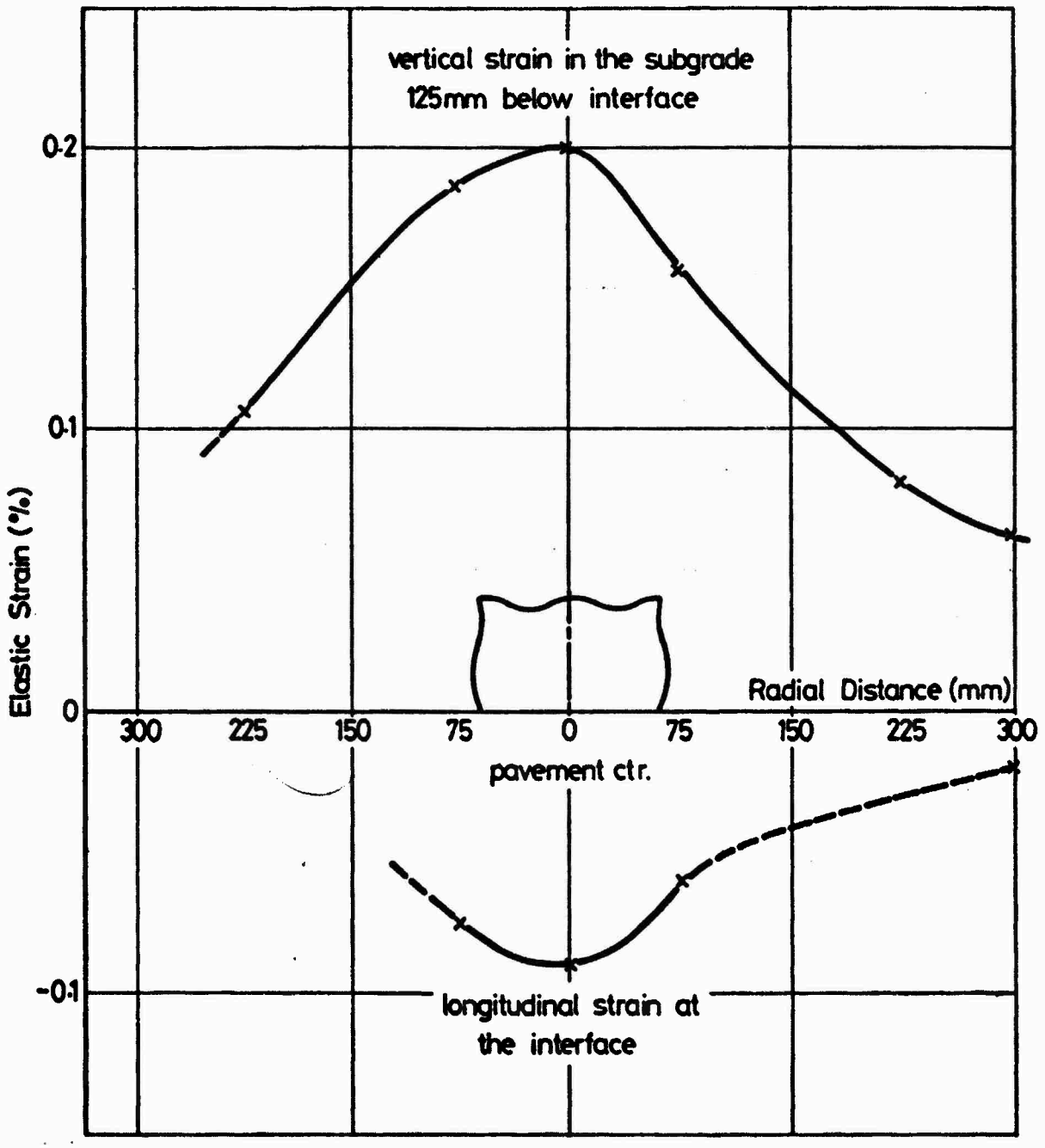

FIG. 5.17 VARIATION OF ELASTIC STRAIN WITH RADIAL DISTANCE FROM PAVEMENT CENTRE, PAVEMENT NO. 2

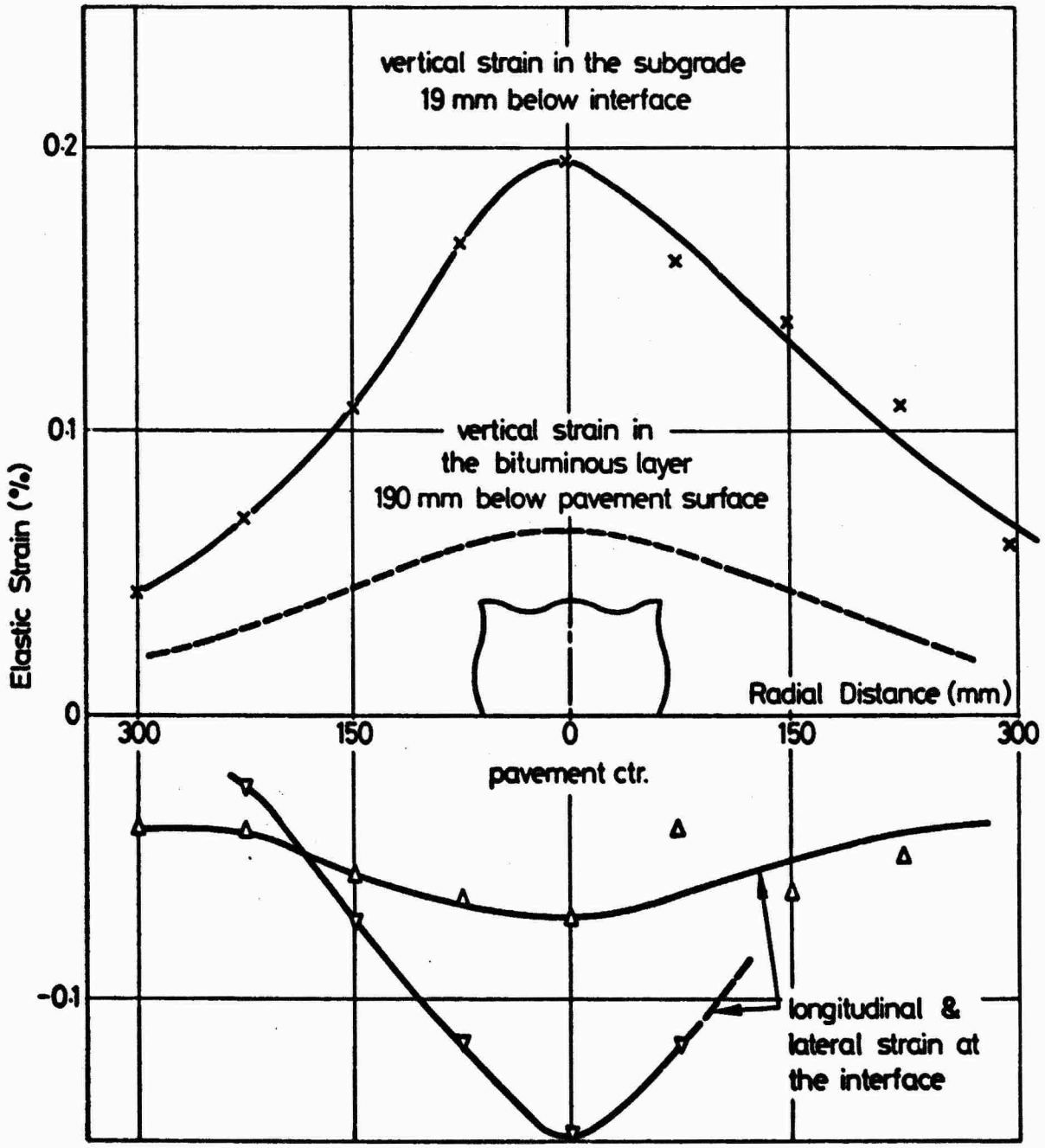

FIG. 5.18 VARIATION OF ELASTIC STRAIN WITH RADIAL DISTANCE

FROM PAVEMENT CENTRE, PAVEMENT NO. 3

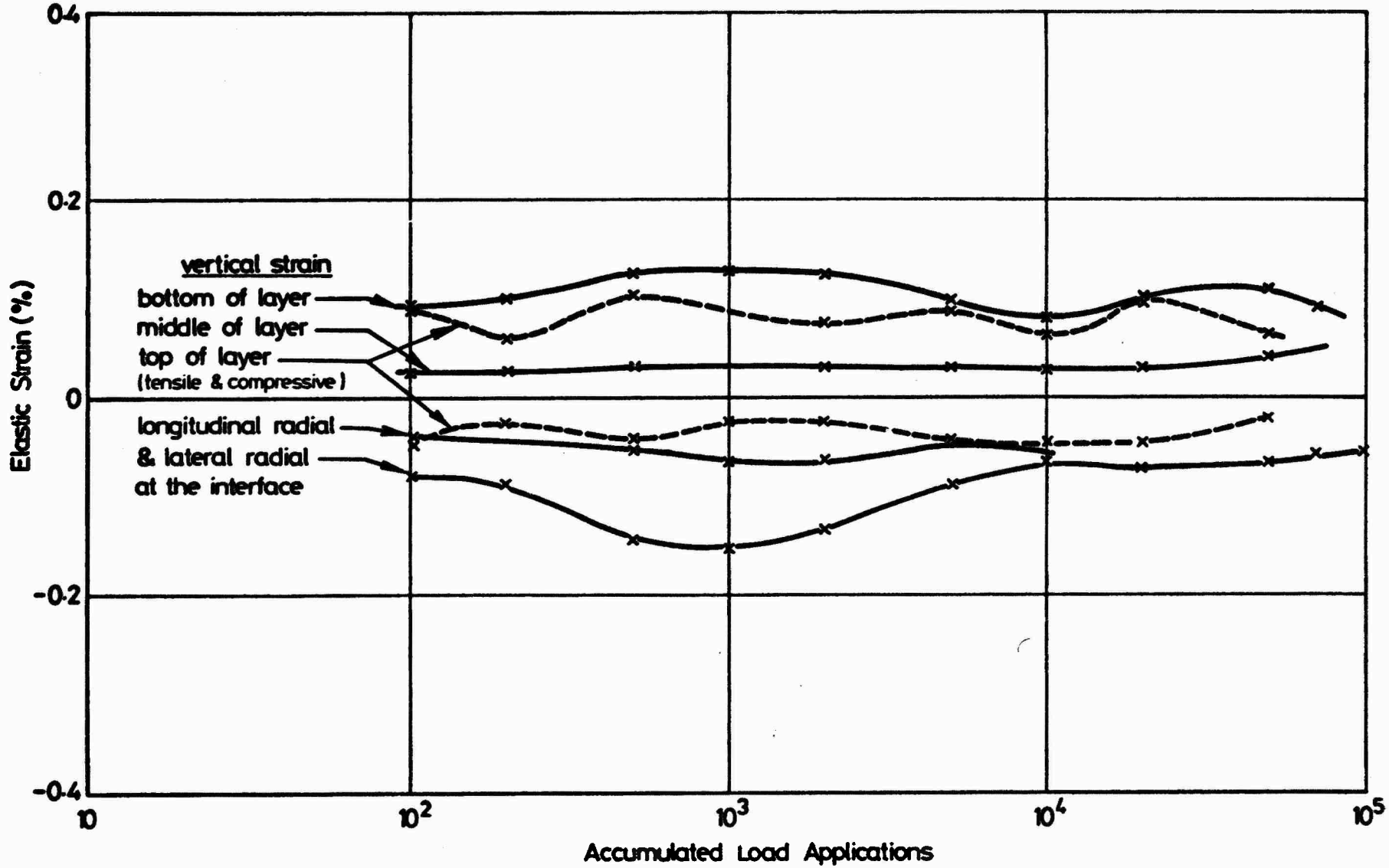

FIG. 5.19 ELASTIC STRAIN DETERMINED FROM STRAIN GAUGES, PAVEMENT NO. 1

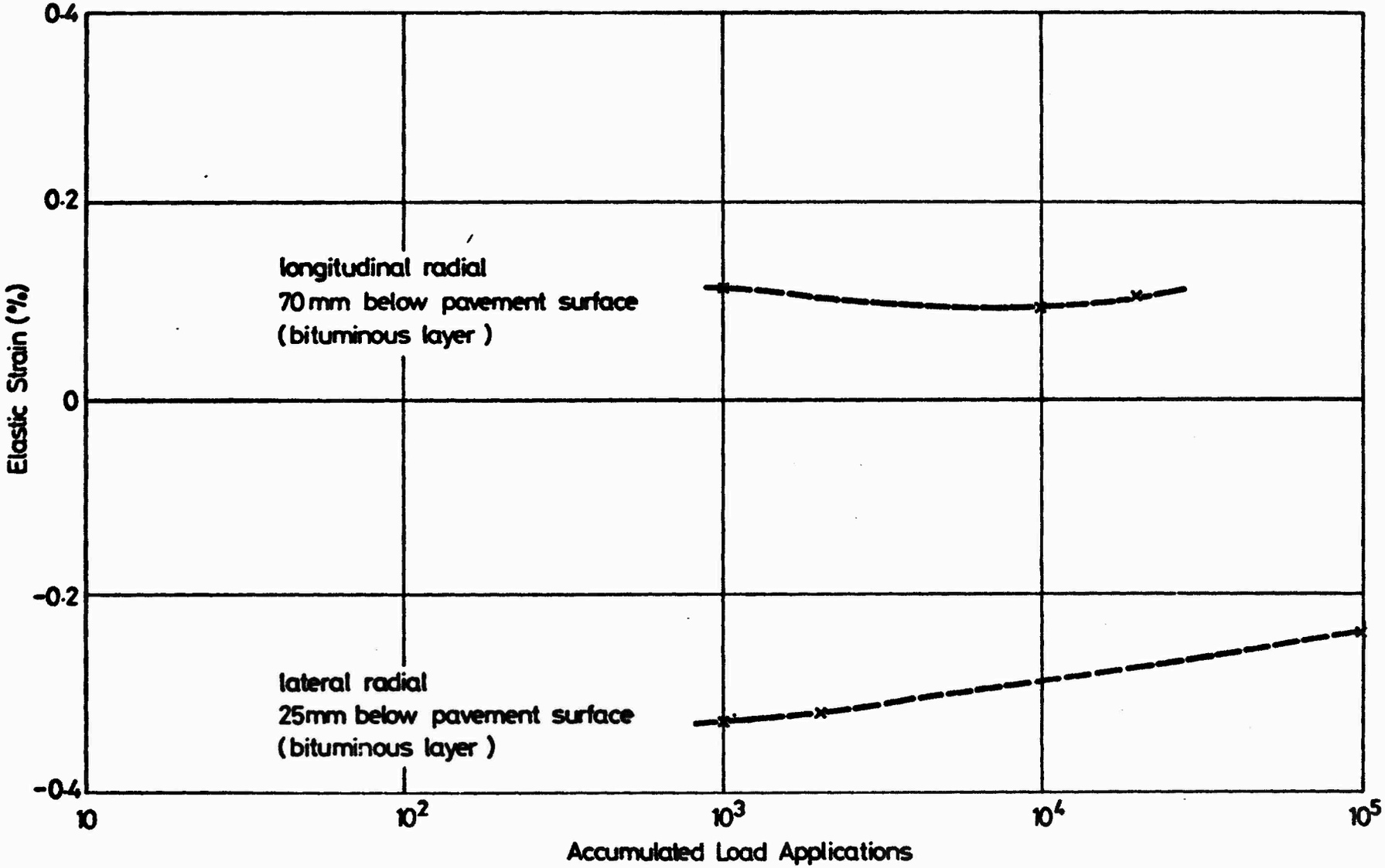

FIG. 5.20 ELASTIC STRAIN DETERMINED FROM STRAIN GAUGES, PAVEMENT NO. 2

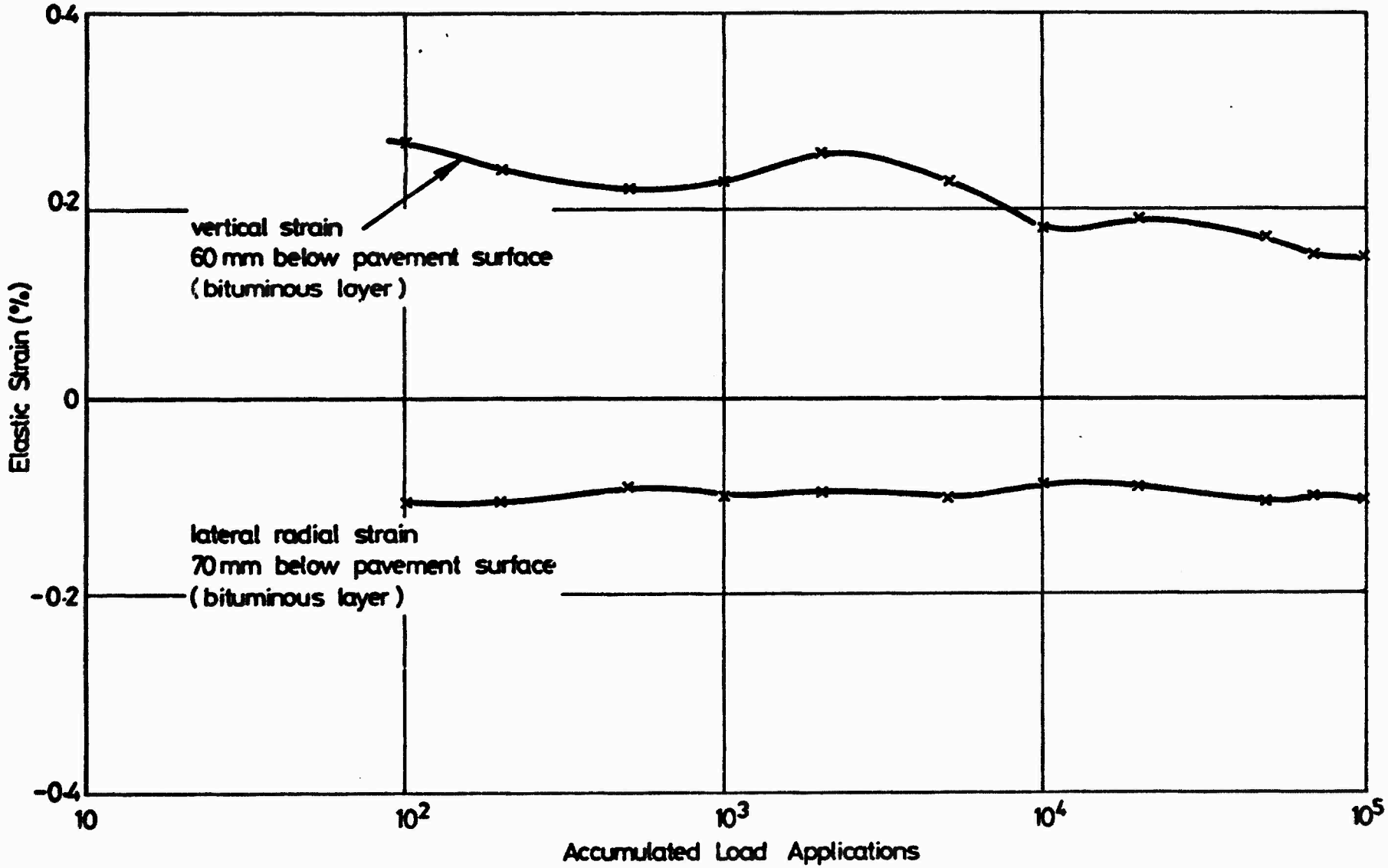

FIG. 5.21 ELASTIC STRAIN DETERMINED FROM STRAIN GAUGES, PAVEMENT NO. 3

limited due to strain gauge failures. The results indicate only a minor variation of elastic strain with load applications. It would appear that the only large variations in elastic strain during the test occurred in the subgrade of pavement 2 from the coils, but there is a gap in the information at the initial stages of the tests.

5.6 STRESS LEVELS

Figs 5.22 and 5.23 show the subgrade stresses measured just below the interface for pavements 2 and 3 in the form of lateral profiles. The values which are plotted were derived from the averages of all the readings taken as the tests progressed since no definite trends in magnitude related to load applications were observed for either pavement. This was not the case for pavement 1 in which the stress levels generally decreased during the tests and insufficient off-axis measurements were taken to define a lateral profile.

The maximum stresses recorded are summarised in Table 5.3. The range of stresses recorded for pavement 1, and the stresses recorded near the end of the tests, for pavements 2 and 3, are shown. The large

Table 5.3 Comparison of pressure cell readings in the subgrade

Pavement No.	Vertical stress (kN/m^2)	Longitudinal stress (kN/m^2)
1	89.6-41.4	6.9-4.8, 34.5-27.6
2	66, 55, 60	25.4, 34.7, 22.1
3	60, 52	15, 17

range of stresses recorded for pavement 1 could be due to the subgrade suffering additional compaction from the trafficking as the test progressed, combined with inaccuracies in the measurements. For the subsequent pavements, the compaction due to trafficking and subsequent stiffening

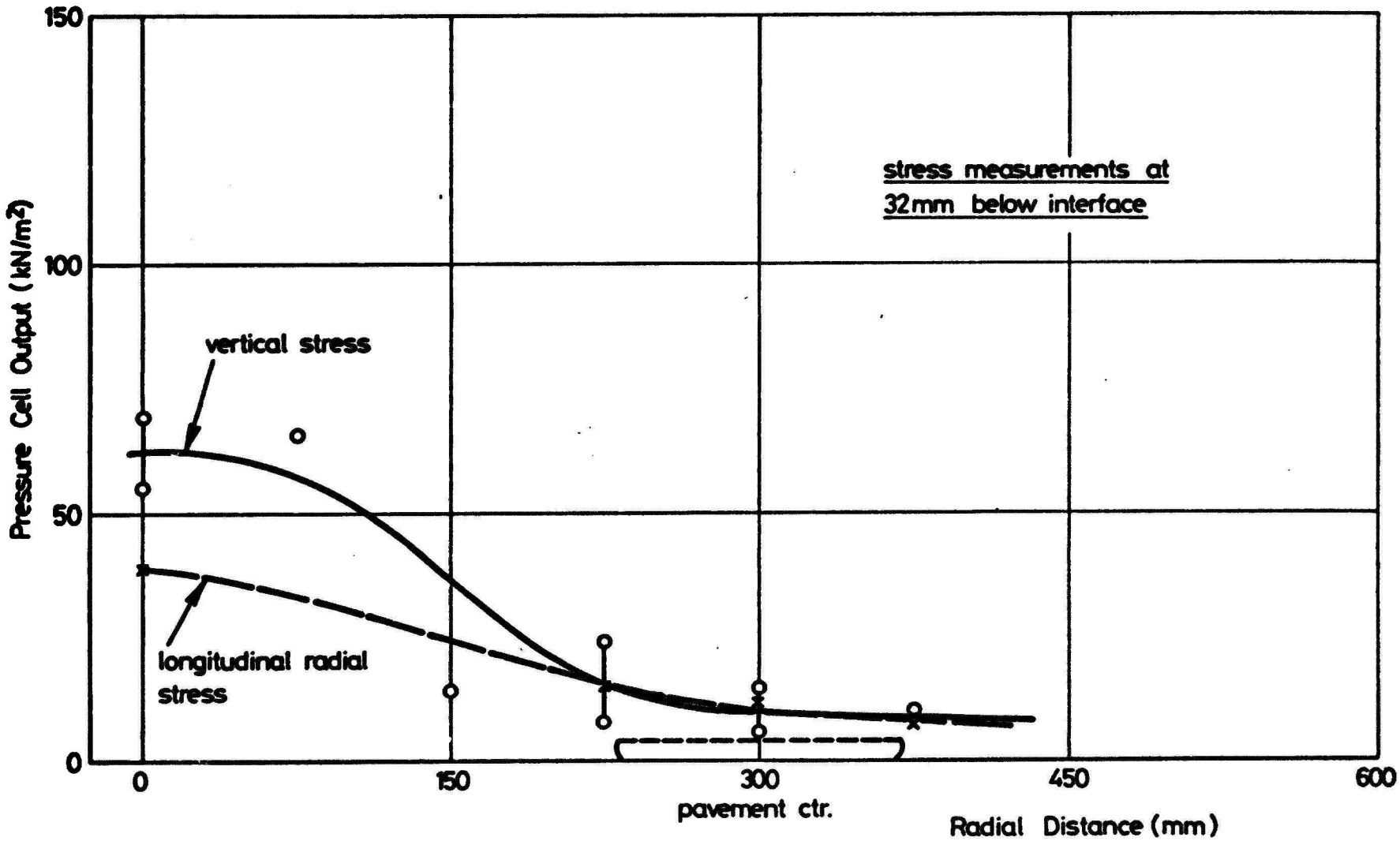

FIG. 5.22 VARIATION OF STRESS WITH RADIAL DISTANCE FROM PAVEMENT CENTRE (SUBGRADE LAYER),

PAVEMENT NO. 2

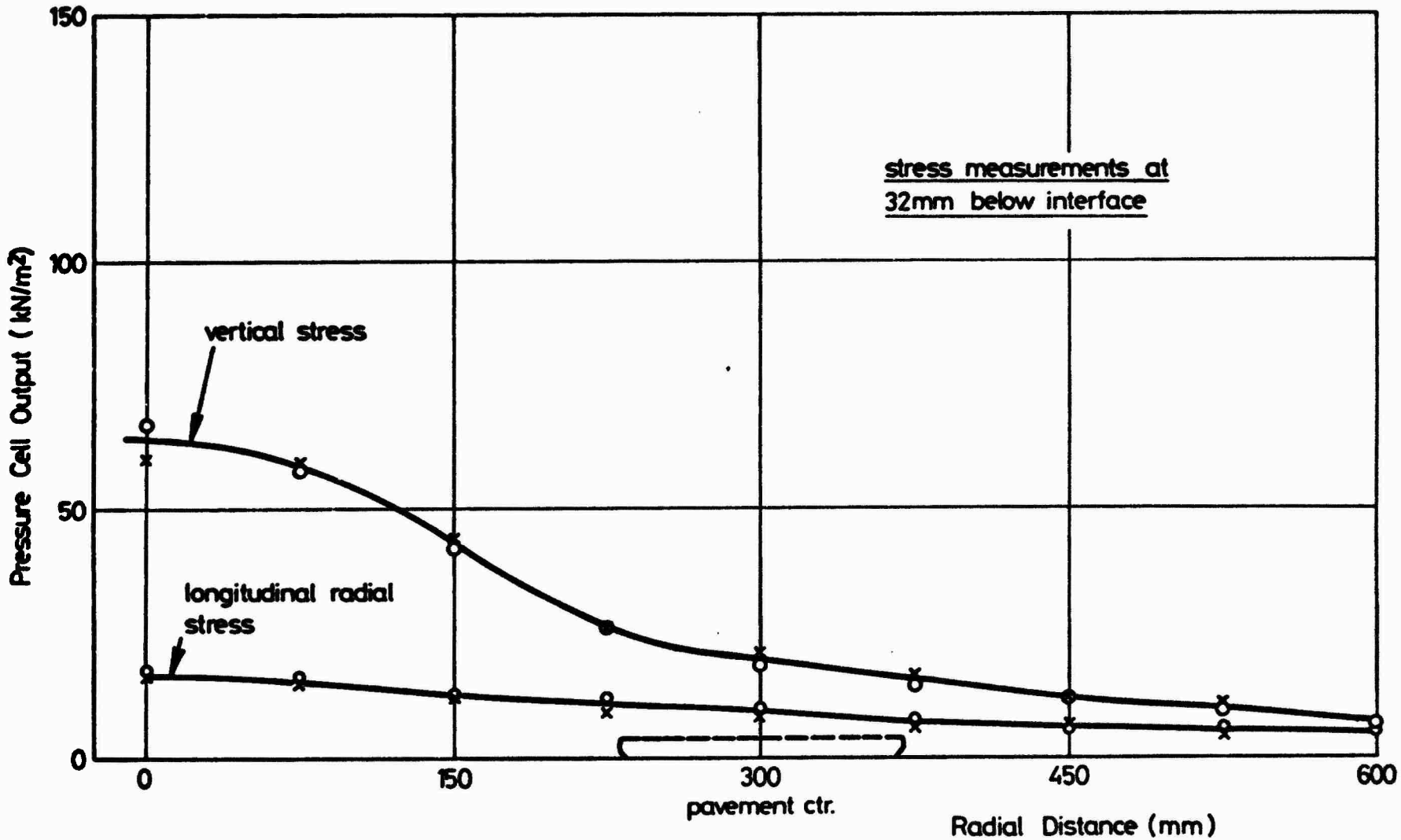

FIG. 5.23 VARIATION OF STRESS WITH RADIAL DISTANCE FROM PAVEMENT CENTRE (SUBGRADE LAYER),

PAVEMENT NO. 3

of the clay, would be much less, and the measurements were repeated with one or two additional cells. Comparison of the vertical stresses recorded at the end of the tests shows that the weaker structures of pavements 2 and 3 have higher values than pavement 1, despite lower contact pressures. The longitudinal stresses recorded in pavement 3 were the lowest which would be expected with a thicker bituminous layer.

The readings from the two sets of cells in the subgrade layer of pavement 3 were in excellent agreement and it is felt that this lateral profile is an accurate representation of the stress levels. A degree of scatter was observed for the subgrade stress measurement for pavement 2 and the lateral profile was not as well defined.

An attempt to measure stresses in the bituminous layer of pavement 3 was carried out with the Nottingham pressure cell. This instrument was designed for use in soil and only one initial calibration in a DBM specimen was possible before installation. A cell registration of 0.94 obtained from this test was applied to the measurements recorded for pavement 3 and the lateral profile shown in Fig. 5.24 was developed. The readings from the three cells monitoring the upper longitudinal horizontal stresses varied considerably under the wheel load and off axis, to one side of the pavement centre. A single cell was installed to measure the longitudinal horizontal stress levels at the bottom of the layer and indicated significant compressive stress combined with an indication of tensile stress since the cell is not designed to register tension. The vertical stress at the same location was 77 kN/m^2, compared with the reading in the subgrade of 64 kN/m^2, thus indicating the continuity of this parameter across the interface (i.e. equilibrium).

As with previous measurements, more information was available for pavement 3 and the readings in the subgrade are considered to be reliable. The scatter for the results in pavement 2 tends to indicate that these

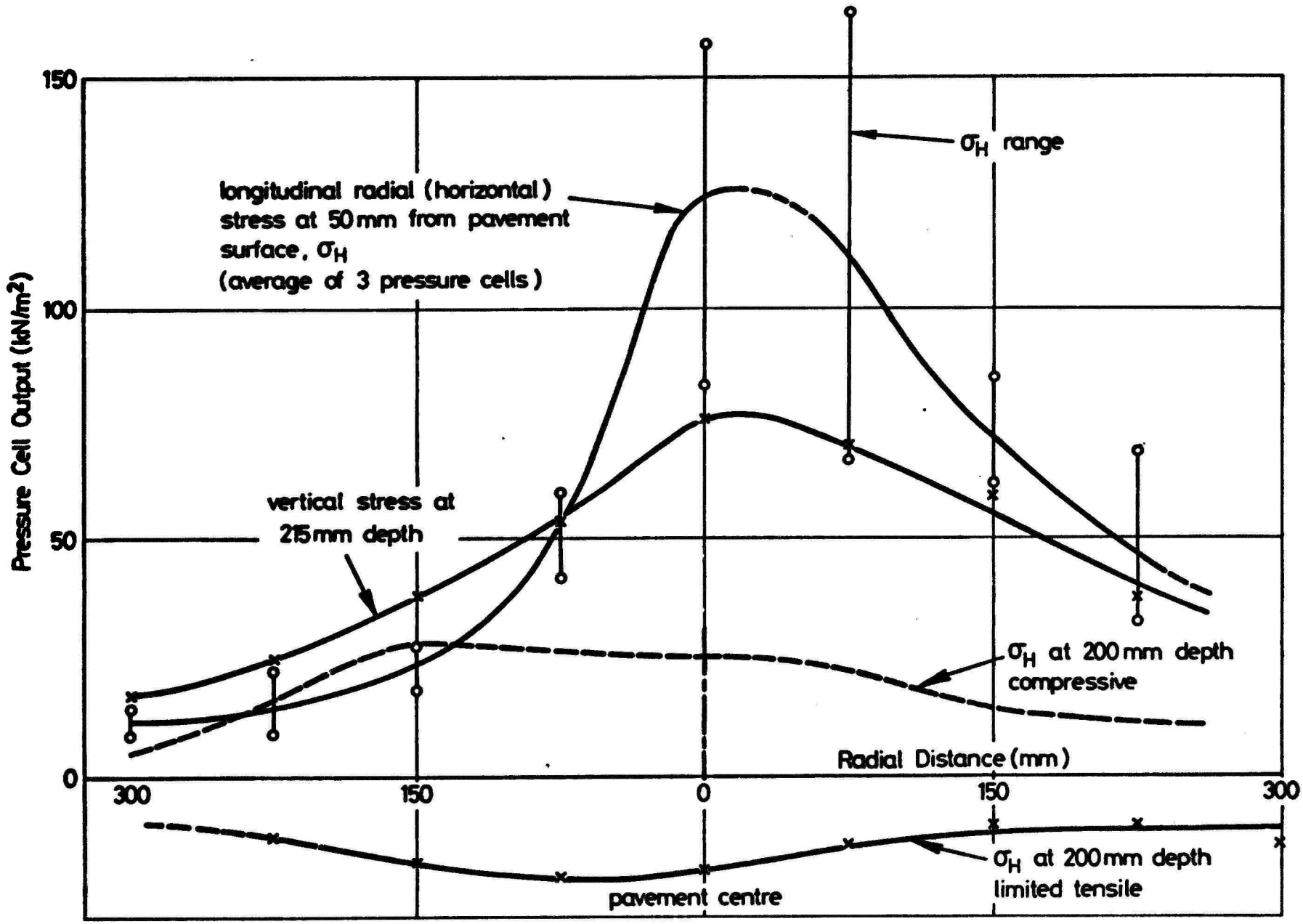

FIG. 5.24 VARIATION OF STRESS WITH RADIAL DISTANCE FROM PAVEMENT CENTRE (BITUMINOUS LAYER), PAVEMENT NO. 3

measurements are generally less reliable. The difference in the readings of horizontal stress in pavement 1 (Table 5.3) illustrates the need for at least three measurements of each parameter, and even this may not be conclusive as the results in the bituminous layer demonstrated.

5.7 PULSE SHAPES

Some typical pulses taken from high speed recorder traces are shown in Figs 5.25 and 5.26. The wheel load strain gauge bridge output is included for correlation purposes in both figures. The peaks on the wheel load traces are due to the position of the carriage reactive bearings about the strain gauges on the main beams and do not correspond to an increase in wheel load. The true value was obtained from the central section, arrowed in the figures, but the load level was constant over the location of the instruments. Phase differences between the peak readings of the instrument are a function of their position in relation to the wheel rather than a material effect, i.e. if the instruments were all vertically aligned, there would be little or no phase difference. However, pulse lengths did vary and these are shown to increase with depth. The readings from the pressure cells are to scale but this does not apply to the coils due to different sensitivity settings during the test.

Fig. 5.25a shows a slight tensile vertical strain response as the wheel approaches followed by the larger compressive pulse. The longitudinal strain at the interface (Fig. 5.25b) is initially compressive but the tensile response was slightly greater and this has been plotted on the elastic strain figures. The lateral strain was wholly tensile and the vertical strain in the subgrade (Fig. 5.25c) was wholly compressive.

The longitudinal radial stress pulse in the upper zone of the

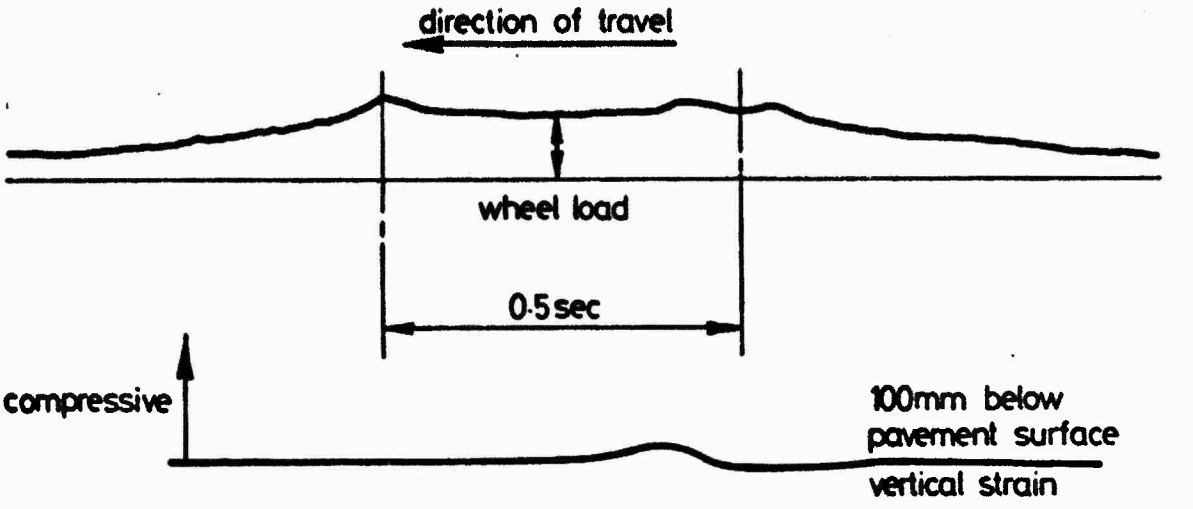

(a) Strain pulse in the bituminous layer

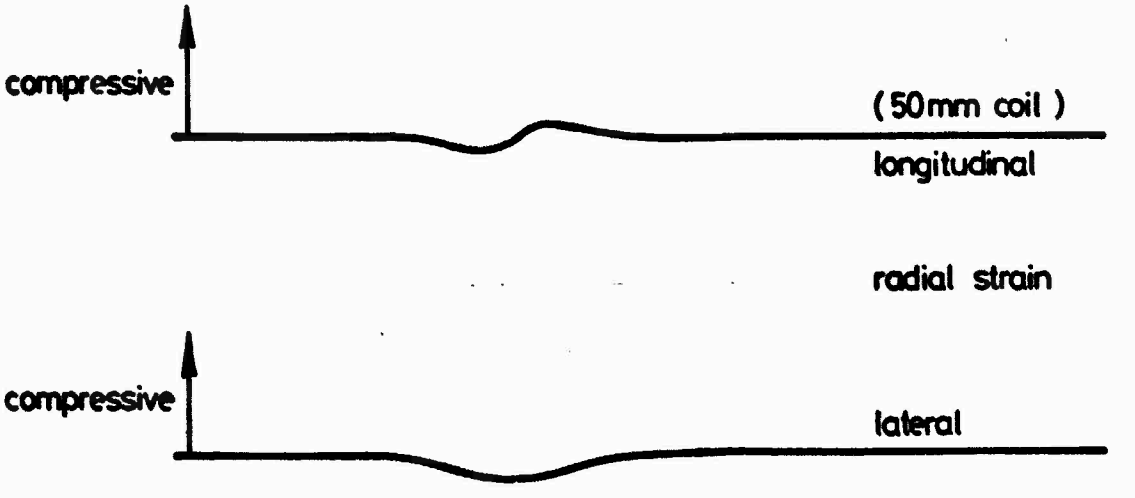

(b) Strain pulses at the interface

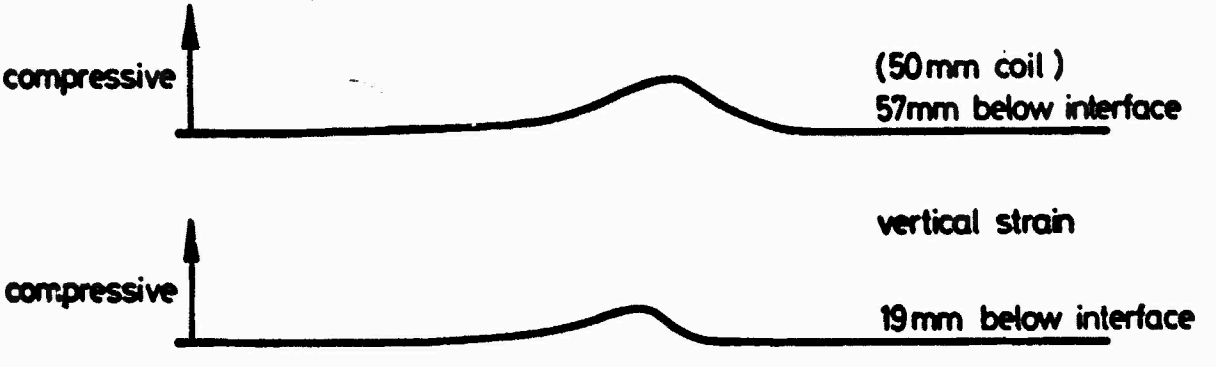

(c) Strain pulses in the subgrade

FIG. 5.25 RESPONSE OF STRAIN COILS, PAVEMENT NO. 3

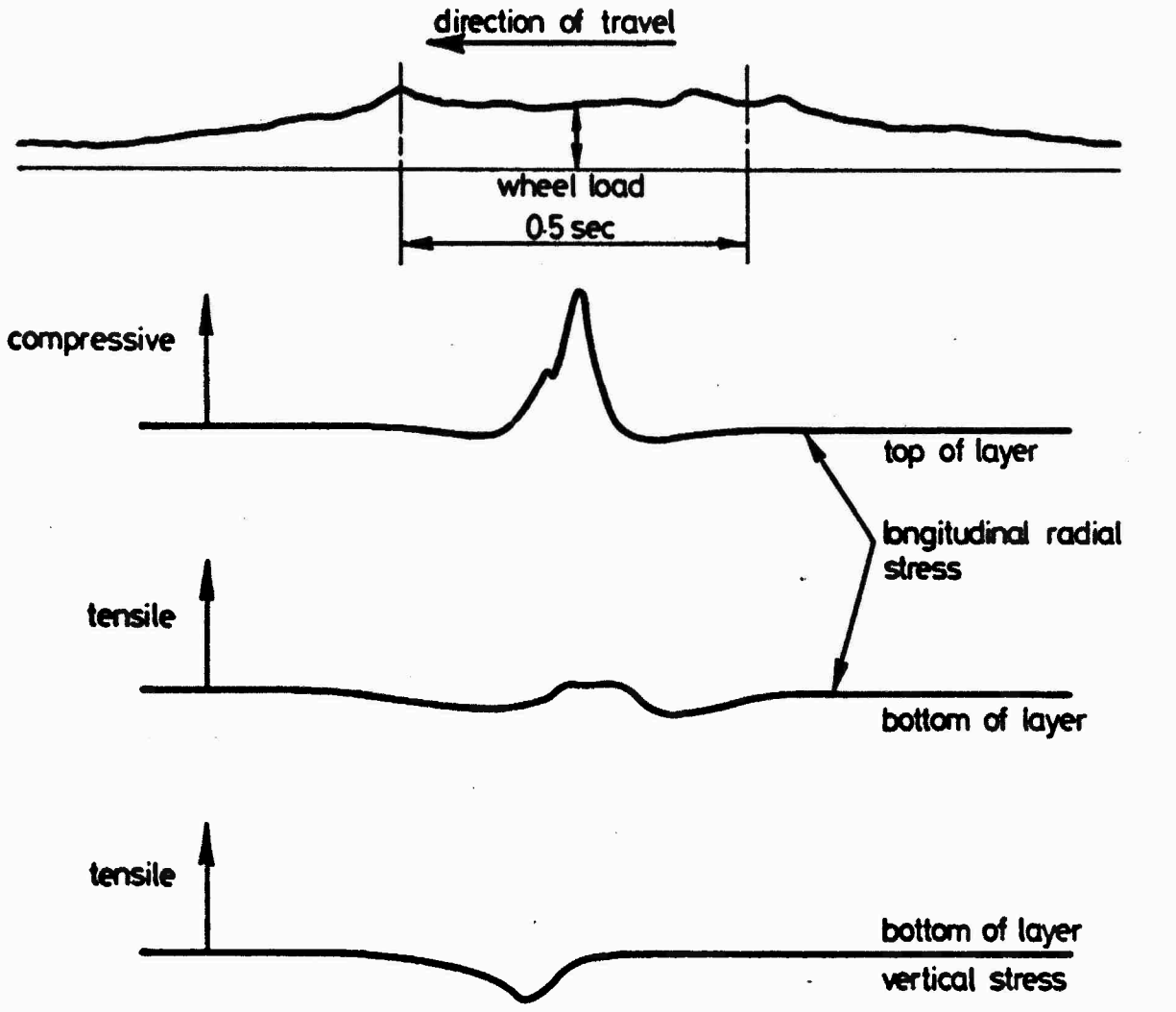

(a) Stress pulses in the bituminous layer

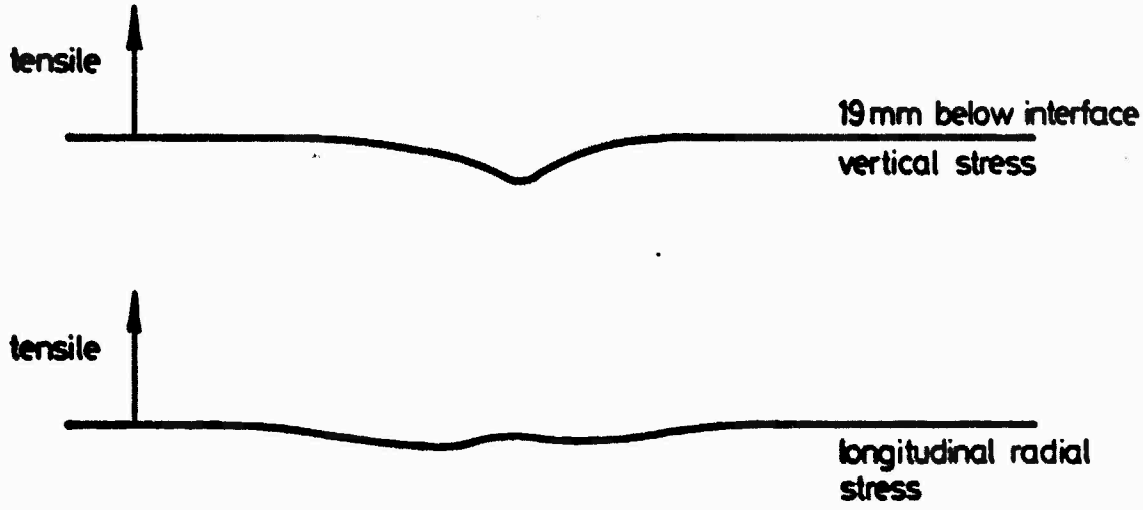

(b) Stress pulses in the subgrade

FIG. 5.26 RESPONSE OF PRESSURE CELLS, PAVEMENT NO. 3

bituminous layer (Fig. 5.26 a) was somewhat complex and consisted of an initial tensile output followed by an unsymmetrical compressive response and a smaller tensile output. The pressure cell at the bottom of the layer indicated compression initially followed by tension, but the pulse is truncated since the cells cannot follow a tensile situation. Stress measurements in the subgrade reveal compressive vertical stresses of long duration and compressive longitudinal radial strains which decrease when the wheel is directly over the cell.

5.8 PERFORMANCE OF THE INSTRUMENTS

One instrument which has not previously been mentioned in the results is the accelerometer. No prior experience had been gained with this instrument and it was introduced as an exercise to determine transient surface deflection under the moving wheel. Initially, a ± 2 g servo type accelerometer (Section 3.3) was used in pavement 2. This was somewhat insensitive and required increased amplification to detect the acceleration signal which was in the region of 0.1 g. Consequently, inherent d.c. drift became significant and the two integrating amplifiers were difficult to balance. A more sensitive accelerometer required a bias circuit to compensate for the effect of gravity on the sensing element as this would inevitably cause the servo system to lock at one end of its range. Unfortunately, the cost and delivery of a new instrument was excessive and so an attempt was made, in pavement 3, to use a piezo-electric accelerometer which was available and of sufficient accuracy.

This was expected to operate below its full potential output as the acceleration pulse was not of the repeated sinusoidal form normally required to maintain the charge across the internal sensing element.

To work successfully, the pulse had to be repeatable in terms of rise, decay and length and it was essential for the accelerometer to be calibrated by creating an identical movement to that experienced by the pavement surface. This was attempted with a vibrator and waveform generator and eventually an acceptable pulse was obtained. Unfortunately, drift still occurred despite the increased signal level and reduced amplification. A commercially available amplifier was then tried which had an internal self zeroing circuit and was extremely stable in the acceleration mode at almost d.c. level. However, when switched to the displacement mode the generating principle of the double integrator again required a sinusoidal input and the response to a deflection pulse of constant magnitude, although stable, varied with pulse duration.

During testing, outputs were obtained on a storage oscilloscope using the manual zeroing facilities on the original double integrator (11). This proved extremely difficult and hence successful readings were not obtained. It was concluded that a very sensitive servo accelerometer of a very high mechanical quality with regard to balance and bearings was necessary to measure deflection.

The strain coils made at Nottingham in their present state are unsatisfactory for in situ pavement experiments since they are insufficiently robust. Modification to the cable connection and improvements to the winding technique would be necessary before using them in pavements. Full advantage was not taken of the sensitivity of the Bison coils in order to prevent overcrowding on the U.V. recording paper and this limited the accuracy of the elastic readings. Furthermore, calibration at low levels of strain is difficult and practical micrometer movements were limited to the equivalent of 70 microstrain.

A peak reading digital voltmeter or a storage oscilloscope with potentiometric voltage measuring facilities would be of considerable advantage for the evaluation of low strain levels. Again, it must be emphasised that the ultimate accuracy depends on the success of the installation and a series of calibrations in specimens of the in situ material is recommended particularly if carrier blocks are to be used. The experience gained in using the strain coils in these pavement experiments has been of immense value and this culminated in a satisfactory set of readings for pavement 3.

The more comprehensive information for the strain gauge measurements of pavement 1 was attributed to the protection of the vertical gauges and the use of three strain gauge pairs to measure longitudinal and lateral strain. A high proportion of failures severely limited the readings for pavements 2 and 3. In all cases, the gauges survived the compaction of the bituminous layers from the point of view of electrical continuity. Approximately half the gauges for all pavements required substantial rebalancing when the bridge voltage was applied and it was these gauges which failed at early stages of the test. This indicated the application of relatively large strains during compaction and some gauges examined after testing were considerably distorted. Another difficulty arose over supporting the unstressed DBM block, carrying the dummy gauges at 30°C. This tended to disintegrate particularly as the air temperature was above 30°C and it was necessary to wedge the block in a hole cored in the pavement.

Despite such problems the gauges which survived were very stable and sensitive. The vertical gauges in all cases require careful alignment and accurately cut carrier blocks are necessary to establish satisfactory external references for judging the gauge verticality.

Positioning of the horizontal gauges is also important, but is perhaps easier to assess. If the gauges are combined on a block as sandwiches, then external markings are required as reference for correct positioning.

It is felt that incorporating strain gauges in bituminous materials requires time, practice and calibration tests in specimens of the material. If this can be accomplished, then considerable information on elastic strains can be collected if several duplicate readings are obtained.

The d.c. soil strain cell exhibited an intermittent electrical fault throughout the tests and this proved difficult to trace between pavement installations, although initial calibration was satisfactory. On completion of the programme the instrument was dismantled and the encapsulated electronics in the base were exposed. This revealed trapped moisture and some decomposition of components, which may have been due to some chemical reaction with the brass body. A higher output was obtained from the a.c. strain cell compared to the elastic strain recorded by the coils. This may have been due to a rather insensitive sensitivity control on the external carrier system or a weak pocket of soil around the instrument.

The pressure cells functioned satisfactorily, particularly for pavement 3 and seemed entirely suitable for the clay subgrade used in these tests. Previous calibrations have been carried out on this material and installation is relatively straightforward. Calibration tests in bituminous specimens are at present underway and at this stage appear to indicate a decrease in registration with increasing stiffness as found in soils. The lack of information on the use of this cell in bituminous materials must be considered for the pavement 3 readings and these should only be treated as a guide to the stress levels at this stage.

CHAPTER SIX

THEORETICAL ANALYSIS

6.1 INTRODUCTION

The basic approach which has been used is similar to that suggested by Romain (14) and Barksdale (15). This involves a linear or non-linear elastic analysis of the pavement to determine the stress distribution over a network of elements. The vertical permanent strain in each of these elements is then predicted from results of repeated load testing on laboratory specimens of the pavement materials. Subsequent integration of permanent strain with depth gives the permanent deformation at the pavement surface.

6.2 PRELIMINARY CALCULATIONS

An estimate of the resilient properties of the two pavement materials was used to calculate a preliminary stress distribution for the first pavement, on the basis of which a provisional test programme was devised. Subsequent testing produced measured values of the resilient properties, which were then used to check whether the programme was adequate.

6.3 THEORY OF STRESS INVARIANTS

A rigorous prediction of permanent deformation depends on the ability to predict the permanent strain in all elements of the pavement within a reasonable distance of the wheel load.

Fig. 6.1 indicates that the repeated load triaxial test can exactly simulate in situ stress conditions on the axis of symmetry of the wheel load, except near the bottom of a bituminous layer where the two horizontal stresses become tensile. One approach to the prediction of

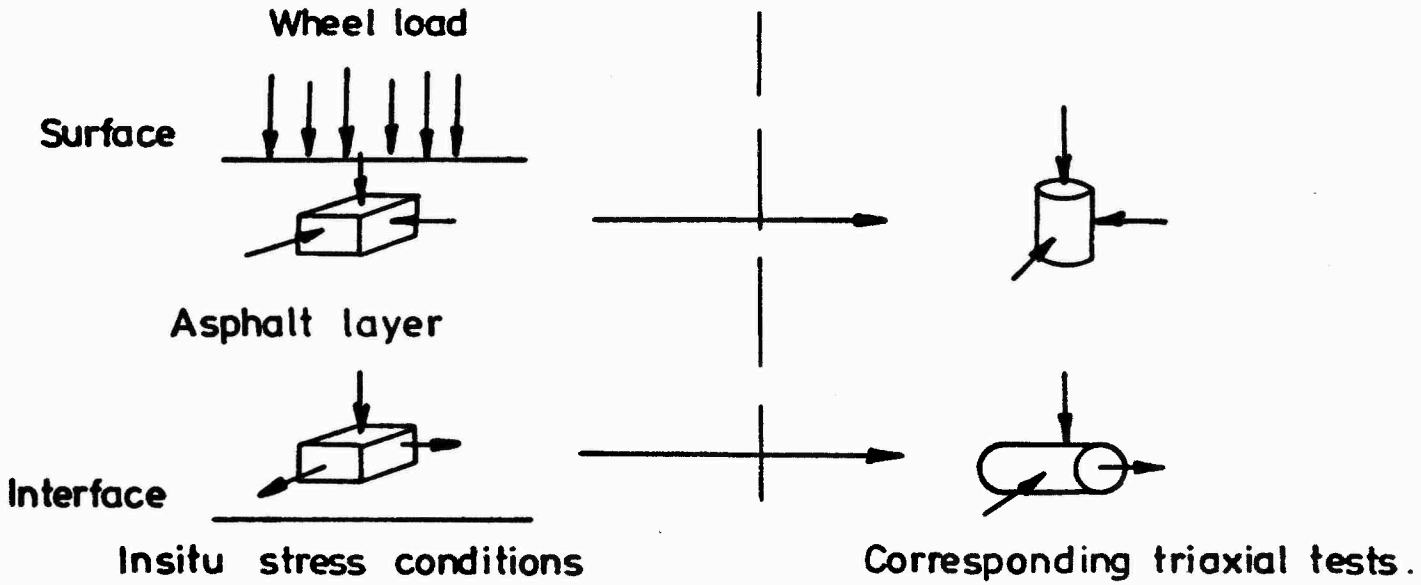

FIG. 6.1 COMPARISON OF IN SITU AND TRIAXIAL STRESS CONDITIONS

permanent strains in this location is illustrated in Fig. 6.1 in which the radial strain on the test sample is taken to be the in situ vertical strain. However, this approach is only approximate since only one tensile stress is applied.

For locations off the axis, all three principal stresses differ and some assumptions need to be made for utilisation of the results from repeated load triaxial tests.

Use of the stress invariants mean normal stress (p) and deviator stress (q) has been suggested by Brown (3) and Brown and Bell (5) to partially overcome these problems. The approach is based on the assumption that permanent strain depends on the levels of shear and normal stress applied to the element causing shear distortion and volume change.

These stress invariants are defined in terms of the three principal stresses as follows:

$$p = \tfrac{1}{3}(\sigma_1 + \sigma_2 + \sigma_3) \qquad (6.1)$$

$$q = \frac{1}{\sqrt{2}}\sqrt{[(\sigma_1 - \sigma_2)^2 + (\sigma_2 - \sigma_3)^2 + (\sigma_3 - \sigma_1)^2]}$$

$$= \frac{3}{\sqrt{2}} \cdot \tau_{oct} \qquad (6.2)$$

where σ_1, σ_2, and σ_3 are the principal stresses and τ_{oct} is the octahedral shear stress. Under conditions of axial symmetry, as occur in the triaxial test, $\sigma_2 = \sigma_3$:

and hence: $$q = (\sigma_1 - \sigma_3) \qquad (6.3)$$

i.e. the deviator stress.

Measurements of permanent vertical and radial strains accruing in the repeated load test enable strain invariants to be computed. These

are volumetric strain (v) and shear strain (ϵ) defined as:

$$v = \epsilon_1 + \epsilon_2 + \epsilon_3 \tag{6.4}$$

$$\text{and } \epsilon = \frac{\sqrt{2}}{3}\sqrt{[(\epsilon_1 - \epsilon_2)^2 + (\epsilon_2 - \epsilon_3)^2 + (\epsilon_3 - \epsilon_1)^2]} \tag{6.5}$$

where ϵ_1, ϵ_2 and ϵ_3 are the principal strains. The coefficient of the shear strain term has again been chosen to suit the triaxial situation where $\epsilon_2 = \epsilon_3$ and hence:

$$\epsilon = \tfrac{2}{3}(\epsilon_1 - \epsilon_3) \tag{6.6}$$

The relative contributions to in situ vertical permanent strain of the shear and volumetric components will depend on the initial compaction of the material. Hence, a poorly compacted mix will undergo volume change and shear distortion, while a well compacted mix will undergo mainly shear distortion.

Ideally, the solution of equations (6.4) and (6.5) would yield values of the principal strains from which a value for the in situ vertical permanent strain could be calculated, and subsequently used to predict permanent deformation. However, there are three unknowns and only two equations, and therefore some simplifying assumption has to be made. The approach adopted in this work was to assume that the in situ permanent vertical strain is equal to the major principal strain in the repeated load test. This is likely to err on the safe side for design purposes.

6.4 LINEAR OR NON-LINEAR ANALYSIS

Initially, linear elastic analysis was used to calculate stress distributions. It was thought that this would be adequate, since previous investigators (16) had found that, provided the resilient modulus and Poisson's ratio were carefully selected, agreement was

obtained with in situ measurements, although this conclusion seems less certain under high temperatures (17).

Results from the characterisation tests showed that the dense bitumen macadam was markedly non-linear, particularly when a tensile stress was applied, and the Keuper marl showed non-linearity typical of a cohesive soil. It was, therefore, decided to adopt a non-linear analysis and to use the finite element computer programme DEFPAV (18). This programme has the added advantage of calculating permanent deformations from "creep-equations" selected by the user from those already existing in the programme, or from the results of independent tests. In this case, the calculations were based on equations derived from the material characterisation tests. The development of these equations is described in Chapter 9.

CHAPTER SEVEN

MATERIALS CHARACTERISATION TESTS

7.1 INTRODUCTION

Both pavement materials were characterised using electro-hydraulic servo-controlled testing machines, which had been previously developed at Nottingham (19, 20, 21). 100 mm diameter cores of Keuper marl were taken prior to the laying of each DBM layer, and 100 mm diameter DBM cores were taken several days after the completion of paving.

The majority of tests carried out on the DBM were on cores from pavement 1. A few DBM cores from the two subsequent pavements, which incorporated nominally the same material, were tested for comparison with that used in pavement 1. All the tests were conducted at 30°C, the temperature of the pavement experiments.

The majority of tests for the Keuper marl were carried out on cores taken in between the testing and excavation of pavement 1 and the laying of the DBM for pavement 2. A number of cores had been taken before the paving of pavement 1 and stored in latex rubber membranes, but these leaked severely, causing the cores to dry. Subsequent cores were sealed in wax before they were stored. A few cores were taken following the excavation of pavement 2 and were tested for comparison with the previous tests.

7.2 DENSE BITUMEN MACADAM

7.2.1 Introduction

The test conditions were based on the results of a linear elastic analysis of pavement 1 and they are shown superimposed in the complete p, q plot for in situ conditions in Fig. 7.1. Once tests had been

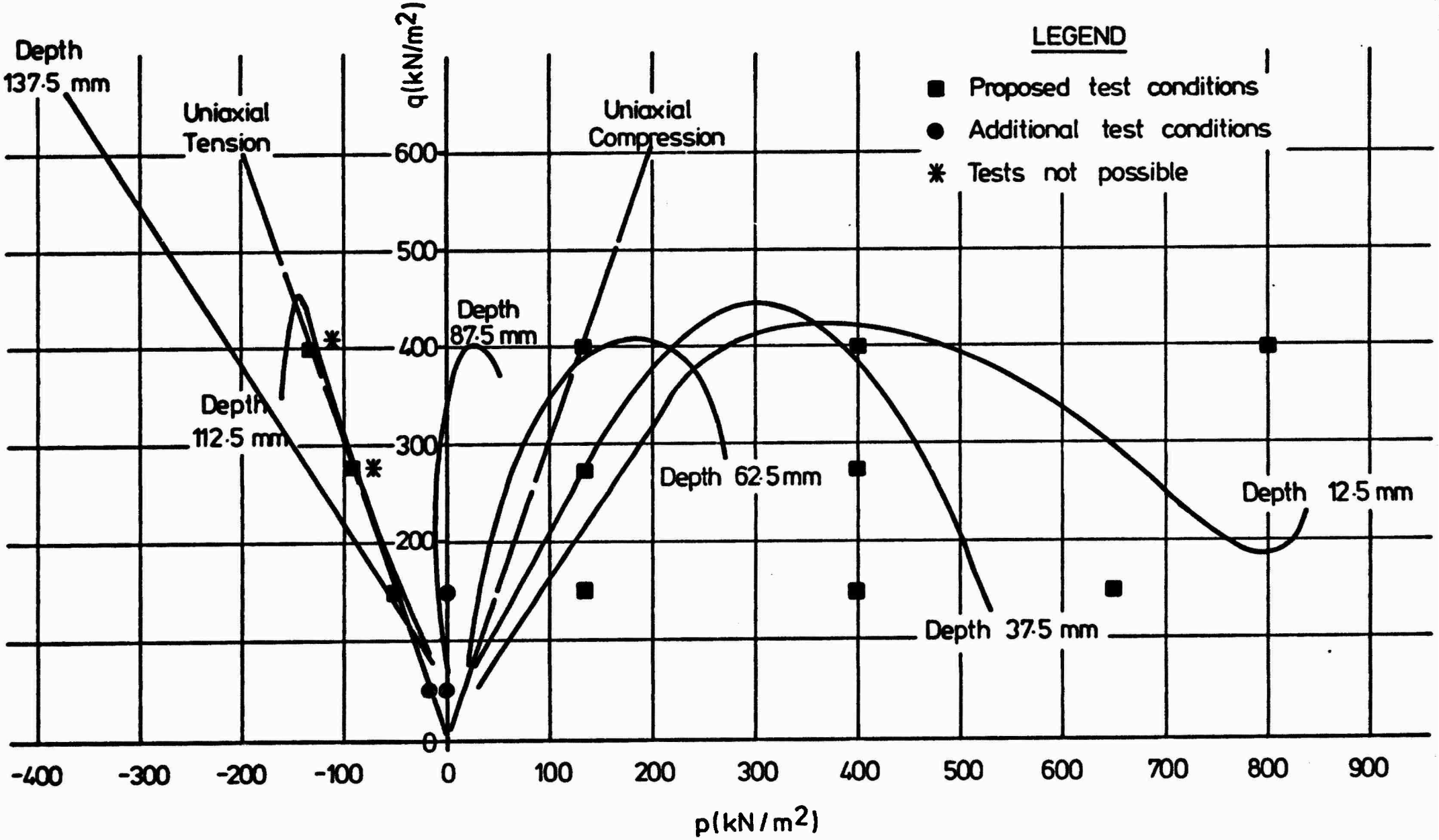

FIG. 7.1 STRESSES IN THE DBM (PAVEMENT NO. 1) BY LINEAR ELASTIC THEORY, WITH LABORATORY TEST CONDITIONS

completed at several of these stress conditions, it became apparent that the material exhibited considerable non-linearity. A non-linear analysis was therefore carried out using the results of these tests to check that the original test conditions would cover this new stress distribution. It was found necessary to add only two more test conditions. The non-linear analysis based on the results of the complete test programme for pavement 1 is shown in Fig. 7.2.

Lines representing uniaxial compression and uniaxial tension are shown in Figs 7.1 and 7.2, having slopes of +3 and -3 respectively*. Tests carried out at any point on one of these lines requires no confining pressure, only a compressive or tensile axial stress respectively. Points to the right of the uniaxial compression line require axial compression plus confining stress (compression tests), and points between the uniaxial compression and tension lines require axial tension plus confining stress (tension tests). The uniaxial tension line represents the limit which can be reached in a triaxial test, i.e. consider the mean normal stress:

$$p = \tfrac{1}{3}(\sigma_1 + 2\sigma_3)$$

$$\text{if } \sigma_3 = 0, \quad p = \sigma_1/3 \quad \text{and} \quad q = \sigma_3 - \sigma_1$$

(for a situation where σ_1 is tensile and σ_3 compressive)

$$\therefore \quad q = -\sigma_1 \quad \text{and} \quad p = -q/3$$

No test condition to the left of the uniaxial tension line can be represented by a triaxial test. However, particularly judging by the

---

* This representation ignores the effect of the third stress invariant and follows the approach suggested by Brown (36).

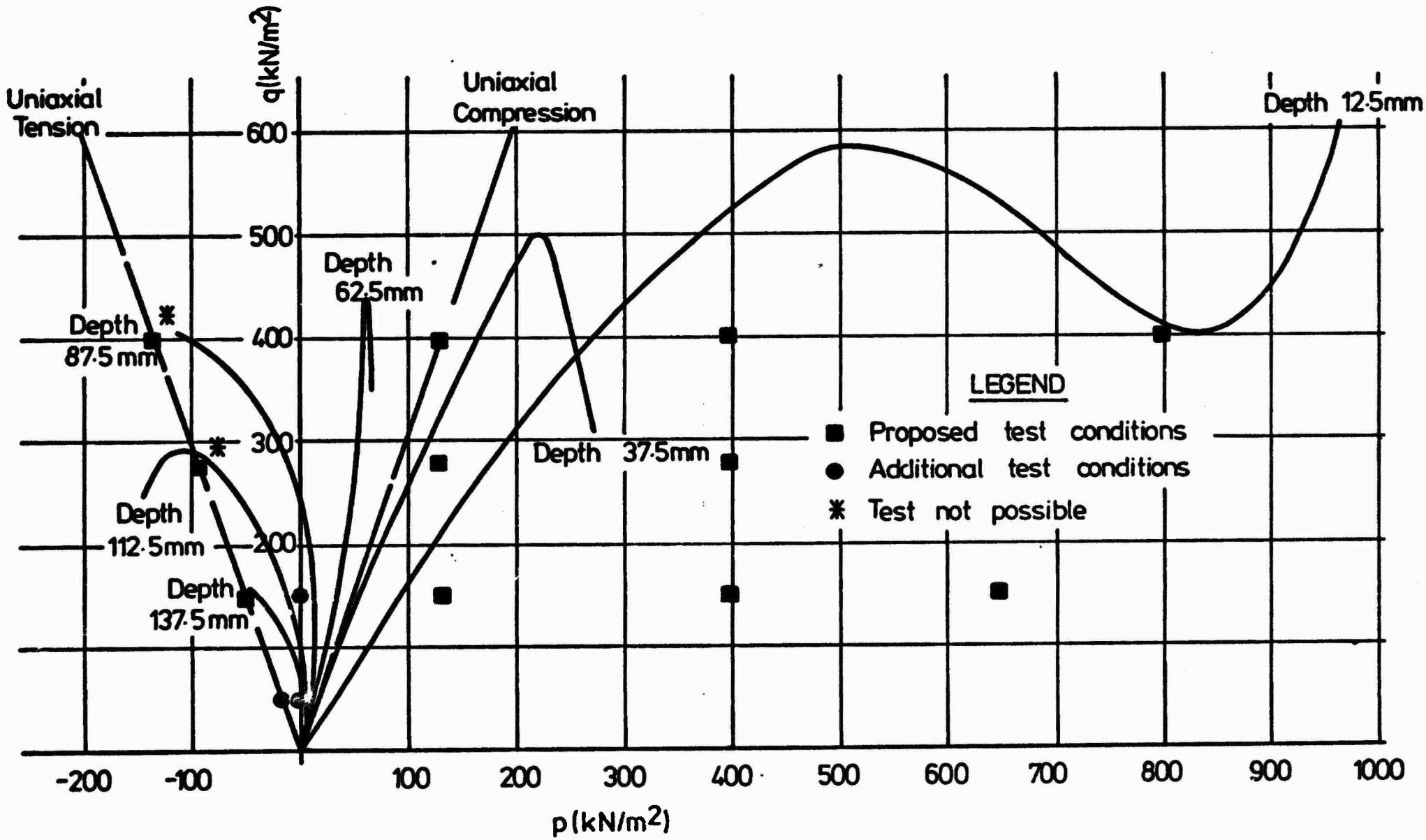

FIG. 7.2 STRESSES IN THE DBM (PAVEMENT NO. 1) BY NON-LINEAR ELASTIC THEORY, WITH LABORATORY TEST CONDITIONS

non-linear analysis (Fig. 7.2) this represents a very small portion of the tension zone in the bituminous layer.

When testing at a particular combination of p and q, which did not lie on either the uniaxial tension or compression lines, a problem arose in selecting the suitable stress path. This was due to the fact that facilities for applying a cyclic confining stress were not available. This meant that the only fluctuation of p would be due to the vertical cyclic stress, and the stress paths would be restricted to lines parallel to either the uniaxial compression or tension lines.

Previous testing of a nominally identical mix by Brown and Snaith (22) indicated that similar permanent strains were obtained in tests with constant and cyclic confining stresses, when the constant value equalled the mean of the cyclic one.

Consequently, the combinations of constant confining stress and vertical cyclic stress were chosen on this basis, as illustrated in Fig. 7.3 for p = 400 kN/m^2 and q = 400 kN/m^2.

7.2.2 Test Programme

The test conditions shown in Figs 7.1 and 7.2 were selected on the basis of analyses of pavement 1 and although it was expected that analyses of pavements 2 and 3 would produce somewhat different stress distributions, the same basic framework was used for all three pavements so that comparisons would be simplified.

Loading frequency: The majority of tests were carried out with continuous sinusoidal loading at a frequency of 1 Hz, rather than at a frequency corresponding to the loading in the pavements. This was used for convenience, since Brown and Snaith (22) found that within a frequency range which included 1 Hz, the permanent deformation was dependent on the

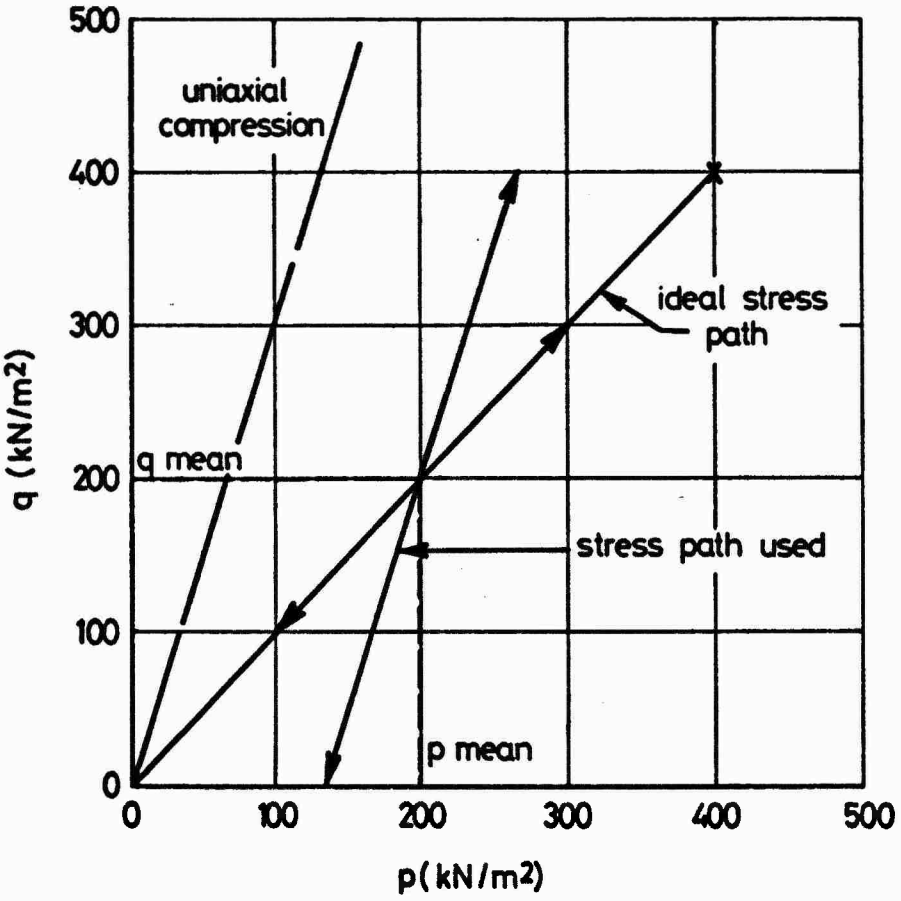

FIG. 7.3 TYPICAL STRESS PATH FOR THE DEM TESTS

total time of loading, rather than the frequency and number of load applications.

Some tests were carried out at a frequency of 3.3 Hz with a 2 second rest period between each stress pulse. This corresponded to a computed loading time for pavements 1 and 2, where the known elapsed time between the wheel passing a particular point was 2 seconds. The frequency was calculated by reference to Barksdale (23), which gave a principal stress pulse time (t_B) of 0.20 seconds at the centre of a 150 mm thick pavement layer, and to Brown (24) who stated that the average loading time was 1.5 t_B. This gave an average stress pulse time of 0.30 seconds, corresponding to a frequency of 3.3 Hz.

Pavement 1: A total of 24 vertical cores were taken from pavement 1 and these were primarily used for compression tests. Initially, four cores were used for compression tests where the end platens were glued to the core, so that the specimen could be bolted into the testing machine. This procedure was adopted so that there would be compatibility between tension and compression tests. However, the cores used in these tests were found to barrel very badly, and it was decided to adopt the more conventional lubricated ends for compression tests (Snaith (25)).

Three tension tests were carried out with vertical cores, but these proved unsuccessful, since the cores fractured along one of the interfaces which had been formed during compaction. It was, therefore, decided to supplement these vertical cores with laboratory manufactured specimens of the same mix, compacted, in moulds to the same void content. Following completion of testing on pavement 1, the DBM was sawn into slabs, and horizontal cores were taken from untrafficked sections.

The manufactured specimens were used for tension testing (10 specimens), and also for an investigation to compare the effects of loading at a frequency of 1 Hz and a frequency of 3.3 Hz with a 2 second rest period (4 specimens). The horizontal cores were also used for tension tests (10 cores), and for an investigation to check the isotropy of the material (3 cores). Some of the horizontal cores used for tension tests were tested at 3.3 Hz with a 2 second rest period. This ensured better control of the test, which was of short duration when continuous loading at a frequency of 1 Hz was used.

Pavement 2: Thirteen vertical and eight horizontal cores were taken from pavement 2. However, because of the high void content of the mix used for this pavement, these cores were of poor quality. It was found that, after storing them at room temperature for only a few days, the majority had deformed under their own weight. Therefore, of the remainder, two cores were tested at one test condition ($p = 133$, $q = 275$ kN/m^2, Figs 7.1 and 7.2) so that a comparison could be made with results from the same test condition on samples from pavement 1. An additional core was used to carry out an investigation of the resilient properties of the mix, by testing for a few cycles at values of p and q covering most of the range for compression tests. Frequencies of 1 Hz and 3.3 Hz with a 2 second rest period were both used.

Pavement 3: The same general approach was used as for pavement 2 in order to minimise testing. Three cores were tested at $p = 133$, $q = 275$ kN/m^2 (Figs 7.1 and 7.2), and one was used to determine the resilient properties of the mix, at both 1 Hz and 3.3 Hz with a 2 second rest period. A summary of the entire test programme is presented in Table 7.1.

Table 7.1 Summary of Test Programme

Test Series	Description of tests carried out
C1	The main series of compression tests on vertical cores from pavement 1.
TV1	Tension tests on vertical cores from pavement 1 and laboratory manufactured specimens of the same mix and void content.
TH1	The main series of tension tests on horizontal cores from pavement 1.
CR1	A supplementary series, on laboratory manufactured specimens to investigate the effect of using the in situ loading frequency (3.3 Hz) with a 2 second rest period.
I1	A supplementary series to investigate the isotropy of the material from pavement 1.
C2	Compression tests on vertical cores from pavement 2.
C3	Compression tests on vertical cores from pavement 3.

7.2.3 Specimen Preparation

Each core was trimmed with a diamond tipped cutting blade so that the ends were perpendicular to the longitudinal axis and the length was approximately 125 mm. For compression tests the cut ends were polished on the side of an abrasive cutting blade. Before the cores were tested, they were weighed in air and water, for void content determination, and after testing, a portion of some cores was used for binder content analysis.

Three pairs of locating pips, for the strain measuring devices, were glued with epoxy resin to the core using a specially prepared jig for accurate positioning. The pips can be seen in position in Fig. 7.4. The top and bottom pairs were used to locate the LVDT's for longitudinal measurements, over a gauge length of 75 mm, and the middle pair was used

FIG. V.4 A SPECIMEN WITH LOAD LOCATING PIPS, AND END PLATENS ATTACHED

to locate a lateral strain collar incorporating another LVDT. If a confining pressure was to be applied in the test, a neoprene rubber membrane was placed over the core.

For compression tests a pair of steel end platens were employed with finely machined surfaces. The contact between the polished ends of the core and the end platens was via two thin latex rubber discs the same diameter as the end platens, which were lubricated with silicone grease. This ensured that the core would deform in the shape of a right cylinder.

For tension tests, the ends of the cores were glued to loading platens (shown in Fig. 7.4) using epoxy resin. The core could then be bolted in place in the testing machine as shown in Fig. 7.5.

7.2.4 Testing Equipment

Electro-hydraulic servo-controlled testing machine: The machine, shown in Fig. 7.5, had been developed for fatigue testing of bituminous materials (21, 26) using a similar test configuration to that adopted for the tension tests. For compression tests the specimen, complete with end platens, was placed on the bottom loading flange, and was loaded via a ball bearing below the top of the upper loading flange. This arrangement is shown in Fig. 7.6.

The hydraulic ram applied a repeated load to the specimen, which could be either unconfined or have a constant confining stress applied by air pressure. The pressure was maintained within a triaxial cell (shown in position in Fig. 7.5) which was raised above the specimen when not in use, as in Fig. 7.6. The cell pressure was monitored by a pressure gauge situated just outside the cell.

Deformation measurement: Longitudinal deformation was measured with

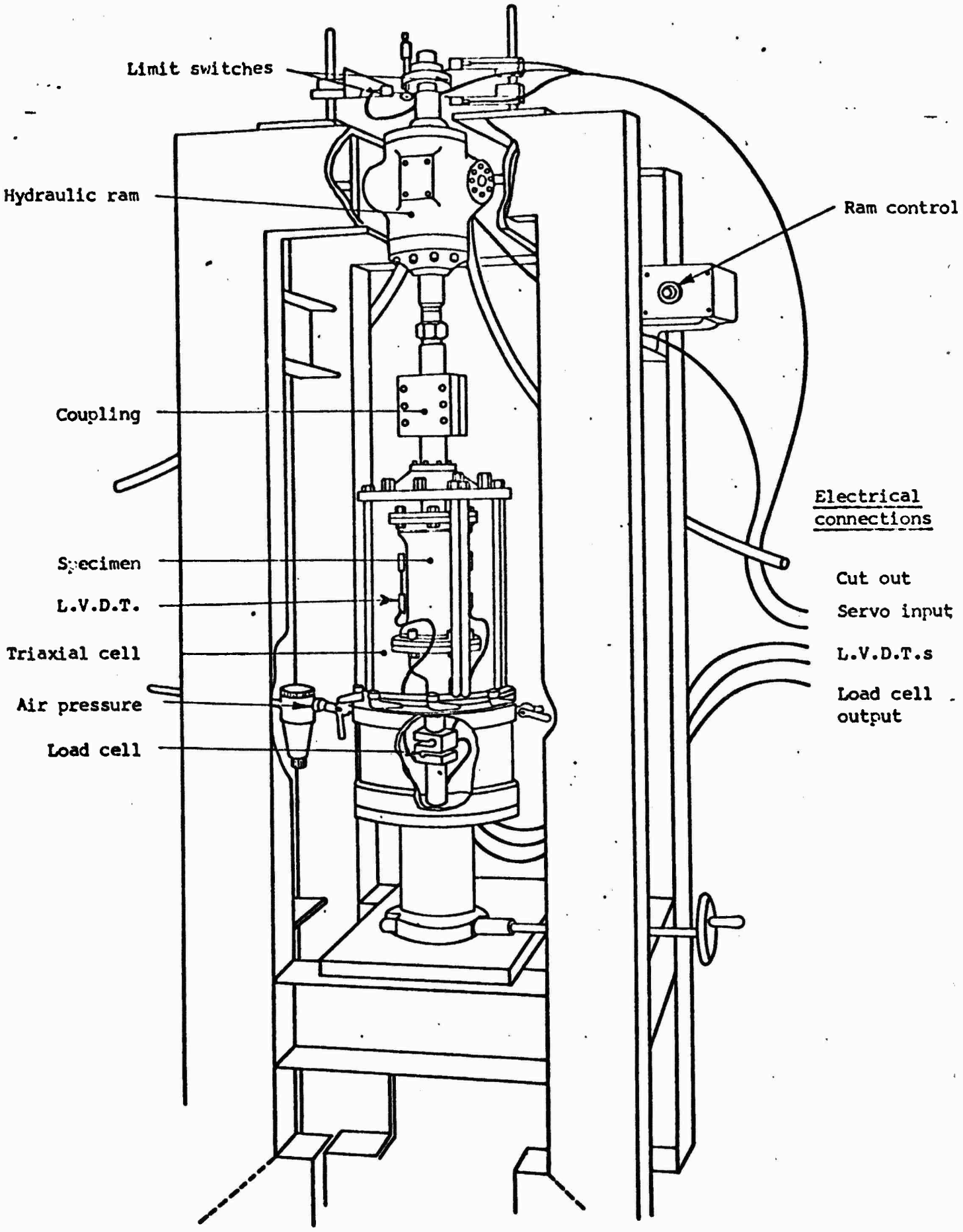

FIG. 7.5 ELECTRO-HYDRAULIC SERVO-CONTROLLED TEST MACHINE FOR TESTING ASPHALTIC MATERIALS

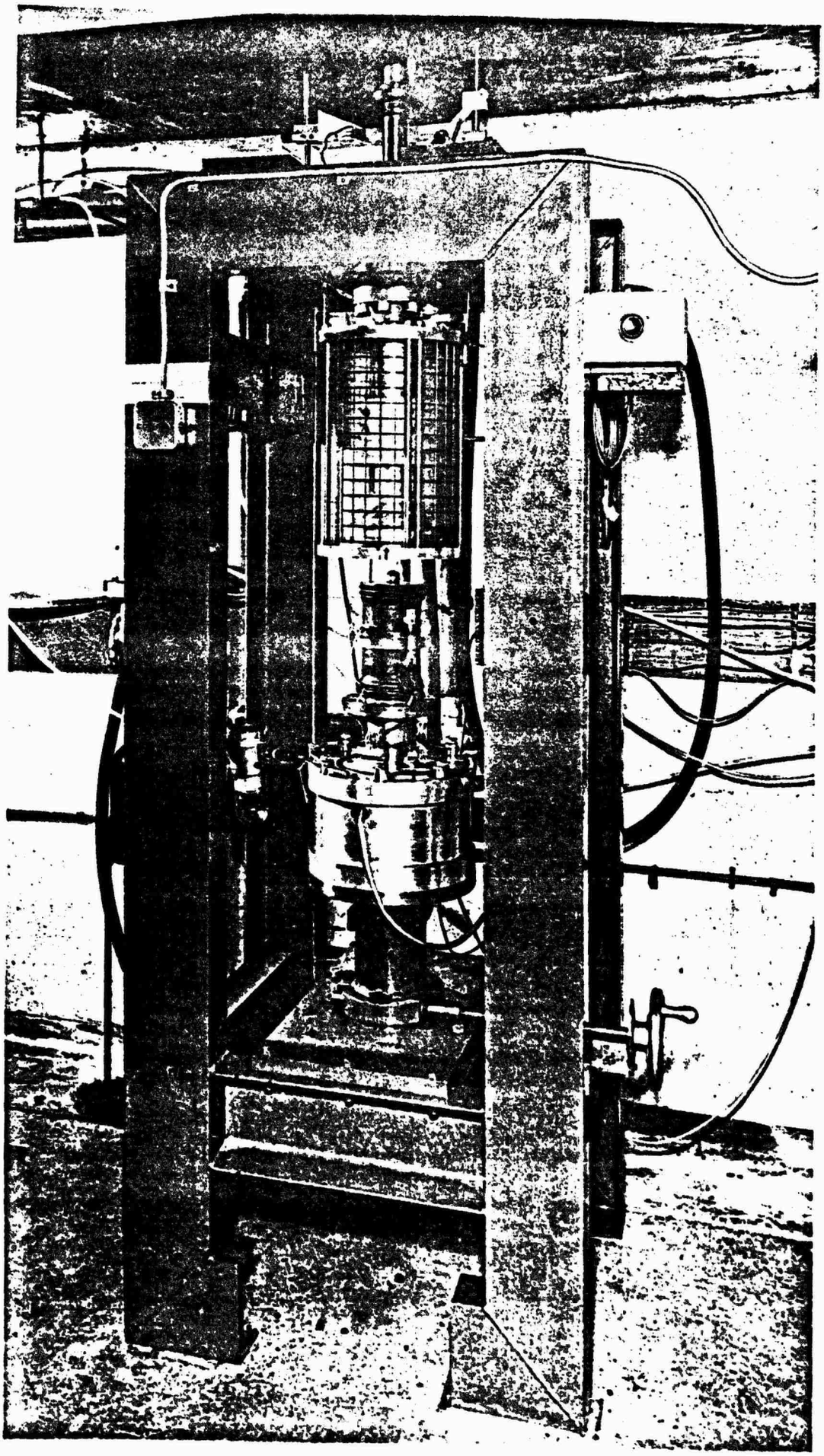

FIG. 7.6 A DBM SPECIMEN SHOWN IN POSITION IN THE TESTING MACHINE

two diametrically opposed LVDT's, over gauge lengths of 75 mm, about the mid-height of the specimen. The LVDT's were fitted across these gauge lengths by screw-fittings to the locating pips, as shown in Fig. 7.7. Thus the measurements were taken away from the areas which could be subject to end effects.

Radial deformation was also measured by an LVDT mounted across the jaws of a hinged strain collar of the type described by Brown and Snaith (27) located on two diametrically opposed targets at the centre of the specimen as shown in Fig. 7.7. As the specimen expanded or contracted laterally, the gap between the free ends of the collar changed and this change was measured by the LVDT.

The monitoring devices which were employed are described within the following section.

7.2.5 Testing Procedure

All tests were carried out at 30°C, the same temperature as the pavement experiments. Prior to testing, each specimen was left in the temperature controlled room, which housed the testing machine, for at least 24 hours, to ensure uniform temperature conditions.

Three monitoring devices were used to provide a visual check on the outputs from the load cell and LVDT's. These were a Digital Voltmeter (DVM), an Ultra Violet (UV) recorder, and a Cathode Ray Oscilloscope (CRO), all of which are shown in Fig. 7.8, together with the control equipment for the testing machine and the LVDT's. The load cell and LVDT's had been calibrated using both the DVM and UV recorder, and as these were both used to record the response of a specimen under test, cross checking of measurements was possible. However, the UV recorder was favoured because of the ability to record simultaneously the outputs from the load cell and the LVDT's.

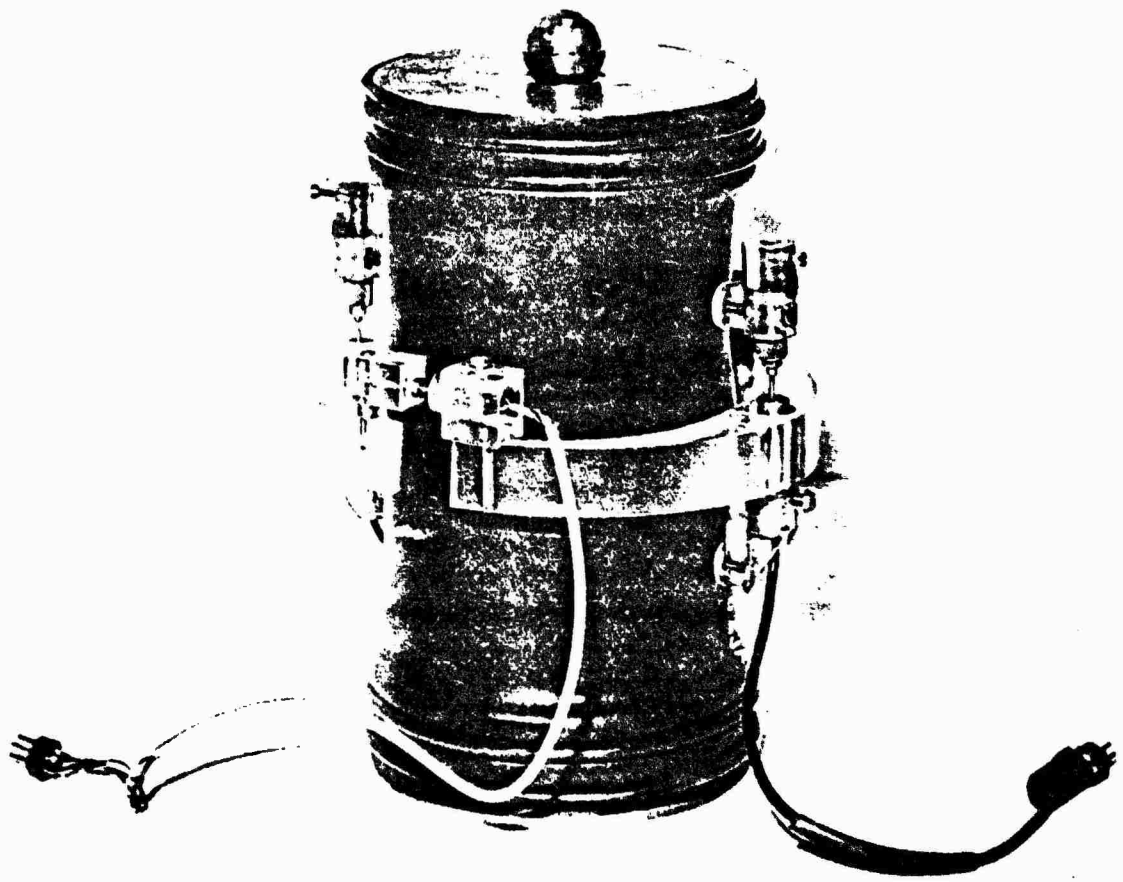

FIG. 7.7 A DBI SPECIMEN WITH LVDT's ATTACHED

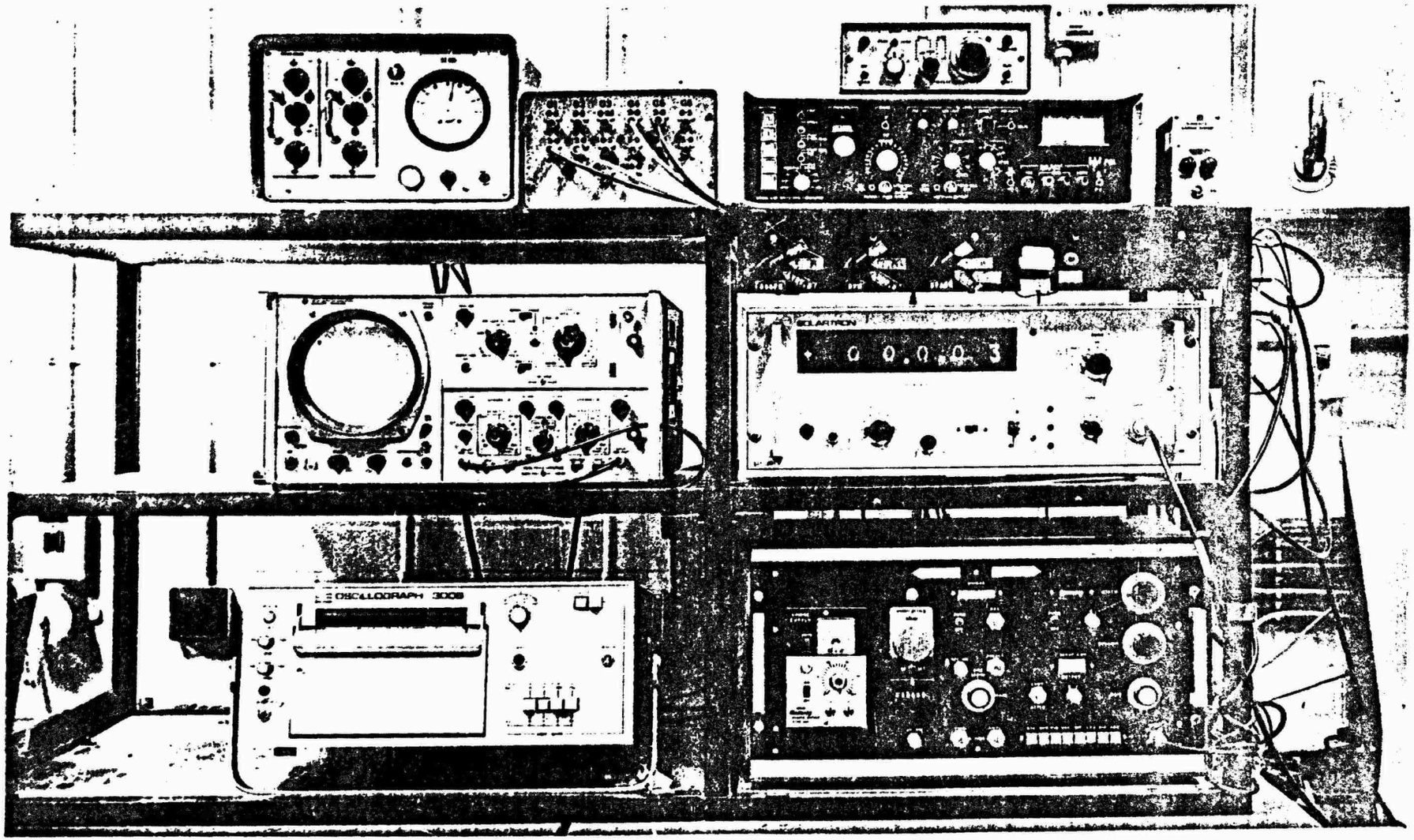

FIG. 7.3 MONITORING AND CONTROL EQUIPMENT FOR DBM TESTS

Each test was continued for either 100,000 cycles, or until excessive deformation had occurred and the core responded erratically, or, in the case of a tension test, when fracture of the specimen had occurred.

7.2.6 Results

Processing: The behaviour of a specimen during a test was recorded on the oscillograph paper, and occasionally, a reading was taken from the DVM. The outputs could, in general, be processed by hand during the course of a test, parallel with the necessary control of the test machine.

At frequent intervals of time, the vertical and radial permanent and resilient strains were computed from the measured deformations. The vertical deformation from each vertical LVDT was monitored separately, and an average value used unless one was obviously in error, a phenomenon which could occur if a locating pip became loose. The resilient modulus and Poisson's ratio were computed from the resilient strains, and were used to check and update the values used in the elastic analyses.

From this information a table of results and graphs of the material behaviour were constructed. For those test conditions where more than one specimen was tested, the results were averaged. Where a test was carried out at a frequency of 3.3 Hz with a 2 second rest period, the number of cycles was divided by 3.3 to obtain the elapsed time.

Presentation: Table 7.2 summarises the results of the seven series of tests outlined in Table 7.1. Where a binder content analysis was carried out on the test specimen, the actual value obtained is shown, otherwise

Table 7.2 Summary of Results of DBM Characterisation Tests

Stress Conditions (kN/m^2)			Test Frequency	Binder Content (%)	Void Content (%)	Resilient Properties			Length of Test (secs)	No. of Tests
p	q	σ_3				Initial Modulus (MN/m^2)	Final Modulus (MN/m^2)	Initial Poisson's Ratio		
TEST SERIES C1										
133	400	0	A	4.5	5.8	700	770	.40	3,200	3
133	275	20.5	A	4.8	4.8	700	780	.40	25,000	2
133	150	41.5	A	4.9	4.8	500	330	.30	100,000	1
400	800	66.5	A	4.7	5.8	1,125	1,175	.11	18,000	2
400	400	133.0	A	4.7	5.3	900	625	.30	65,000	1
400	275	154.0	A	4.6	6.0	750	500	.50	50,000	1
400	150	175.0	A	4.7	5.8	1,000	675	.38	100,000	2
150	650	300.0	A	4.7	5.2	925	500	.30	100,000	2
800	800	267.0	A	4.7	5.8	1,540	1,650	.40	70,000	1
800	400	333.0	A	4.9	5.0	1,300	1,000	.43	100,000	2
TEST SERIES TV1										
0	50	8.3	A	4.7	6.3	100	80	-	900	1
0	150	25.0	A	4.7	5.9	250	100	-	110	2
-16.6	50	0	A	4.7	6.2	100	50	-	200	3
-50	150	0	A	4.7	5.8	100	70	.40	140	3
TEST SERIES TH1										
0	80	13.3	B**	4.9	4.6	400	400	.45	420	1
0	240	40.0	B	4.9	4.6	275	225	.35	180	2
-16.6	50	0	A*	4.9	4.1	250	180	-	1,000	3
-50	150	0	A	4.7	5.2	300	250	.40	80	3
TEST SERIES I1										
133	275	20.5	A	4.9	4.6	1,175	820	.45	10,000	3
TEST SERIES C2										
133	275	20.5	A	4.9	9.7	450	500	.70	1,500	2
Very			A & B	4.9	9.7	-	-	-	-	1
TEST SERIES C3										
133	275	20.5	A	4.95	8.3	400	420	.50	20,000	3
Very			A & B	4.95	8.3	-	-	-	-	1

* A = 1 Hz ** B = 3.3 Hz + 2 secs rest

an average value for the set of specimens from each pavement is shown. The void content was obtained from a knowledge of the binder content and bulk specific gravity of a specimen and the specific gravities of the binder and aggregate.

The initial resilient modulus was based on the resilient strain near the beginning of a test, once the desired amplitude of vertical cyclic stress had been correctly set. The final resilient modulus was that determined just before the end of a test. The initial resilient Poisson's ratio was the ratio of the radial to longitudinal resilient strain measured at the same time as the initial resilient modulus.

The results of the investigation of the effect of rest periods, series CR1, are not tabulated. Two tests were conducted with continuous cycling, and two with rest periods, and although not conclusive, the results did show that after equal periods of time, the vertical permanent strains were similar. This conclusion is supported by Cooper et al (28) and Brown and Snaith (22). It was henceforth assumed that the permanent deformation was time dependent, and the most convenient form of loading was used in each test. For analysis of results, the number of cycles was subsequently converted to time.

Permanent Strain Behaviour: Figs 7.9 to 7.23 show both the vertical and radial permanent strain results plotted against time on a semi-logarithmic basis, which conveniently presents the results for an entire test. It was found that, when the results were plotted on a completely logarithmic basis, as will be shown in Chapter 9, they were in a more convenient form to evolve a permanent strain model.

The results of test series C1 indicated the sensitivity of the behaviour of the material to the stress parameters p and q. In general, increasing q increased the permanent strain, and increasing p decreased

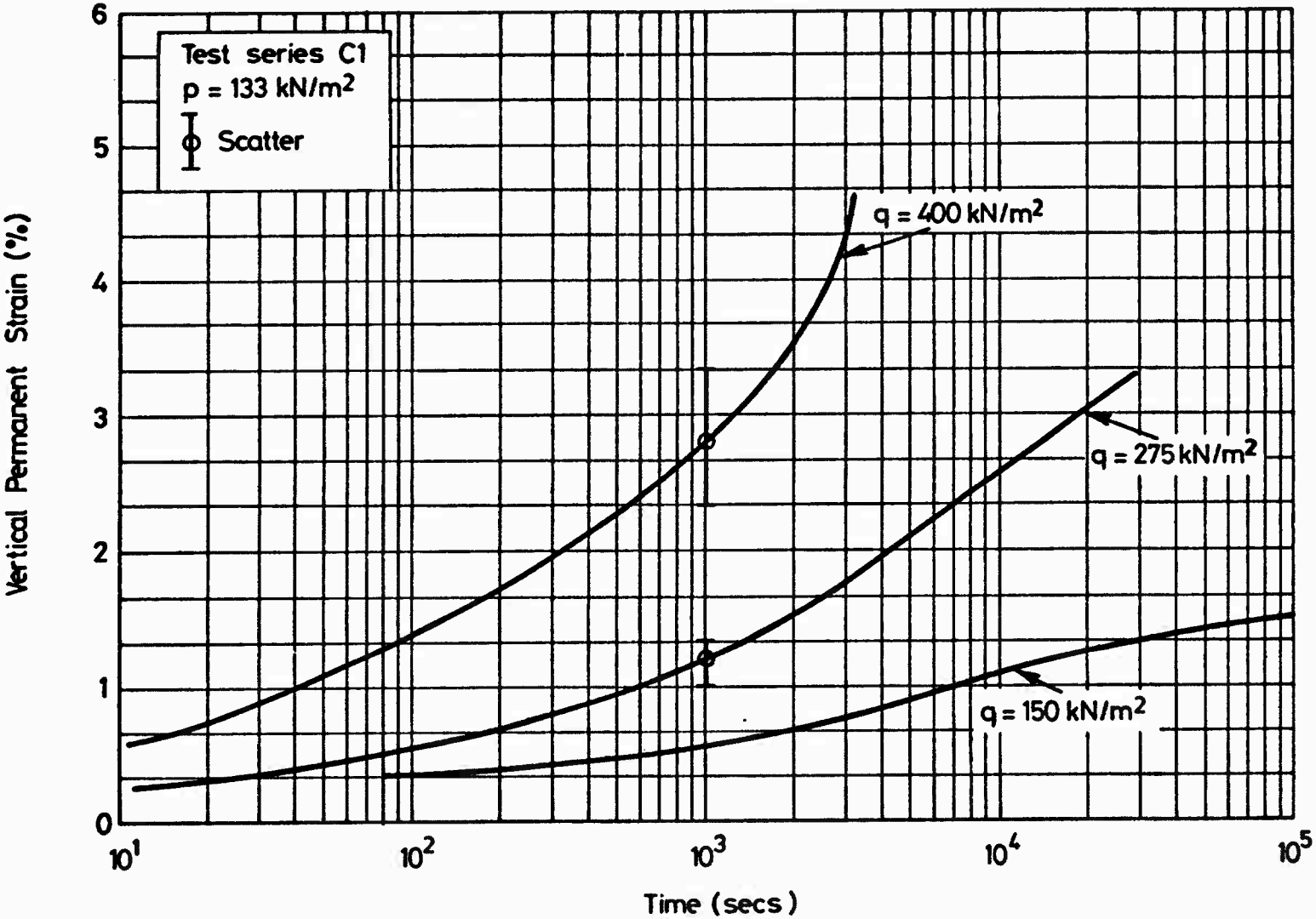

FIG. 7.9 THE INFLUENCE OF q ON VERTICAL PERMANENT STRAIN OF DBM, p = 133 kN/m^2

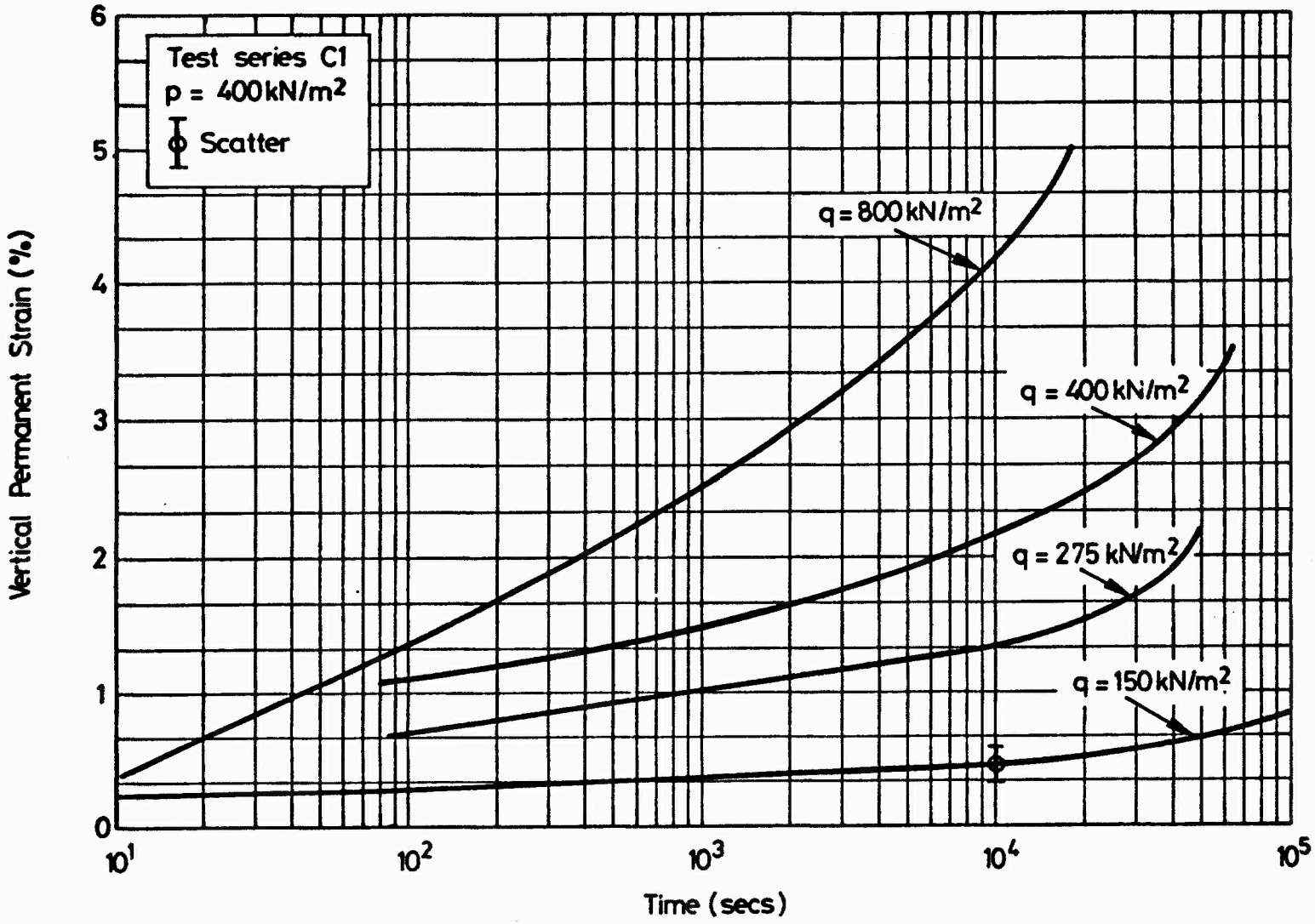

FIG. 7.10 THE INFLUENCE OF q ON VERTICAL PERMANENT STRAIN OF DBM, p = 400 kN/m^2

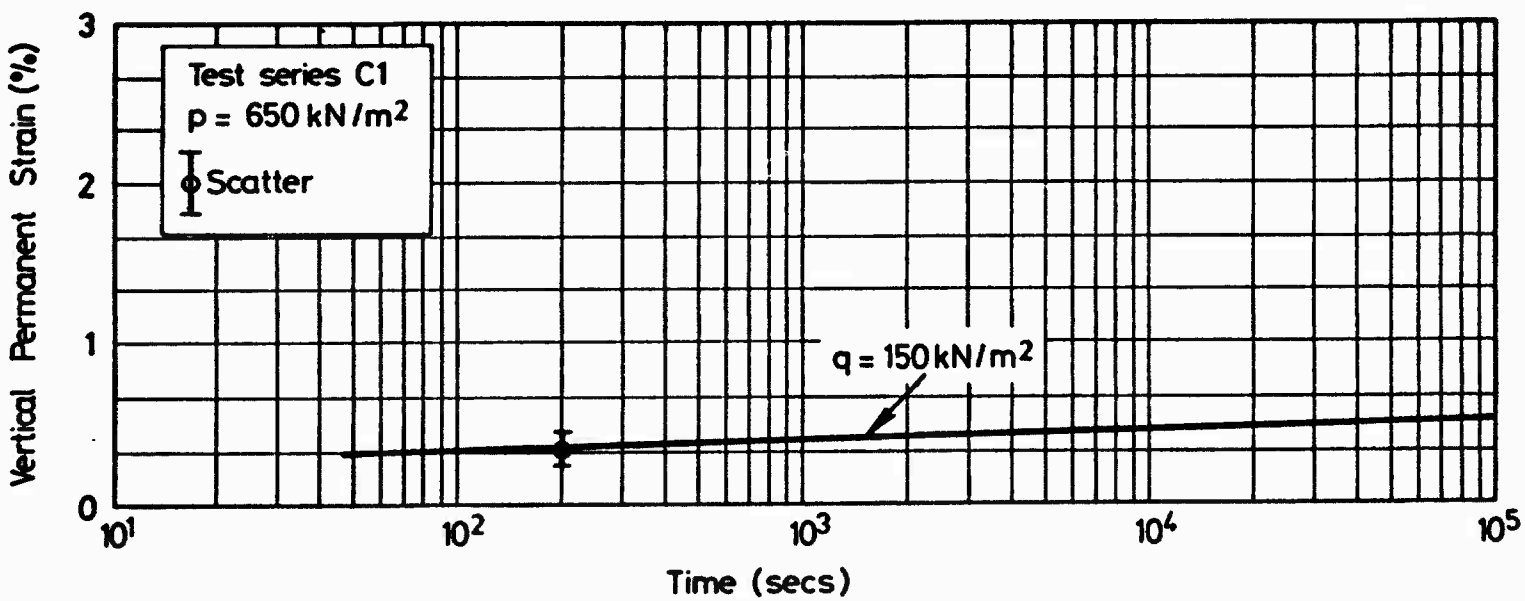

FIG. 7.11 THE INFLUENCE OF q ON VERTICAL PERMANENT STRAIN OF DBM, p = 650 kN/m^2

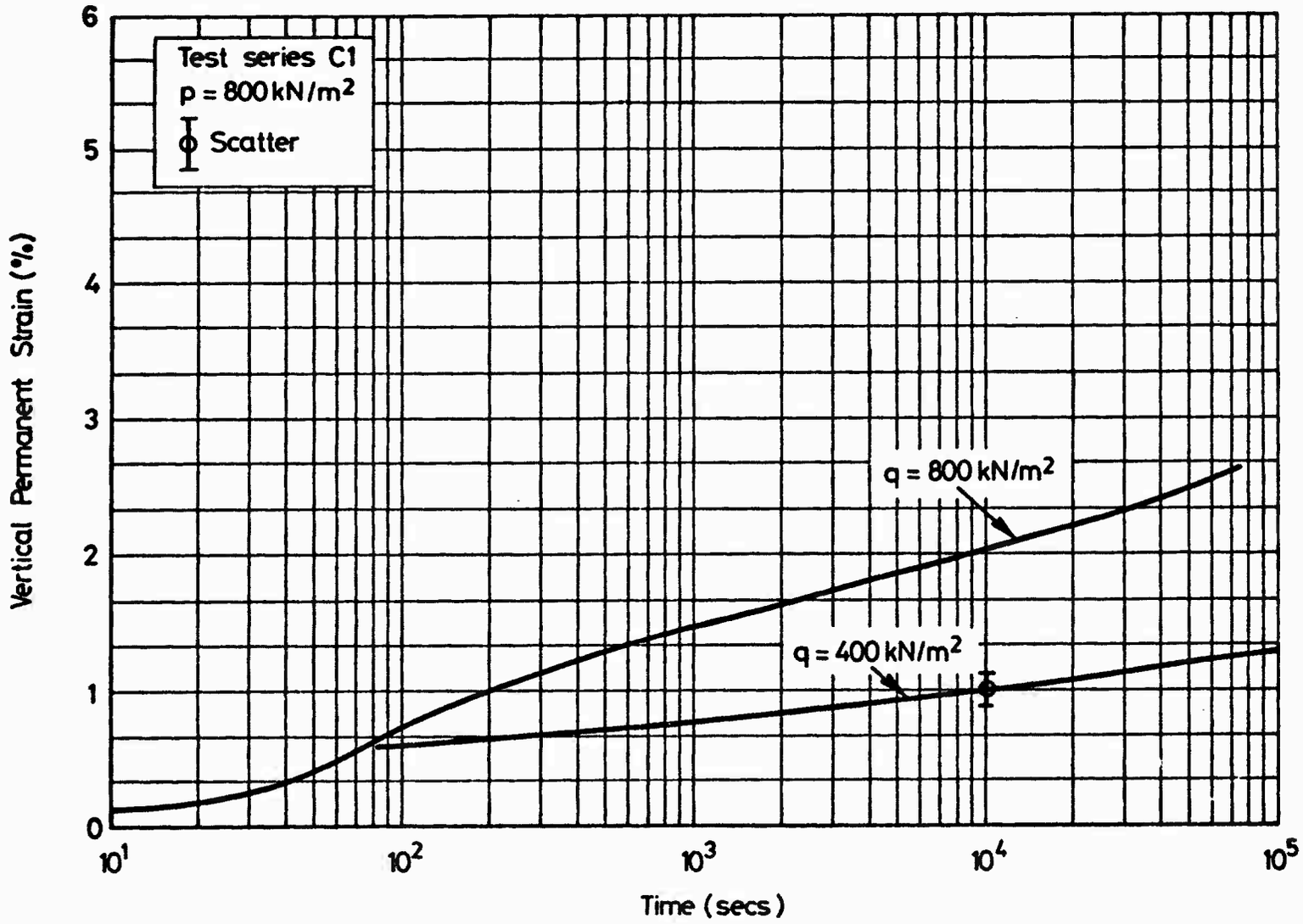

FIG. 7.12 THE INFLUENCE OF q ON VERTICAL PERMANENT STRAIN OF DBM, p = 800 kN/m^2

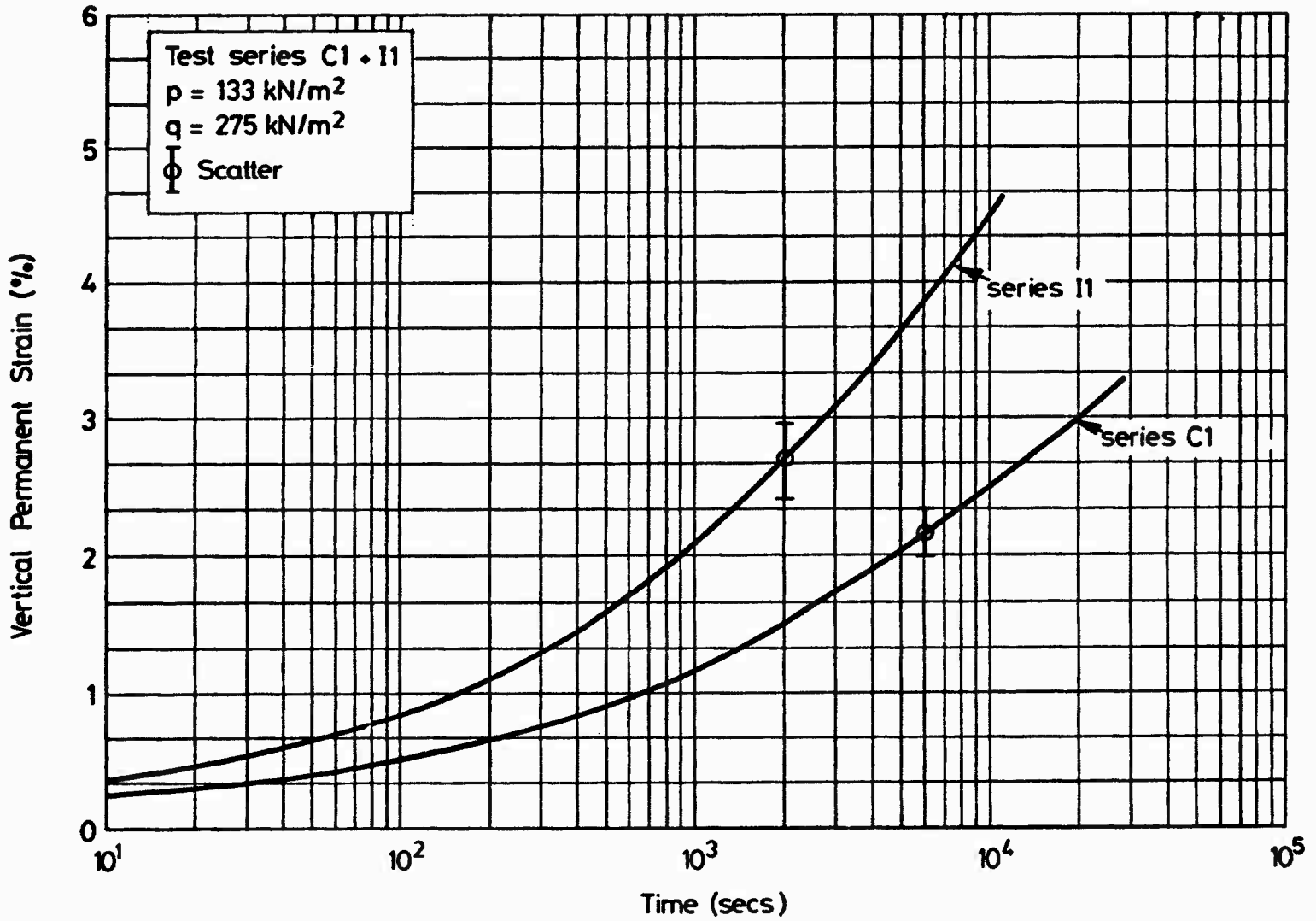

FIG. 7.13 COMPARISON OF VERTICAL PERMANENT STRAINS ACHIEVED WITH DBM CORES TAKEN VERTICALLY AND HORIZONTALLY

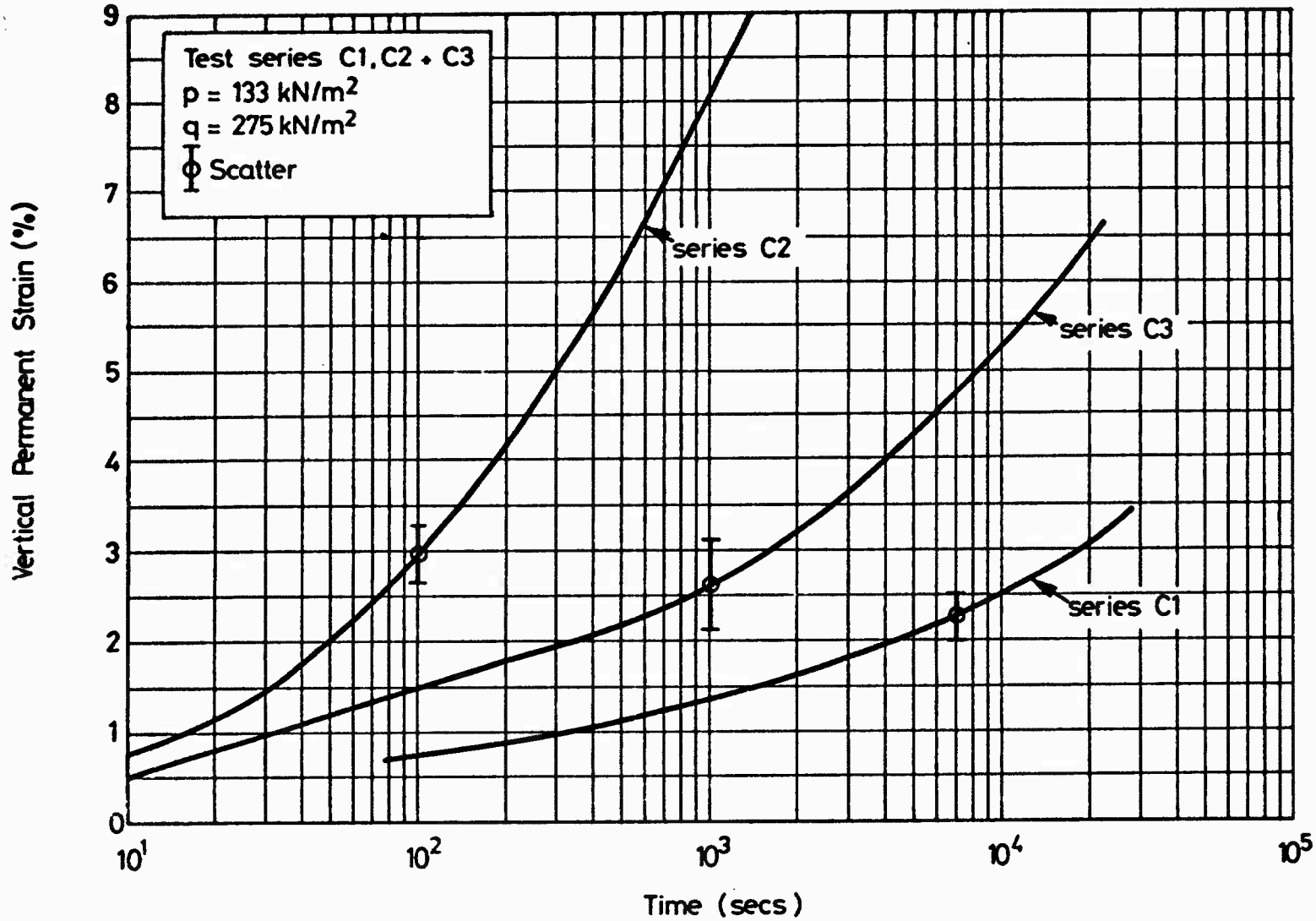

FIG. 7.14 COMPARISON OF VERTICAL PERMANENT STRAINS ACHIEVED WITH DBM CORES TAKEN FROM EACH PAVEMENT

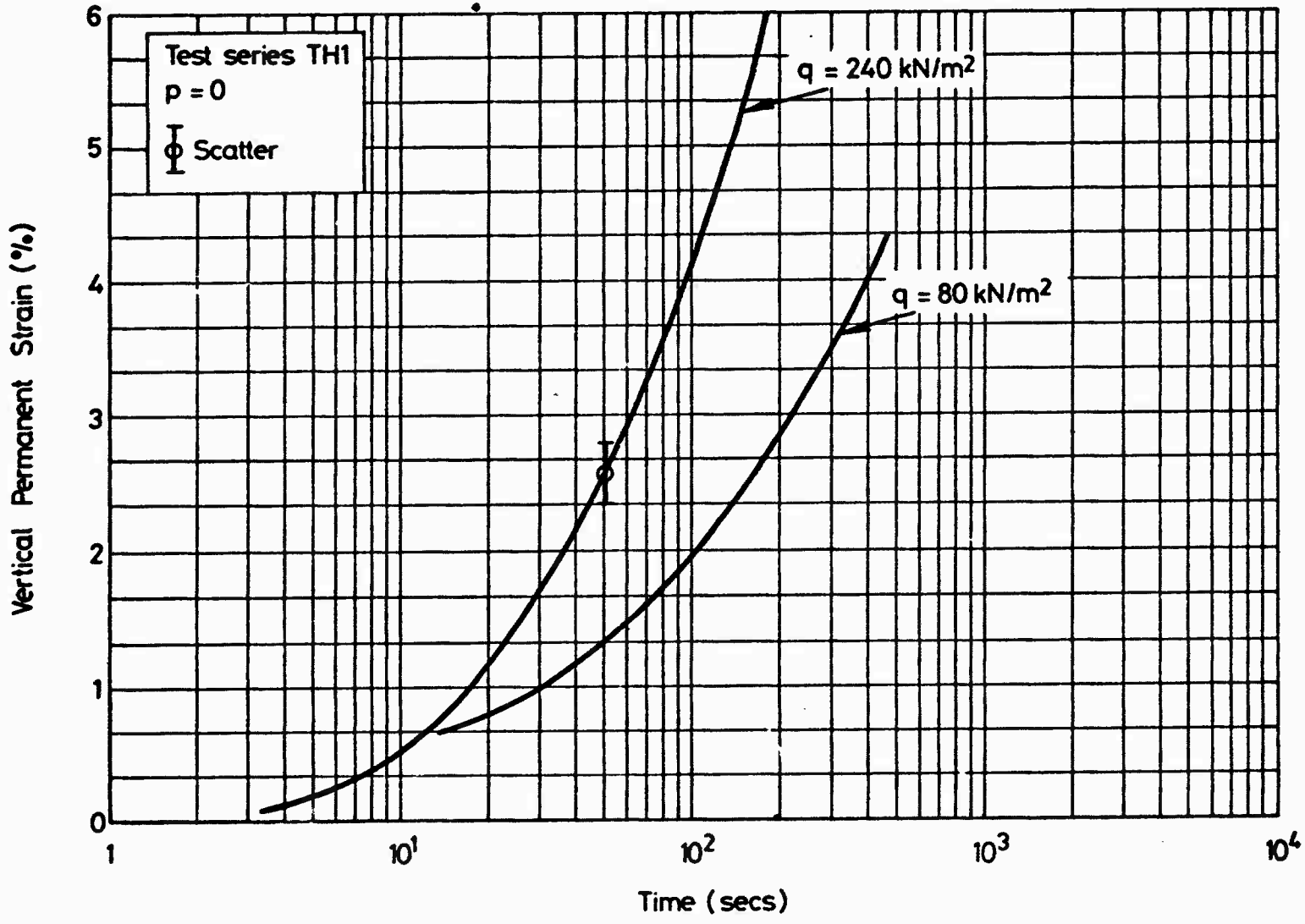

FIG. 7.15 THE INFLUENCE OF q ON VERTICAL PERMANENT STRAIN OF DBM, p = 0

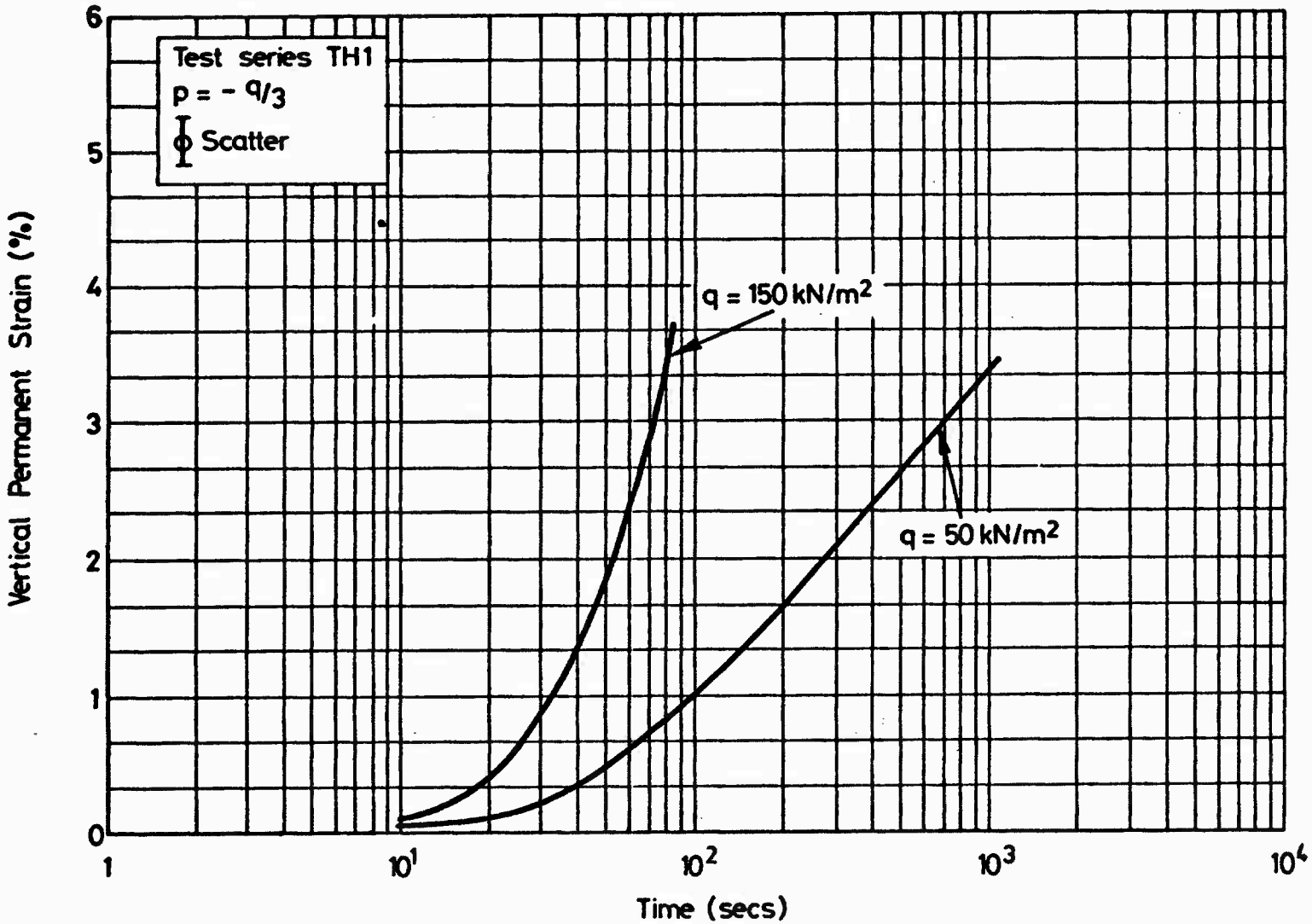

FIG. 7.16 THE INFLUENCE OF q ON VERTICAL PERMANENT STRAIN OF DBM, p = -q/3

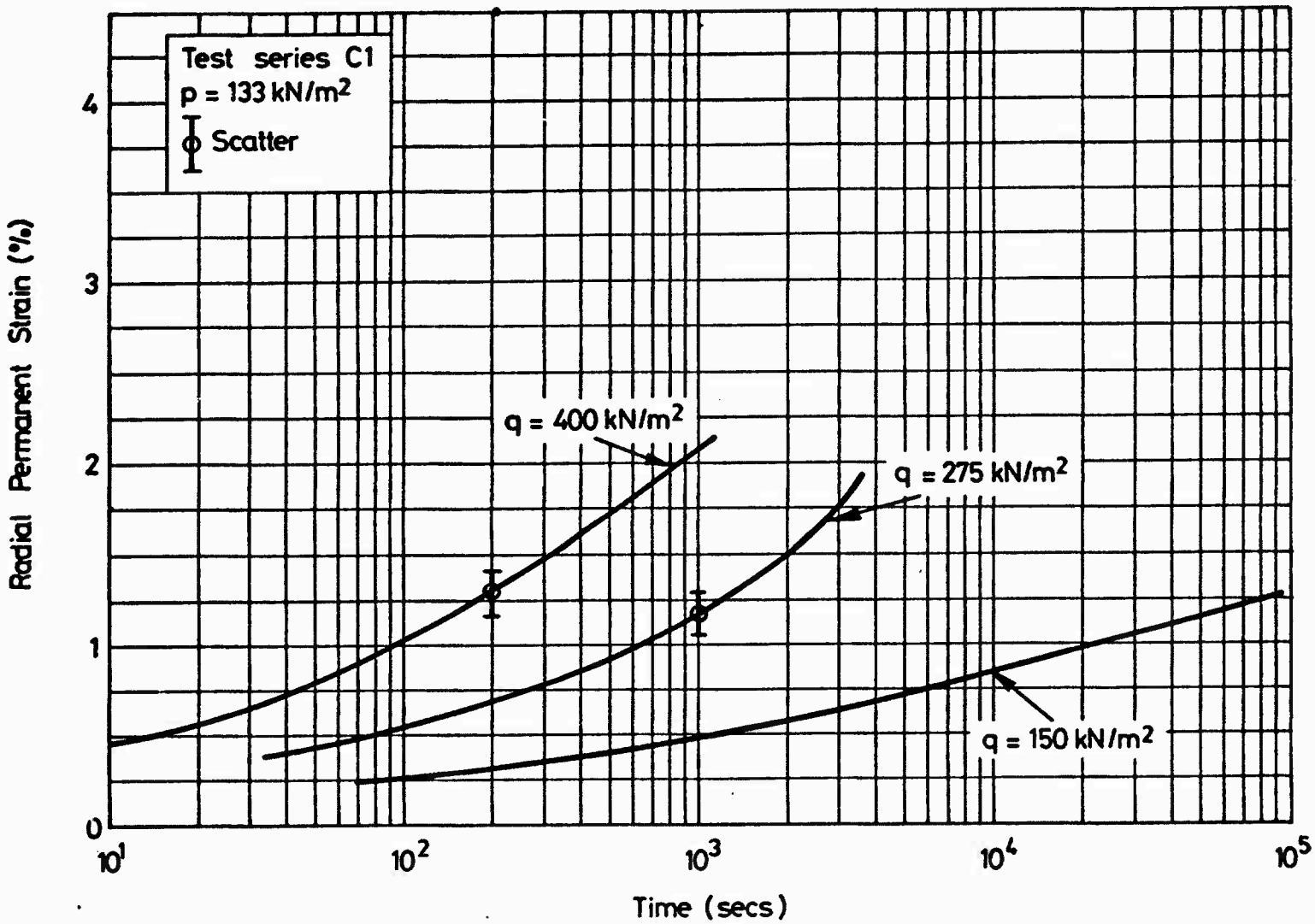

FIG. 7.17 THE INFLUENCE OF q ON RADIAL PERMANENT STRAIN OF DBM, p = 133 kN/m^2

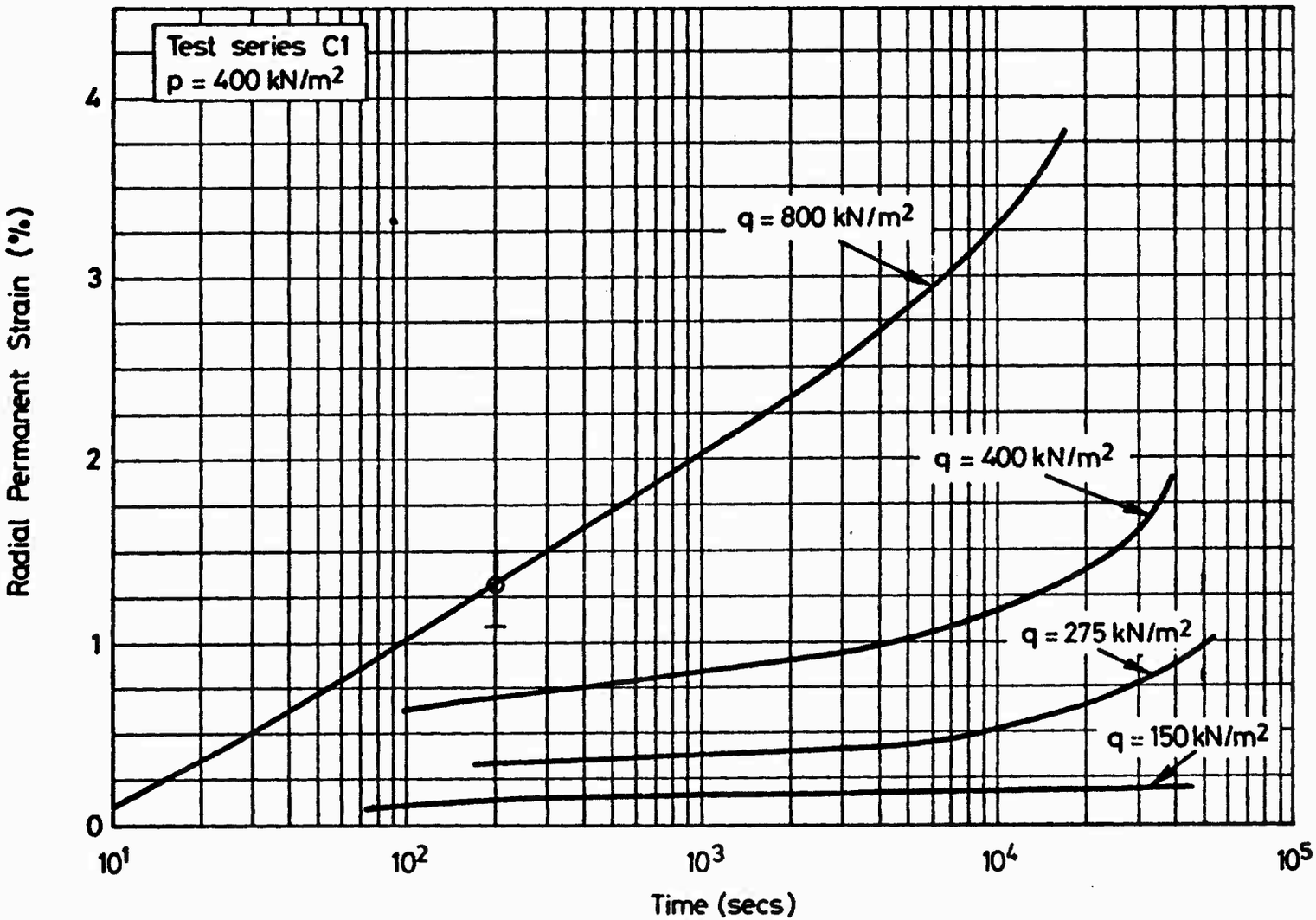

FIG. 7.18 THE INFLUENCE OF q ON RADIAL PERMANENT STRAIN OF DBM, p = 400 kN/m^2

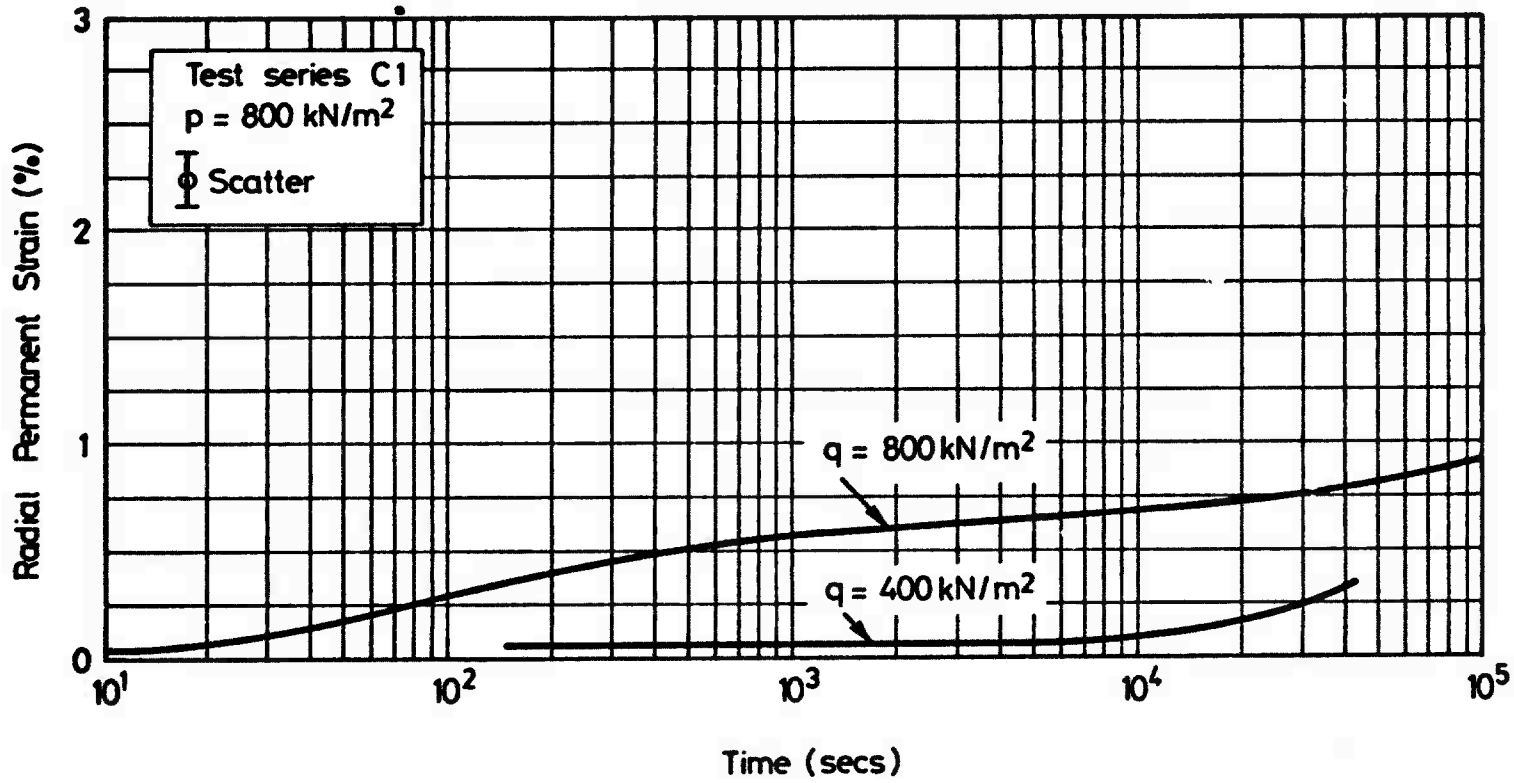

FIG. 7.19 THE INFLUENCE OF q ON RADIAL PERMANENT STRAIN OF DBM, p = 800 kN/m^2

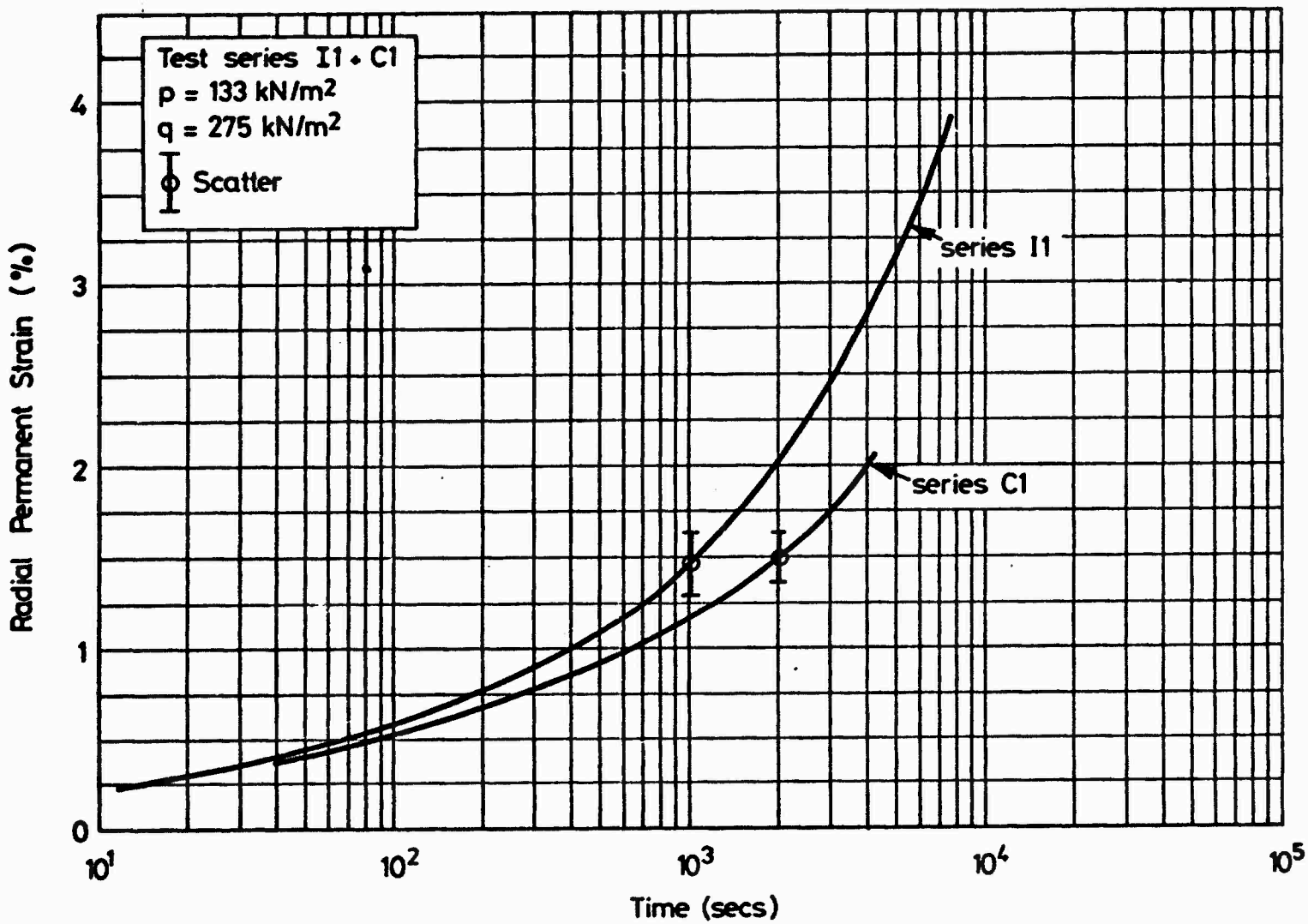

FIG. 7.20 COMPARISON OF RADIAL PERMANENT STRAINS ACHIEVED WITH DBM CORES TAKEN VERTICALLY AND HORIZONTALLY

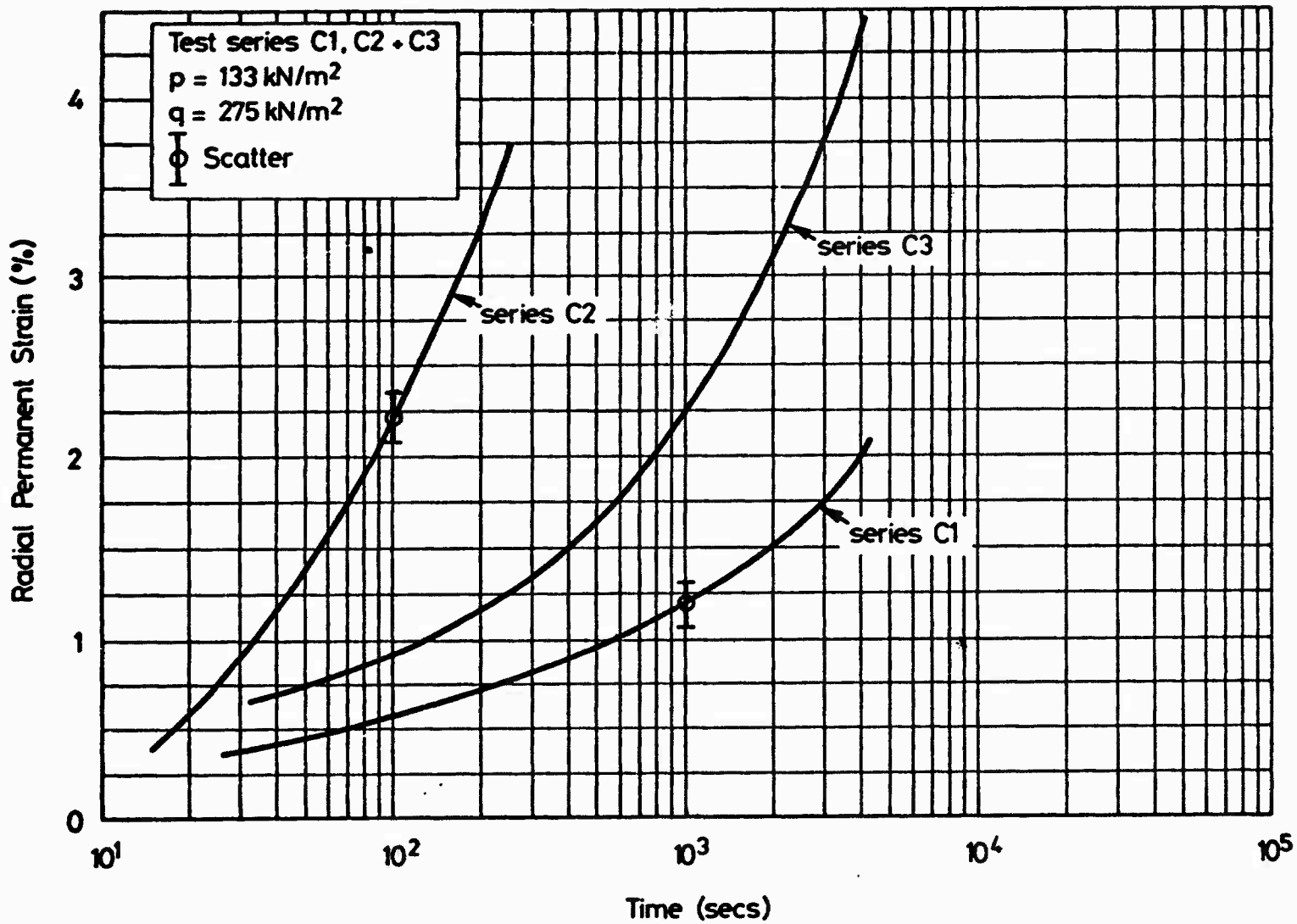

FIG. 7.21 COMPARISON OF RADIAL PERMANENT STRAINS ACHIEVED WITH DBM CORES TAKEN FROM EACH PAVEMENT

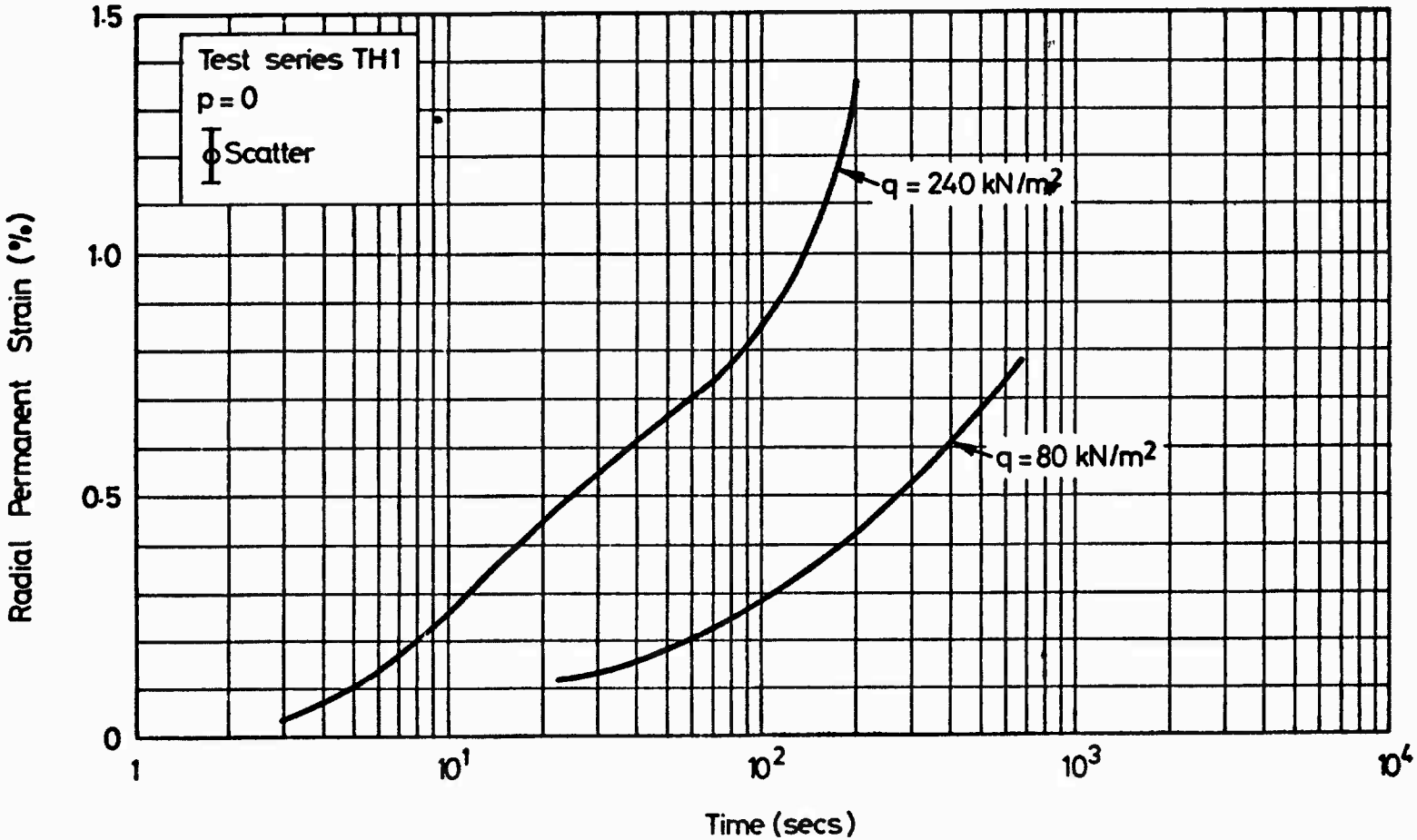

FIG. 7.22 THE INFLUENCE OF q ON RADIAL PERMANENT STRAIN OF DBM, p = 0

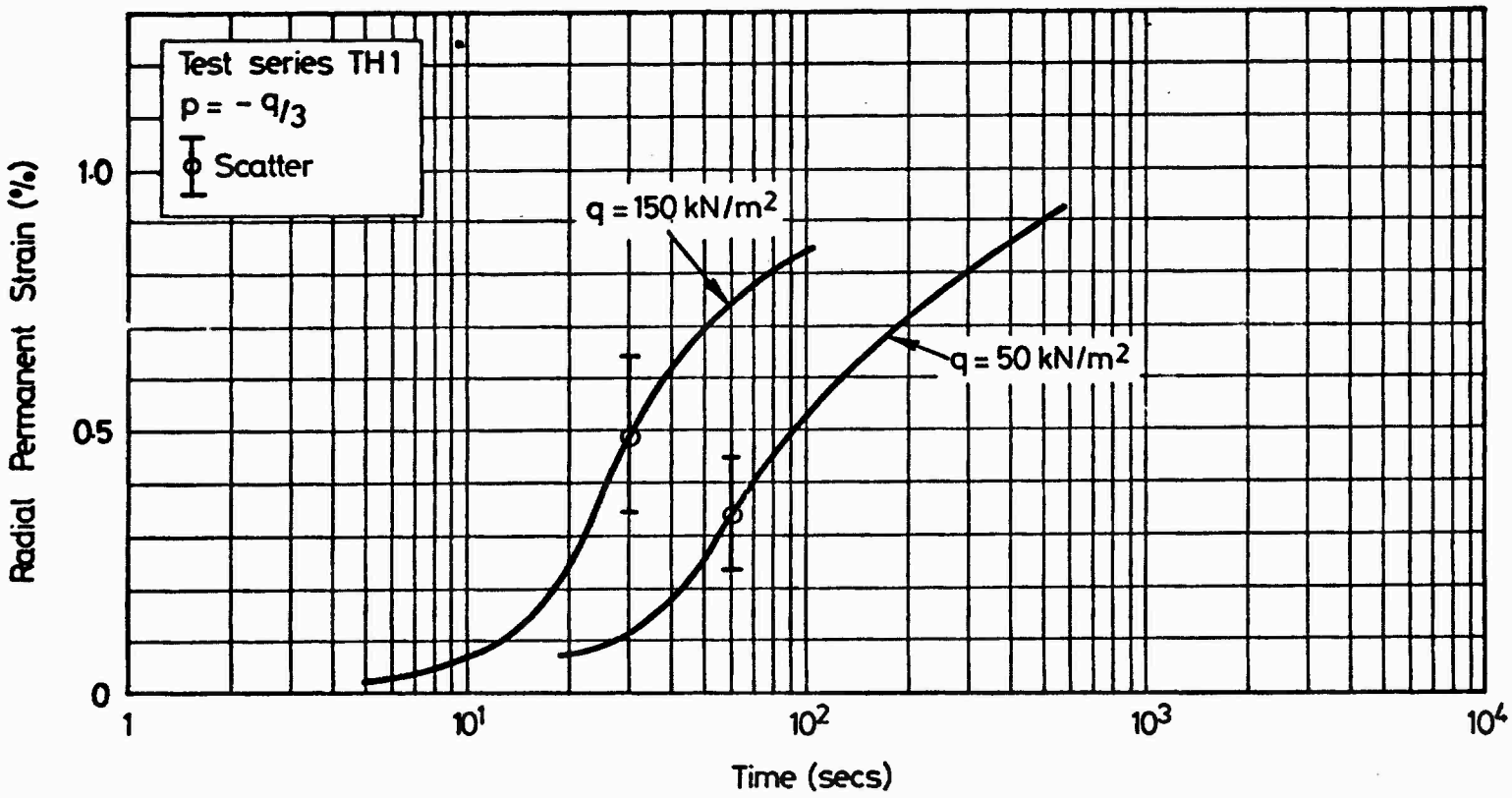

FIG. 7.23 THE INFLUENCE OF q ON RADIAL PERMANENT STRAIN OF DBM, p = -q/3

it, the most critical combination being when p was low and q was high, which resulted in high deformations and early failure of the material. This was particularly true for the tension tests (series TH1, Figs 7.15, 7.16, 7.22 and 7.23) where, with a zero or negative p value, the test specimens were able to sustain only a low value of q for a few cycles of load.

The plot of radial permanent strain versus time for p = 650 kN/m^2 and q = 150 kN/m^2 is not shown due to the very small strains obtained.

The results of both test series TV1 and TH1 are shown in Table 7.2. The TH1 results were more consistent and thought to be more representative, since the repeated axial tension was applied in the same direction as in situ.

The results from series I1 (Figs 7.13 and 7.20) show that the horizontal cores underwent more deformation than the vertical ones, a fact also observed in comparing the results of series TV1 and TH1. This is probably due to the noticeable orientation of the larger aggregate particles, which would result in the aggregate interlock in the two directions being different.

The results from series C1, C2 and C3 are compared in Figs 7.12 and 7.14, and indicate that the materials from pavements 2 and 3 underwent more deformation than from pavement 1. This could be attributed to the higher void contents of the materials from pavements 2 and 3, resulting from a combination of poorer aggregate grading and compaction, compared with pavement 1.

Resilient Properties: Figs 7.24 to 7.26 show plots of resilient modulus versus p for each pavement. The plot for pavement 1 includes results from all the tests in series C1 and TH1. The plots for pavements 2 and 3 are from much more limited data, the majority of points being obtained

Pavement 1

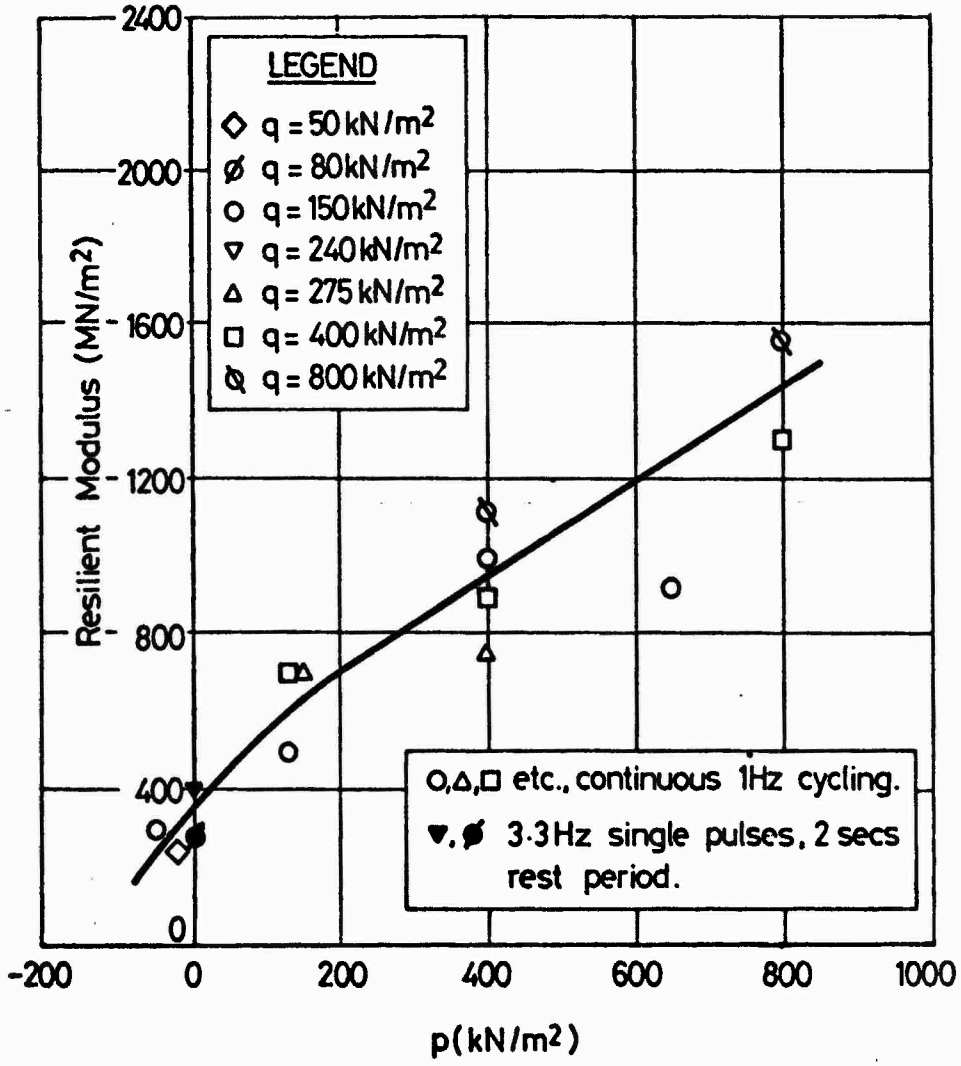

FIG. 7.24 THE EFFECT OF p AND q ON THE RESILIENT MODULUS OF DBM CORES FROM PAVEMENT NO. 1

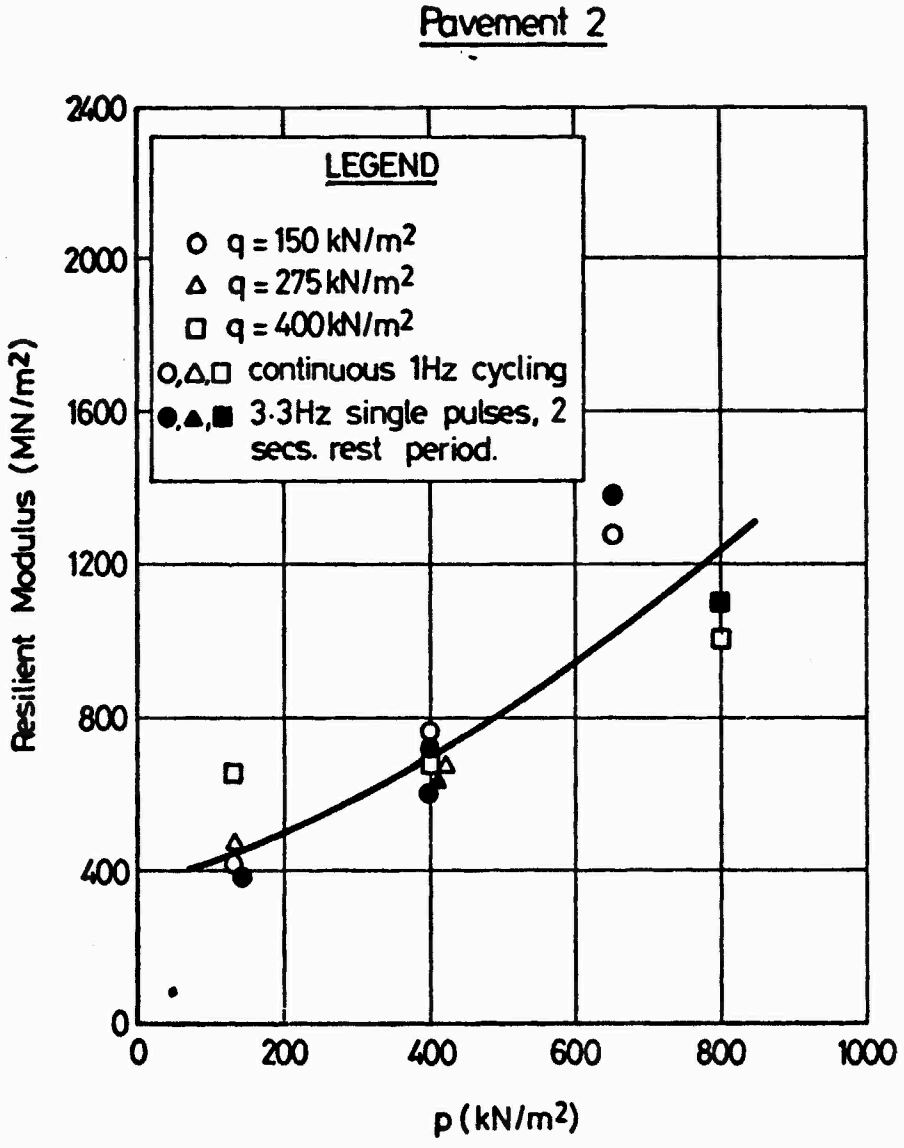

FIG. 7.25 THE EFFECT OF p AND q ON THE RESILIENT MODULUS OF DBM CORES FROM PAVEMENT NO. 2

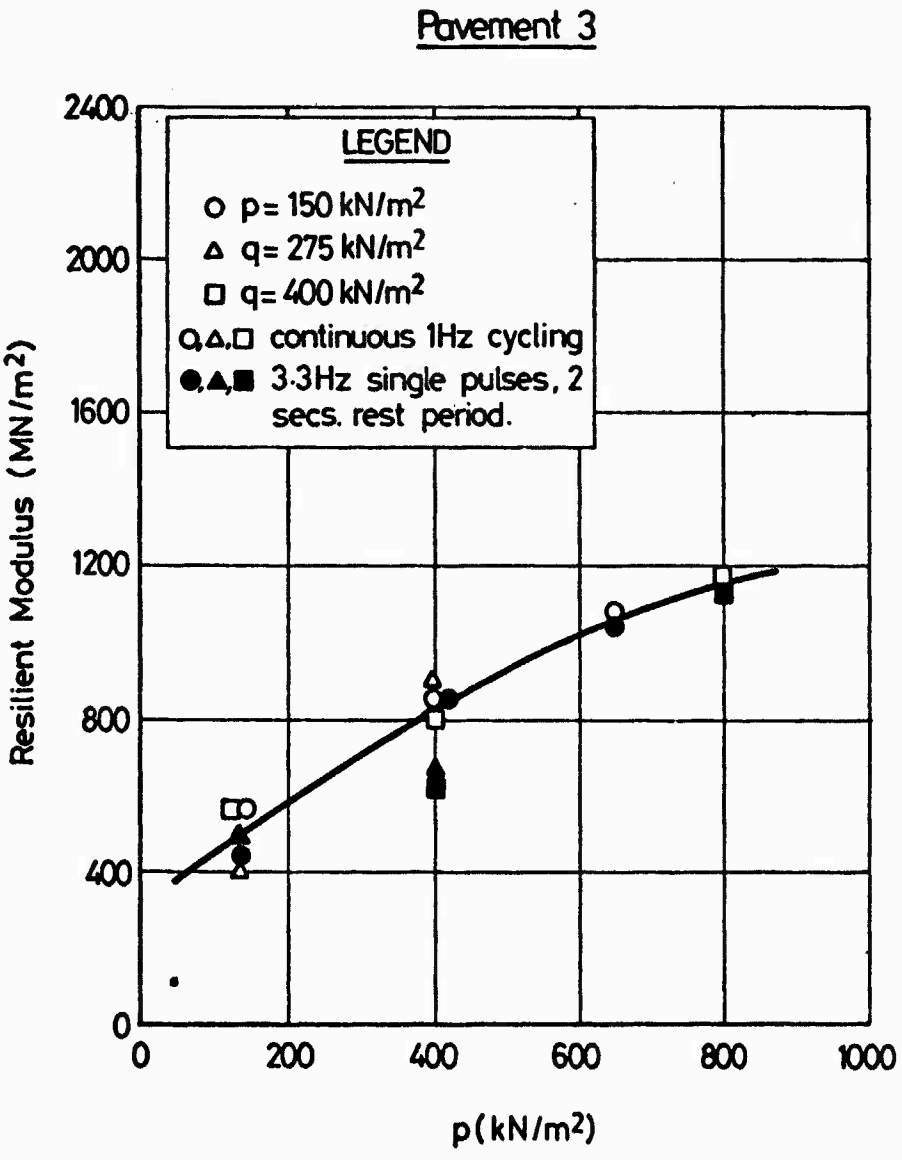

FIG. 7.26 THE EFFECT OF p AND q ON THE RESILIENT MODULUS OF DBM CORES FROM PAVEMENT NO. 3

from a number of tests on one specimen.

Broadly speaking, the resilient modulus behaviour for all three pavements followed the same trend, exhibiting considerable non-linearity, as would be expected under the test conditions of high temperature and fairly long loading times. From the limited data available, there appeared to be little difference in the moduli measured at 1 Hz and 3.3 Hz with a 2 second rest period. This is probably because the material was able to recover more during the rest period, and thus the measured deformations were comparable for the two modes of loading. Had both modes utilised continuous cycling, the higher frequency would result in a higher modulus.

The values of the initial resilient Poisson's ratio were not plotted since no distinct relationship emerged. However, the values measured are shown in Table 7.2 and for series C1 and TH1 (pavement 1) have an average value of approximately 0.40. Snaith (25) found that the value of Poisson's ratio was particularly dependent on temperature, which was constant for all tests carried out in this project. He also found that Poisson's ratio decreased with increasing confining pressure, which is roughly equivalent to increasing p. No such trend could be distinguished from the results presented herein.

7.3 KEUPER MARL SUBGRADE

7.3.1 Introduction

The stress conditions for tests on the clay cores were determined from linear elastic analysis, assuming a modulus based on the empirical relationship:

$$E = 10 \times CBR \ (MN/m^2)$$

Standard CBR tests on the clay indicated a value of 5% thus, initially,

the modulus was taken as 50 MN/m^2. However, preliminary tests gave a measured resilient modulus for stress conditions thought to exist at the surface of the subgrade, of 35 MN/m^2. The results of the analysis using this modulus are shown in Fig. 7.27 with the test conditions superimposed. The number of tests required was comparatively small due to the small spread of the stress distribution.

After completion of several tests, it became apparent that the non-linearity of the clay was too great to approximate with a linear analysis, and hence a non-linear analysis was adopted. The results of this are shown in Fig. 7.28, compared with the linear analysis. It can be seen that the spread of the stress conditions to be covered is wider than for the linear analysis, but still thought to be sufficiently narrow to be approximated by a straight line. Therefore, the test conditions chosen from the linear analysis were retained, so as to avoid extensive additional tests in the limited time which was available.

The limitation on the form of the test path used was similar to that which applied to the DBM characterisation tests, i.e. constant confining stress. The selection of appropriate stress paths was identical to that outlined for the DBM tests.

7.3.2 The Test Programme

The test conditions for the basic programme are shown in Figs 7.27 and 7.28. However, in order to develop a more rigorous model for the permanent deformation behaviour of the clay, one more test condition was added, at q = 70 kN/m^2. Hence, all tests were carried out on the line q = 5.0 + 1.75 p, at one of the following values of q: 15, 30, 40, 50 and 70 kN/m^2.

Ten cores were taken following the testing and excavation of pavement 1. These cores were found to be dryer and more dense than those taken

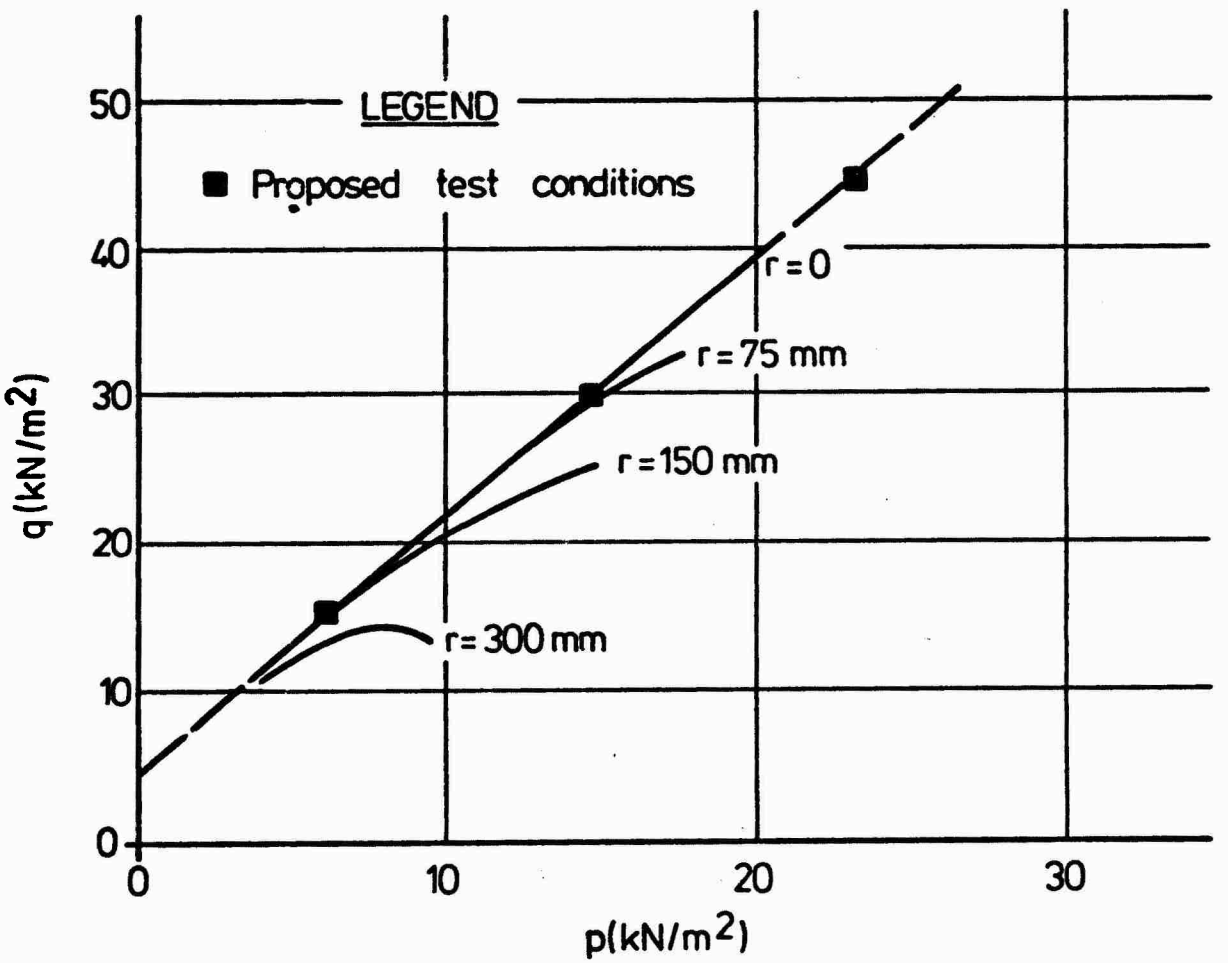

FIG. 7.27 STRESSES IN THE SUBGRADE (PAVEMENT NO. 1) BY LINEAR ELASTIC THEORY, WITH LABORATORY TEST CONDITIONS

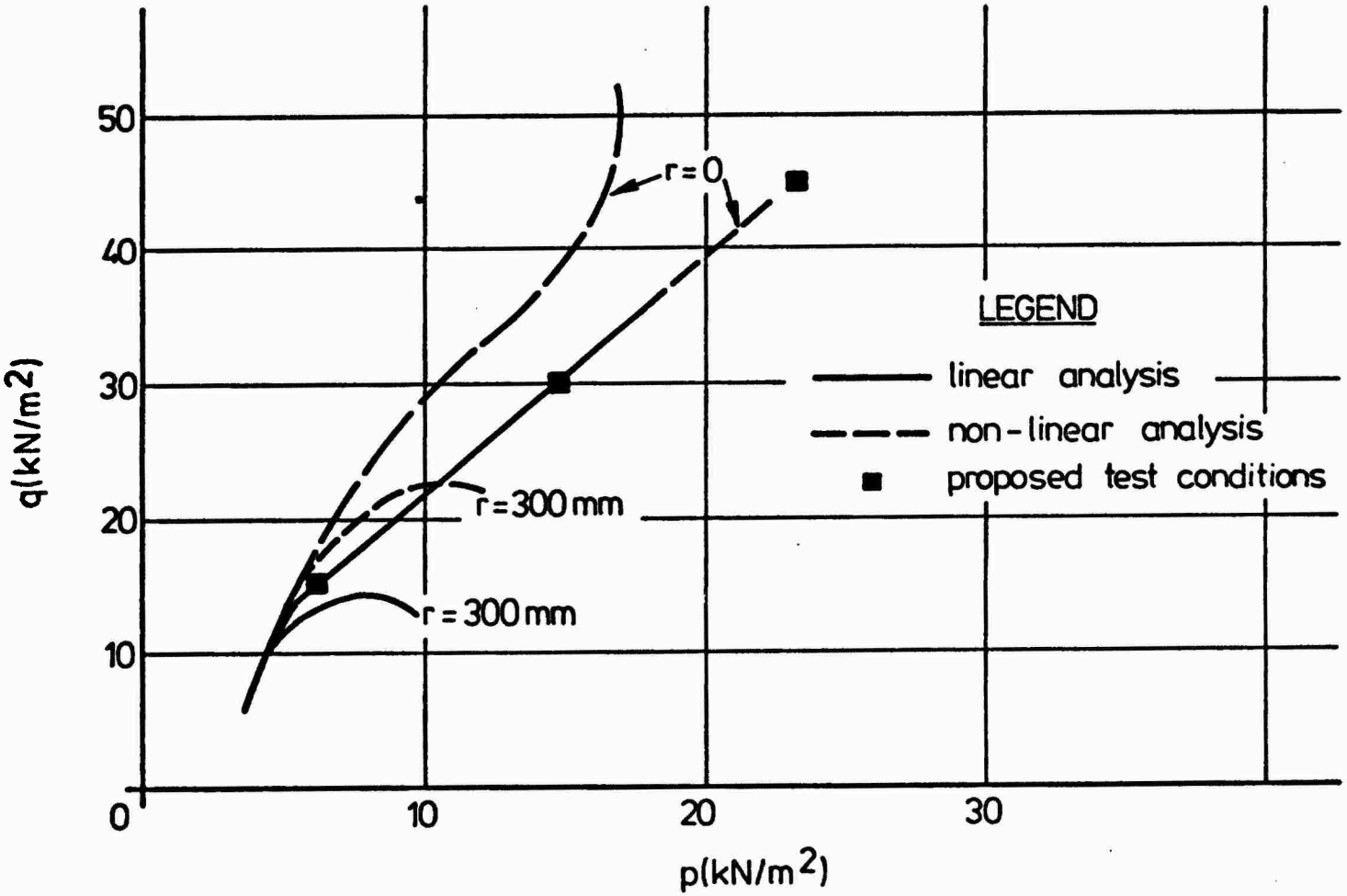

FIG. 7.28 COMPARISON OF STRESSES IN THE SUBGRADE (PAVEMENT NO. 1) BY LINEAR AND NON-LINEAR ELASTIC THEORY

at the time of construction, as may be seen in Fig. 7.29, where the dry density versus moisture content plot is shown. It was therefore decided to use these cores largely for a preliminary investigation, and to establish a testing technique. This group of tests was designated series K1.

A further ten cores were taken before the construction of pavement 2, from new material which had been used to replace that lost after the excavation of pavement 1. These cores were of a similar density and moisture content to those taken before construction of pavement 1 (Fig. 7.29). The test carried out on these cores constituted the main series designated K2.

Finally, a batch of cores was taken following the testing and excavation of pavement 2, of which three were used for characterisation tests (series K3). The densities and moisture contents of these cores, shown in Fig. 7.29, were again higher and lower respectively than cores taken before construction. It was therefore clear that the subgrade dried out and became more compact during testing, causing a reduction in moisture content of about 1.5%. The air voids in the material remained almost constant in both cases.

A small dead load equivalent to the overburden pressure, was applied to the specimen throughout a test. This had been calculated using a linear elastic analysis, for a number of positions in the subgrade, covering the range of values of q from 15 to 70 kN/m^2.

Test Frequency: All the tests were carried out at a frequency of 4 Hz, and with a 2 second rest period between pulses. The frequency was obtained by reference to Barksdale (23), and corresponded to a principal stress pulse time of 0.25 seconds which was appropriate for a position just below the surface of the subgrade.

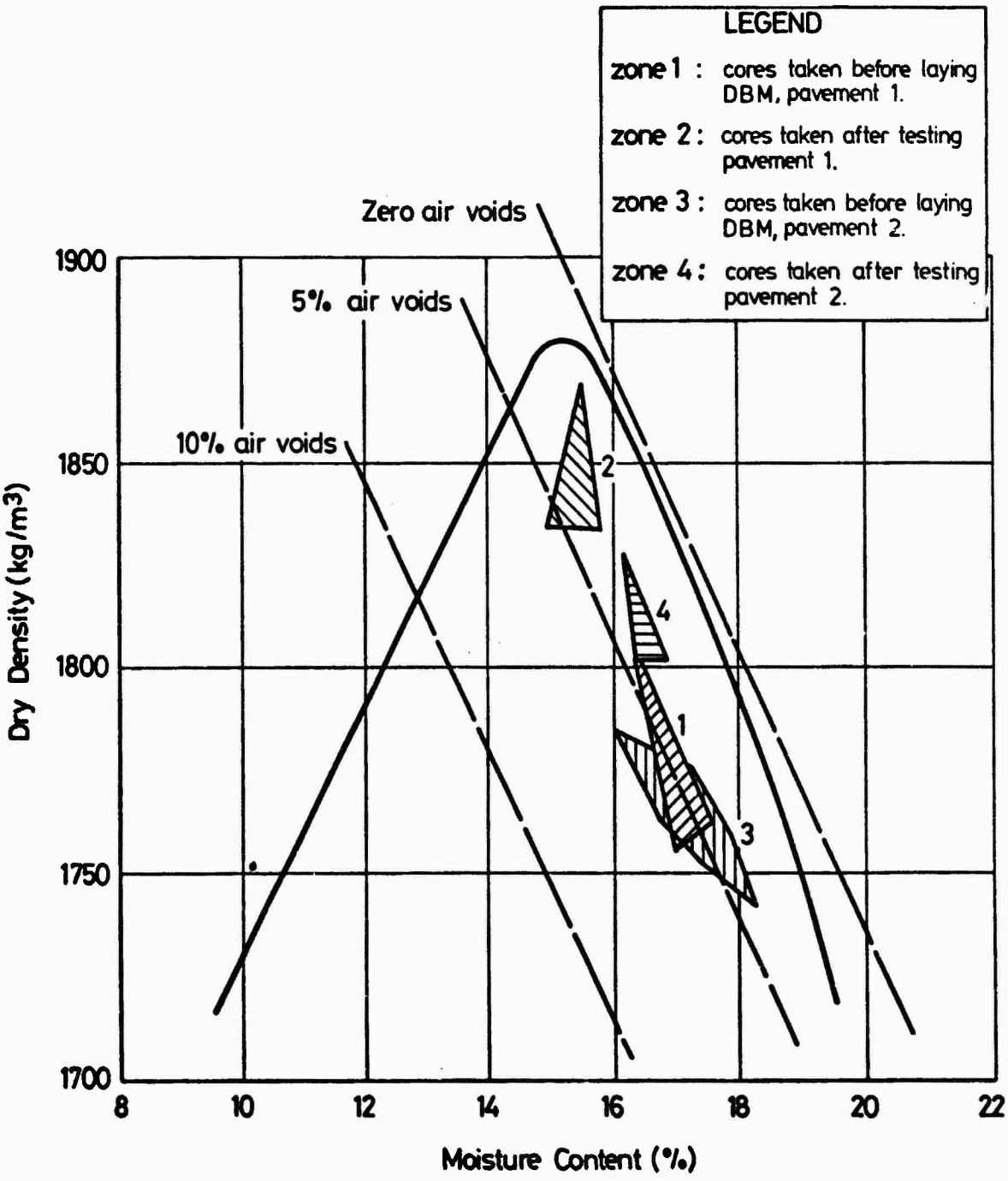

FIG. 7.29 DRY DENSITY VERSUS MOISTURE CONTENT RELATIONSHIP FOR KEUPER MARL, WITH RESULTS FROM CORES

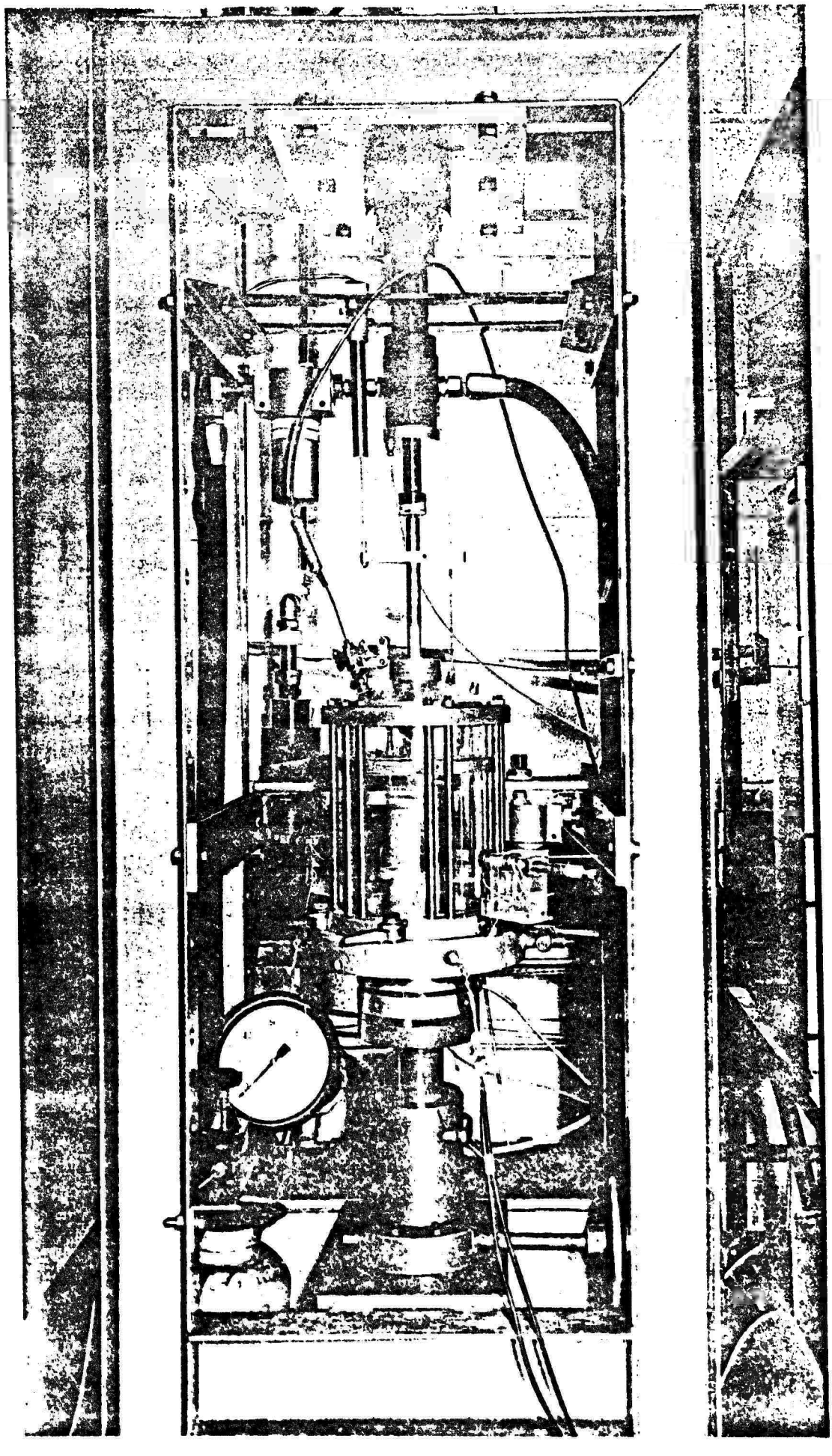

FIG. 7.30 A KEUPER MARL SPECIMEN SHOWN IN POSITION IN THE TEST MACHINE

This is at variance with the DBM tests where an average stress pulse was used. The DBM tests were carried out at a later stage than the clay tests, when it was considered more realistic to use an average stress pulse. However, the use of the exact pulse loading time is not essential for permanent strain characterisation which depends on total time. For DBM the resilient modulus at a different loading time can be found by utilising Van der Poel's nomograph, and for clay, Lashine (29) showed that resilient modulus was independent of frequency over the range considered here.

7.3.3 Specimen Preparation

The equipment used for the characterisation tests was normally used for testing 75 mm diameter specimens. Therefore, when the cores were removed from wax they were trimmed to this diameter using a soil lathe. Each core was then placed in a 75 mm diameter split mould and the ends trimmed to a final length of approximately 113 mm. The trimmings from both operations were used for moisture content determination.

Lubricated ends consisting of two latex rubber membranes and silicone grease on polished loading platens were used to minimise lateral end restraint.

7.3.4 Test Equipment

Electro-hydraulic Servo-controlled Test Machine: A machine designed specifically for testing soils (19, 20) was used for the clay characterisation tests and is shown in Fig. 7.30. In principal, this machine was identical to that used for the DBM tests. However, the triaxial cell was different, being entirely detachable from the machine. The load was transmitted to the specimen via a loading piston passing through a bearing at the top of the cell. The contact between the piston and

the loading ram was through a half ball-bearing.

The load cell was located below the triaxial cell and hence any friction between the loading piston and the cell would be included in the measurement. This friction was minimised by lubricating the bearing and piston with "Vaxiella" oil before each test, and maintaining the level of oil in a small reservoir around the top of the bearing where the piston entered the cell.

The testing equipment was capable of cycling the cell pressure, but to simplify the test procedure, and maintain compatibility with the DBM tests, a constant cell pressure was used. The confining medium was de-aired water, and the cell pressure was measured by a transducer located at the top of the cell.

Drainage connections on the cell were blocked off, as were tappings for a pore-pressure measuring device, since drainage could not occur in the test pavement, and pore-pressure measurements could not be made in this partially saturated material.

Deformation Measurement: Longitudinal deformation was measured by an LVDT, mounted rigidly to the loading frame as shown in Fig. 7.30. The cyclic output from the LVDT thus included the deformation of the whole vertical loading system. This effect could be calibrated out by measuring the cyclic deformation of the system with a rigid specimen in place of the soil. The error was largely due to the cyclic deformation of the lubricated latex rubber discs used to create "free" end conditions between the test specimen and the end platens. Thus, the calibration operation was carried out before each test using the same lubricated latex discs which were to be used in the test.

The radial deformation was measured at the centre of the test specimen by two pairs of 25 mm diameter strain coils whose response was

monitored by a Bison instrument, each pair mounted on diametrically opposite sides of the specimen as shown in Fig. 7.31. The inner coil of each pair was attached to the specimen, and the outer one mounted onto a carrier whose movement was controlled by a micrometer. Calibration of the coils was carried out before each test, using the micrometers to alter the separation of each pair by a known amount, and recording the change in signal on a UV recorder.

The coils were identical to those used in the test pavement, and reference should be made to Chapter 3 for a description of the principles of operation.

7.3.5 Testing Procedure

Following the preparation of the test specimen, the triaxial cell top was clamped to the base, the loading piston inserted and the cell filled with de-aired water. The cell was then placed on the loading pedestal, the cell pressure line connected, and all electrical connections made. The cell pressure transducer was de-aired, and zeroed, and the output from the load cell zeroed. Finally, the LVDT for measuring vertical strain was placed in position, so that it was at one end of its range.

Three devices (DVM, UV recorder and CRO) were again used to monitor outputs from the load cell, strain coils, and the LVDT, and are shown in Fig. 7.32 with the control equipment for the testing machine. The load cell and LVDT had been calibrated using both the DVM and the recorder and the strain coils using the recorder only. The UV recorder was used to register the behaviour of a specimen under test with intermediate checks from the DVM.

A test was continued for either 100,000 cycles or until excessive deformation had occurred. In some cases, premature failure of the

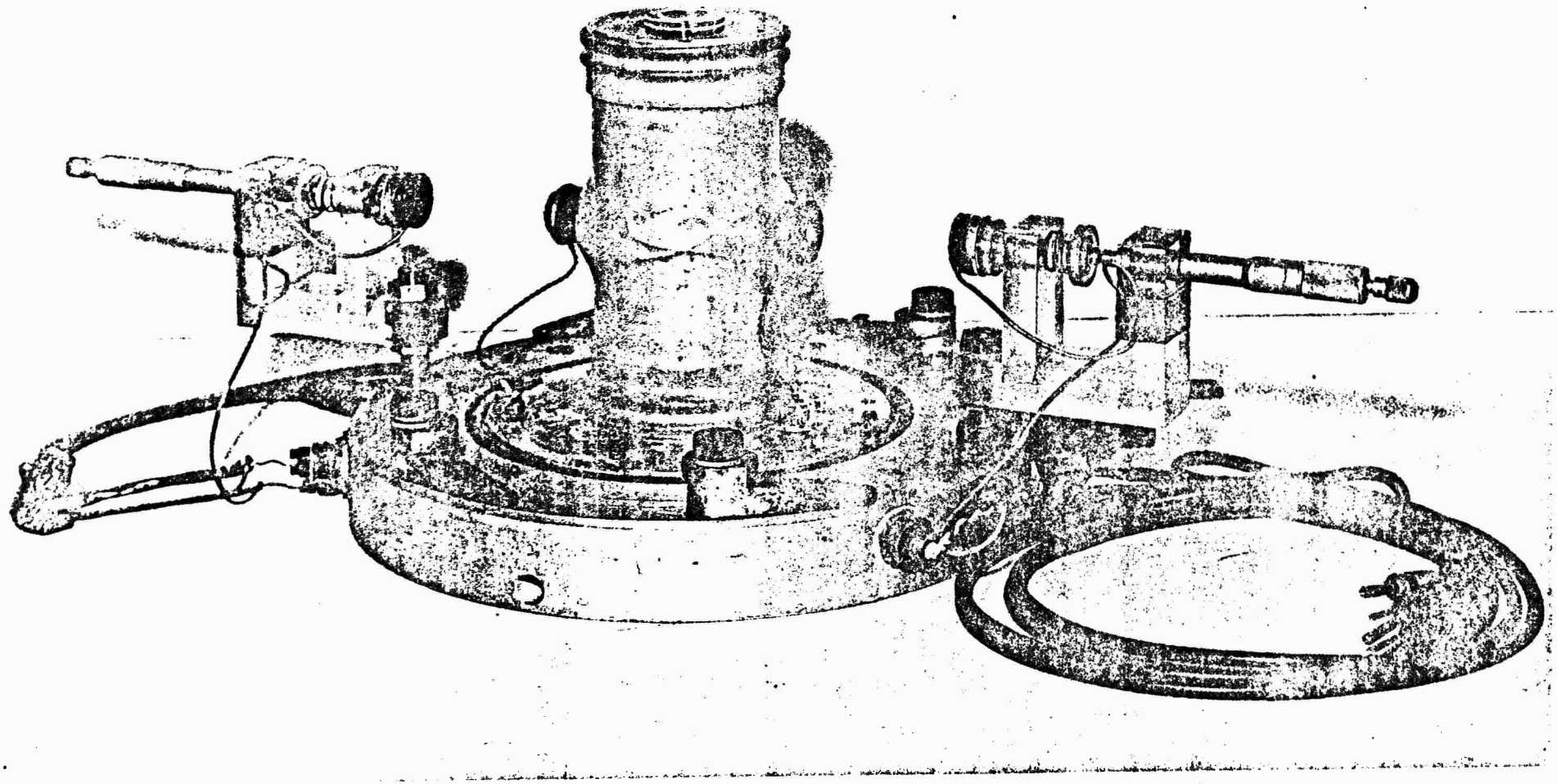

FIG. 7.31 A KEUPER MARL SPECIMEN SET UP ON THE CELL-BASE WITH THE STRAIN COILS IN POSITION

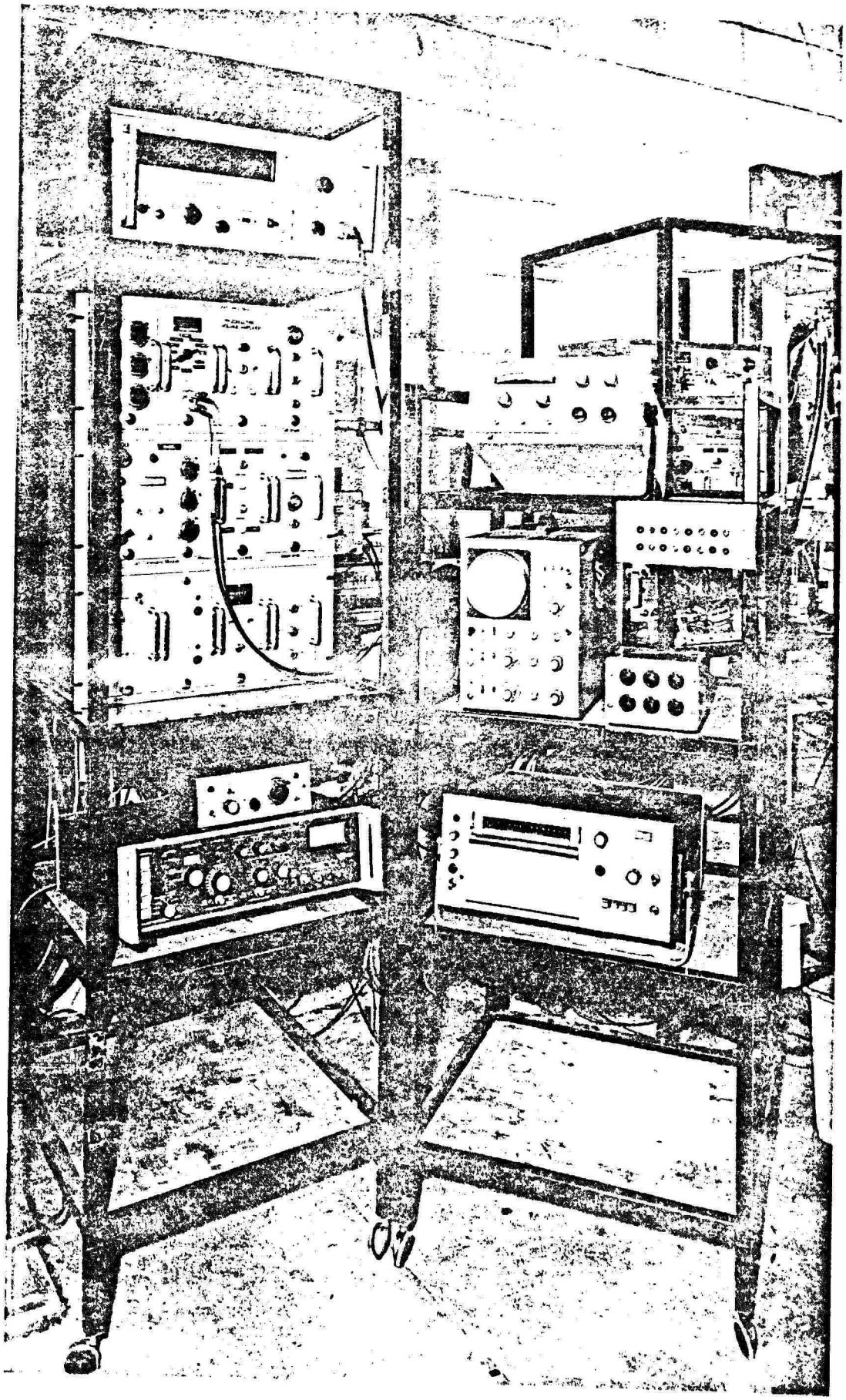

FIG. 7.32 MONITORING AND CONTROL EQUIPMENT FOR THE REUPER NAIL TESTS

specimen occurred due to a 'spike' of electrical noise being picked up by the control equipment and causing a sudden surge of load. As a result of this phenomenon, several tests did not fulfil their potential.

7.3.6 Results

Processing: The results were processed from the UV recorder paper, by hand during the course of the test. The vertical and radial permanent and resilient strains were computed at frequent intervals, and the resilient modulus and Poisson's ratio computed from the resilient strains. A table and graphs of the material behaviour were constructed. Where more than one test was carried out at any test condition, the results were averaged, any obviously erratic results being discarded.

Presentation: A summary of all the successful tests is provided in Table 7.3. The initial resilient modulus was that measured at the start of a test, once the desired amplitude of vertical stress had been achieved. The final resilient modulus was that measured just before the end of a test. The initial resilient Poisson's ratio was the ratio of the radial to longitudinal resilient strain measured at the same time as the initial resilient modulus.

Permanent Strain Behaviour: Figs 7.33 to 7.35 show the vertical permanent strain plotted against the number of cycles, on a semi-logarithmic basis, for the three test series. In most cases, the lines were straight, which was convenient in developing the permanent strain model. The results for the radial permanent strain are not shown, but they were such that, in all tests, the volumetric strain was compressive, thus compaction always occurred.

Resilient Properties: Fig. 7.36 shows the plot of resilient modulus

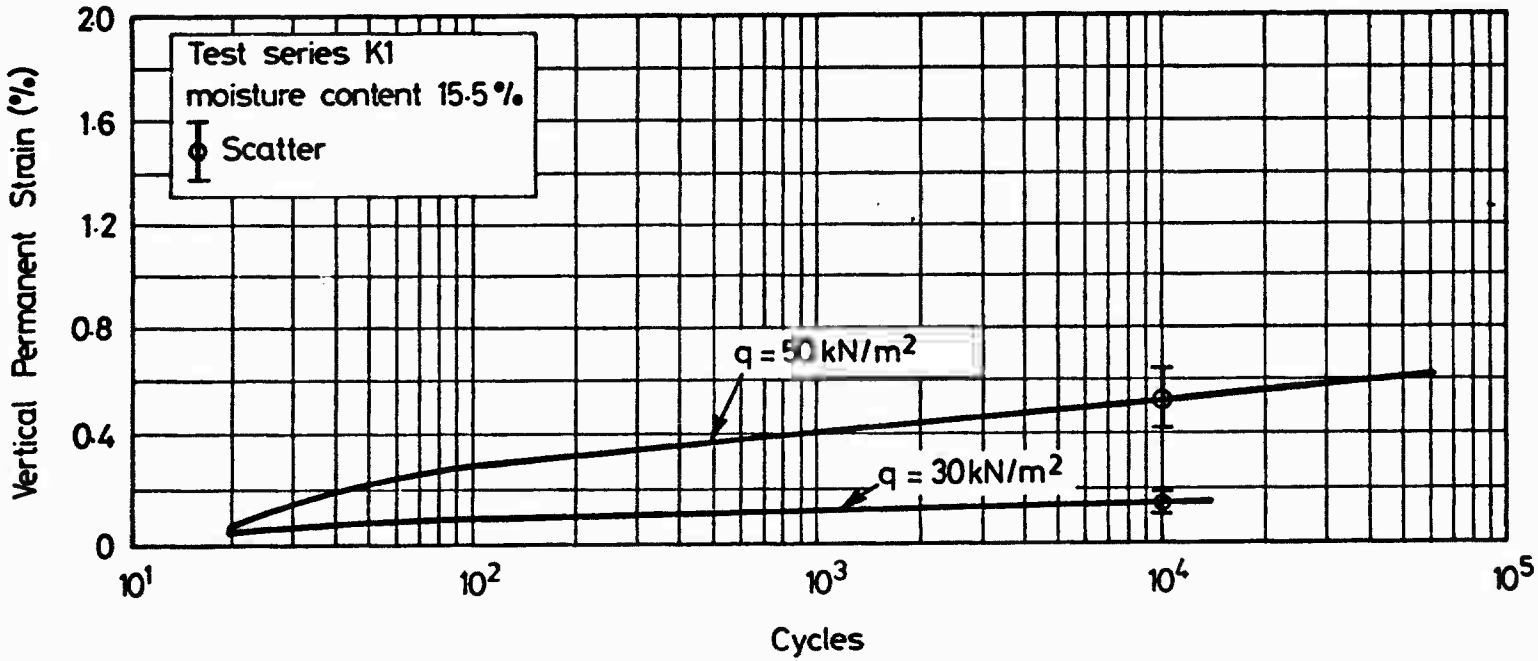

FIG. 7.33 THE EFFECT OF q ON THE VERTICAL PERMANENT STRAIN OF KEUPER MARL, TEST SERIES K1

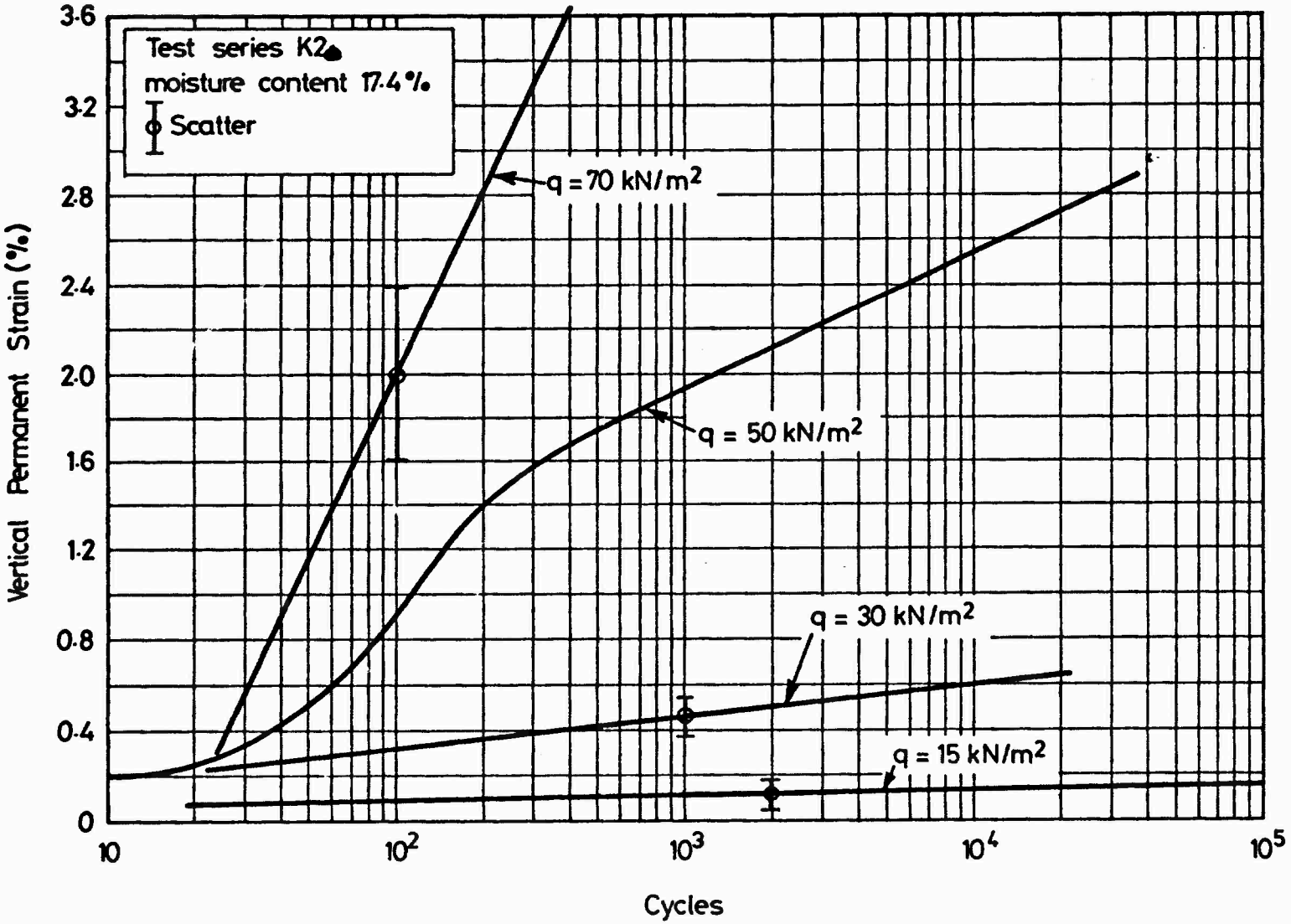

FIG. 7.34 THE EFFECT OF q ON THE VERTICAL PERMANENT STRAIN OF KEUPER MARL, TEST SERIES K2

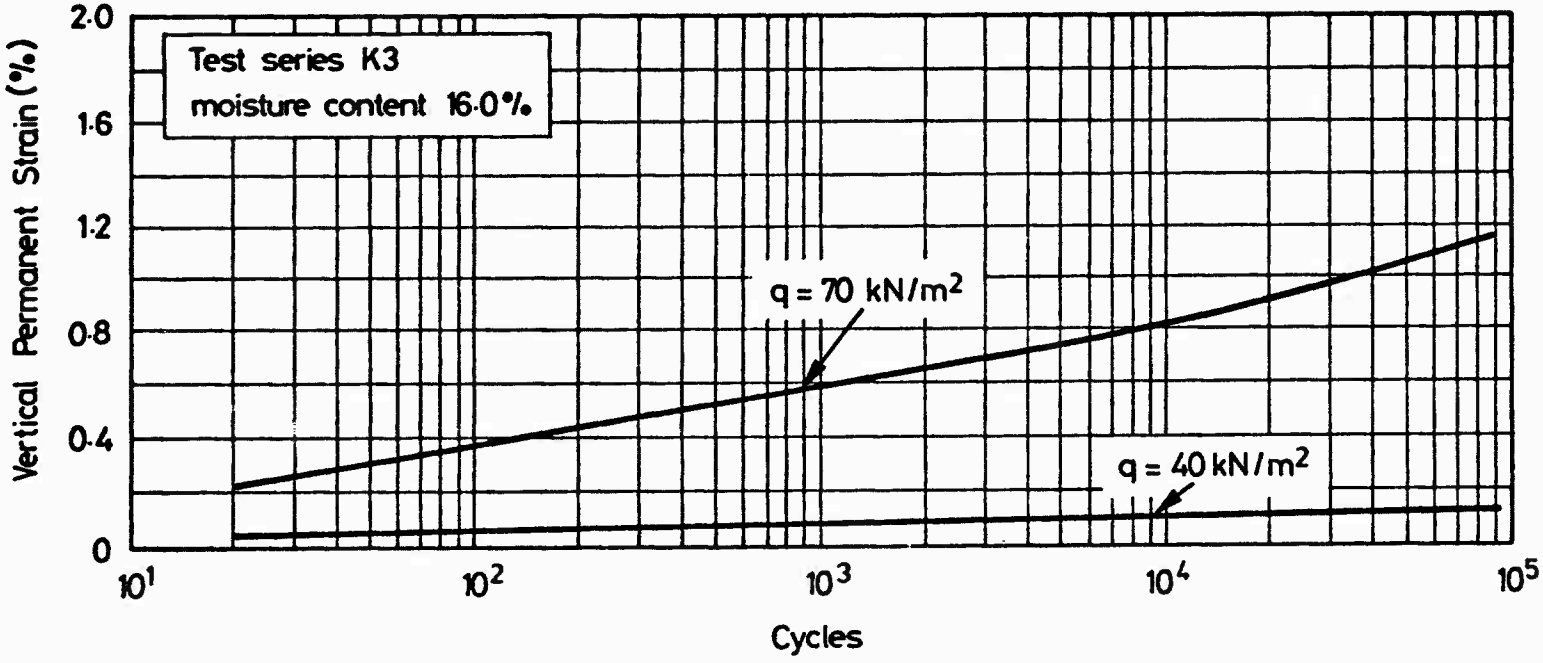

FIG. 7.35 THE EFFECT OF q ON THE VERTICAL PERMANENT STRAIN OF KEUPER MARL, TEST SERIES K3

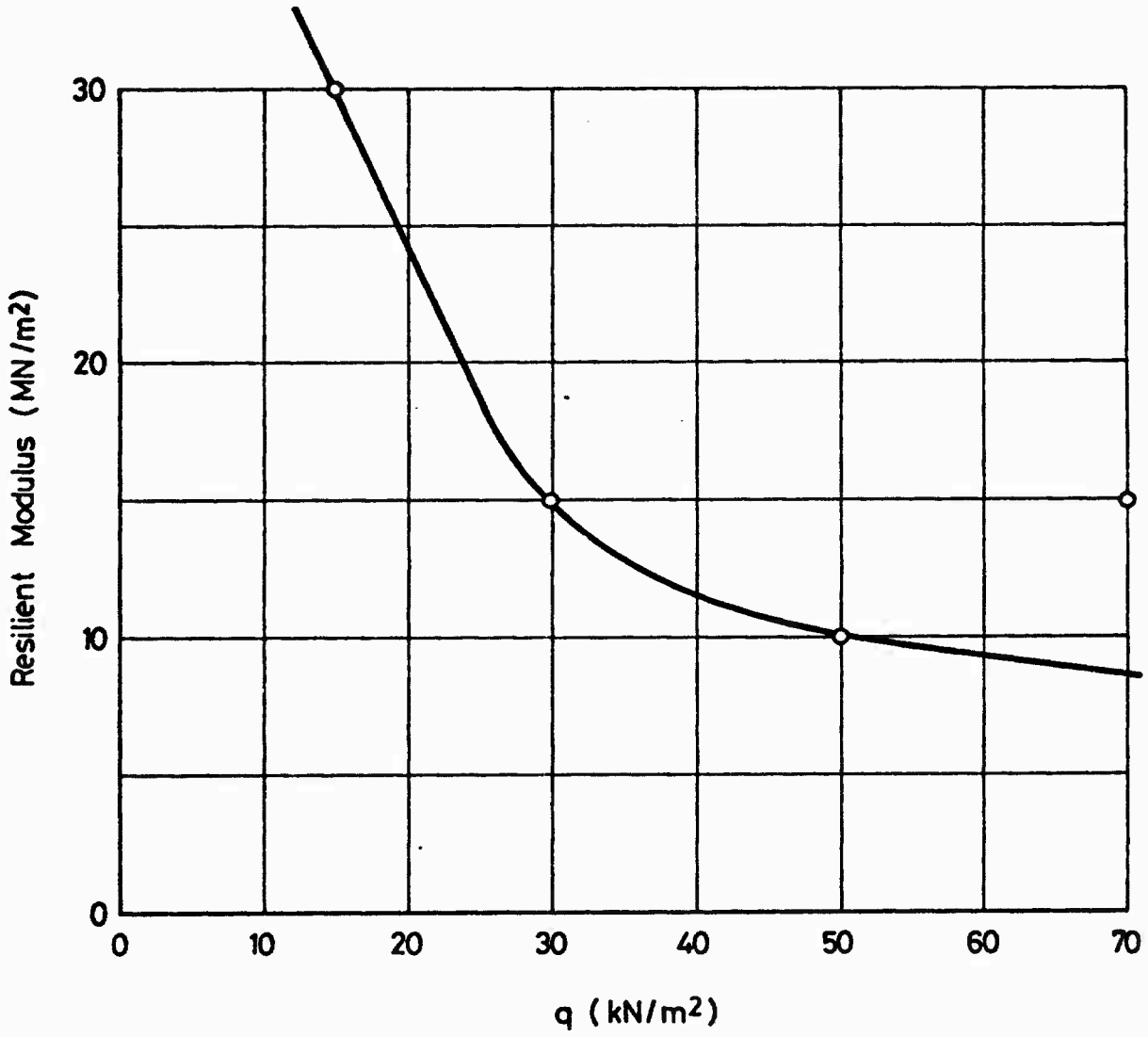

FIG. 7.36 THE EFFECT OF q ON THE RESILIENT MODULUS OF KEUPER MARL, TEST SERIES K2

Table 7.3 Summary of Results of Keuper Marl Characterisation Tests

Stress Conditions (kN/m^2)			Moisture Content (%)	Dry Density (lb/ft^3)	Resilient Properties			Cycles in Test	No. of Tests
p	q	σ_3			Initial Modulus (MN/m^2)	Final Modulus (MN/m^2)	Initial Poisson's Ratio		
TEST SERIES K1									
14.3	30	1.8	15.4	114.6	70	65	.28	14,000	2
25.7	50	2.0	15.5	116.1	38	33	.44	60,000	3
TEST SERIES K2									
5.7	15	1.8	17.4	109.8	30	30	.33	100,000	3
14.3	30	2.0	17.5	110.6	15	15	.27	20,000	4
25.7	50	3.9	17.0	110.9	10	10	.48	34,000	2
37.1	70	6.9	17.7	110.0	15	15	.35	14,000	2
TEST SERIES K3									
20.0	40	2.8	16.0	114.2	42	42	.30	100,000	1
37.1	70	6.9	16.0	113.0	40	31	.45	90,000	1

versus q for test series K2. The modulus for q = 70 kN/m^2 was higher than expected, which was probably due to the fact that the two tests carried out, at this condition, were on cores which had already been tested at a lower value of q. The material showed the usual stress softening non-linearity associated with cohesive materials.

The results for resilient Poisson's ratio are not plotted, but, as can be seen from Table 7.3, there appears to be a trend of increasing Poisson's ratio with increasing q. Again, the result shown for series K2 where q = 70 kN/m^2 is at variance with the general trend.

CHAPTER EIGHT

PREDICTIONS OF RESILIENT BEHAVIOUR

8.1 INTRODUCTION

As described in Chapter 5, measurements of resilient stresses and strains were taken in each pavement at various positions. Comparison of these measurements with those predicted by elastic analysis (linear or non-linear) provided an indication of the accuracy of the analysis.

The most comprehensive set of results from each pavement was provided by the strain coils, which supplied strain distributions with depth in each pavement, and radial strains at the interface in pavements 2 and 3. Strain gauges used in all three pavements in the DBM provided additional information, as did two strain cells in the subgrade, although instrument failure was common with both these types.

Pressure cells provided measurements of stress in each pavement. Radial stresses and strains were measured at the surface of the subgrade in pavements 1 and 2; not very successfully in the first case. Additional cells were installed in the DBM for pavement 3, to measure radial stresses in the top and bottom of the layer. Emphasis was placed on the measurement of the compressive radial stress at the top of the layer since this parameter was likely to be more difficult to determine theoretically than vertical stress.

The following sections present comparisons of measurements with predictions from both linear and non-linear analyses, using resilient constants obtained from the materials characterisation tests described in Chapter 7. The linear elastic analysis, utilised layer theory (BISTRO) (30), whereas the non-linear analysis used finite elements (DEFPAV) (18).

8.2 SELECTION OF ELASTIC CONSTANTS

Discussion in Chapters 6 and 7 showed that both pavement materials had markedly non-linear elastic properties. For this reason a computer programme capable of carrying out a non-linear analysis was favoured (DEFPAV), and the relationships plotted in Figs 7.24 to 7.26 and 7.36 were used as input data for the resilient moduli of the DBM and Keuper marl. A constant Poisson's ratio was used for each material, since the characterisation tests had not highlighted any particular trend in relation to the stress conditions. However, Snaith (25) showed that such trends do exist although usually overshadowed by temperature effects, and work has been carried out at Nottingham (31) so that a variable Poisson's ratio can be used with DEFPAV.

Although a non-linear analysis was favoured, a linear analysis was not discounted, since development of the permanent deformation prediction techniques could show an approximate approach using linear analysis to be adequate. Non-linear analysis is generally much more expensive, in terms of computing time, than the linear approach, and therefore an approximate approach may be necessary in order to make the prediction procedure viable for design purposes.

Linear analyses were carried out using the computer programme BISTRO, compensating partly for the effects of non-linearity by dividing the two-layer pavement system into a number of sub-layers and selecting appropriate moduli and Poisson's ratios. Normally, this procedure involves a certain amount of manual iteration in order to ensure that the moduli correspond to the expected stresses, as determined by Figs 7.24 to 7.26 and 7.36. It should be noted that even if such a procedure results in an adequate analysis, the need for manual calculations and possible alteration of modulus values negates the

advantage gained by saving computing time. The values of moduli actually used in the linear analyses, for which results are presented in this chapter, were in fact chosen from the results of the DEFPAV non-linear calculations and hence manual iteration was not necessary.

8.3 COMPARISON OF MEASURED AND PREDICTED STRESSES

In the case of pavement 1, only four pressure cells were installed in the subgrade, two to measure vertical stress and two to measure radial stress. Only one of the vertical cells survived construction of the pavement, and this gave extremely variable measurements of stress during testing. Although both radial cells gave measurements of stress throughout the tests, the results were again variable. Thus, comparisons between measured and predicted values were virtually impossible, although it could be concluded that they were of the same order.

Measurements of stresses were much more successful with pavements 2 and 3. Two more cells were installed in the clay for pavement 2, resulting in three measurements of vertical stress and three of radial stress, since all six cells survived construction. The results of these measurements were shown in Chapter 5, and are reproduced in Fig. 8.1 with the predicted values superimposed for comparison. The measured vertical stresses are higher than both the linear and non-linear predictions, particularly near the axis of the load. The measured radial stresses are also higher and at all radial distances.

For pavement 3, four cells were included in the subgrade, with an additional five cells in the DBM, three near the top of the layer to measure radial stress, and one of each to measure vertical and radial stresses near the bottom of the layer. The results from all cells, except those measuring radial stress at the bottom of the DBM,

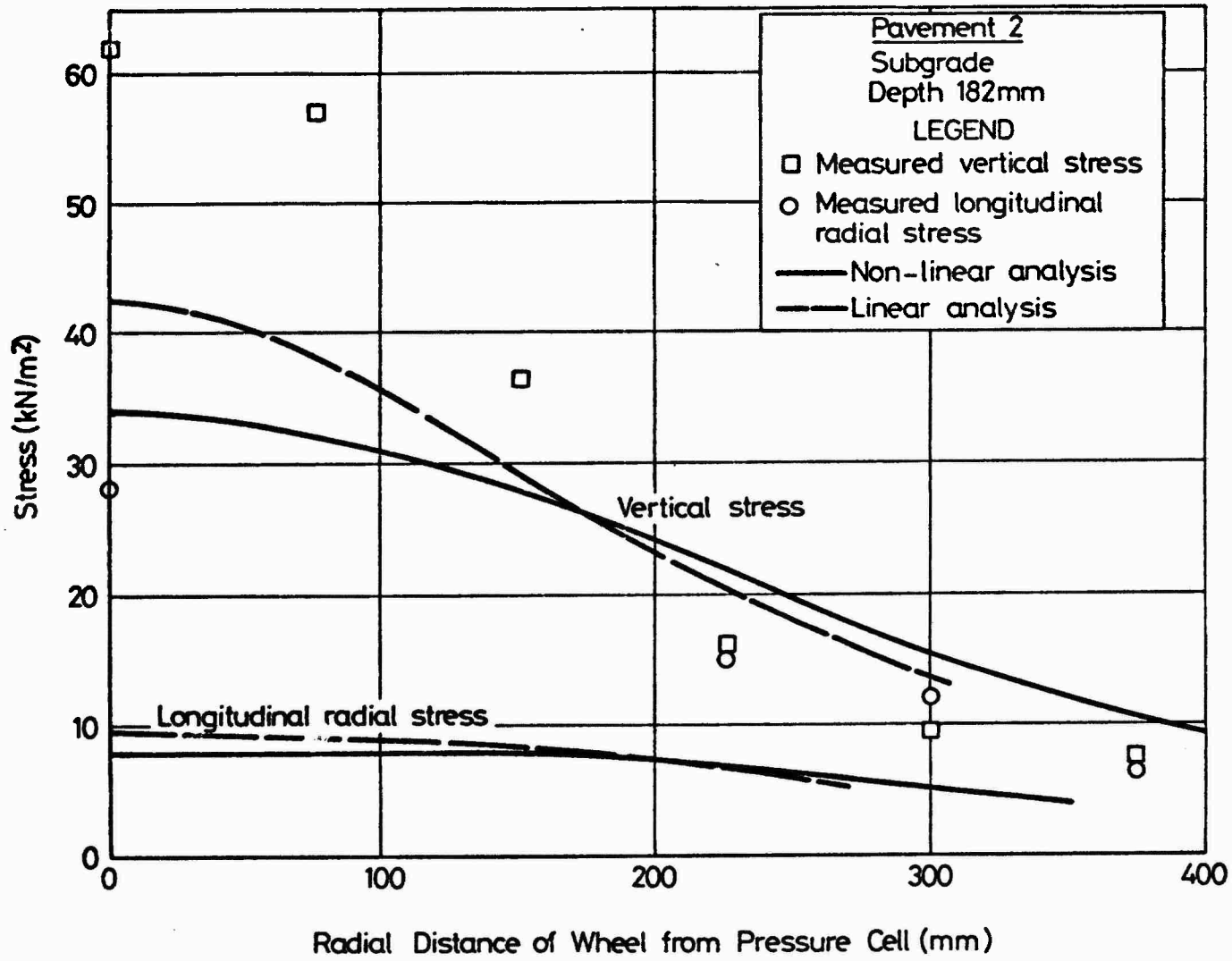

FIG. 8.1 COMPARISON OF MEASURED AND PREDICTED STRESSES (PAVEMENT NO. 2)

were reasonable, and are shown compared with predicted values in Figs 8.2 and 8.3. Because of the development of tensile stress at the bottom of the DBM, quantitatively correct results could not be obtained at this location (see Section 5.6).

Fig. 8.2 is for the stresses in the DBM and shows reasonable comparison between the measured radial stress at the top of the layer, near the axis and the predicted values. However, the measured vertical stress at the bottom of the layer was higher than the predicted value. Fig. 8.3 is for the stresses in the clay and shows the same trends as Fig. 8.1 for pavement 2. Both the measured vertical and radial stresses are greater than the predicted values, with the measurement for the radial stress considerably larger than the predicted value. Earlier research also showed that measured radial stresses were higher than predicted values (32).

8.4 COMPARISON OF MEASURED AND PREDICTED STRAIN

Figs 8.4 to 8.6 show the results of strain measurements for each pavement, with the maximum vertical strain plotted against depth and compared with the corresponding predicted strains. The results from pavements 2 and 3 (Figs 8.5 and 8.6) are the average of readings from two stacks of strain coils, whereas those for pavement 1 (Fig. 8.4) are for only one stack, which showed much more variability, and included the results from the strain gauges, which were found to operate better in this pavement than the subsequent ones.

The measurement of vertical strain at the top of the DBM layer was higher, in all cases, than the predictions; otherwise no trend occurred in the DBM, with the comparison for pavement 3 being very good. The predictions of strain in the subgrade were lower than the measured strains for all three pavements.

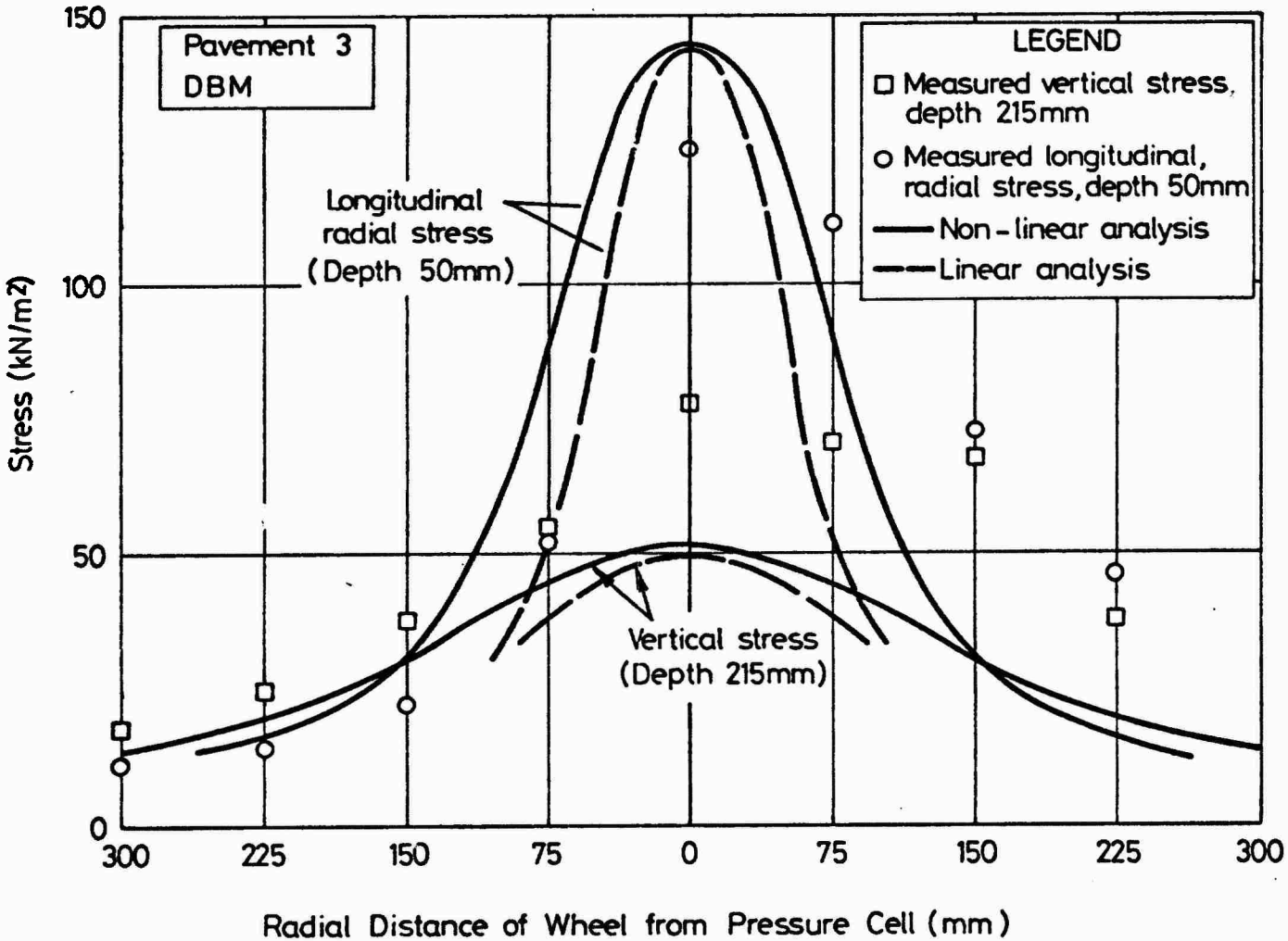

FIG. 8.2 COMPARISON OF MEASURED AND PREDICTED STRESSES IN DBM (PAVEMENT NO. 3)

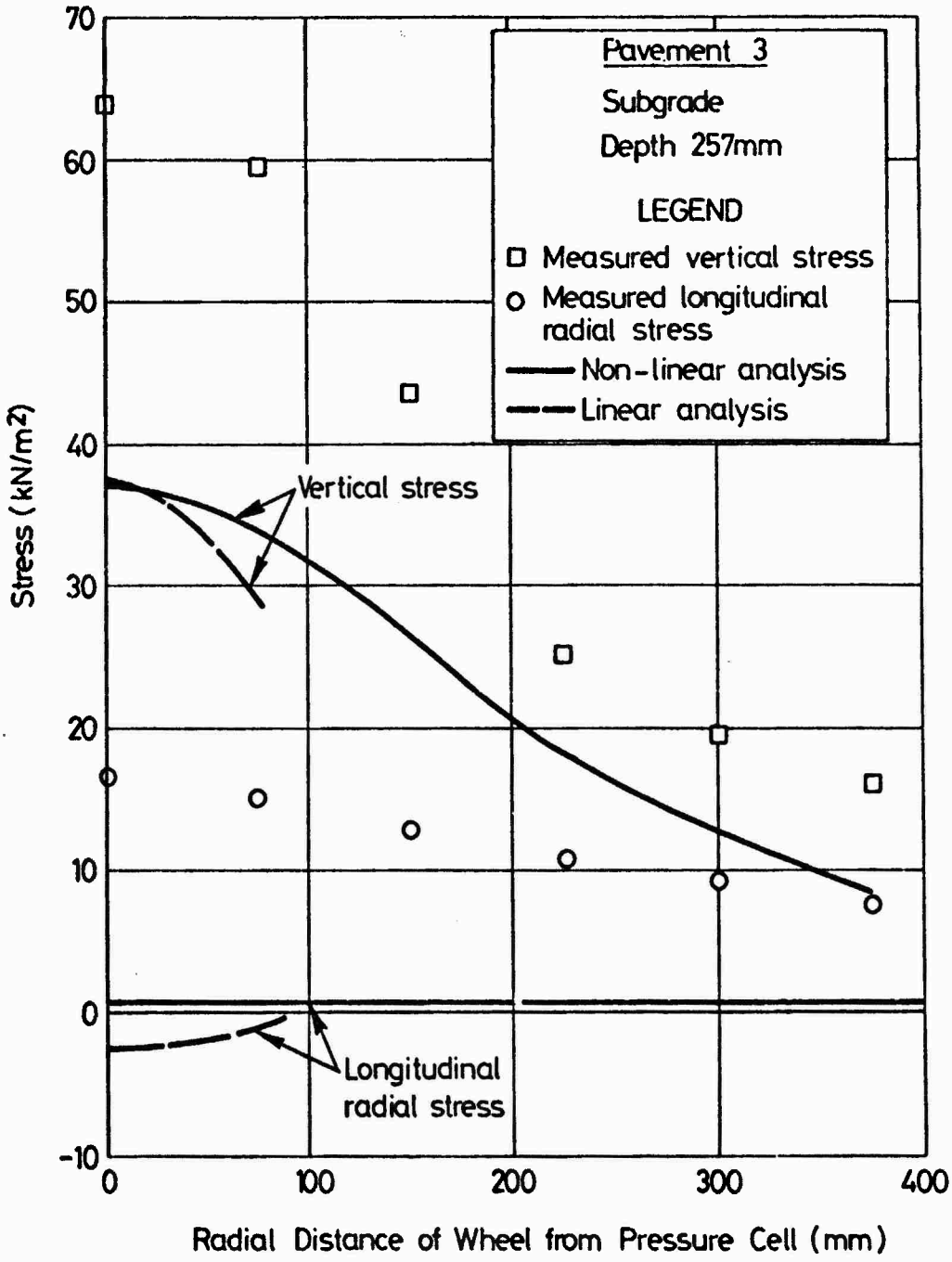

FIG. 8.3 COMPARISON OF MEASURED AND PREDICTED STRESSES IN SUBGRADE (PAVEMENT NO. 3)

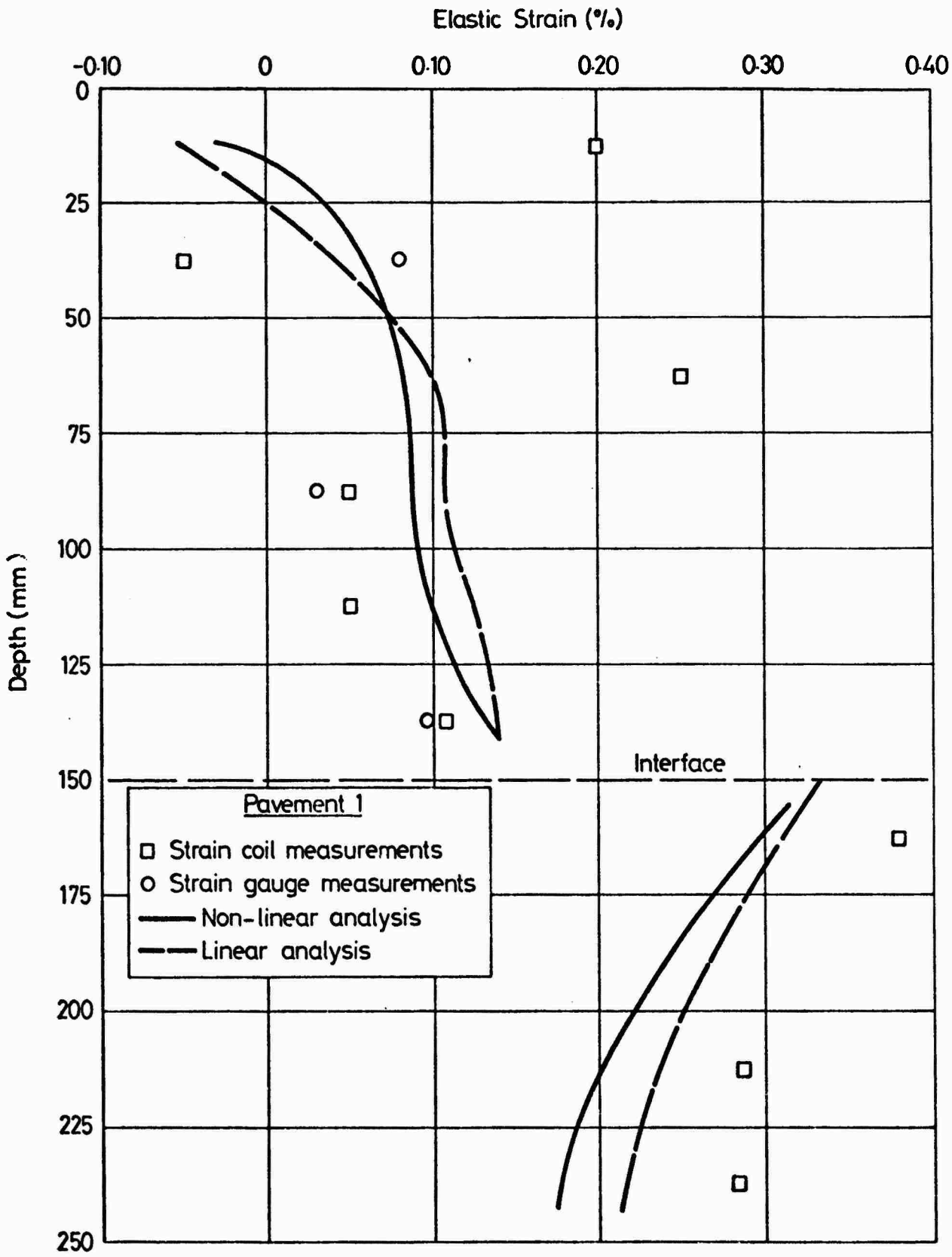

FIG. 8.4 COMPARISON OF MEASURED AND PREDICTED VERTICAL STRAINS

(PAVEMENT NO. 1)

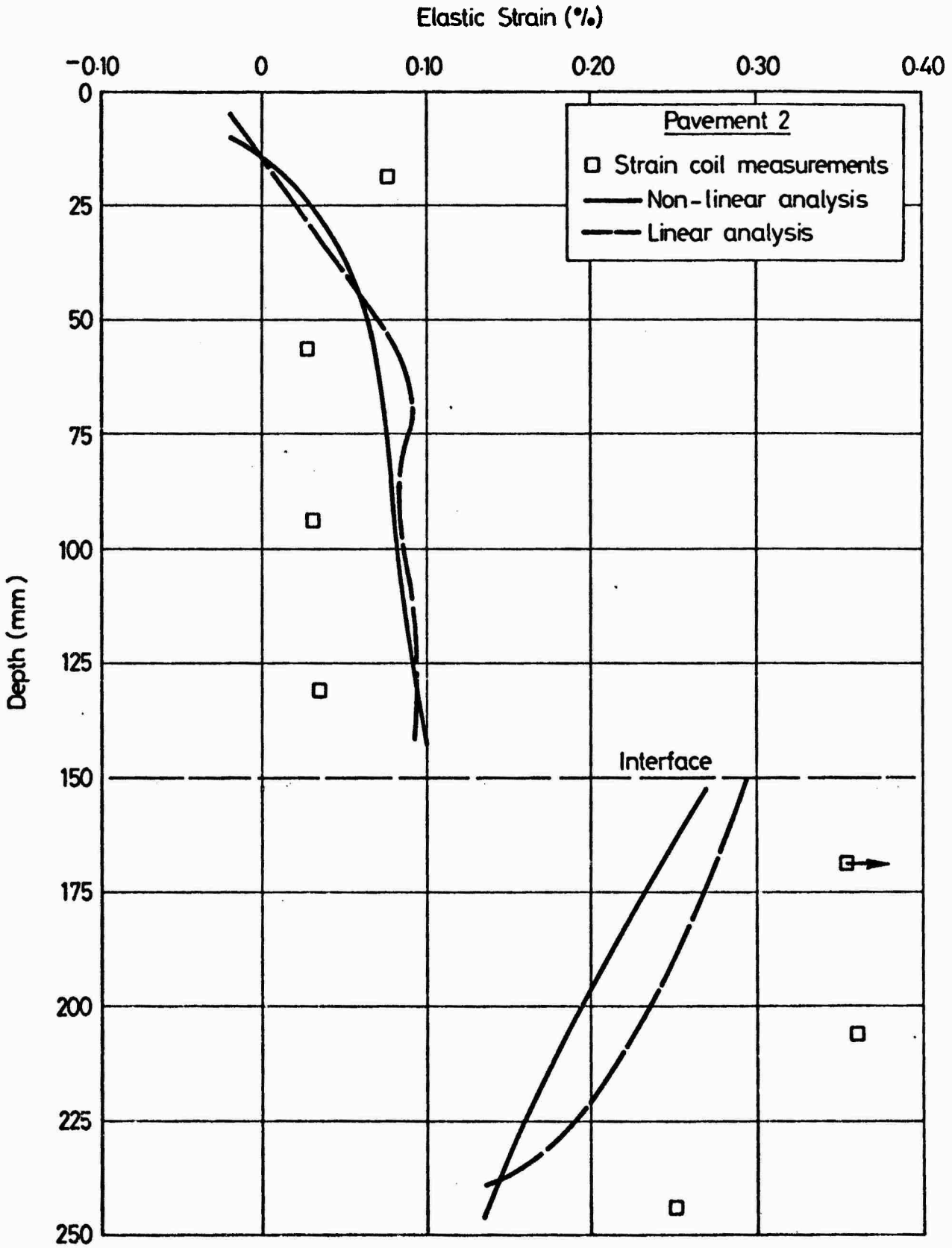

FIG. 8.5 COMPARISON OF MEASURED AND PREDICTED VERTICAL STRAINS

(PAVEMENT NO. 2)

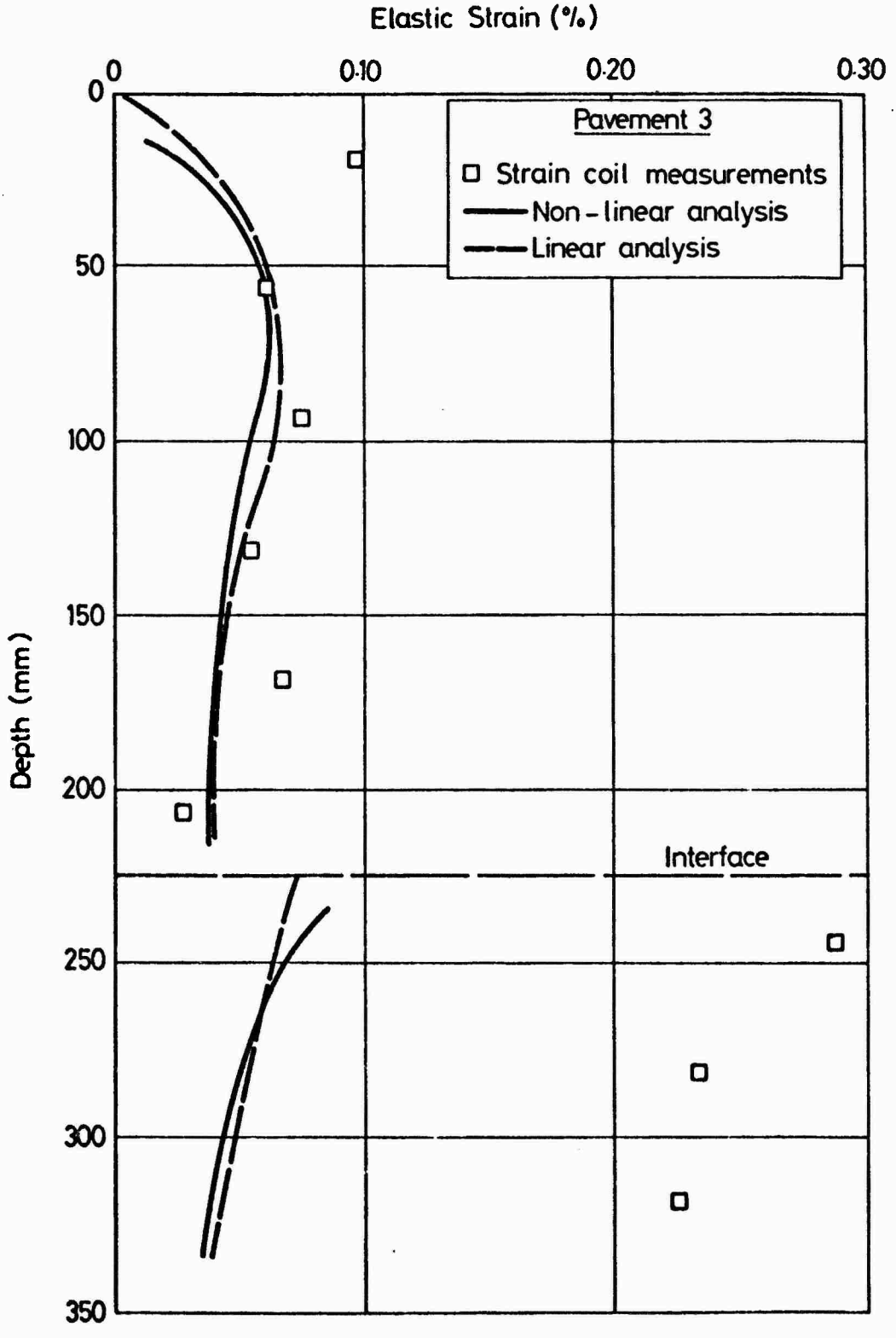

FIG. 8.6 COMPARISON OF MEASURED AND PREDICTED VERTICAL STRAINS

(PAVEMENT NO. 3)

Figs 8.7 to 8.9 show how the strains varied with radial distance for pavements 2 and 3, for those positions where sufficient information was available. For pavement 2, measurements were available for the vertical strain at 275 mm depth in the subgrade, where the measured values were again much higher than the predictions, and for the radial longitudinal strain at the interface where agreement was very good. For pavement 3, more measurements were available, with two sets of vertical measurements compared for the subgrade, and both the lateral and longitudinal radial strains at the interface. In all cases, the predicted values are much less than the measured ones.

8.5 RESILIENT CONSTANTS DERIVED FROM IN-SITU MEASUREMENTS

For a three-dimensional stress field with principal stresses σ_1, σ_2 and σ_3, the generalised Hooke's law can be applied, so that the principal strains are given by equations of the form

$$\epsilon_1 = \frac{1}{E}\left[\sigma_1 - \nu(\sigma_2 + \sigma_3)\right]$$

This is an approximation where the materials are non-linear.

Thus, if the stresses and strains at a point are known, simultaneous equations may be obtained, and solved for E and ν.

For the three pavement experiments, measurement of stresses had been very limited, and it was only possible to compute the resilient constants for one position in the subgrade, 32 mm below the interface. This was for a position on the axis of the load, thus the two horizontal stresses and strains should be equal, and only two simultaneous equations were obtained.

An alternative method of computation, which is more appropriate for non-linear behaviour, is to calculate G and K, from:

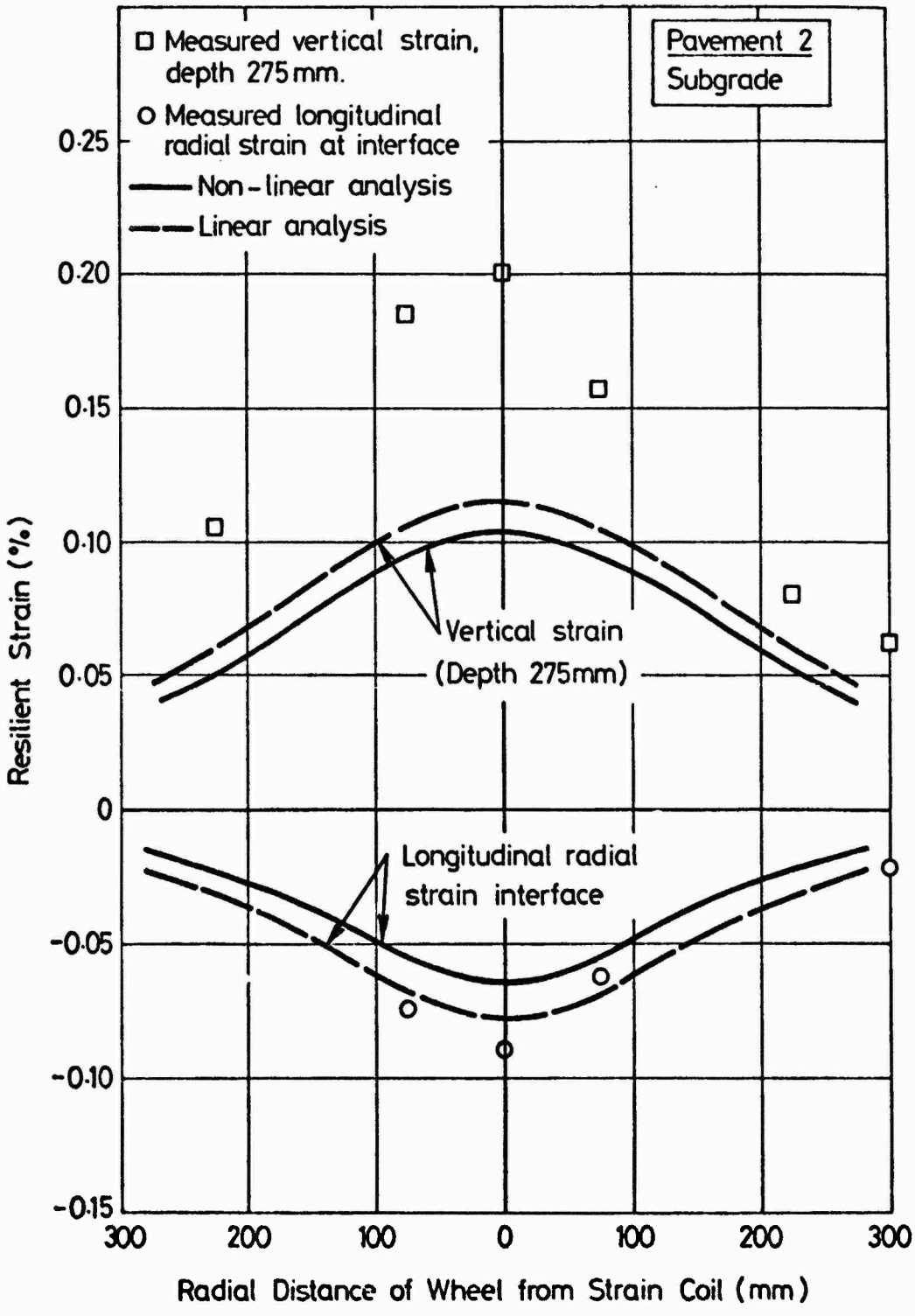

FIG. 8.7 COMPARISON OF MEASURED AND PREDICTED STRAIN VARIATION WITH RADIUS (PAVEMENT NO. 2)

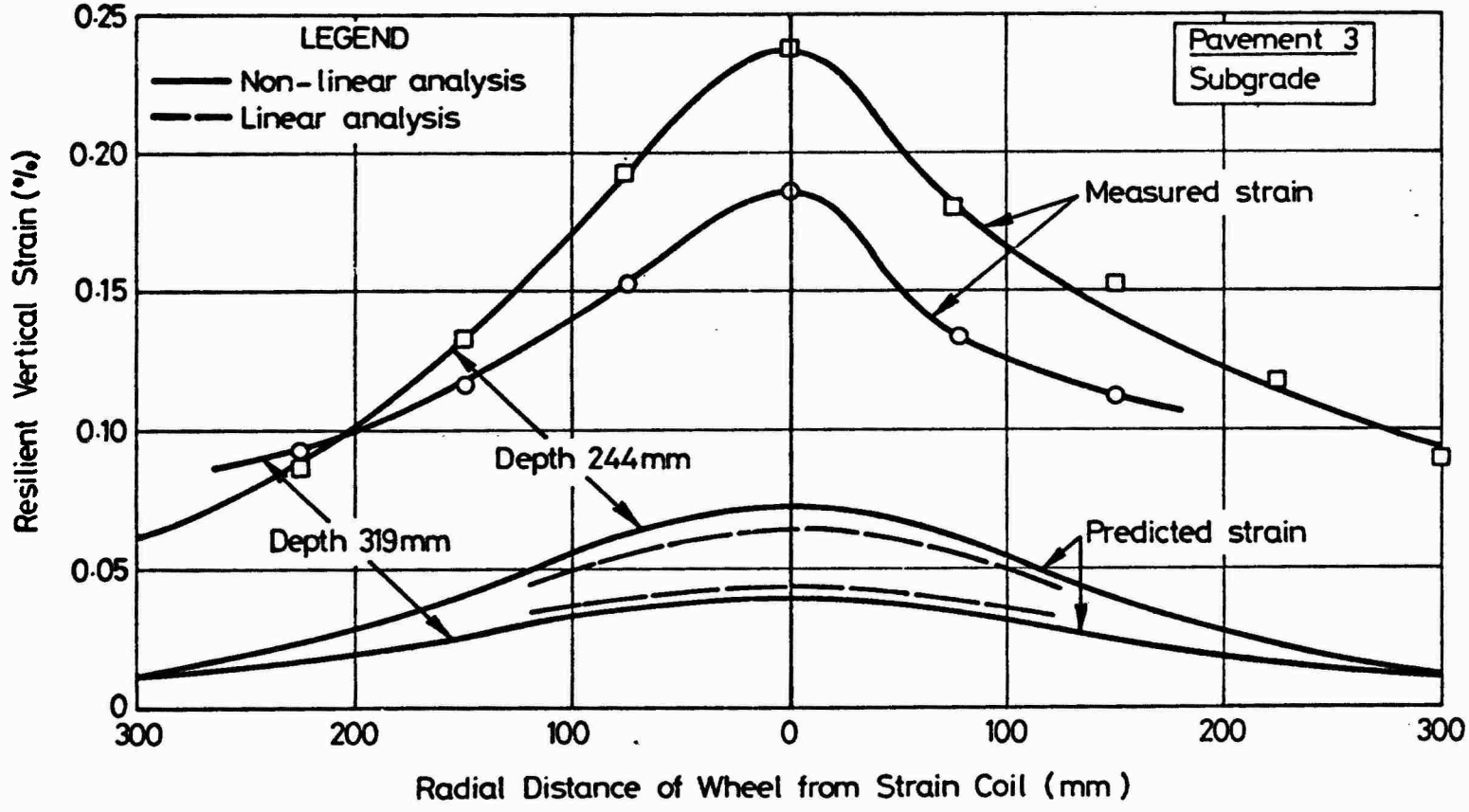

FIG. 8.8 COMPARISON OF MEASURED AND PREDICTED VERTICAL STRAIN VARIATION WITH RADIUS (PAVEMENT NO. 2)

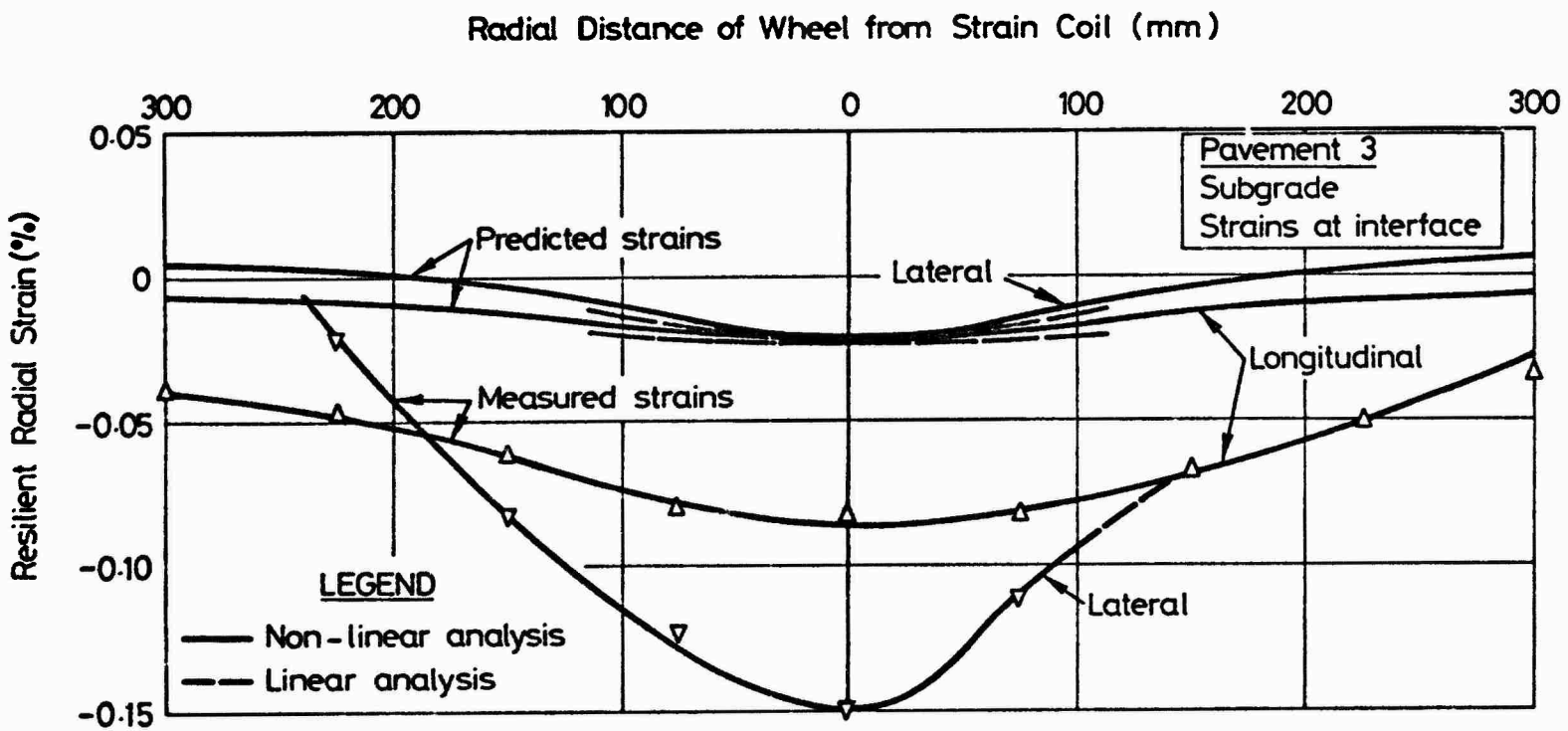

FIG. 8.9 COMPARISON OF MEASURED AND PREDICTED HORIZONTAL STRAIN VARIATION WITH RADIUS (PAVEMENT NO. 3)

$$K = \frac{p}{v} \quad \text{and} \quad G = \frac{\tau_{oct}}{\gamma_{oct}}$$

where p is the mean normal stress, v is the volumetric strain, τ_{oct} is octahedral shear stress and γ_{oct} the octahedral shear strain, and:

$$p = \tfrac{1}{3}(\sigma_1 + \sigma_2 + \sigma_3)$$

$$v = \varepsilon_1 + \varepsilon_2 + \varepsilon_3$$

$$\tau_{oct} = \tfrac{1}{3}\sqrt{[(\sigma_1 - \sigma_2)^2 + (\sigma_2 - \sigma_3)^2 + (\sigma_3 - \sigma_1)^2]}$$

$$\gamma_{oct} = \tfrac{2}{3}\sqrt{[(\varepsilon_1 - \varepsilon_2)^2 + (\varepsilon_2 - \varepsilon_3)^2 + (\varepsilon_3 - \varepsilon_1)^2]}$$

For an axisymmetric situation, $\sigma_2 = \sigma_3$, and:

$$\tau_{oct} = \frac{\sqrt{2}}{3}(\sigma_1 - \sigma_2)$$

$$\gamma_{oct} = \frac{2\sqrt{2}}{3}(\varepsilon_1 - \varepsilon_2)$$

The resilient constants E and ν can be found by solving simultaneous equations obtained from the following expressions, though these assume linear elastic behaviour in their derivation:

$$K = \frac{E}{3(1 - 2\nu)} \quad \text{and} \quad G = \frac{E}{2(1 + \nu)}$$

The resilient moduli and Poisson's ratios obtained by these two approximate methods are shown in Table 8.1 and show good agreement. The values of Poisson's ratio obtained from the generalised Hooke's law indicate that the clay may be very nearly incompressible.

For pavement 1, two distinct measurements of vertical and radial stress were obtained and therefore two values of the constants were computed which are substantially different.

Table 8.1 Resilient constants derived from in situ measurements in subgrade

Pavement No.		Method of Calculation	
		Generalised Hooke's Law	From G & K
1	E MN/m^2	16.9 & 4.8	16.9 & 8.7
	ν	0.37 & 0.48	0.37 & 0.40
2	E MN/m^2	6.8	8.0
	ν	0.5	0.39
3	E MN/m^2	22.1	21.1
	ν	0.53	0.47

When the computed resilient moduli for the softer clay from pavements 1 and 2 (see Section 7.3) are plotted with those obtained from the characterisation tests (Fig. 8.10), a stress stiffening effect is indicated. Since the computation of the moduli depends on the measurement of three parameters in each case, and only three moduli are available, this effect could be a result of erratic measurements. However, such an effect has been reported by previous researchers at high deviator stresses (33).

A non-linear analysis was carried out for pavement 2, using this stress-stiffening relationship for the clay. It resulted in similar stresses and strains in the DBM to those obtained with the original stress-softening relationship, but the strains in the subgrade showed better agreement with measured values, with the stresses even lower than before.

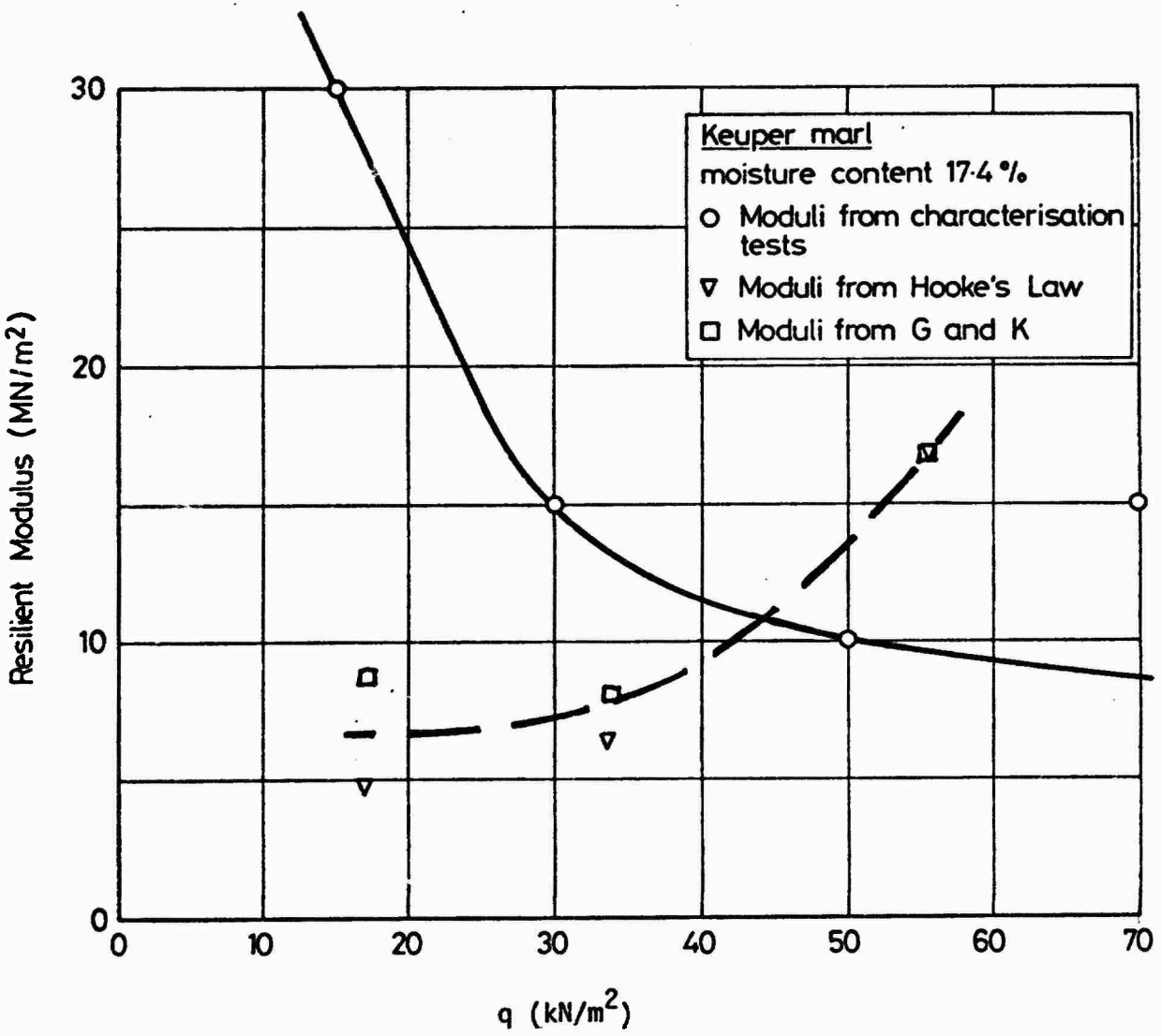

FIG. 8.10 COMPARISON OF RESILIENT MODULUS OF SUBGRADE DETERMINED FROM IN SITU MEASUREMENTS AND FROM CHARACTERISATION TESTS

8.6 SUMMARY

This chapter has compared the measurements of the resilient behaviour of the test pavements with corresponding predictions from linear and non-linear analyses based on resilient constants obtained from the repeated load triaxial tests on the materials described in Chapter 7. Generally, the predicted stresses, particularly radial ones, were lower than measured values, and the predicted strains in the subgrade were much lower than measured values. The prediction of vertical strain at the top of the DBM was always lower than the measurement, and tended towards a tensile value, whereas the measurement was always a high compressive strain.

Comparison of the two elastic analyses shows good agreement, particularly for positions on the axis of the load. This may be attributed to the facts that selection of the constants for the linear analysis was based on the results of the non-linear analysis, and that the pavement structure was divided into five or six sublayers in order to deal with non-linearity. Thus, the more economical linear analysis may be used providing the constants are selected carefully. However, the particular analysis used (BISTRO) does not incorporate the permanent strain calculations, required for rut depth predictions, at the present time. For research purposes, the non-linear analysis using finite elements (DEFPAV) was found to be much more convenient since, apart from the computing time used, the associated work was far quicker.

The resilient constants determined from the in situ measurements in the subgrade implied a stress-stiffening relationship for that material. This was thought to be due to an accumulation of errors and could not be taken as conclusive since only three measurements were available.

Several attempts to produce better agreement between the measured and predicted stresses and strains in each pavement by adjusting the resilient constants proved largely unsuccessful. Generally, the vertical strain at the top of the DBM and throughout the subgrade was under-predicted, as were stresses at the top of the subgrade. Theoretically, reduction of the modular ratio and adjustment of Poisson's ratio should compensate for these differences, but the non-linearity of the materials makes such adjustment very difficult.

An additional problem which arises when analysing pavements is that of anisotropy, which may be introduced into the layers due to rolling during construction. In this case, cores taken from the DBM in each pavement indicated that the aggregate, which was very flakey, was orientated with the longer axis of each aggregate particle in a horizontal direction. An investigation of the anisotropy of the material from pavement 1 with respect to permanent deformation (Figs 7.13 and 7.20), indicated a greater tendency to deformation with cores taken horizontally than with cores taken vertically, although their stiffnesses were comparable. However, the anisotropy encountered with permanent strains could equally well apply with resilient strains, which, combined with non-linearity of the materials, make analysis very difficult.

CHAPTER NINE

PREDICTIONS OF PERMANENT DEFORMATION

9.1 INTRODUCTION

The materials testing results reported in Chapter 7 have been used in this chapter to develop models relating vertical permanent strain to the applied stresses both for the DBM mixes and the Keuper marl used in each of the three pavements. These models are incorporated in the computer programme DEFPAV (18) as "creep equations". Following the calculation of stresses in DEFPAV, the vertical permanent strains are calculated for each element in the chosen network, and these strains are then used in the final calculation of permanent deformation. The final calculation procedure is not incorporated in DEFPAV as yet, but is relatively easy to carry out.

9.2 DEVELOPMENT OF THE DBM PERMANENT DEFORMATION MODELS

9.2.1 Introduction

The results which were plotted in Figs 7.9 to 7.12 and Fig. 7.14 have been replotted in Figs 9.1 to 9.4 using a logarithmic scale for the permanent strain. A model was developed for the DBM used in each pavement, from these figures, using the results from pavement 1 (test series C1 and TH1) as guidelines to the behaviour of pavements 2 and 3 for which only a few results were available.

9.2.2 Model for pavement 1

Figs 9.1 to 9.3 show that, for a particular value of p, a series of parallel lines represented the response of the material to q and to time. Snaith (25) found that the permanent strain behaviour of a DBM could be represented by a series of straight lines, although not parallel,

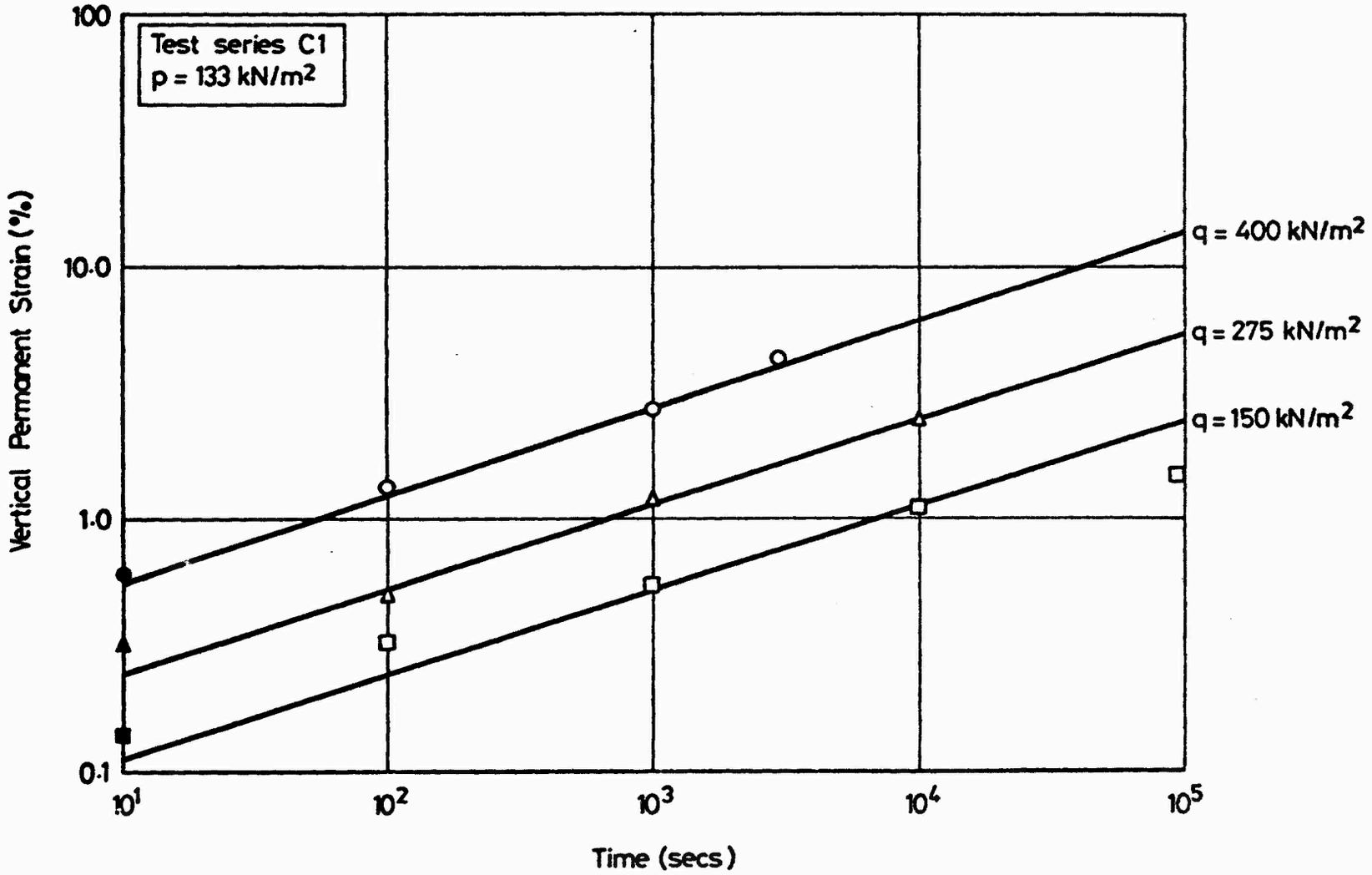

FIG. 9.1 THE INFLUENCE OF q ON VERTICAL PERMANENT STRAIN OF DBM, p = 133 kN/m^2

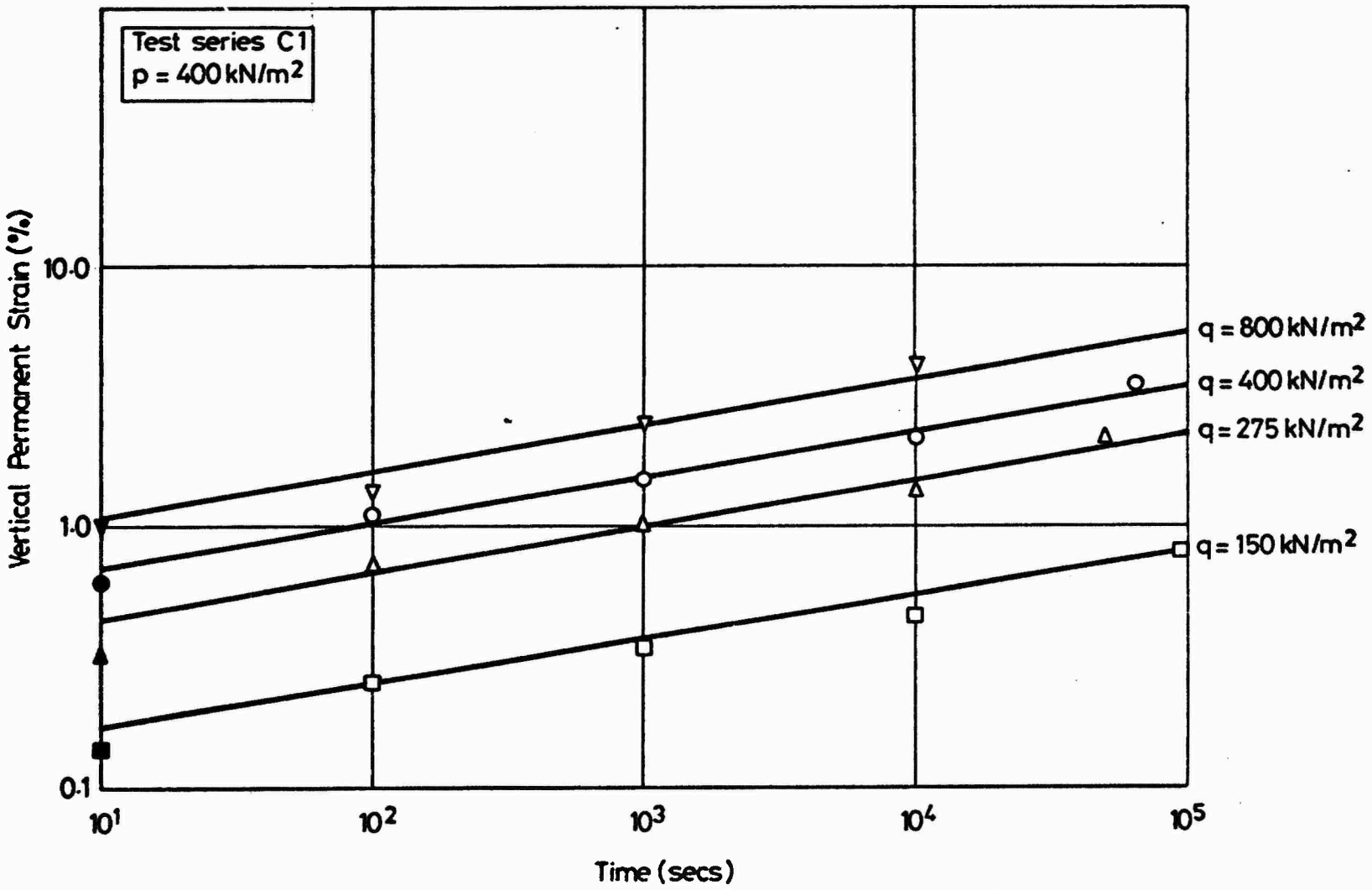

FIG. 9.2 THE INFLUENCE OF q ON VERTICAL PERMANENT STRAIN OF DBM, p = 400 kN/m^2

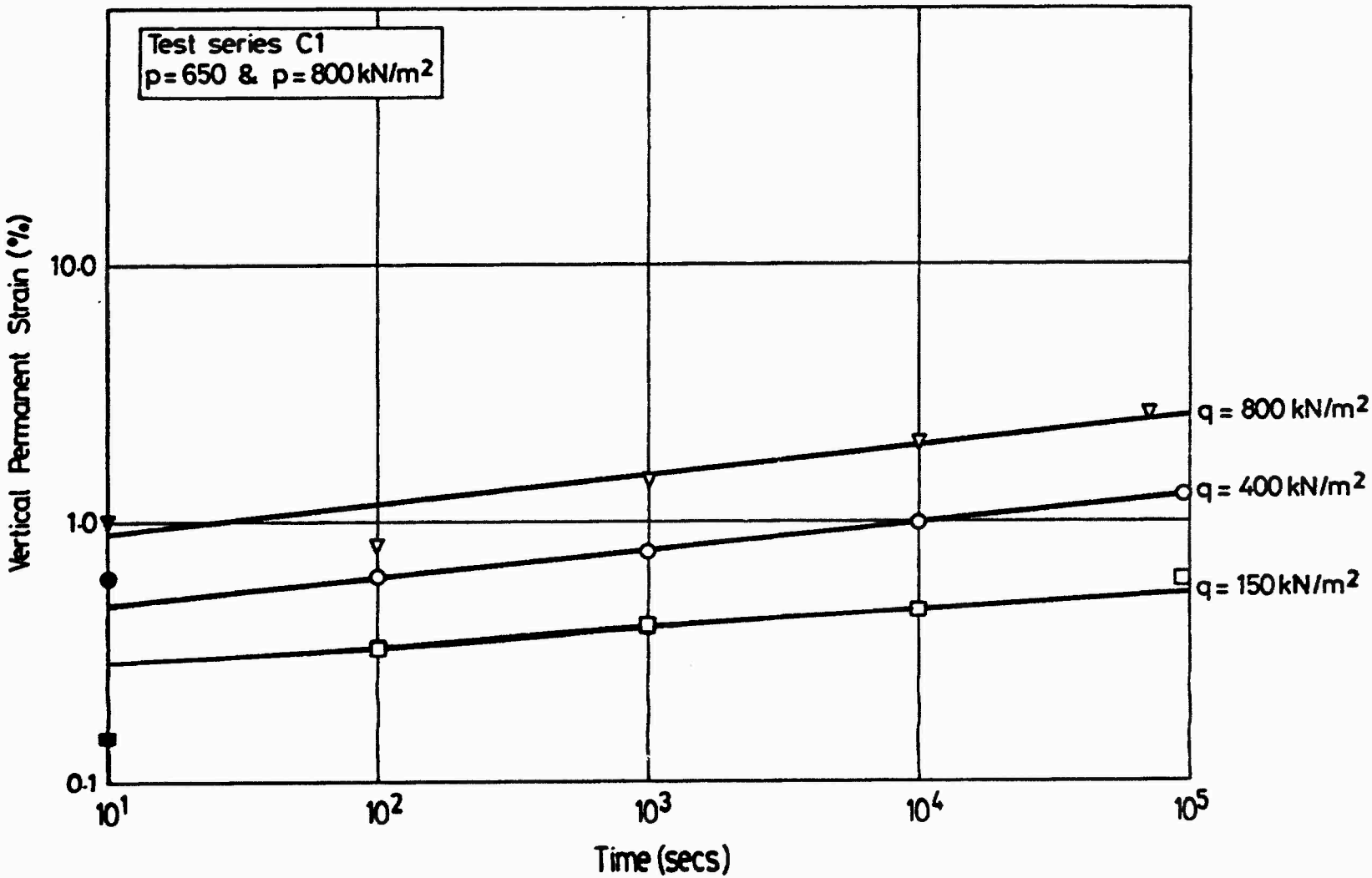

FIG. 9.3 THE INFLUENCE OF q ON VERTICAL PERMANENT STRAIN OF DBM, p = 650 and 800 kN/m^2

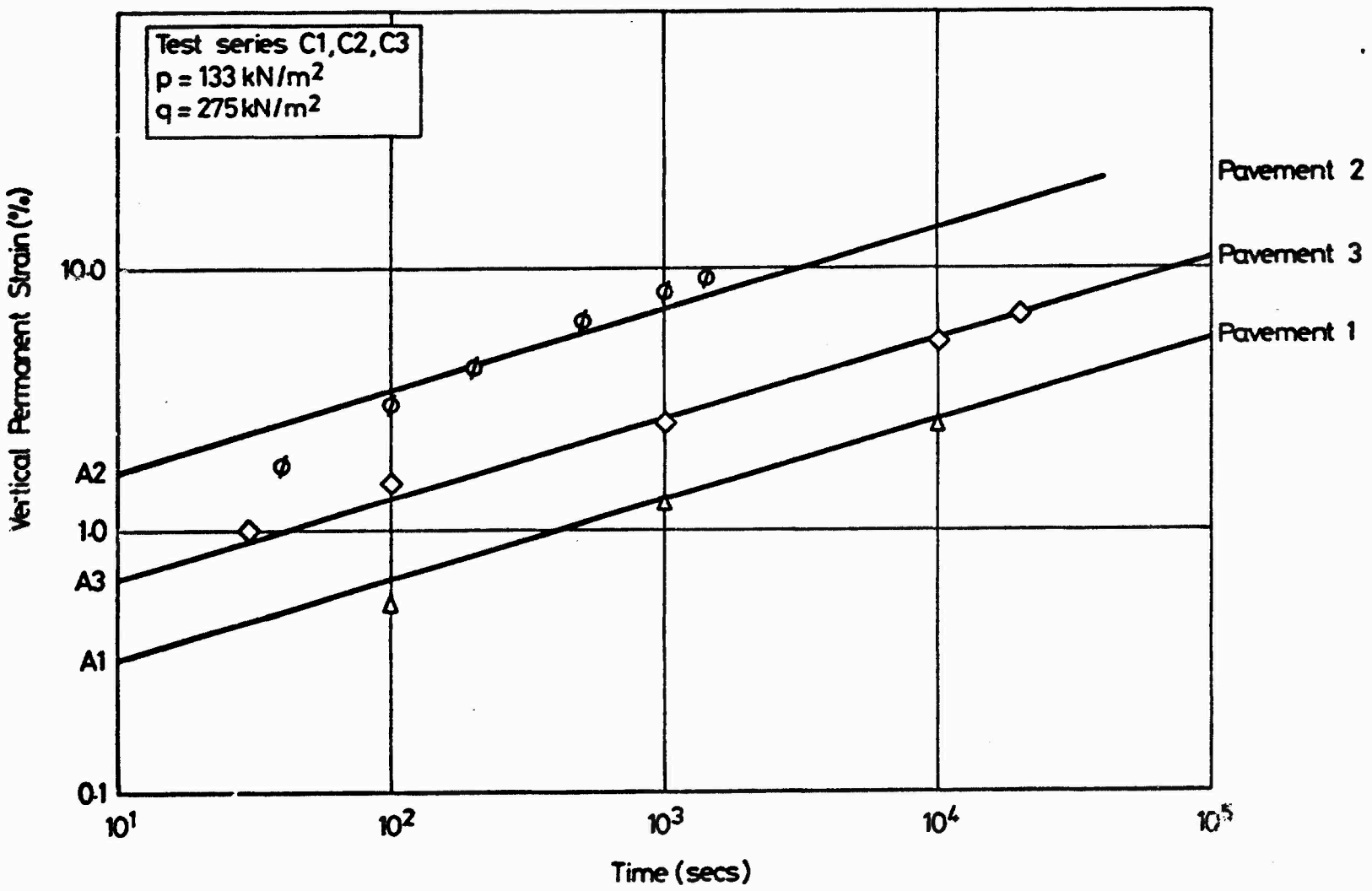

FIG. 9.4 COMPARISON OF VERTICAL PERMANENT STRAINS ACHIEVED WITH DBM CORES FROM EACH PAVEMENT

since his tests were at different values of p. He developed a model for his material by determining an intercept and a slope value and related these to the test conditions. Snaith's original model was improved in the first year of this project and the results were reported earlier (1). The same general approach has been followed in analysing the latest results.

The intercepts with the vertical axis in Figs 9.1 to 9.3 were moved such that they coincided for all values of p, at a particular value of q. This adjustment did not affect the accuracy of the representation significantly. The plot for p = 650 kN/m^2 and q = 150 kN/m^2 (Fig. 9.3) did not comply with the trend established at the other test conditions, which was probably due to the difficulty of measuring the deformations, which were very small under these conditions. Thus, this plot was weighted lightly when choosing the adjusted intercepts, which were approximately the average values from the other test conditions. The adjusted intercepts are shown as closed symbols in Figs 9.1 to 9.3.

It was very difficult to interpret the results of the tension tests since they had been of short duration, and accurate measurements of strain had been difficult. In order to reproduce the in situ stress conditions, at positions where two of the principal stresses are tensile (biaxial tension), it was necessary to apply an axial tension (uniaxial tension) in the triaxial test. This necessitated a much higher tensile stress in the test than exists in situ and therefore resulted in higher permanent strains. This fact was corroborated by the results which, when plotted on a logarithmic basis, did not fall within the pattern established for the compression tests; the intercepts and slopes of the lines being higher. Therefore, in the development of the model, the intercepts were assumed to have the same values as those for the

compression tests, and the slope values were assumed to fall on a smooth curve developed from the compression tests (Fig. 9.6).

A representation of the straight line logarithmic plots is given in Fig. 9.5. The equation of this general line is:

$$\log \epsilon_{vp} = A + B(\log t - 1) \qquad (9.1)$$

Thus, to obtain a value for the permanent vertical strain (ϵ_{vp}), all that is required are values of the intercept (A), and slope (B) of the line, and the total time (t). The intercept depends on q, and the slope on p. Plots of A versus q, and B versus p are shown in Figs 9.6 and 9.7 respectively. For convenience, the actual value of A was used, rather than the logarithm, thus equation 9.1 becomes:

$$\log \epsilon_{vp} = \log A + B(\log t - 1) \qquad (9.2)$$

A computerised curve fitting procedure (34) was used to fit a Chebyshev polynomial to the plots in Figs 9.6 and 9.7, obtaining equations of the form:

$$w = \tfrac{1}{2} a_{i0}T_0(X) + a_{i1}T_1(X) + a_{i2}T_2(X) \ldots\ldots$$

$$\ldots\ldots a_{ii}T_i(X) \qquad (9.3)$$

where $T_0(X) = 1$, $T_1(X) = X$, $T_2(X) = 2X^2 - 1$

$T_3(X) = 4X^3 - 3X$

$T_4(X) = 8X^4 - 8X^2 + 1$

$T_5(X) = 16X^5 - 20X^3 + 5X$ etc.

and X is the independent variable after a change of origin and scale, i.e. in this case X is given by:

$$X = (2x - xmax - xmin)/(xmax - xmin) \qquad (9.4)$$

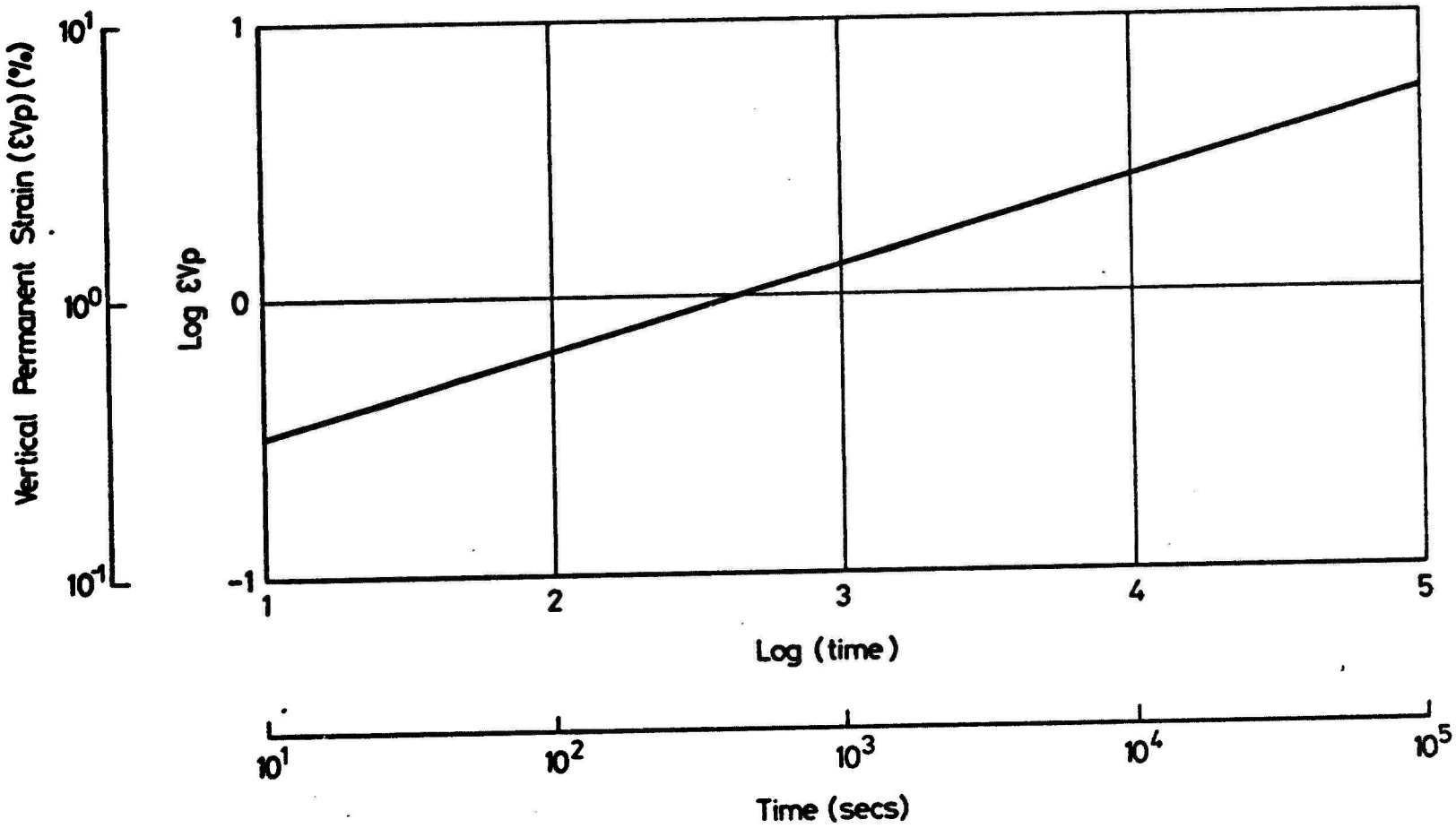

FIG. 9.5 IDEALISED LOGARITHMIC PLOT OF VERTICAL PERMANENT STRAIN VERSUS TIME

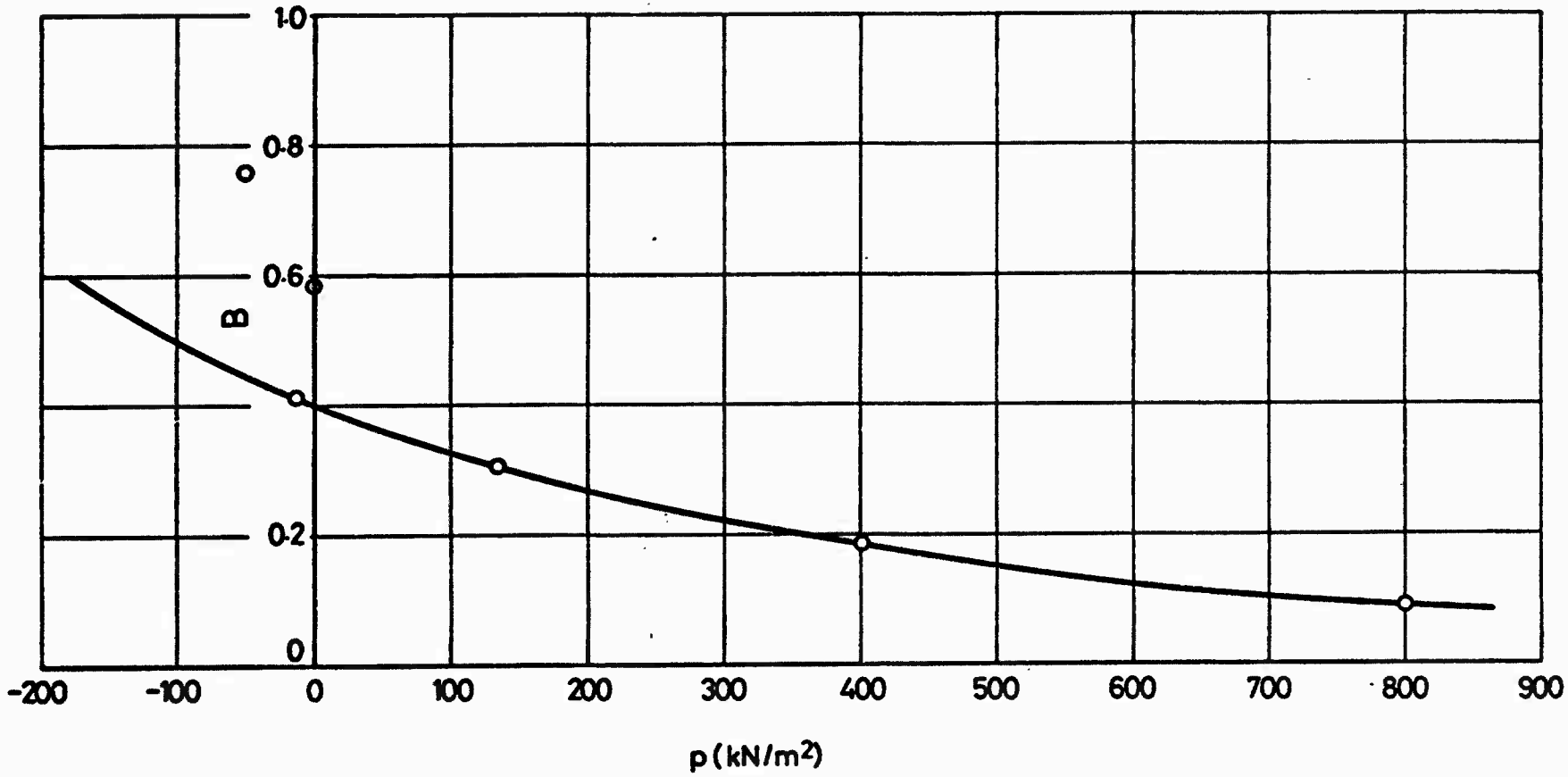

FIG. 9.6 SLOPE FACTOR VERSUS MEAN NORMAL STRESS DBM, PAVEMENT NO. 1

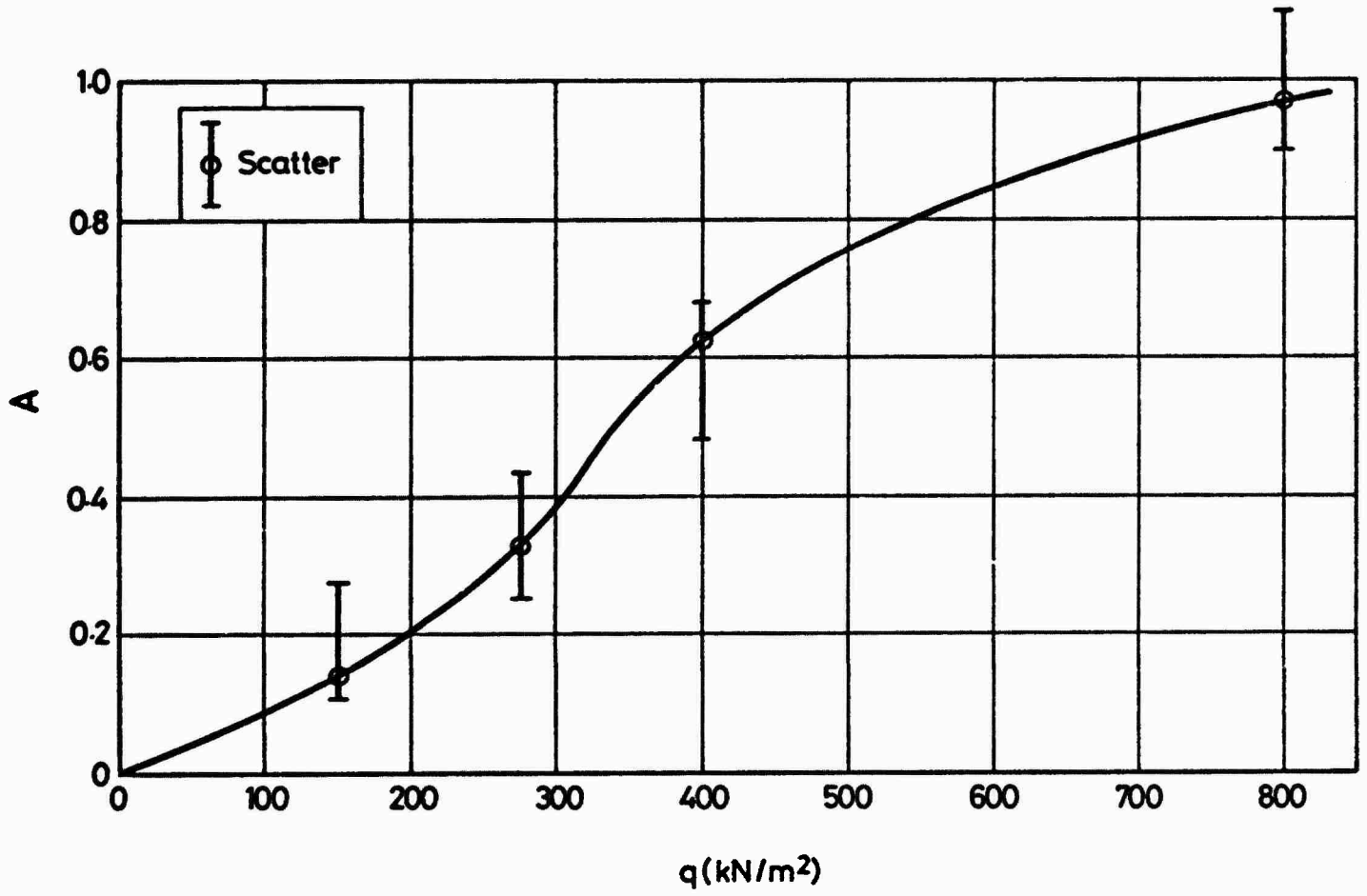

FIG. 9.7 INTERCEPT VALUE VERSUS OCTAHEDRAL SHEAR STRESS (PAVEMENT NO. 1)

Thus, for Fig. 9.7, x = q, qmax = 800, qmin = 0, and:

$$X = (2q - 800)/800 \qquad (9.5)$$

The resulting equations for A and B were as follows:

$$A = .5164 + .5321T_1(X) - .0500T_2(X) - .0538T_3(X) + .0238T_4(X) \qquad (9.6)$$

$$B = .2575 - .2199T_1(Y) + .0546T_2(Y) - .0156T_3(Y) \qquad (9.7)$$

where $$Y = (2(p + 150) - 1000)/1000 \qquad (9.8)$$

Thus, a value for ϵ_{vp} may be obtained, providing the values of p, q and t are known.

9.2.3 Model for pavements 2 and 3

Fig. 9.4 shows the logarithmic plot comparing behaviour of the mixes in the three pavement experiments, at the same stress conditions ($p = 133$ kN/m^2, $q = 275$ kN/m^2). The lines were parallel, with that for pavement 2 showing the greatest susceptibility to deformation. It was therefore assumed that for all other values of p, the slope values for each pavement would be the same as for pavement 1. The intercept values were found by assuming that differences between the intercepts for pavements 2 or 3 and those for pavement 1 at all values of q would be the same as at $q = 275$ kN/m^2.

Hence: $$\log A_2 = \log A_1 + .731 \qquad (9.9)$$

$$\log A_3 = \log A_1 + .301 \qquad (9.10)$$

where A_1, A_2 and A_3 are the intercepts for pavements 1, 2 and 3 respectively, as shown in Fig. 9.4.

Therefore, providing p, q and t are known, the vertical permanent strain may be found from equations 9.2, 9.6 and 9.7, as for pavement 1,

by substituting the appropriate value of A_2 or A_3, obtained from equation 9.9 or 9.10, into 9.2.

9.3 DEVELOPMENT OF KEUPER MARL PERMANENT DEFORMATION MODELS

Discussion in Chapter 7 indicated that the results for vertical permanent strain of Keuper marl when plotted semi-logarithmically, were in a convenient form for the development of models. The plots in Figs 7.33 to 7.35 were adjusted slightly so that all lines passed through the origin, as in Fig. 9.8, which shows Fig. 7.34 replotted. The general form of the equation for any line is thus:

$$\epsilon_{vp} = b \log N \qquad (9.11)$$

where ϵ_{vp} is the vertical permanent strain, b is the slope of the line, and N is the number of load cycles. Thus, to obtain a value of ϵ_{vp} after a particular number of cycles (N), all that is required is a value of b, which is simply a function of q. Since the test programme for the Keuper marl was based on a unique line, theoretically the value of b could depend on p or q. However, as discussed in Chapter 7, a constant confining pressure was employed in the testing, and only the mean values of p and q were reproduced. The magnitudes of q used in the testing were equivalent to those in situ and hence this parameter was chosen to define b.

The main series of tests for this material was series K2 (Fig. 9.8) which used cores taken from new material installed for pavement 2, that was similar to the material in pavement 1. Fig. 9.9 shows the plot of b_1 versus q for this series, and again, a Chebyshev polynomial was fitted to the plot to give the following equation for b_1:

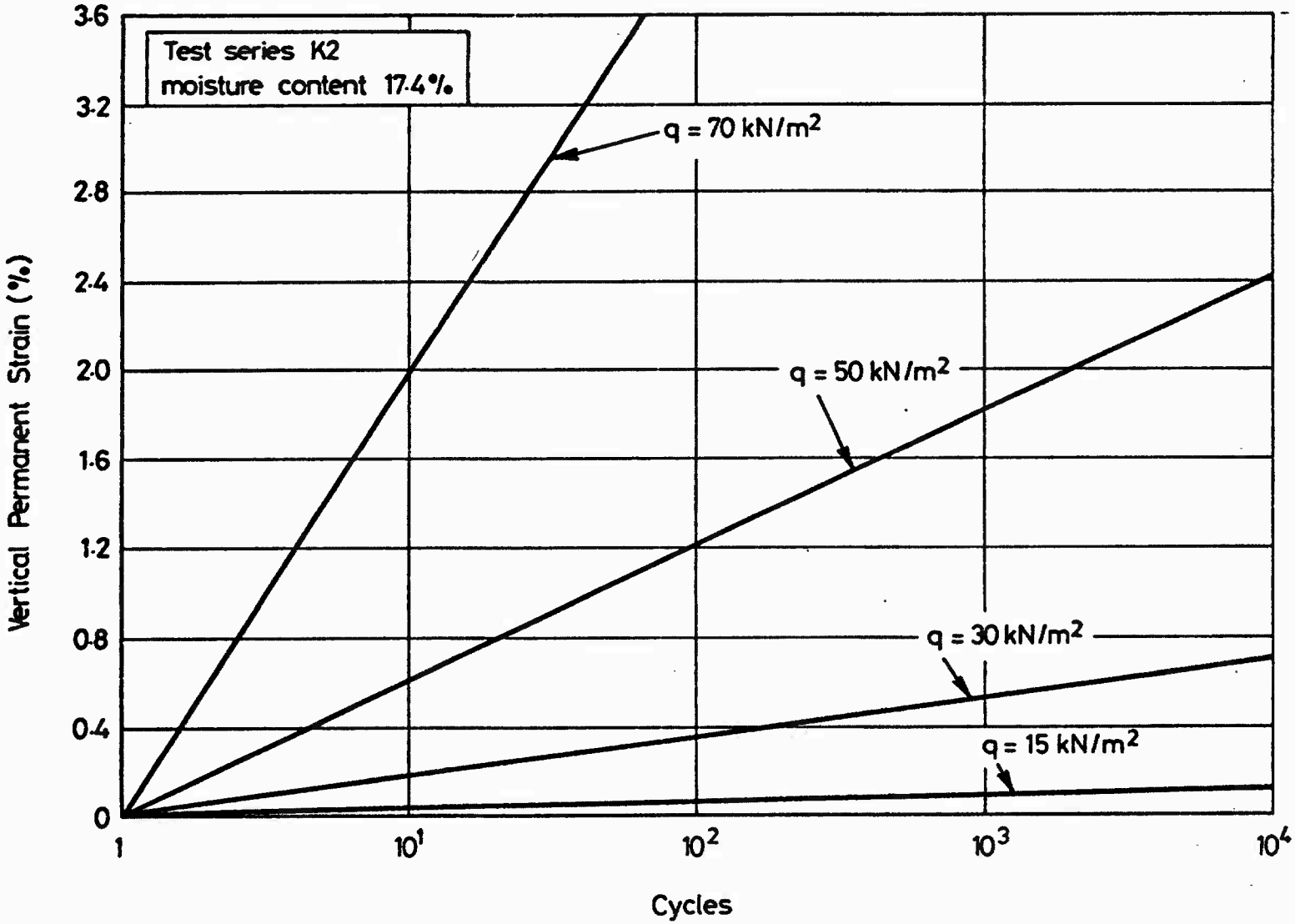

FIG. 9.8 ADJUSTED PLOT SHOWING EFFECT OF q ON VERTICAL PERMANENT STRAIN OF KEUPER MARL

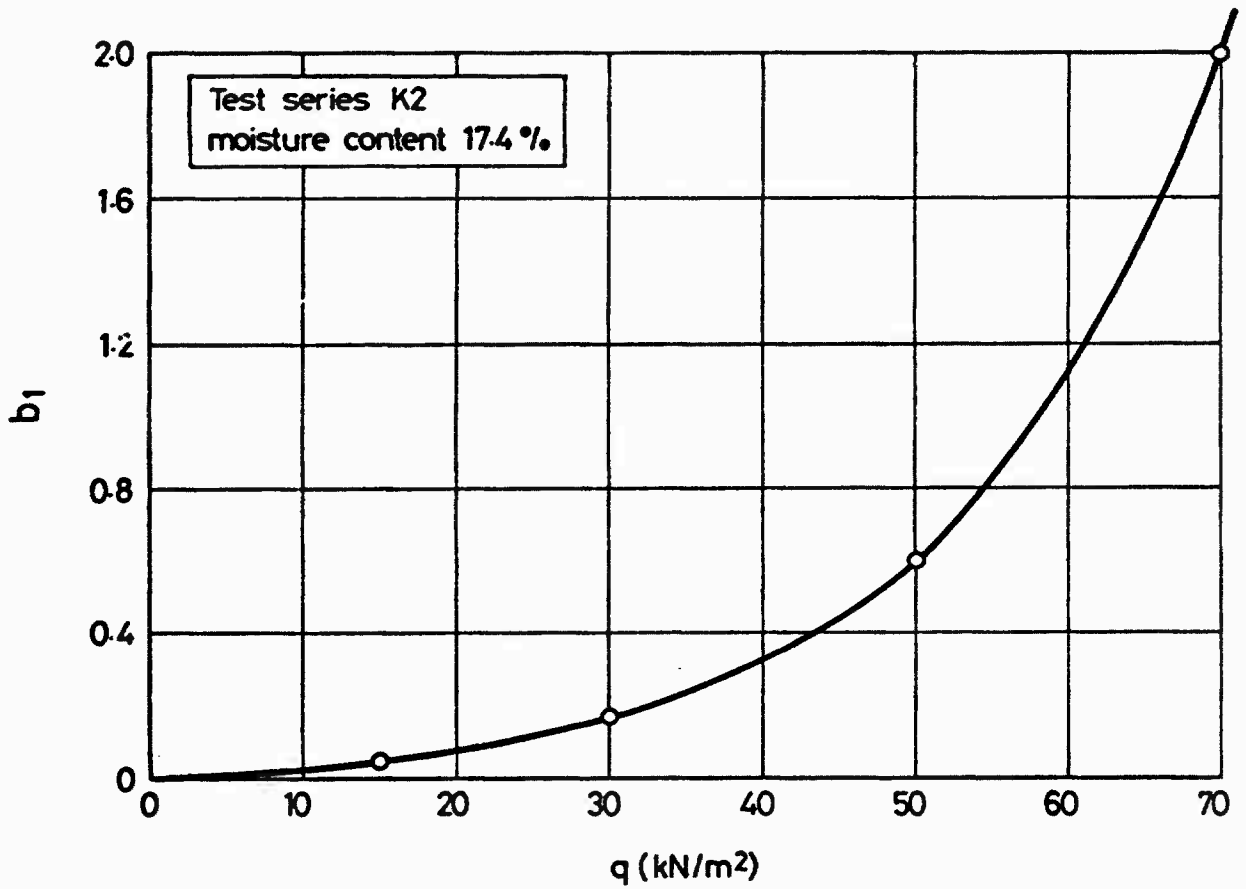

FIG. 9.9 SLOPE FACTOR VERSUS OCTAHEDRAL SHEAR STRESS (KEUPER MARL, TEST SERIES K2)

$$b_1 = .59159 + 88784T_1Z + .37704T_2(Z) + .10584T_3Z$$

$$+ .03058T_4Z + .00198T_5(Z) \qquad (9.12)$$

where $$Z = (q - 70)/70 \qquad (9.13)$$

A simpler equation represents the curve, for $q \leq 40$ kN/m^2:

$$\epsilon_{vp} = (q/70)^2 \log N \qquad (9.14)$$

where $b_1 = (q/70)^2$.

This equation was found to be more satisfactory than the Chebyshev polynomial for $q \leq 40$ kN/m^2, and was therefore adopted because of its simple form. In fact, it was found that, using the non-linear analyses for all three pavements, the value of q was never greater than 40 kN/m^2.

A similar model was developed for the dryer materials tested in series K1 and K3, which were combined because of their similar moisture contents, and together, the results provided sufficient information to construct a b_2 versus q plot (shown in Fig. 9.10). An equation of similar form to 9.14 was found to provide a best fit line through the points, over the entire range tested, giving:

$$\epsilon_{vp} = (q/130)^2 \log N$$

where $b_2 = (q/130)^2$.

The model developed from test series K2 was used for predictions on pavement 1 and for the layer of new material added during the construction of pavement 2. The model developed from series K1 and K3 was used for predictions on pavement 3 and for the old material in pavement 2.

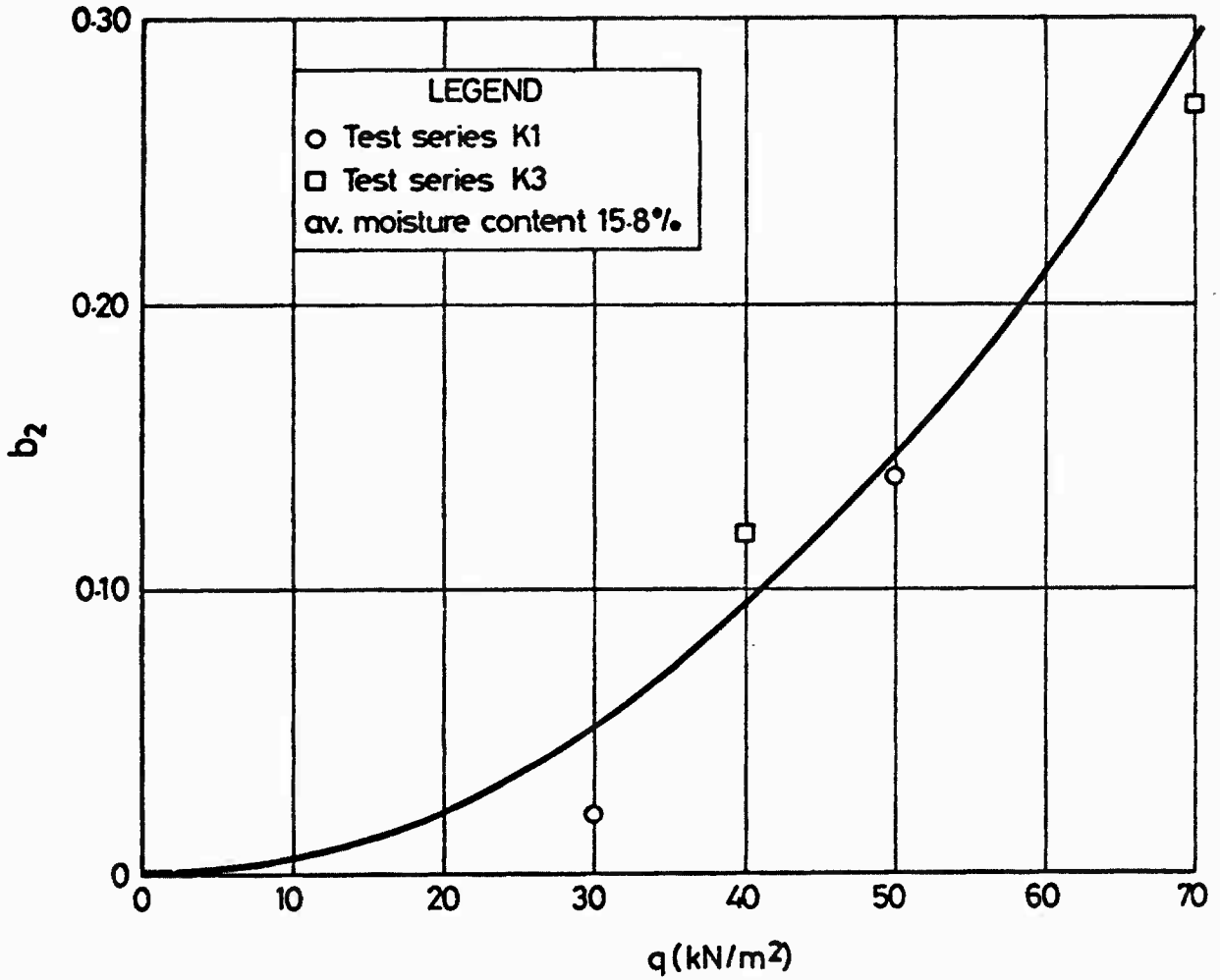

FIG. 9.10 SLOPE FACTOR VERSUS OCTAHEDRAL SHEAR STRESS (KEUPER MARL, TEST SERIES K1 AND K3)

9.4 PREDICTION PROCEDURE

9.4.1 Multi-track tests

The permanent strain models were incorporated in DEFPAV which computed vertical permanent strain for a network of elements after any number of load repetitions in a single wheel track.
However, the main experiment for each test pavement was a multi-track test, consisting of a pseudo-normal distribution of load repetitions in nine equally spaced wheel tracks over a 600 mm width of pavement. Therefore, in order to obtain values of rut depth and rut profile, it was necessary to obtain the vertical permanent strain in each element due to the wheel travelling in each of the nine tracks. This was achieved by adopting a "time hardening" cumulative loading procedure (35). This procedure is illustrated in Fig. 9.11 with an alternative "strain hardening" procedure. The former was favoured, because it is simpler to apply and had been validated by tests on nominally the same DBM (28). A cumulative loading procedure is thus used to predict the strain accruing in an element subjected to differing stresses, which may be caused by loads of differing magnitude passing directly over the element, or by loads of the same magnitude at different radii from the element, which is the case here.

Cumulative loading procedure: Fig. 9.12 shows the distribution of wheel passes used in the multi-track tests, for a total number of passes of 10^5. Rather than calculate the permanent deformation at the points on the centre line of each wheel track, points midway between adjacent wheel tracks were chosen, since all elements below such a point were affected equally by each adjacent track. There is no great advantage in either method, however, although the second is easily combined with a finite element analysis. The permanent strains accruing in the columns of

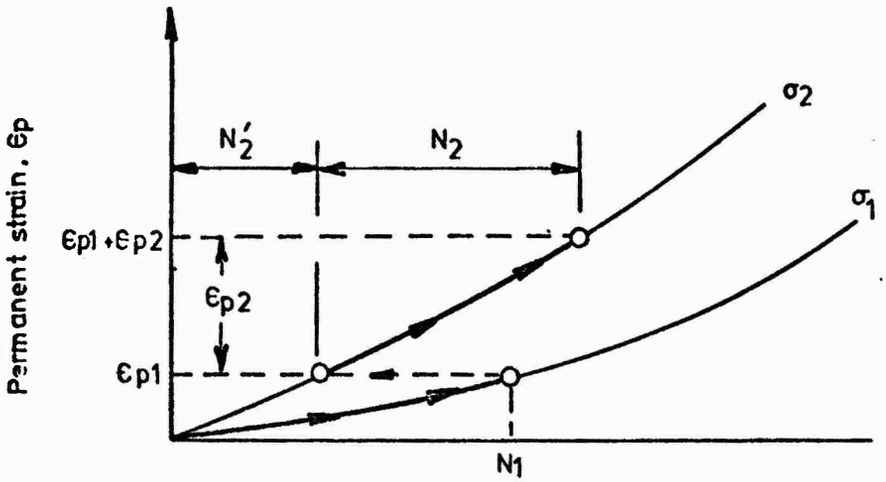

(a) "Time hardening" procedure

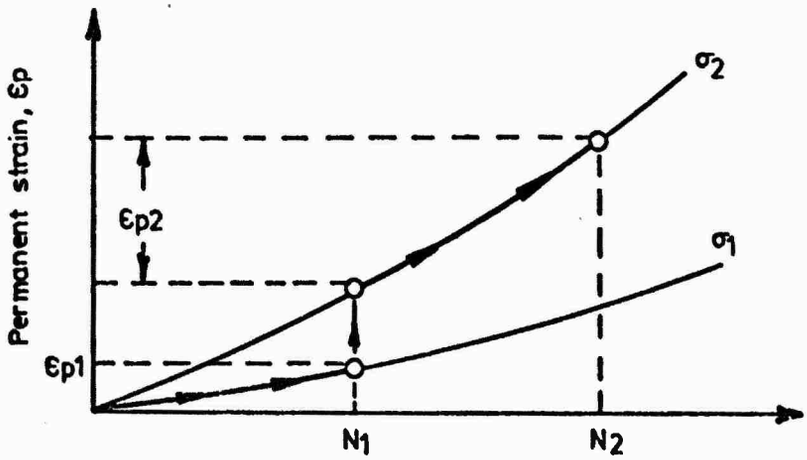

(b) "Strain hardening" procedure

FIG. 9.11 TIME HARDENING AND STRAIN HARDENING CUMULATIVE LOADING PROCEDURES

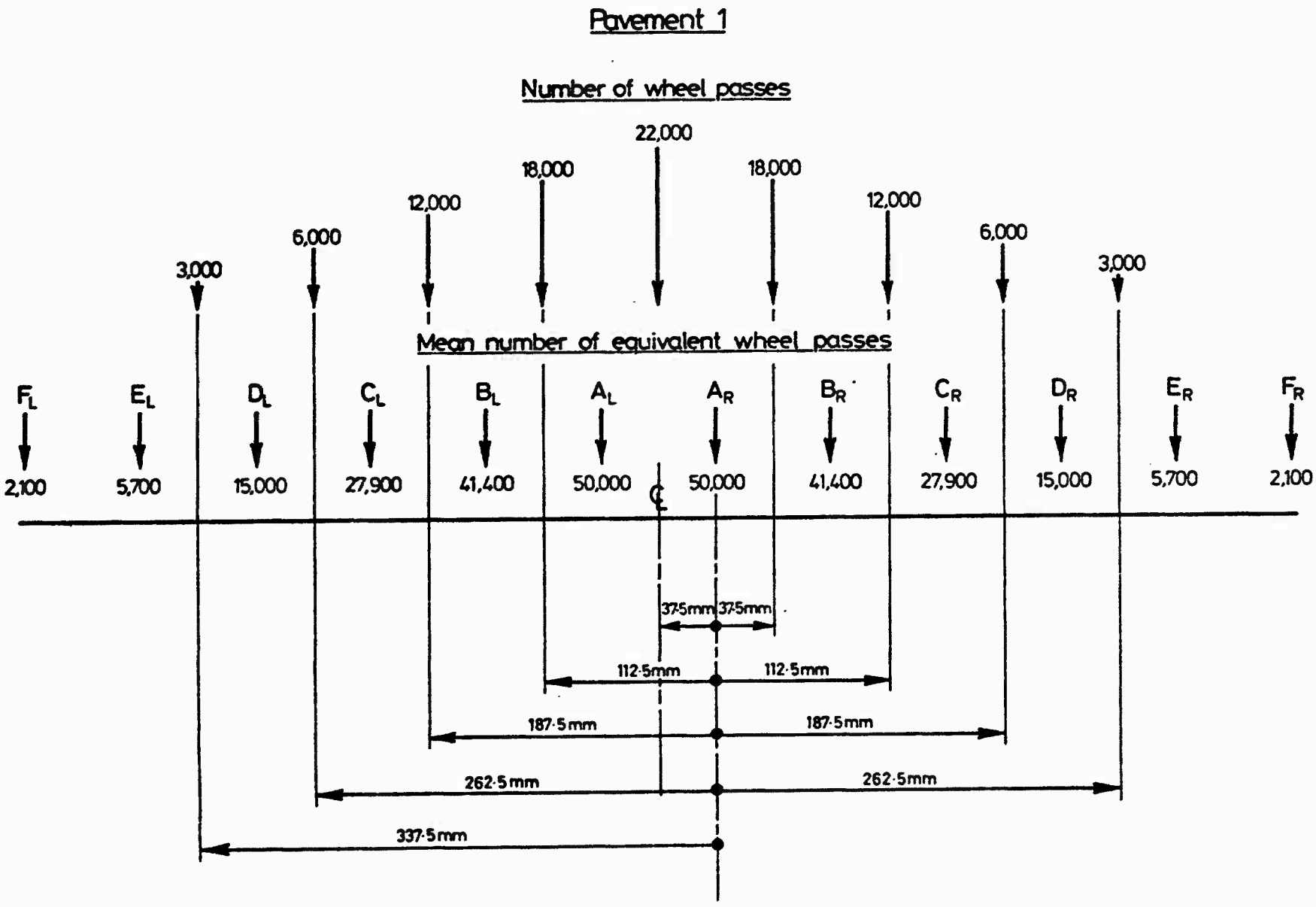

FIG. 9.12 DISTRIBUTION OF WHEEL PASSES USED IN THE MULTI-TRACK TESTS, WITH MEP VALUES FOR PAVEMENT NO. 1

elements below points A_R to F_R were found, and those in the columns below A_L to F_L were exactly the same. The reasons for using points E_R and F_R, E_L and F_L are explained later in the text.

The cumulative loading construction used to determine the permanent strain accruing in an element 62.5 mm below point A_R in Fig. 9.12, is shown in Fig. 9.13. This was for pavement 1 assuming a DBM layer thickness of 150 mm, the nominal thickness of the surfacing for this structure. The actual depth of DBM, found from measurement of cores and slabs taken after testing, was 145 ± 5 mm. As may be seen in Fig. 9.12, the point A_R is affected by wheel loads at radii of 37.5 mm (22,000 plus 18,000), 112.5 mm (18,000 + 12,000), 187.5 mm (12,000 + 6,000), 262.5 mm (6,000 + 3,000), and 337.5 mm (3,000). In order to obtain the total permanent strain due to the wheel acting at these five radii, the stress conditions in the element were calculated, and a strain line obtained for each radius. This was achieved by using DEFPAV, and obtaining permanent strain outputs for a suitable range of load repetitions.

The construction assumed that the wheel moved from right to left in Fig. 9.12, when changing tracks, and that 3,000 passes occurred at a radius of 262.5 mm continuously, then 6,000 at a radius of 187.5 mm and so on, until finally 3,000 passes again occurred at a radius of 337.5 mm. This was at variance with the actual loading pattern where small numbers of passes occurred at each position, and, in the case of pavements 2 and 3, in a random order, until the total number of passes (100,000) was achieved. However, the final computed result would be the same in each case.

The path followed in the cumulative loading construction is indicated by arrows in Fig. 9.13. Initially, 3,000 passes at a radius

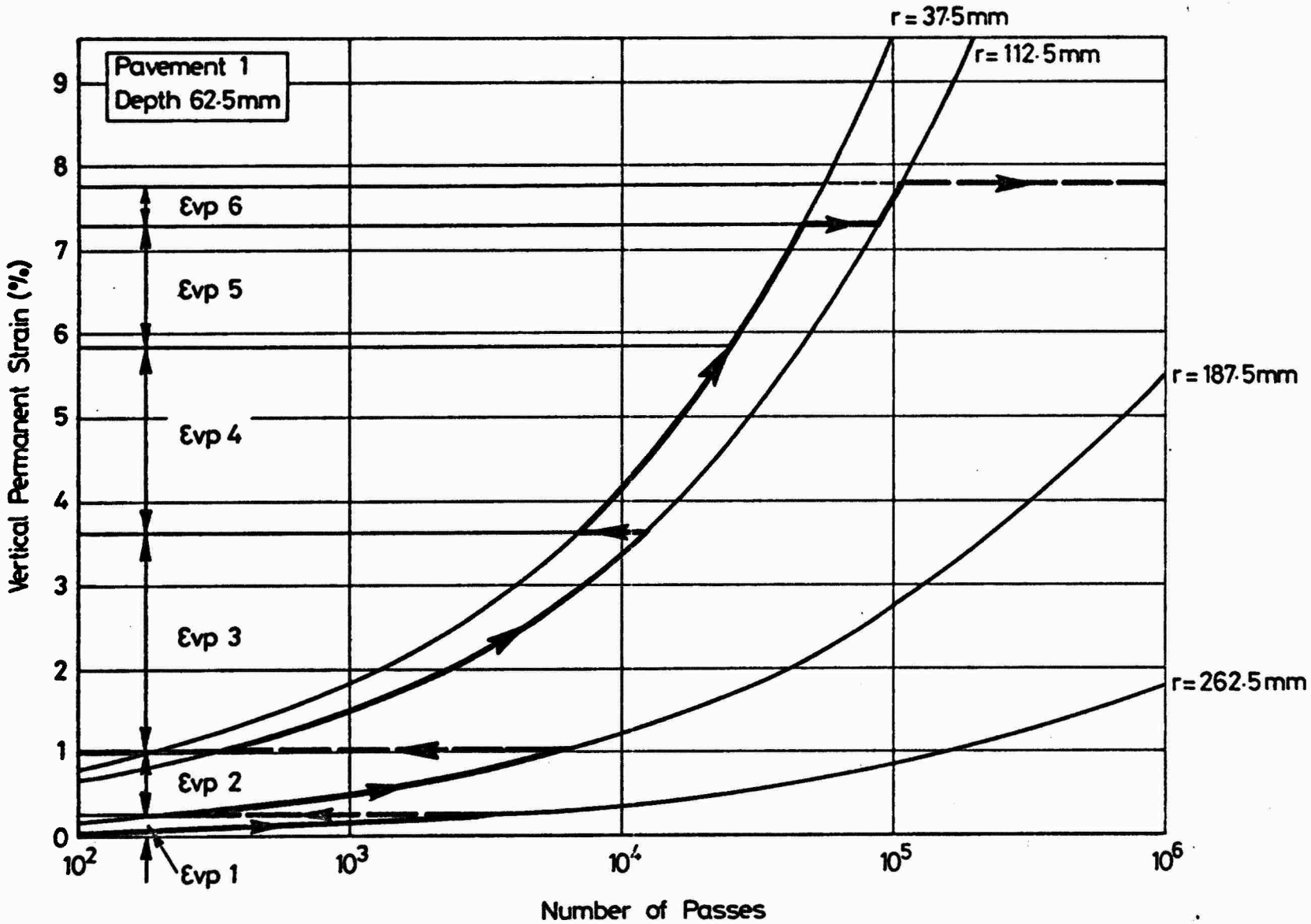

FIG. 9.13 TIME HARDENING CUMULATIVE LOADING PROCEDURE FOR A POSITION IN PAVEMENT NO. 1

of 262.5 mm resulted in a vertical permanent strain of ϵ_{vp1}. This was approximately equivalent to 200 passes at r = 187.5 mm. A further 6,000 passes at r = 187.5 mm resulted in an additional permanent strain ϵ_{vp2}, and a total of ϵ_{vp1} plus ϵ_{vp2}, and so on. The fourth and fifth stages of loading occur at the same radius, r = 37.5 mm, and therefore 40,000 passes result at that radius. The seventh stage of loading was for 12,000 passes at a radius of 187.5 mm. However, it may be seen from Fig. 9.13 that horizontal projection from point α on the r = 112.5 mm strain line, to the r = 187.5 mm strain line, would pass through more than one decade, and the resulting additional permanent strain achieved would be negligible. The same would apply to the remaining two stages. Thus, the total vertical permanent strain accruing in this element, after 10^5 wheel passes, was the value at α; 7.8%.

The equivalent number of passes: Fig. 9.13 shows that the total vertical permanent strain achieved after 10^5 total passes would have been achieved by 57,000 passes had they all been applied at a radius of 37.5 mm. This number of passes was termed the "equivalent number of passes". A similar construction procedure to that outlined above was carried out for all the other elements vertically below point A_R, resulting in the equivalent passes, permanent strains and element deformations shown in Table 9.1. The total surface deformation shown (at this radius of 37.5 mm) was assumed to be the rut depth, since it was not possible with finite elements to obtain the deformations at the exact centre of the spectrum of wheel passes. The stress distribution occurring there would be only slightly different from that at r = 37.5 mm, resulting in a very similar deformation.

Table 9.1 Pavement 1

Results of time hardening cumulative loading construction

r = 37.5 mm (Point A_R)

Depth (mm)	Equivalent Passes (N)	ϵ_{vp} (%)	Deformation (mm)	ϵ_{vp} (%)	Deformation (mm)
		After N passes		After 50,000 passes (MEP)	
12.5	70,000	3.26	.815	3.17	.793
37.5	63,000	5.23	1.308	5.09	1.273
62.5	57,000	7.80	1.895	7.39	1.848
87.5	46,000	10.00	2.500	10.35	2.588
112.5	43,000	12.75	3.188	13.37	3.343
137.5	50,000	8.25	2.063	7.99	1.999
162.5	40,300	1.330	.333	1.373	.343
187.5	41,000	.875	.219	.909	.227
212.5	42,000	.625	.156	.641	.160
237.5	50,000	.465	.116	.469	.117
262.5	58,000	.385	.096	.388	.097
287.5	59,000	.338	.085	.329	.082
350	54,000	.226	.226	.228	.228
500	50,000	.086	.172	.860	.172
900	65,000	.021	.126	.020	.120
Total (Surface Deformation) = 13.49				Total = 13.49	

The mean number of equivalent passes: It was found possible to select a number of passes approximately equal to the average of the number of equivalent passes for all elements at a radius of 37.5 mm, that would give the same surface deformation. This number was termed the mean

number of equivalent passes (MEP). Table 9.1 shows the permanent strains and deformations resulting in all elements below A_R after 50,000 passes at a radius of 37.5 mm, with a surface deformation very similar to that obtained by the detailed procedure of Fig. 9.13. This information was obtained directly from an output of DEFPAV, and involved no graphical construction. The individual permanent strains and deformations are very similar to those obtained by the cumulative loading construction since the strain lines are not particularly sensitive to the number of passes over the range 4×10^4 to 7×10^4.

Determination of MEP's for other radial positions: The surface deformation accruing at a radius of 37.5 mm (below point A_R, Fig. 9.12), was assumed to be the rut depth. However, to obtain a rut profile, similar deformations at points B_R to F_R were required. These deformations could be obtained by a cumulative loading construction, but this would be extremely time consuming, and an approximate method was developed based on the selection of an MEP for each position.

The constructions for point A_R in pavement 1 indicated that only the wheel passes at radii of 37.5 and 112.5 mm contributed significantly to the deformation at any point, hence the need to calculate deformations at points E_R, F_R, E_L and F_L for the outermost wheel positions. For point A_R the number of significant passes contributing to an MEP of 50,000 was 70,000. Therefore, to obtain an MEP for other points, the total number of passes at radii of 37.5 and 112.5 mm was multiplied by 5/7 (the MEP factor). Hence, for point B, 22,000 plus 6,000 passes were applied at a radius of 112.5 mm, and 18,000 plus 12,000 passes at a radius of 37.5 mm, giving a total of 58,000 significant passes. Thus, the mean number of equivalent passes is given by:

$$MEP = 5/7 \times 58,000$$

$$= 41,400$$

Similar calculations for points C to F resulted in the MEP's shown in Fig. 9.12.

Positions of maximum permanent strain: Table 9.2 shows a section of output from DEFPAV for permanent strain calculations over a network of elements after 50,000 total passes, on pavement 1. This particular section of output was used to obtain the deformation for an MEP of 50,000, i.e. below the point A_R (Fig. 9.12), at a radius of 37.5 mm. The strains shown have not been converted to percentages.

The table shows that in the upper half of the DBM layer, the maximum permanent strain at a particular depth (shown enclosed) does not occur at the position nearest to the point of loading, i.e. when the wheel is 37.5 mm from A_R (the second column in this case). Fig. 9.14 shows a plan view of the pavement surface with the wheel travelling along the path MN. Table 9.2 indicates that the maximum permanent strain 12.5 mm below A_R occurs when the centre of the wheel is 95 mm from A_R (at point 0 in Fig. 9.14). Similarly, the maximum permanent strains 37.5 and 62.5 mm below A_R are when the wheel is 95 mm and 75 mm from A_R respectively. At larger depths the maximum strain does occur when the wheel passes closest to the point.

Thus, the deformation accruing below point A_R, 37.5 mm from the line of travel of the wheel, is determined by choosing the maximum strain at each depth, and carrying out the usual summation procedure (Table 9.1). The deformations below all the other points may be found by obtaining outputs from DEFPAV for the particular values of MEP at each point, or by constructing a plot of deformation versus MEP, from

Table 9.2 Permanent strain output after 50,000 passes

RADIUS OF CENTRE OF ELEMENT (mm)

	12.5	37.5	60.0	75.0	85.0	95.0	112.5	145.0	187.5	262.5	382.5	550.0
	ELEMENT COLUMN NUMBER											
Depth (mm)	1	2	3	4	5	6	7	8	9	10	11	12
12.5	0.01540	0.01420	0.01431	0.01831	0.02570	0.03163	0.03148	0.02510	0.01131	0.00374	0.00208	0.00166
37.5	0.02558	0.03026	0.03916	0.04776	0.05083	0.05087	0.04658	0.03069	0.01451	0.00391	0.00158	0.00162
62.5	0.06018	0.06588	0.07213	0.07392	0.07179	0.06625	0.05935	0.03915	0.02064	0.00598	0.00156	0.00197
87.5	0.11339	0.10354	0.09297	0.08373	0.07676	0.06975	0.05859	0.03966	0.02297	0.00777	0.00184	0.00158
112.5	0.16011	0.13365	0.10686	0.08906	0.07744	0.06739	0.05352	0.03611	0.02145	0.00844	0.00260	0.00147
137.5	0.08190	0.07988	0.07611	0.07153	0.06749	0.06210	0.05251	0.03969	0.02091	0.00921	0.00415	0.00182
162.5	0.01463	0.01373	0.01281	0.01213	0.01155	0.01087	0.00958	0.00642	0.00469	0.00320	0.00123	0.00039
187.5	0.00947	0.00909	0.00864	0.00829	0.00803	0.00775	0.00698	0.00564	0.00403	0.00293	0.00126	0.00040
212.5	0.00663	0.00641	0.00614	0.00593	0.00579	0.00564	0.00531	0.00422	0.00386	0.00270	0.00122	0.00042
237.5	0.00482	0.00469	0.00455	0.00440	0.00430	0.00443	0.00428	0.00393	0.00349	0.00249	0.00115	0.00043
262.5	0.00393	0.00383	0.00389	0.00349	0.00386	0.00385	0.00375	0.00346	0.00302	0.00225	0.00107	0.00043
287.5	0.00333	0.00329	0.00328	0.00326	0.00324	0.00322	0.00316	0.00298	0.00265	0.00200	0.00099	0.00042
350.0	0.00232	0.00228	0.00225	0.00222	0.00220	0.00217	0.00211	0.00198	0.00181	0.00136	0.00082	0.00038
500.0	0.00086	0.00086	0.00085	0.00084	0.00083	0.00082	0.00080	0.00077	0.00076	0.00066	0.00049	0.00026
900.0	0.00020	0.00020	0.00020	0.00020	0.00020	0.00020	0.00020	0.00019	0.00019	0.00018	0.00016	0.00012

RUT DEPTH (mm)

- 13.390

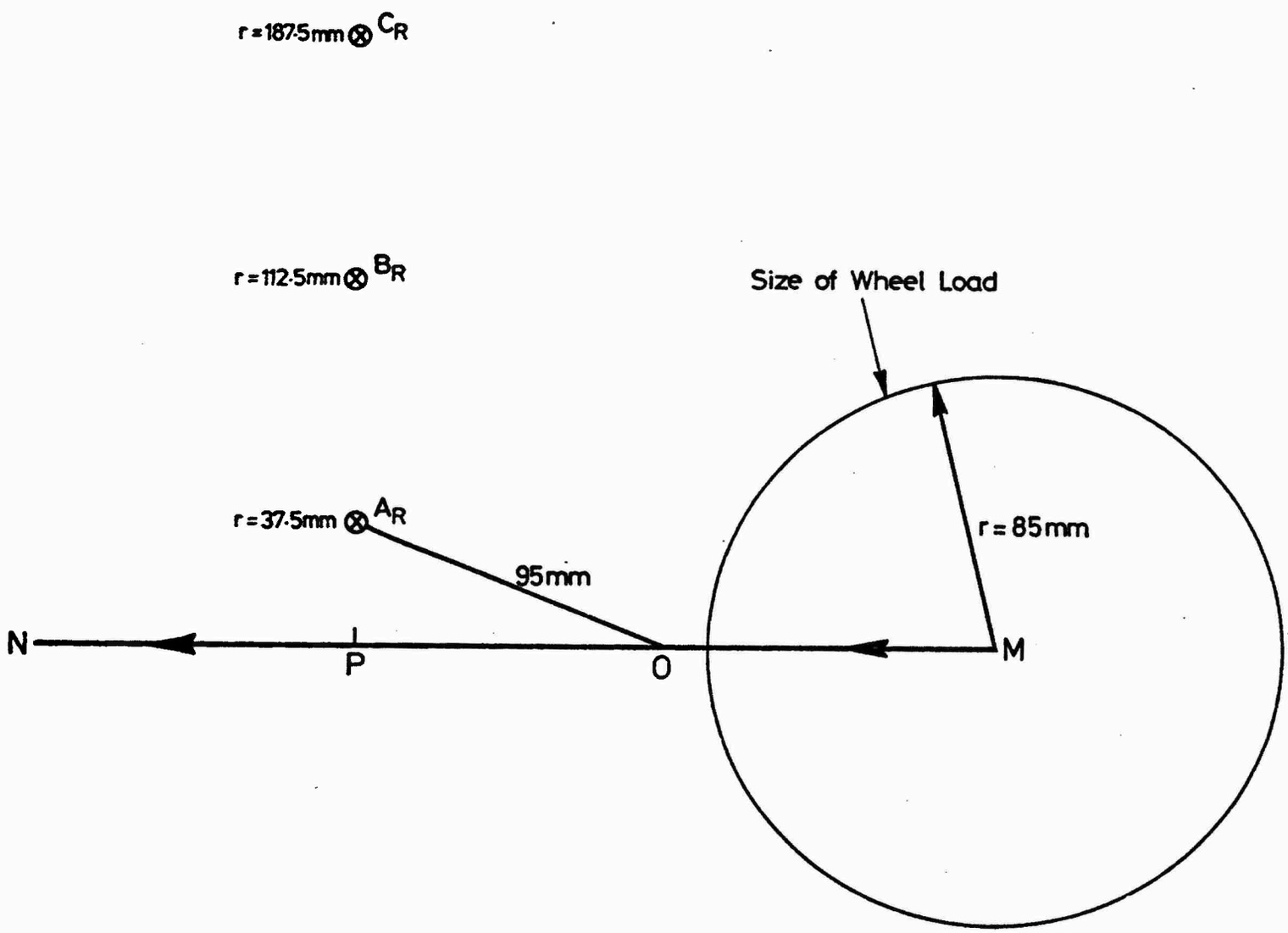

FIG. 9.14 PLAN VIEW OF PAVEMENT SURFACE

a set of outputs covering a suitable range of MEP, and reading off the relevant deformations.

The plot of deformation versus MEP for pavement 1 is shown in Fig. 9.15. Thus, a knowledge of the deformation accruing below each point enables a rut profile to be constructed.

Summary: The following steps were required to predict the rut-depth and rut profile for a particular pavement:

(a) Determine the deformation at point A (r = 37.5 mm) by a series of cumulative loading constructions for a column of elements. This is assumed to be the rut depth.

(b) Determine the "equivalent number of passes" for each element at this radius and compute the average.

(c) Determine the "mean number of equivalent passes" (MEP) by comparing the deformation from (a) with those from a number of DEFPAV outputs for a range of passes including the average equivalent number of passes.

(d) Divide the MEP from (c) by the total number of passes at radii of 37.5 and 112.5 mm from A (significant passes) to determine an MEP factor.

(e) Determine the MEP's at points B to F by multiplying the number of "significant passes" by the MEP factor.

(f) Construct a plot of deformation versus MEP from a suitable range of DEFPAV outputs and read off the deformations corresponding to the MEP's for points B to F, to construct the rut profile.

9.4.2 Single track tests

In this case, the predictions were much more straightforward.

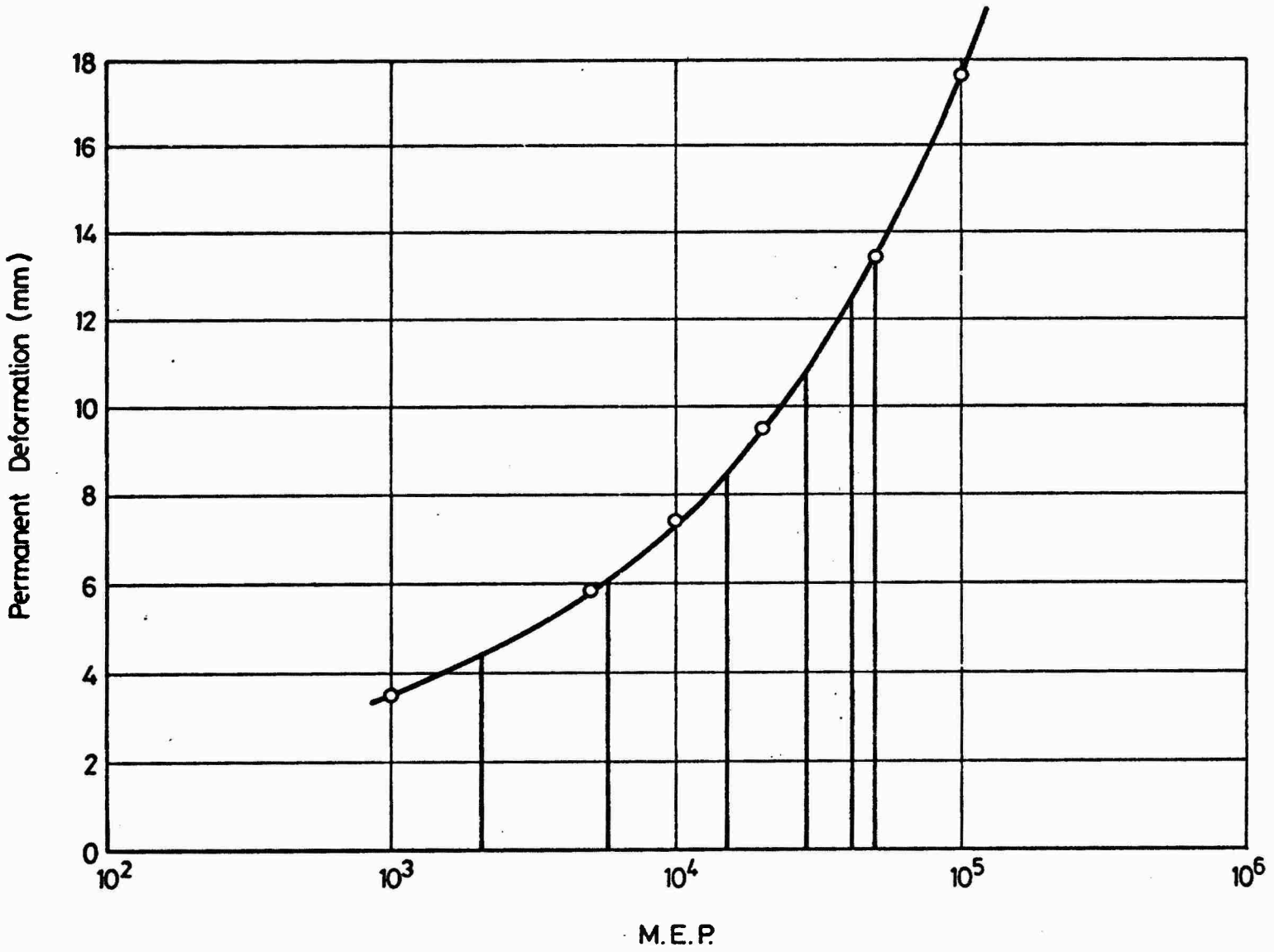

FIG. 9.15 PERMANENT DEFORMATION VERSUS MEAN NUMBER OF EQUIVALENT PASSES

For the three single track tests carried out, 22,000 wheel passes were applied in one track, the same number as were applied in the central track of the multi-track tests. One run with DEFPAV, giving the permanent strains after 22,000 passes, provided all the information required to predict the rut depth and rut profile.

The output for pavement 1 is shown in Table 9.3, with the positions where maximum permanent strain occur shown enclosed. With reference to Fig. 9.14 in this case the permanent strains accruing below the point P are required. The maximum strains at depths of 12.5, 37.5 and 62.5 mm occur at radii of 95, 95 and 75 mm. For depths greater than these the maximum strains occur at a radius of 12.5 mm, the closest point to the line of travel of the wheel. The rut depth was found by carrying out the usual integration process, multiplying the maximum strain at each depth by the thickness of the element and summing.

The surface profile was found by summing the maximum deformations at each radius. The procedure for a radius of 12.5 mm has been described, and is similar to that followed for the other radii, but, as the radius increases, only the strains occurring below positions of greater radius were considered when determining the maximum strain in a particular element. For instance, for the column of elements at a radius of 85 mm, the maximum strain at a depth of 12.5 mm occurs in column 6. Thereafter, the maximum strains are all in column 4. For radii of 95 mm and above, the maximum strains occur within the column of elements at that radius.

9.5 PREDICTIONS

9.5.1 Presentation

Figs 9.16 to 9.21 show the predictions of rut depths and profiles

Table 9.3 Permanent strain output after 22,000 passes

Depth (mm)	RADIUS OF CENTRE OF ELEMENT (mm)											
	12.5	37.5	60.0	75.0	85.0	95.0	112.5	145.0	187.5	262.5	382.5	550.0
	ELEMENT COLUMN NUMBER											
	1	2	3	4	5	6	7	8	9	10	11	12
12.5	0.01444	0.01332	0.01336	0.01674	0.02280	0.02709	0.02592	0.01815	0.00956	0.00373	0.00149	0.00119
37.5	0.02057	0.02469	0.03181	0.03836	0.03999	0.04060	0.03657	0.02545	0.01036	0.00286	0.00113	0.00117
62.5	0.04481	0.04919	0.05372	0.05489	0.05330	0.05076	0.04431	0.02910	0.01524	0.00436	0.00113	0.00142
87.5	0.07835	0.07215	0.06527	0.05902	0.05434	0.04957	0.04200	0.02869	0.01669	0.00565	0.00134	0.00114
112.5	0.10486	0.08877	0.07192	0.06043	0.05288	0.04629	0.03720	0.02550	0.01532	0.00610	0.00189	0.00107
137.5	0.05470	0.05349	0.05110	0.04811	0.04547	0.04191	0.03508	0.02335	0.01473	0.00464	0.00303	0.00132
162.5	0.01365	0.01273	0.01188	0.01124	0.01070	0.01007	0.00883	0.00633	0.00435	0.00296	0.00114	0.00036
187.5	0.00877	0.00843	0.00801	0.00763	0.00744	0.00713	0.00647	0.00523	0.00374	0.00272	0.00117	0.00038
212.5	0.00614	0.00594	0.00569	0.00549	0.00537	0.00522	0.00492	0.00391	0.00353	0.00250	0.00113	0.00039
237.5	0.00447	0.00435	0.00421	0.00409	0.00398	0.00403	0.00397	0.00364	0.00315	0.00231	0.00106	0.00040
262.5	0.00364	0.00359	0.00361	0.00361	0.00358	0.00357	0.00348	0.00321	0.00280	0.00208	0.00099	0.00040
287.5	0.00309	0.00305	0.00304	0.00302	0.00300	0.00298	0.00293	0.00276	0.00245	0.00185	0.00092	0.00039
350.0	0.00215	0.00212	0.00208	0.00206	0.00204	0.00201	0.00196	0.00184	0.00167	0.00126	0.00076	0.00035
500.0	0.00080	0.00079	0.00078	0.00077	0.00077	0.00076	0.00074	0.00072	0.00071	0.00061	0.00045	0.00024
900.0	0.00019	0.00019	0.00019	0.00019	0.00018	0.00018	0.00018	0.00018	0.00018	0.00016	0.00014	0.00011
	SURFACE DEFORMATION (mm)											
	10.500	9.861	9.162	8.606	8.164	7.699	6.762	4.832	2.950	1.418	0.663	0.391

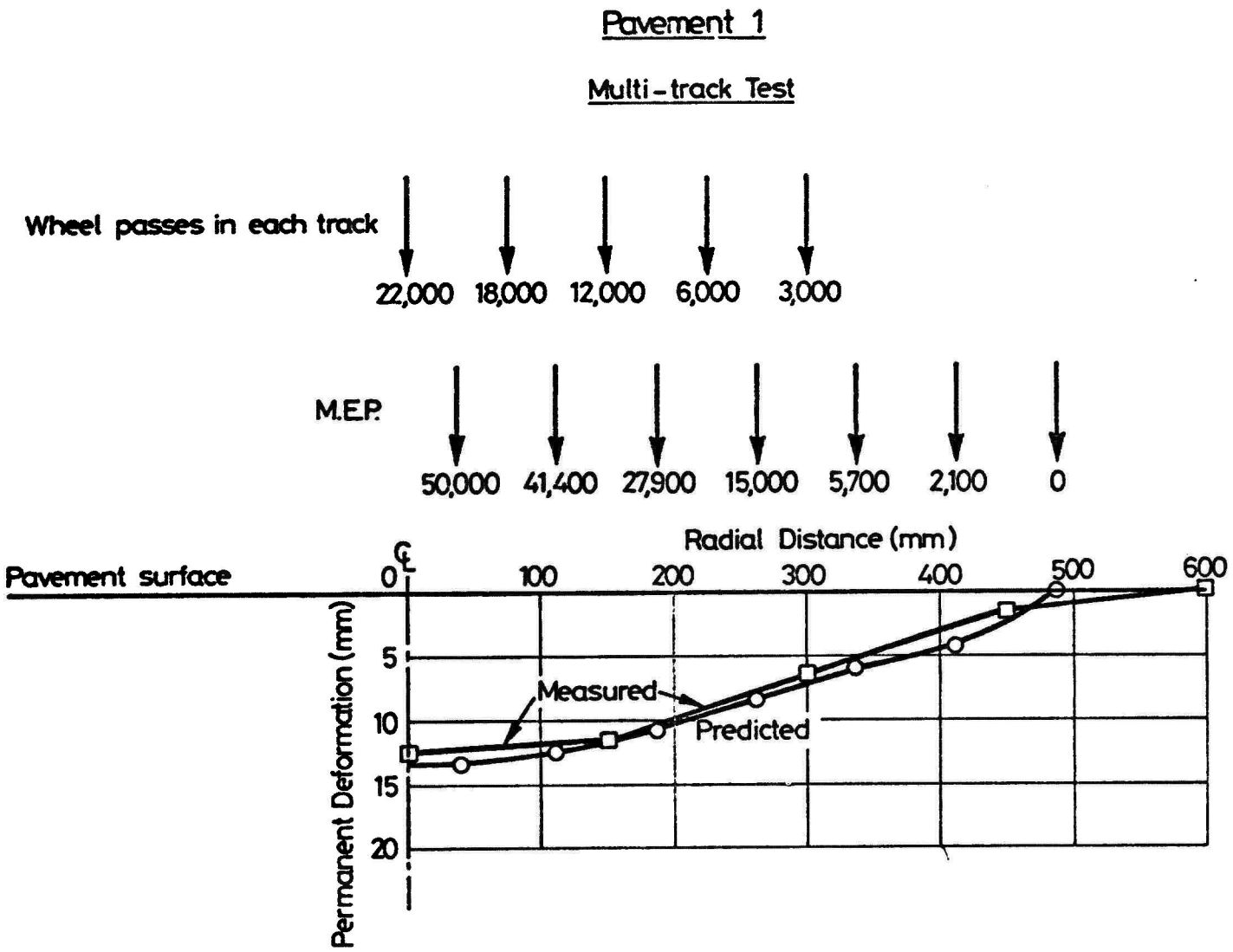

FIG. 9.16 MEASURED AND PREDICTED RUT PROFILES FOR THE MULTI-TRACK TEST (PAVEMENT NO. 1)

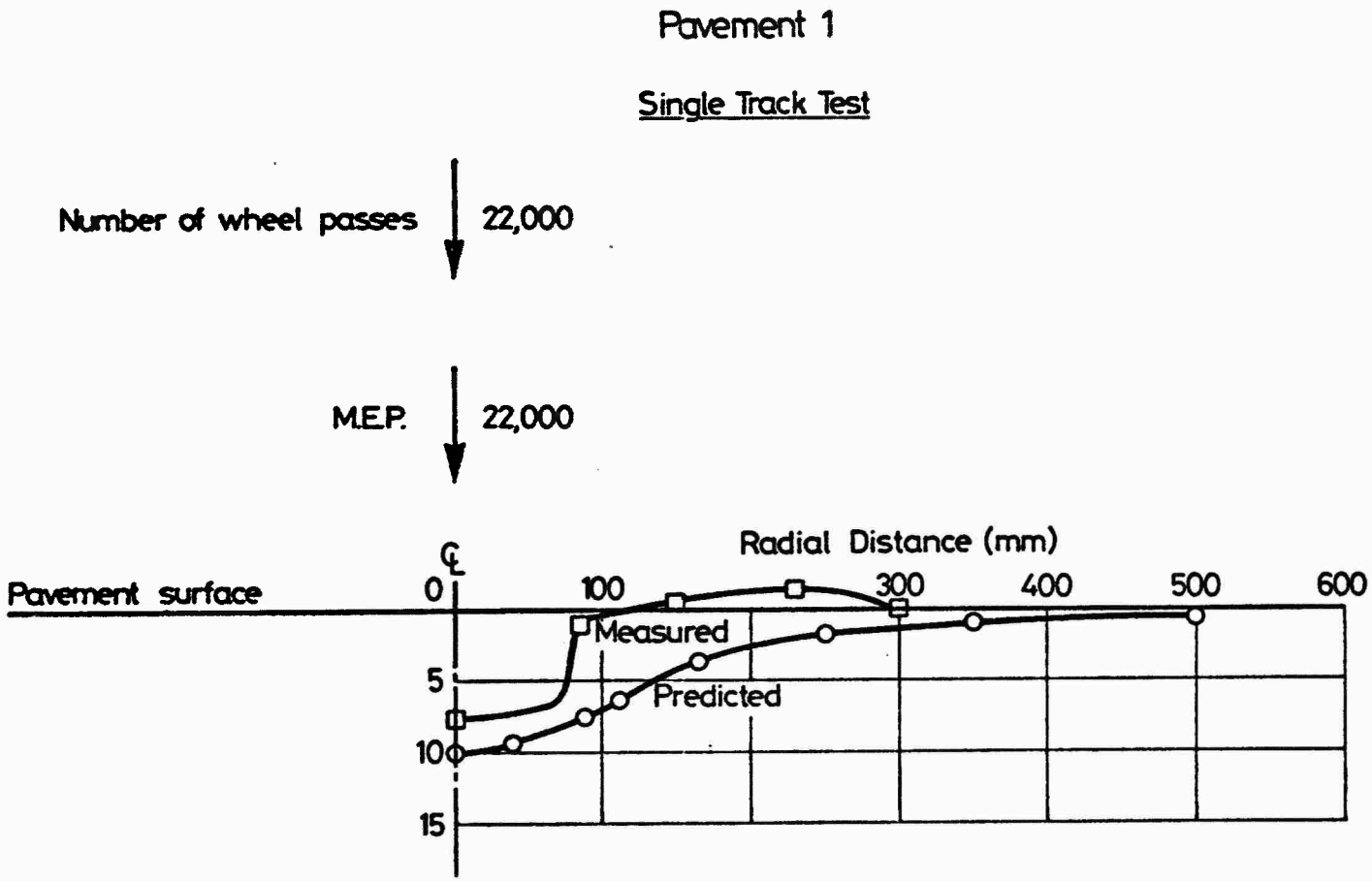

FIG. 9.17 MEASURED AND PREDICTED RUT PROFILES FOR THE SINGLE TRACK TEST (PAVEMENT NO. 1)

Pavement 2

Multi-track Test

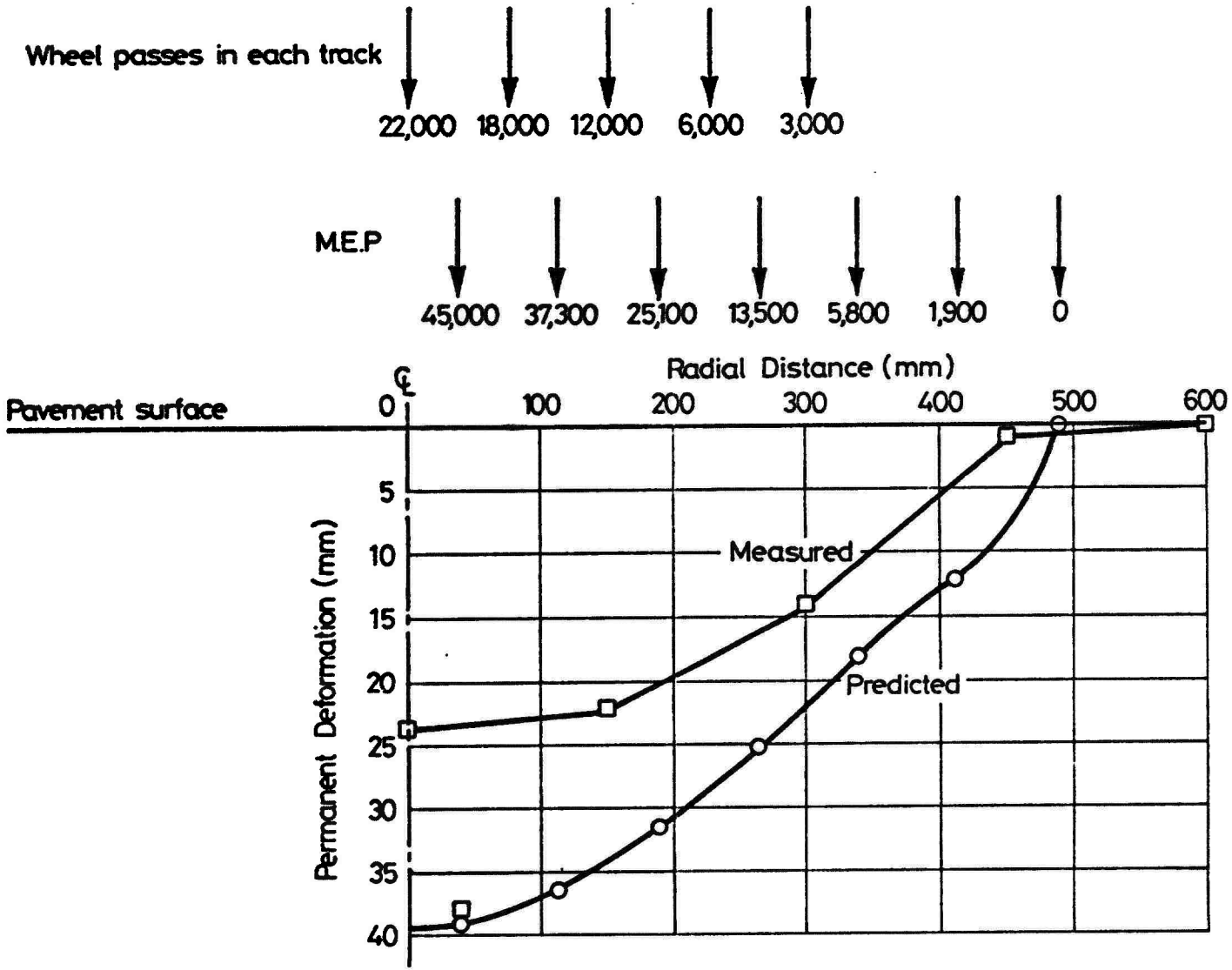

FIG. 9.18 MEASURED AND PREDICTED RUT PROFILES FOR THE MULTI-TRACK TEST (PAVEMENT NO. 2)

Pavement 2

Single Track Test

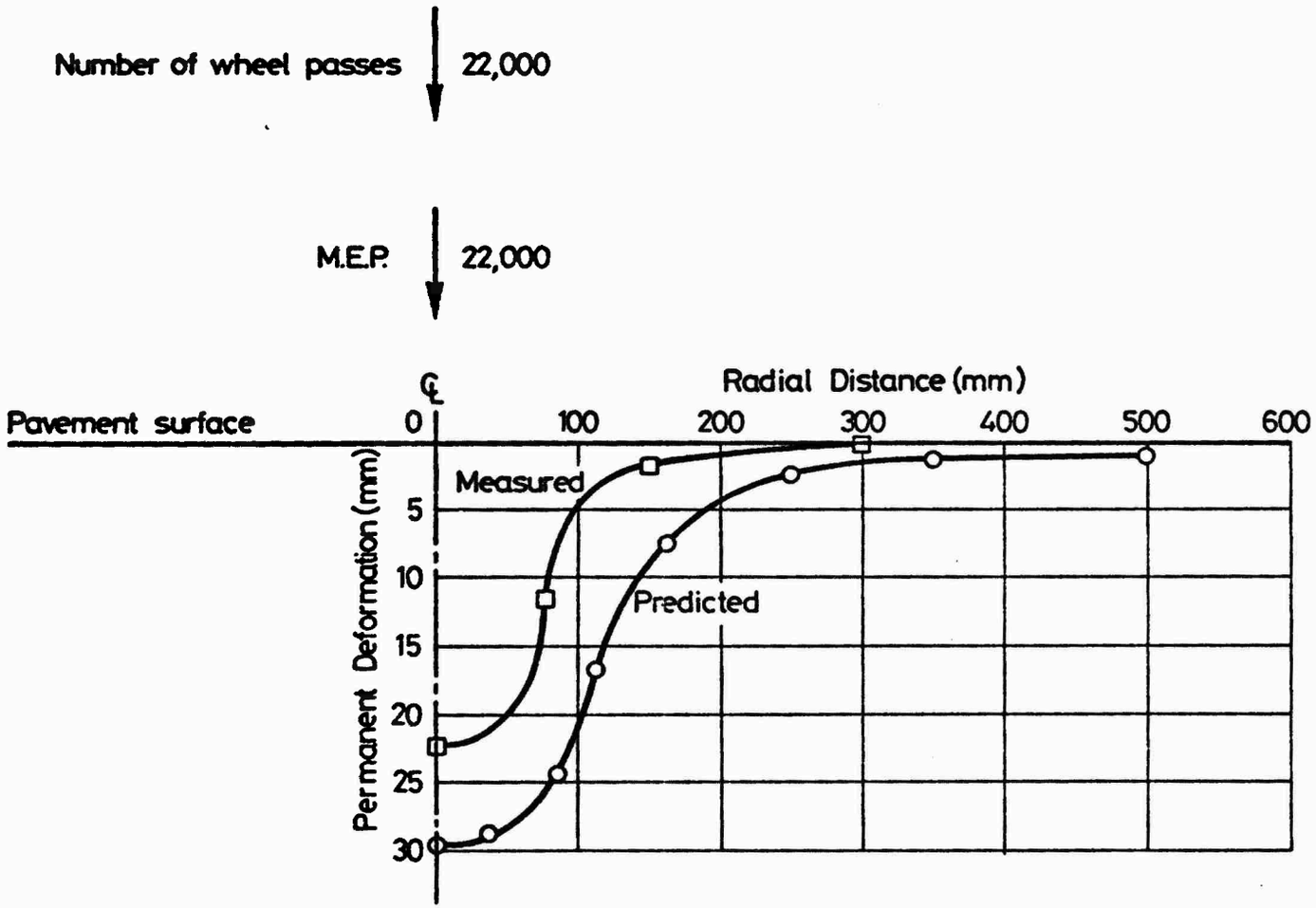

FIG. 9.19 MEASURED AND PREDICTED RUT PROFILES FOR THE SINGLE TRACK TEST (PAVEMENT NO. 2)

Pavement 3

Multi-track Test

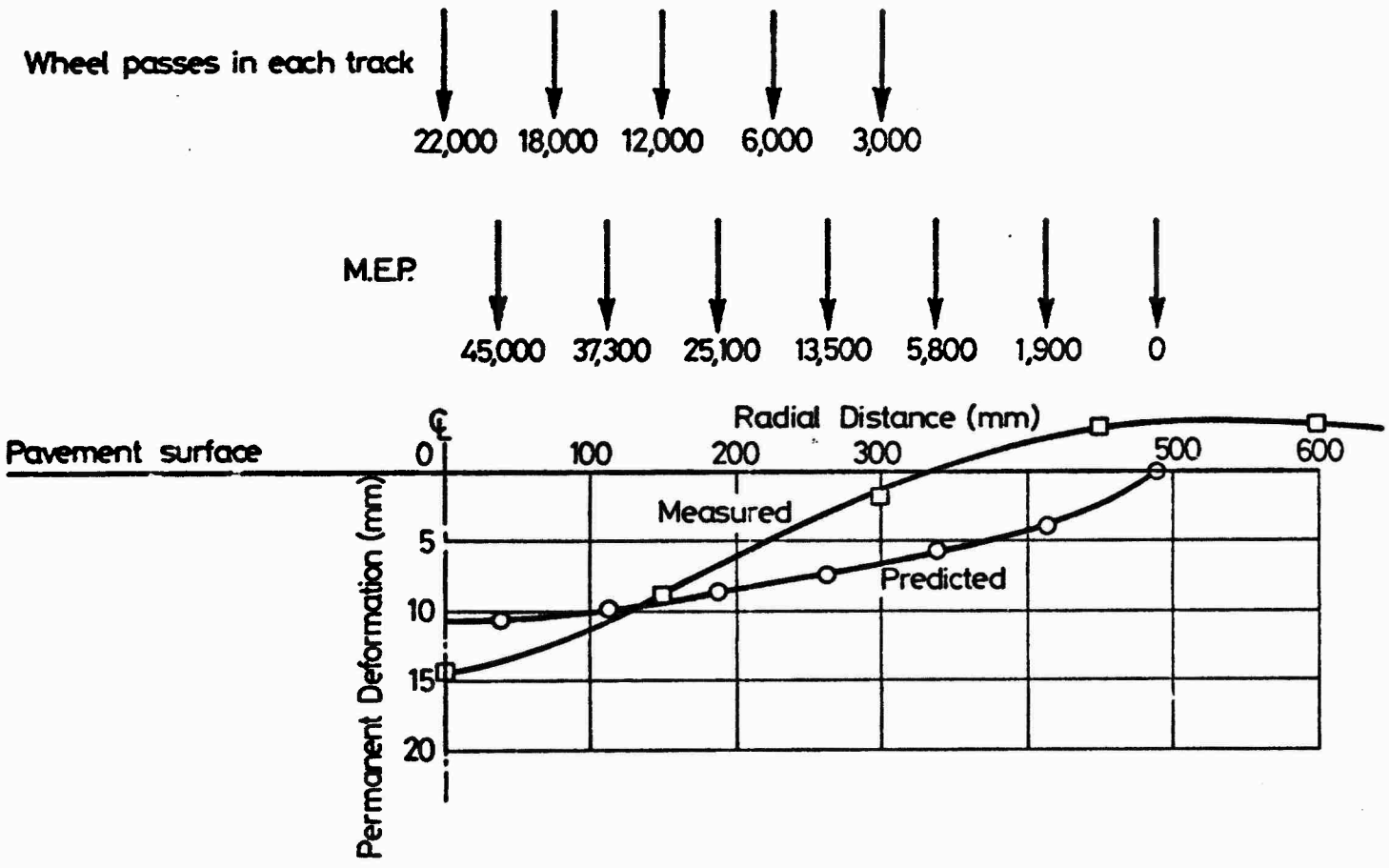

FIG. 9.20 MEASURED AND PREDICTED RUT PROFILES FOR THE MULTI-TRACK TEST (PAVEMENT NO. 3)

Pavement 3

Single Track Test

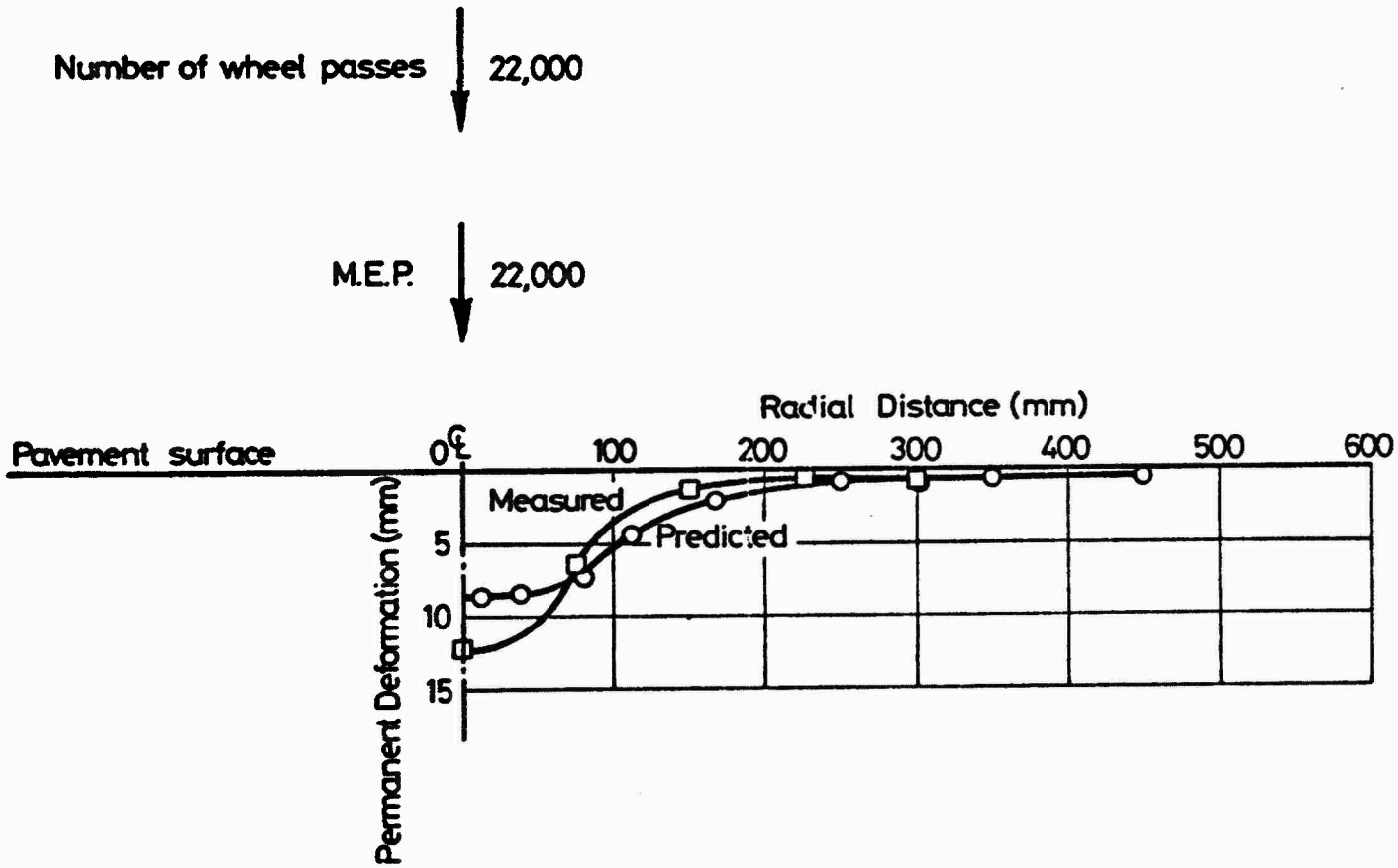

FIG. 9.21 MEASURED AND PREDICTED RUT PROFILES FOR THE SINGLE TRACK TEST (PAVEMENT NO. 3)

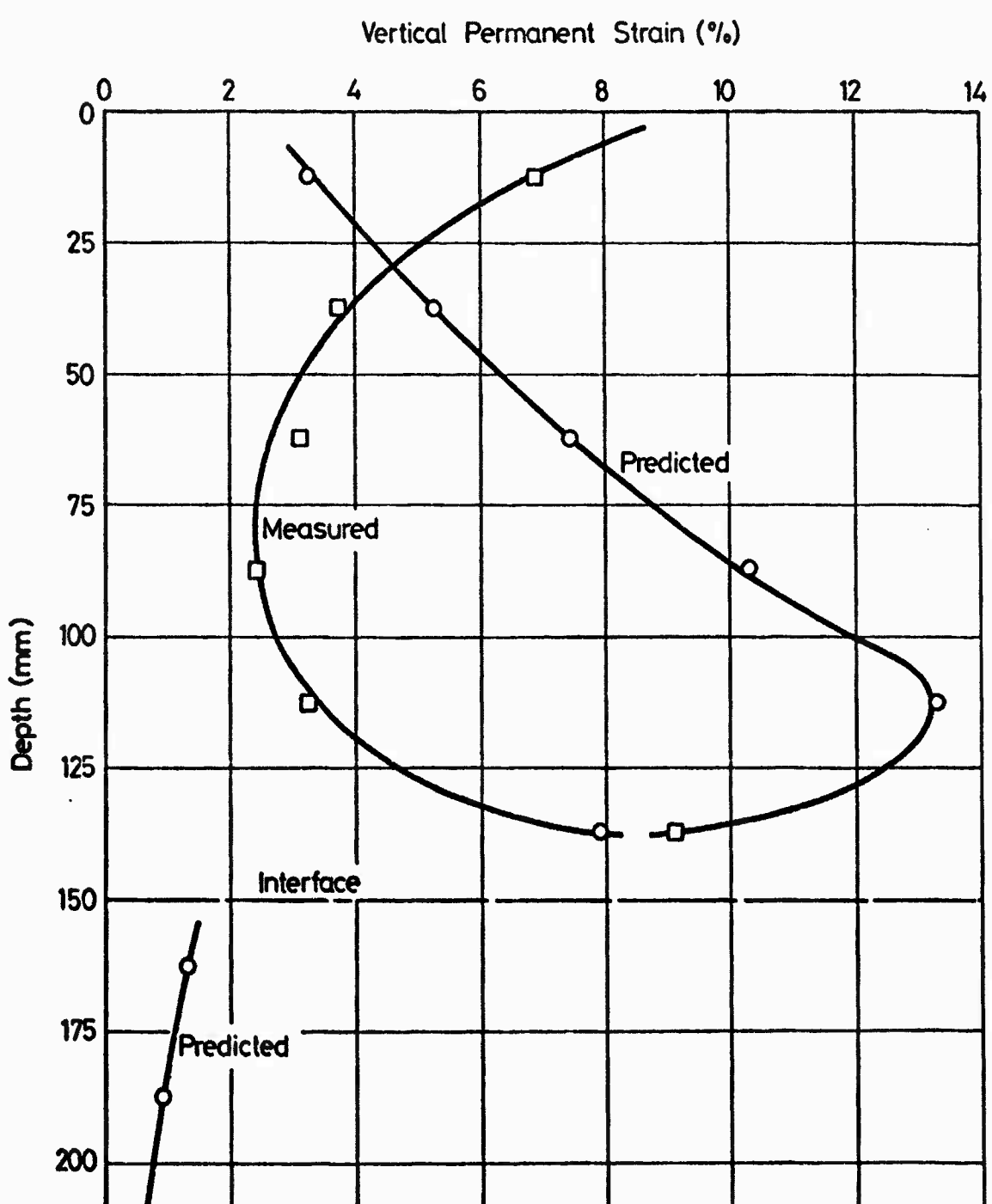

FIG. 9.22 COMPARISON OF MEASURED AND PREDICTED VERTICAL PERMANENT STRAIN (PAVEMENT NO. 1)

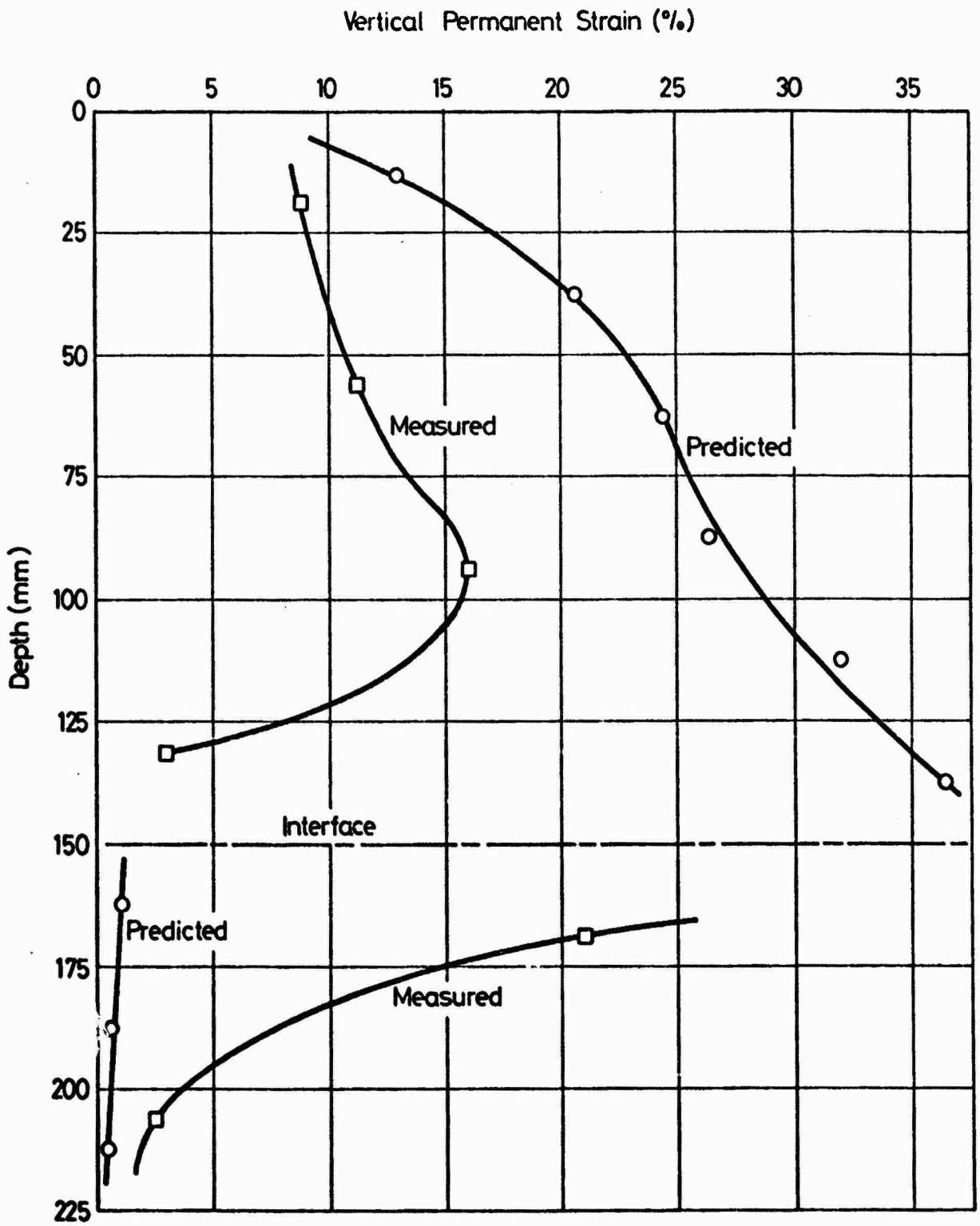

FIG. 9.23 COMPARISON OF MEASURED AND PREDICTED VERTICAL PERMANENT STRAIN (PAVEMENT NO. 2)

Pavement 3

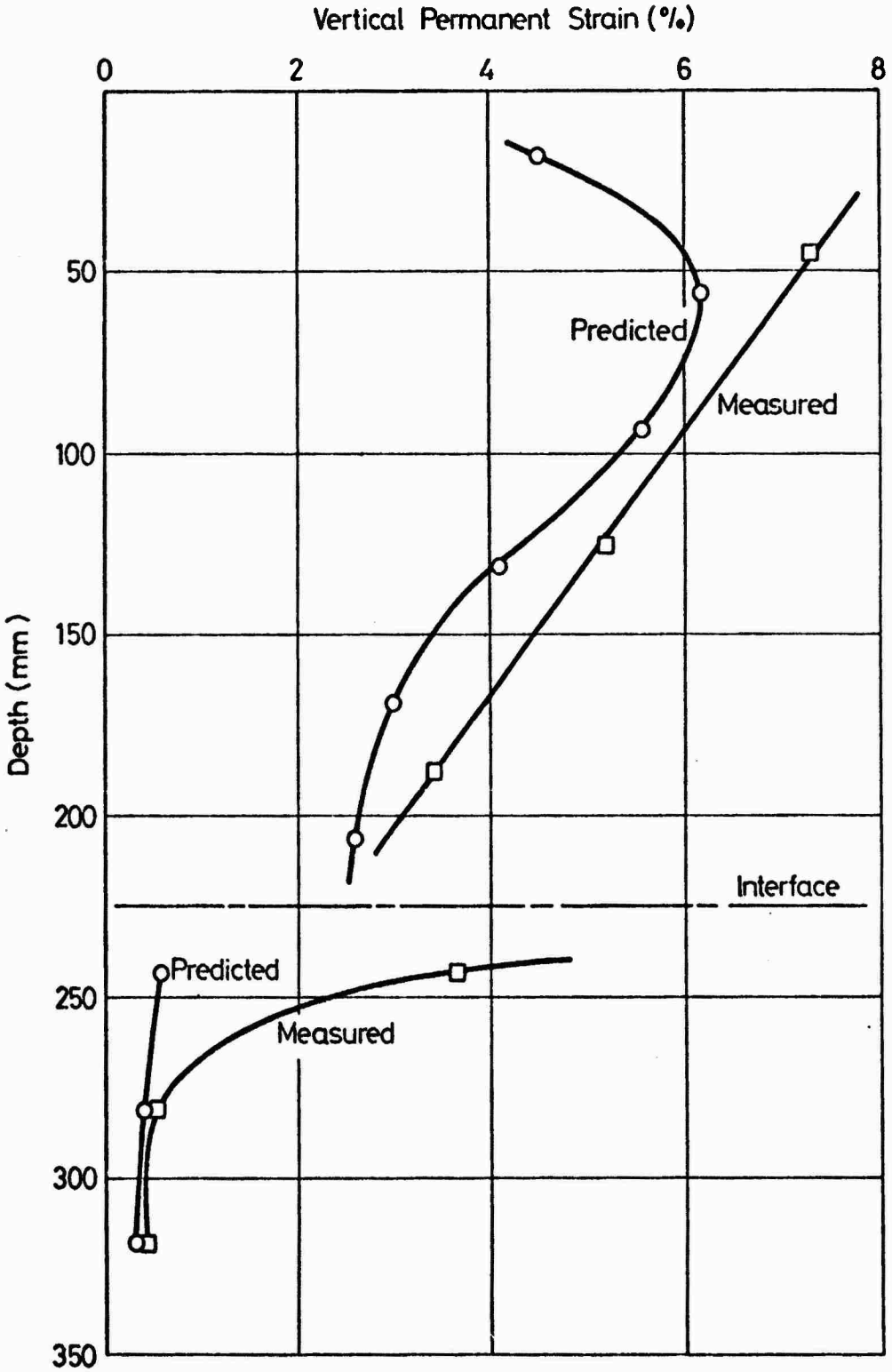

FIG. 9.24 COMPARISON OF MEASURED AND PREDICTED VERTICAL PERMANENT STRAIN (PAVEMENT NO. 3)

for the single and multi-track tests for each pavement, after 22,000 and 100,000 passes respectively. An exception for the single-track tests was pavement 1, where 44,000 passes were applied. The predictions for pavements 2 and 3 were carried out in the manner outlined for pavement 1 in Section 9.4, resulting in an MEP factor of 9/14 in each case, i.e. the MEP at a distance of 37.5 mm from the central wheel track was 45,000 in each case with the significant number of passes 70,000 as before. Figs 9.16 to 9.21 also showed the measured profiles of the rut for comparison with those predicted. A summary of the rut depth predictions and measurements is presented in Table 9.4.

Figs 9.22 to 9.24 show the predictions of the vertical permanent strain versus depth, for the multi-track tests after 100,000 passes, compared with the corresponding measured values. Figs 9.25 to 9.27 show plots of rut depth against MEP at r = 37.5 mm for the multi-track tests, and against the number of passes for the single track tests. For the single track tests the MEP is equal to the total number of passes, since all passes are applied in the same track. Comparison should be made with Figs 5.1 to 5.3 where rut depth is plotted against the total number of passes.

9.5.2 Comparison with measurements

Table 9.4 shows that the predictions of rut depth are adequate, since, with the exception of the multi-track test for pavement 2, all are within 33% of the measured values. For pavements 1 and 2 the predictions were higher than the measured values, and for pavement 3 they were lower. The separate predictions of the deformation in each material show that there was a tendency to overpredict the deformation in the DBM and to under-predict in the Keuper marl. Hence, compensating errors tended to produce a more accurate total deformation (rut depth).

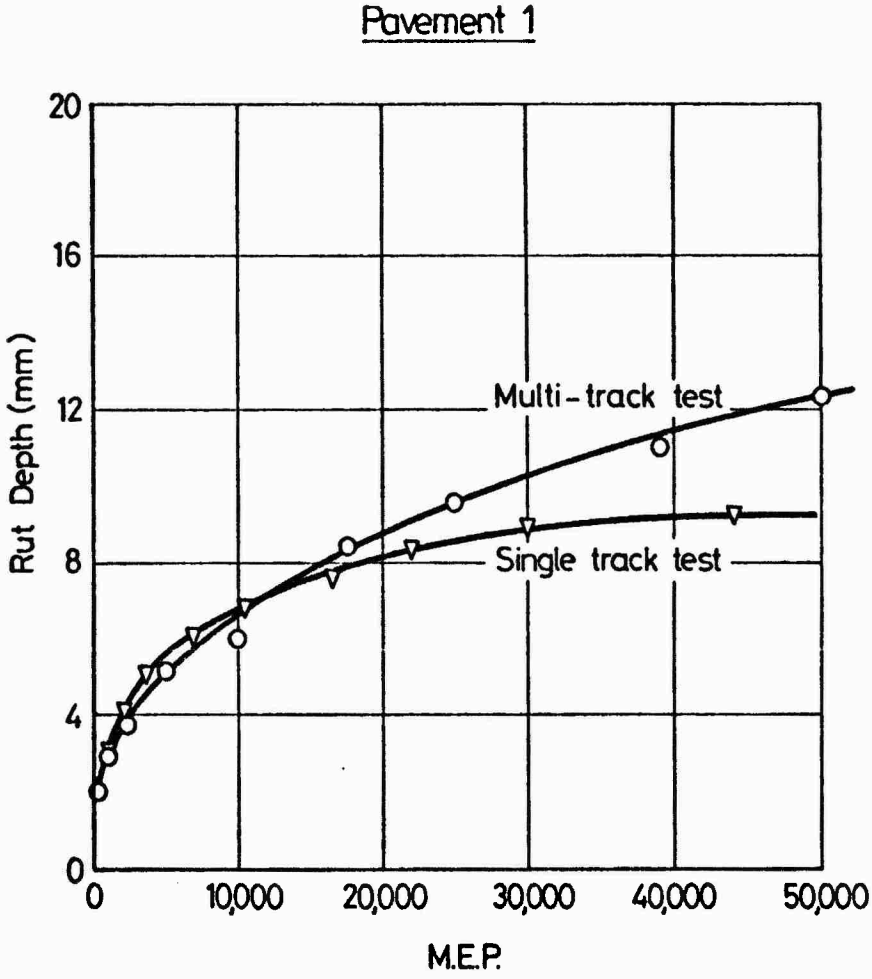

FIG. 9.25 RUT DEPTH VERSUS MEAN NUMBER OF EQUIVALENT PASSES

(PAVEMENT NO. 1)

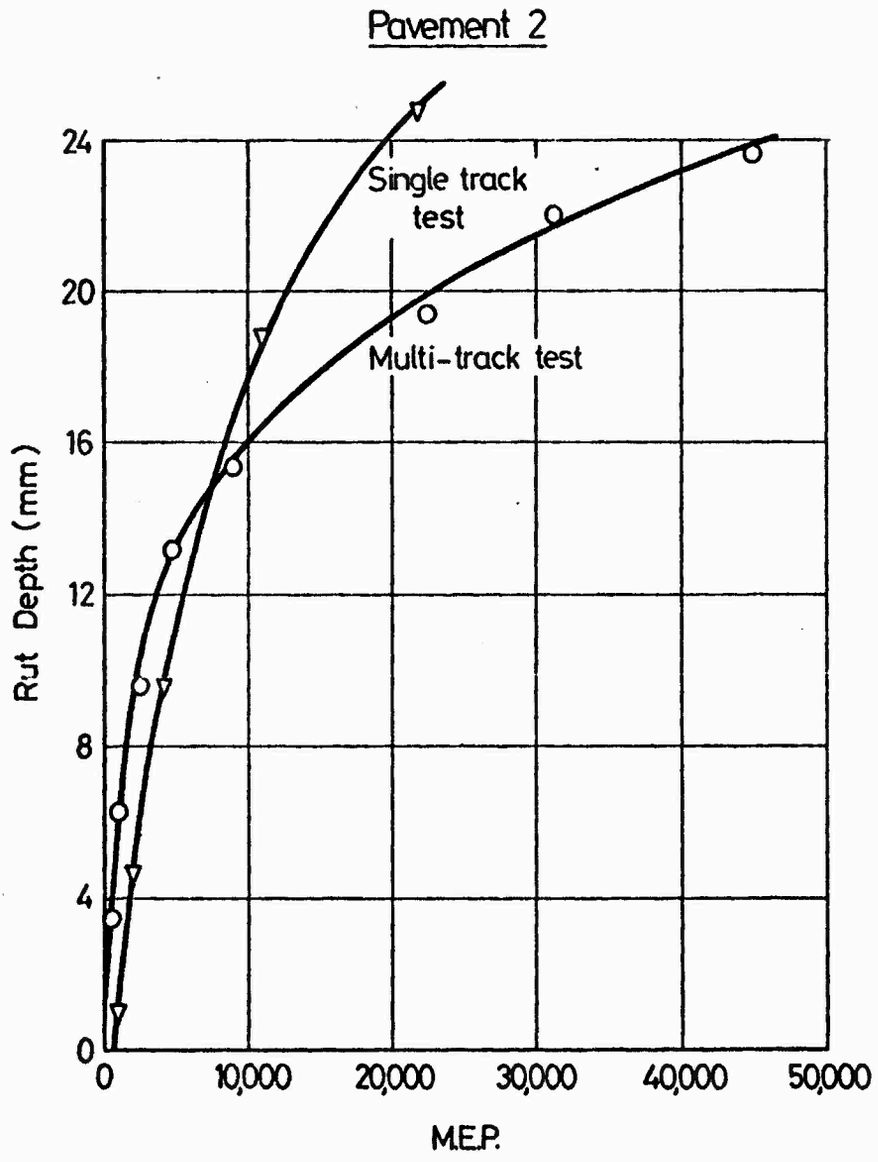

FIG. 9.26 RUT DEPTH VERSUS MEAN NUMBER OF EQUIVALENT PASSES

(PAVEMENT NO. 2)

Pavement 3

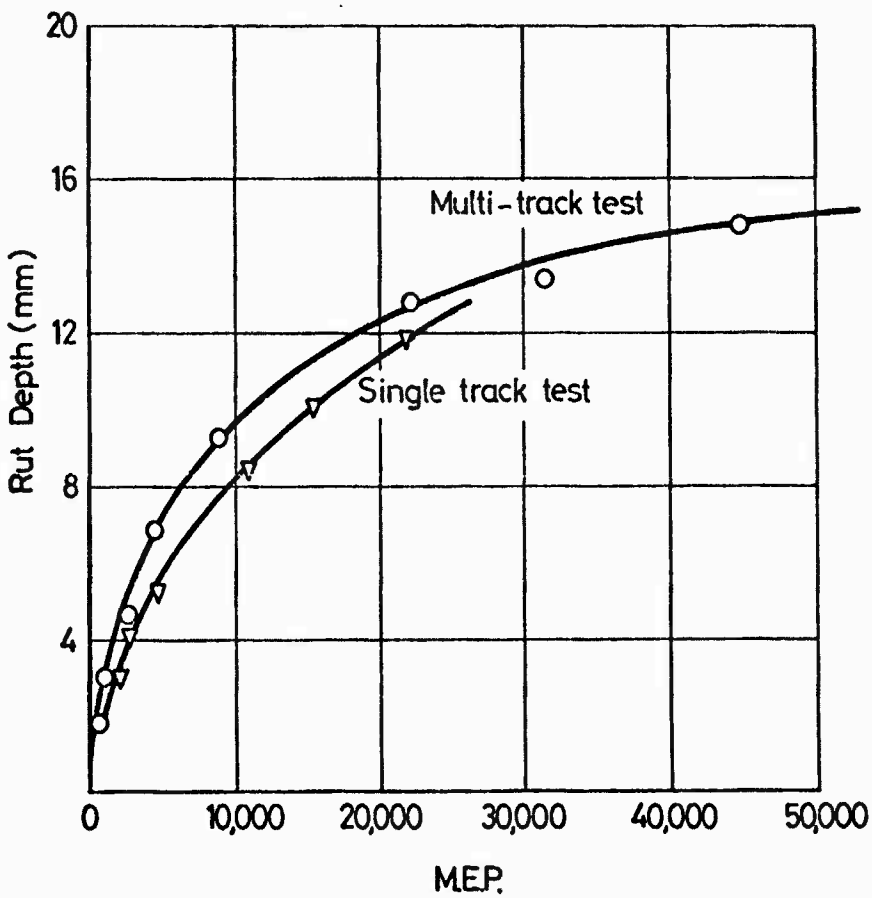

FIG. 9.27 RUT DEPTH VERSUS MEAN NUMBER OF EQUIVALENT PASSES

(PAVEMENT NO. 3)

Table 9.4 Comparison of measured and predicted rut depths

Test	Source of result	Deformation (mm)		Rut Depth (mm)
		DBM	Subgrade	
Pavement 1 Multi-track 10^6 passes	Measurement	7.4	5.0	12.4
	Prediction	12.0	1.5	13.5
Pavement 1 Single track 22,000 passes	Measurement	-	-	8.4
	Prediction	9.0	1.5	10.5
Pavement 2 Multi-track 10^6 passes	Measurement	13.5	10.6	24.1
	Prediction	38.5	1.0	39.5
Pavement 2 Single track 22,000 passes	Measurement	-	-	24.7
	Prediction	29.5	0.9	30.4
Pavement 3 Multi-track 10^6 passes	Measurement	12.5	2.0	14.5
	Predicted	9.8	0.8	10.6
Pavement 3 Single track 22,000 passes	Measurement	-	-	12.3
	Prediction	7.7	0.5	8.2

It is very difficult to assess quantitatively the accuracy of the predictions, because of the many stages in the development of the models. The non-linear analysis did not predict the in situ stresses very accurately (see Section 8.3), the method of triaxial testing was approximate, the deformation measuring devices were subject to errors, and the samples of material varied, sometimes considerably, hence the scatter in the results (Chapter 7). The development of the permanent deformation models introduces more errors, which are particularly difficult to assess in the DBM where tensile stresses occur. It is also very important to remember that errors exist in the measurement of deformations in the pavements, particularly those giving the

distribution of permanent strain with depth from which the permanent deformations in each material are computed. For instance, Table 9.5 shows the results of the three methods of measuring the component deformation in each material for pavement 1. In this case, the DBM deformation was measured together with the total rut depth, the Keuper marl deformation being assumed to be the difference. The difference between the deformation determined by measurements on slabs and from the strain coil stack was 33% of the latter. However, the measurements of rut depth were made with a surveying level for pavements 1 and 2 and with a profilometer for pavements 2 and 3, and both methods were considered to be accurate to within 0.5 mm. Hence, comparison of total predicted deformations with total measured deformations are considered to be more reliable.

Comparison of the predicted and measured permanent strain versus depth plots (Figs 9.22 to 9.24) show that, with the exception of pavement 3, the predictions are much higher than the measured values in the lower half of the DBM. This is caused largely by the problems of representing tensile stresses in the DBM by use of the triaxial test. Comparison also shows that the predictions at the very top of the DBM for pavements 1 and 3 are approximately 50% lower than the measured values. This could be caused by variations in the contact pressure between the tyre and pavement (36). These variations between the predicted and measured permanent strain distributions partly explain the inaccuracies in predicted total deformation in the DBM.

The under-prediction of deformation in the Keuper marl is more difficult to explain. Fig. 9.23 shows that in pavement 2, the measured permanent strain at the surface of the subgrade, after 10^5 passes, was approximately 20% whereas the predicted value was 0.83%.

Table 9.5 Measurements of deformation in each material for pavement 1

Method of Measurement	Deformation of DBM (mm)	Deformation of subgrade (mm)	Total rut depth (mm)
Strain coil stack	6.3	6.1	12.4
Large coils	7.4	5.0	12.4
Measurements on slabs	8.4	4.0	12.4
Average	7.4	5.0	12.4

This discrepancy is partly due to the difference between the measured in situ stresses and those predicted, which are lower. The predicted stresses at the surface of the subgrade in pavement 1 give a value of q of approximately 33 kN/m^2 which gives a value of permanent strain of 1.37% after 10^5 passes. The measured stresses could give a value of q as high as 55 kN/m^2 which would correspond to a permanent strain of approximately 4.0%. Measurements tended to show that the stresses could be even higher at the beginning of a test, a fact corroborated by the form of the pavement strain accumulation at the surface of the clay in pavement 2 (Fig. 5.2) where the majority of the strain was achieved after 10^4 passes. The predictions for the rut profiles are variable, that for the multi-track test in pavement 1 being very close indeed, and for the same test in pavement 2 being 60% too large. However, the general shape of the predicted profiles is good for the multi-track tests and fair for the single-track tests.

The rut formed in the multi-track test for pavement 3 shows a distinct heaving at the edges (Fig. 9.20), a condition impossible to predict by the model used here, which assumes that the in situ vertical

strain is equal to the major principal strain in the triaxial test, which is always compressive. However, it is often the case that for positions near the surface of the pavement which are outside the loaded area, the principal planes rotate sufficiently to cause a tensile minor principal strain to be closest to the vertical, which may cause heaving. To develop a model which could predict this phenomenon would be far more complicated than that developed herein, and would still require approximations to be made for the values of vertical and radial strains if characterisation was to be based on the triaxial test (see Section 6.3).

Comparison of the plots of rut depth versus MEP (Figs 9.25 to 9.27) with those of rut depth versus the total number of wheel passes shows that a multi-track test could be approximated by a single track test, provided that the MEP is used. When plotted in this way, the rut depths in each test were always with 25%.

CHAPTER TEN

DISCUSSION AND CONCLUSIONS

10.1 INTRODUCTION

The aims of this project were to develop a suitable pavement test facility and to use it for producing experimental data which could be checked against theoretical predictions of performance in order to assess the validity of the theory.

In general terms the first part of this objective has been achieved since the test facility has proved very successful although some improvements are desirable for the future. The second objective of checking validity of theory is a much wider and longer term matter, but progress has been made on a limited scale. Only three pavements were tested and these were all of the same basic construction and all were tested at 30°C. A contribution to knowledge has been made on the response of pavements with thick asphaltic layers and this has been possible by obtaining fairly detailed in situ measurements of stress and strain, particularly permanent strain.

A lot of time was spent carrying out materials characterisation tests to provide essential input data for the theoretical calculations and this highlighted some of the problems of doing this on a comprehensive scale.

10.2 THE PAVEMENT TEST FACILITY

One of the criticisms which can be made of the pavement tests reported herein is that the loaded wheel was moved in both directions whereas in practice, pavements are only loaded in one direction. The difference in stress regime relates to the reversal of shear stress

which could have a significant effect on the build up of permanent deformation. There are a number of experimental difficulties associated with the introduction of one-way tests and because of time limitations these were not tackled. However, a comparison of the two modes of loading should be investigated in future experiments. Apart from this limitation, the test facility is regarded as most successful and could be used for a range of experimental projects at relatively low cost. It would not be difficult to increase its load capability, but increased speeds would require a longer travel. The principles of design could easily be adapted for the construction of a larger scale facility.

10.3 INSTRUMENTATION

The strain coils proved successful for the measurement of both permanent and elastic strain. It was possible to check the permanent strain measurements via measured rut depths and this exercise indicated good agreement, thus giving confidence to both the elastic and permanent strain results. The problem of matching the stiffness of carrier blocks to that of the surrounding bituminous material was demonstrated both for coils and bonded strain gauges. If the blocks are too soft damage occurs during compaction, but if they are too stiff, low strain readings are obtained. More care is required with strain gauges than with coils. The Bison instrument coils proved very robust after some strengthening to the cable entry. Out of 63 which were installed, only two mechanical failures resulted.

Although further calibration tests are required, the final pavement experiment showed that it is possible to obtain stress measurements in an asphalt layer.

The experience gained with using accelerometers for transient surface deflection measurements indicated that this method is by no means straight forward. The limited range of a servo accelerometer means that the correct instrument is required for a particular job. The piezoelectric devices only work satisfactorily on pulses of sinusoidal form applied either continuously or in single pulses of short duration. These conditions did not apply in this project.

The most difficult variable to quantify in the use of in situ instrumentation is the error due to installation technique. The effects of this can be minimised by carrying out careful calibration tests in which the particular instrument is installed in a representative sample of the site material using the same placement techniques.

10.4 MATERIALS TESTING

The use of stress invariants provided a good basis for planning the materials tests. It led to the development of permanent strain models for both materials which were expressed in terms of the stress invariants mean normal stress (p) and deviator stress (q). These models were more readily adaptable to predictions of in situ performance than those developed hitherto although certain approximations had to be introduced to overcome the inherent limitations of the triaxial testing stress system.

Both the dense bitumen macadam, at 30°C, and the Keuper marl proved to be very non-linear in their elastic response. This indicated that a non-linear or pseudo non-linear analysis procedure was necessary for evaluating stresses and elastic strains in the pavements.

The tensile tests carried out on the DBM demonstrated the difficulty of obtaining results at low or tensile mean normal stress

levels. This is because tension can only be applied in one direction during the test and hence large tensile strains result leading in most cases to early failure.

A comparison of results from vertical and horizontal cores from the test pavements indicated a degree of anisotropy so far as permanent strain was concerned. The aggregate was somewhat flaky and was aligned by the rolling action thus resulting in higher strains for horizontal cores and creep curves under repeated loading of a different shape from those obtained on vertical cores.

10.5 VALIDITY OF THE THEORY

The main aim of this work was to develop a satisfactory procedure for the prediction of permanent deformation in asphalt pavements. The basic approach which was adopted calculated stresses by means of an elastic analysis and then, in a separate procedure, calculated the vertical permanent strains. Integration of this strain with depth gave the permanent deformation of the surface.

If the procedures which were used are judged solely in terms of rut depth prediction, reasonable success can be claimed. However, this is a mistake which has been made in the past (39,40) and the present project was designed to provide more detailed checks on various stages of the calculation procedure.

The DEVPAV computer program proved to be a very useful tool both for the non-linear elastic analysis of pavements and for the subsequent calculations of permanent strain. However, even when using the non-linear stress-elastic strain relationships derived from the materials testing, the predicted values of stress and elastic strain were generally much lower than the measured values. The subsequent use of these

calculated stresses to predict permanent strains was therefore unlikely to produce very accurate results. This second part of the computation procedure was checked by using measured stresses as the input and this showed some improvement in the resulting permanent strain values. However, this could only be done at the few locations where in situ stresses were measured.

A series of trial and error calculations subsequently revealed that the measured and predicted stresses and elastic strains could only be correlated if the top of the DBM layer and all the soil were assumed to have much lower moduli than in the original calculations. Physical reasons for such a model are not immediately apparent.

There are two possible explanations for the poor correlation of measured and predicted stresses and elastic strains. Firstly, at the high temperature (30°C) used for these experiments, the assumption of elastic behaviour is rather dubious and the usual engineering expedient of using a stiffness appropriate to the temperature and loading time conditions for the bituminous layer does not seem to have worked. Alternatively, the actual values of modulus for both materials obtained from the repeated load sample tests may not be representative of the in situ conditions. Some procedure, such as the wave propagation method or falling weight deflectometer, which could be used to evaluate in situ moduli should perhaps be investigated. However, these methods will not be suitable for producing the detailed data necessary for a non-linear analysis.

In view of the difficulties encountered in calculating stresses it is not possible to comment in detail about the validity of the second part of the predictive method dealing with permanent deformation.

The detailed treatment given to analysis of permanent strain

resulting from a given lateral distribution of wheel load passes resulted in the proposal for using "mean number of equivalent passes" (MEP) as a simplification for design purposes. The need for further simplifications before the concepts investigated herein are extended to practice, has also become apparent. However, the philosophy which the Authors have adopted is that a detailed understanding must be obtained before rational simplifications can be introduced, particularly if the resulting design method is to be applicable to a range of situations.

10.6 DEFORMATIONS FOR RIGID SUPPORT CONDITIONS

At the verbal request of engineers at the Waterways Experiment Station, short sections of lean concrete were placed below the DBM layer at either end of test pavements 2 and 3 (Fig. 2.1). This was intended to provide some indication of the permanent deformation to be expected in asphalt overlays on rigid or semi-rigid pavements.

The location of the lean concrete sections was such that the wheel load was either accelerating or decelerating over it and accurate data could not be expected. However, the rut depths in this area were very similar to those over the main test section of each pavement (Figs 5.2 and 5.3). This implies that the deformation in the DBM must have been greater since that in the lean concrete was negligible. This is in keeping with the lower stiffness of the DBM under the slower speed conditions occurring over the lean concrete areas.

10.7 CONCLUSIONS

This section details the major conclusions to be drawn from this work:

(1) A pavement test facility capable of applying realistic wheel loads

and speeds to semi-full scale pavements has been successfully developed.

(2) Strain coils can be successfully used to obtain detailed information on permanent and elastic strains in bituminous materials and clay.

(3) Carrier blocks for strain measuring devices in bituminous materials should only be used if it is unavoidable and their stiffness should closely match that of the surrounding material.

(4) The need for as many duplicate measurements of a particular in situ stress or strain as possible has been confirmed.

(5) The use of stress invariants to specify in situ stress conditions proved useful in planning material characterisation tests and in developing stress-strain models.

(6) The limitations of the triaxial test configuration for reproducing in situ conditions in a bituminous layer were demonstrated, particularly with regard to the tensile stress zone at the bottom of such a layer.

(7) Under the relatively high temperature conditions ($30^{o}C$) and for the particular materials (dense bitumen macadam and a silty clay) used in these experiments, non-linear elastic theory tended to underpredict stresses and elastic strains.

(8) A detailed procedure for calculating the rut profile resulting from a given lateral distribution of wheel passes was developed with the aid of the computer program, DEFPAV.

(9) The overall predictions of rut depth were reasonably good, but the method tended to overestimate the contribution from the bituminous layer and underestimate that from the subgrade.

ACKNOWLEDGEMENTS

The Authors are grateful for the support they have received from various colleagues in carrying out this research. In particular, they would like to acknowledge the financial support provided by ERO and the Department of Civil Engineering under Professor R.C. Coates and the provision of laboratory and workshop facilities therein. The active interest and advice of Professor P.S. Pell is also gratefully acknowledged. The computing facilities of the Cripps Computing Centre proved indispensible in carrying out the theoretical work. Extensive assistance was provided by a number of technicians in the Department of Civil Engineering under Mr. J.G. Redfern, and in particular by Messrs A. Leyko, D. Lockyer, W. Robinson and G. Stokes. Advice over electronics problems was freely given by Mr. F. Brooks of the Applied Science Faculty Workshops. The large number of figures were prepared by Miss R. Allen and the typing and final production of the report were carried out by Miss J.L. Clerbaut.

The bituminous material for each test pavement was supplied and laid by Tarmac Roadstone Holdings Ltd and their assistance is gratefully acknowledged. The Authors are also indebted to Dr. R.W. Kirwan, Trinity College, Dublin, for making the DEFPAV computer programme available, and to Dr. M.S. Snaith and Dr. T.E. Glynn for advice on its use.

REFERENCES

1. Brown, S.F., Bell, C.A. and Brodrick, B.V., "Permanent deformation of flexible pavements", Research Report to ERO, U.S. Army, Univ. of Nottingham, 1974.
2. Highway Research Board, "Structural design of asphalt concrete pavements to prevent fatigue cracking", Special Report 140, 1973.
3. Brown, S.F., "State-of-the-art on laboratory testing for use in the prediction of rutting in asphalt pavements", Proc. Transportation Research Board Symp., 1976.
4. Proceedings of the 4th International Conference on the Structural Design of Asphalt Pavements, Vol. 1, 1977.
5. Ibid Brown, S.F. and Bell, C.A., "The validity of design procedures for the permanent deformation of asphalt pavements".
6. Brown, S.F. and Brodrick, B.V., "Stress and strain measurements in flexible pavements", Proc. Conf. on Measurement in Civil Engineering, Newcastle, England, 1977.
7. Brown, S.F., "State-of-the-art on field instrumentation for pavement experiments", Prepared for Technical Committee A2K01, "Strength and deformation characteristics of pavement sections" Transportation Research Board, 1976.
8. Brown, S.F. and Brodrick, B.V., "The performance of stress and strain transducers for use in pavement research", Science Research Council Report No. SFB/BVB/593.13, Dept. of Civil Engineering, Univ. of Nottingham.
9. Paterson, W.D.O., "Measurement of pavement deformation using inductance coils", RRU Bulletin No. 13, National Roads Board, New Zealand, 1972.

10. Stuart, E., Miyaoka, Y., Skok, E.L. and Wenck, N.C., "Field evaluation of an asphalt stabilised sand pavement design using the elastic layered system", Proc. Assn Asphalt Paving Technologists, Vol. 43, 1974, pp. 77-108.

11. Bohn, A., Ullidtz, P., Stubstad, R. and Sørensen, A., "Danish experiments with the French falling weight deflectometer", Proc. 3rd Int. Conf. on the Struct. Design of Asphalt Pavements, Vol. 1, London, 1972, pp. 1119-1128.

12. Tory, A.C. and Sparrow, R.W., "The influence of diaphragm flexibility on the performance of an earth pressure cell", Journ. Sc. Instruments, 44, 1967, pp. 781-785.

13. Ministry of Transport, "Specifications for roads and bridge works", HMSO, London, 1969.

14. Romain, J.E., "Rut depth prediction in asphalt pavements", Proc. 3rd Int. Conf. on the Struct. Design of Asphalt Pavements, Vol. 1, London, 1972, pp. 705-710.

15. Ibid Barksdale, R.D., "Laboratory evaluation of rutting in base course materials", pp. 161-174.

16. Klomp, A.J.G. and Niesman, Th.W., "Observed and calculated strains at various depths in asphalt pavements", Proc. 2nd Int. Conf. on the Struct. Design of Asphalt Pavements, Ann Arbor, Michigan, 1967, pp. 671-688.

17. Thrower, E.N., Lister, N.W. and Potter, J.F., "Experimental and theoretical studies of pavement behaviour under vehicular loading in relation to elastic theory", Proc. 3rd Int. Conf. on the Struct. Design of Asphalt Pavements, London, 1972, pp. 521-535.

18. Kirwan, R.W. and Snaith, M.S., "Further investigations towards a rational method of design for flexible pavements", Final Technical Report to US Army, Trinity College Dublin, April 1975.

19. Cullingford, G., Lashine, A.K.F. and Parr, G.B., "Servo controlled equipment for dynamic triaxial testing of soils", Geotechnique, Vol. 22, No. 3, Technical Note, 1972, pp. 526-529.

20. Lashine, A.K.F., Brown, S.F. and Pell, P.S., "Dynamic properties of Soils", Research Report to Shell, Univ. of Nottingham, 1971.

21. McElvaney, J., "Fatigue of a bituminous mixture under compound--loading", Ph.D. thesis, Univ. of Nottingham, 1972.

22. Brown, S.F. and Snaith, M.S., "The permanent deformation characteristics of a dense bitumen macadam subjected to repeated loading", Proc. Assn Asphalt Paving Technologists, Vol. 43, 1974, pp. 224-252.

23. Barksdale, R.D., "Compressive stress pulse times in flexible pavements for use in dynamic testing", Highway Research Record No. 345, 1971, pp. 32-44.

24. Brown, S.F., "Determination of Young's modulus for bituminous materials in pavement design", Highway Research Record No. 431, 1973, pp. 38-49.

25. Snaith, M.S., "Deformation characteristics of dense bitumen macadam subjected to dynamic loading", Ph.D. thesis, Univ. of Nottingham, 1973.

26. Pell, P.S. and Cooper, K.E., "The effect of testing and mix variables on the fatigue performance of bituminous materials", Proc. Assn Asphalt Paving Technologists, Vol. 44, 1975, pp. 1-37.

27. Brown, S.F. and Snaith, M.S., "The measurement of recoverable and irrecoverable deformations in the repeated load triaxial test", Geotechnique, June 1974, Technical Note, pp. 255-259.

28. Cooper, K.E., Brown, S.F., McElvaney, J. and Pell, P.S., "Permanent deformation of bituminous materials", Research Report submitted to TRRL, Univ. of Nottingham, 1975.

29. Lashine, A.K.F., "Some aspects of the chacteristics of Keuper marl under repeated loading", Ph.D. thesis, Univ. of Nottingham, 1971.

30. Peutz, M.G.F., Van Kempen, H.P.M. and Jones, A., "Layered systems under normal surface loads", Highway Research Record No. 228, 1968, pp. 34-45.

31. Pappin, J.W., Private Communication, Univ. of Nottingham, 1976.

32. Brown, S.F. and Pell, P.S., "An experimental investigation of the stresses, strains and deflections in a layered pavement structure subjected to dynamic loads", Proc. 2nd Int. Conf. on the Struct. Design of Asphalt Pavements, Ann Arbor, Michigan, 1967, pp. 487-504.

33. Seed, H.B., Chan, C.K. and Lee, C.E., "Resilience characteristics of subgrade soils and their relation to fatigue failures in asphalt pavements", Proc. Int. Conf. on the Struct. Design of Asphalt Pavements, Ann Arbor, Michigan, 1962, pp. 611-636.

34. Cox, M.G. and Hayes, J.G., "Curve fitting: a guide and suite of algorithms for the non-specialist user", National Phys. Lab. Report NAC 26, 1973.

35. Monismith, C.L., Ogawa, N. and Freeme, C.R., "Permanent deformation characteristics of subgrade soils due to repeated loading", Transportation Research Record 537, 1975, pp. 1-17.

36. Lister, N.W. and Jones, R., "The behaviour of flexible pavements under moving wheel loads", Proc. 2nd Int. Conf. on the Struct. Design of Asphalt Pavements, Ann Arbor, Michigan, 1967, pp. 1021-1035.

37. Brown, S.F., "An improved framework for predicting permanent deformation in asphalt layers", Transportation Research Record 537, 1975, pp. 18-30.

38. Brown, S.F. and Bush, D.I., "Dynamic response of model pavement

structures", Journ. Trans. Eng., Proc. ASCE, No. TE4, November 1972, pp. 1005-1022.

39. Morris, J., Haas, R.C.G., Reilly, P. and Hignell, E., "Permanent deformation in asphalt pavements can be predicted", Proc. Assn Asphalt Paving Technologists, Vol. 43, 1974, pp. 41-76.

40. Brown, S.F., Discussion of "Permanent deformation in asphalt pavements can be predicted" by Morris et al, Proc. Assn Asphalt Paving Technologists, Vol. 43, 1974, pp. 67-70.

APPENDIX 1

SERVO CONTROL ELECTRONIC UNIT

A block diagram of the control circuit is shown in Fig. A1.1 for the closed loop condition. The open loop circuit would not include the feedback transducers and only limited control of the carriage motion would be possible, and drift would be inevitable. Introduction of the transducers eliminates drift and, providing cable tension is maintained, a stable carriage response is achieved.

The operational cycle commences when the AUTO button is pressed and triggers a 10 second timer which sounds an audible warning device. At the end of 10 seconds the right bistable is set by a pulse initiating a 0.5 second "ramp up" from the shaper. This command signal to the servo amplifier is then transmitted to the servo valve controlling the hydraulic motor, causing the carriage to accelerate to the right (in this case relative to the operator's view at the control unit). The signal and feedback to the servo amplifier are automatically switched to the velocity command mode in AUTO and the setting on the velocity potentiometer determines the carriage speed. The carriage reaches constant speed and the "position sensing LVDT" output is driven more positive until the right comparator operates. This resets the right bistable and initiates a 0.5 second "ramp down" causing the carriage to decelerate. When it has nearly stopped the signal level from the tachogenerator operates the right zero detector which sets the left bistable and the carriage accelerates to the left. As the ultimate carriage velocity is attained the LVDT signal falls from positive through zero (carriage at the centre) thus becoming more negative. The tachogenerator feedback signal is also "negative going" and the

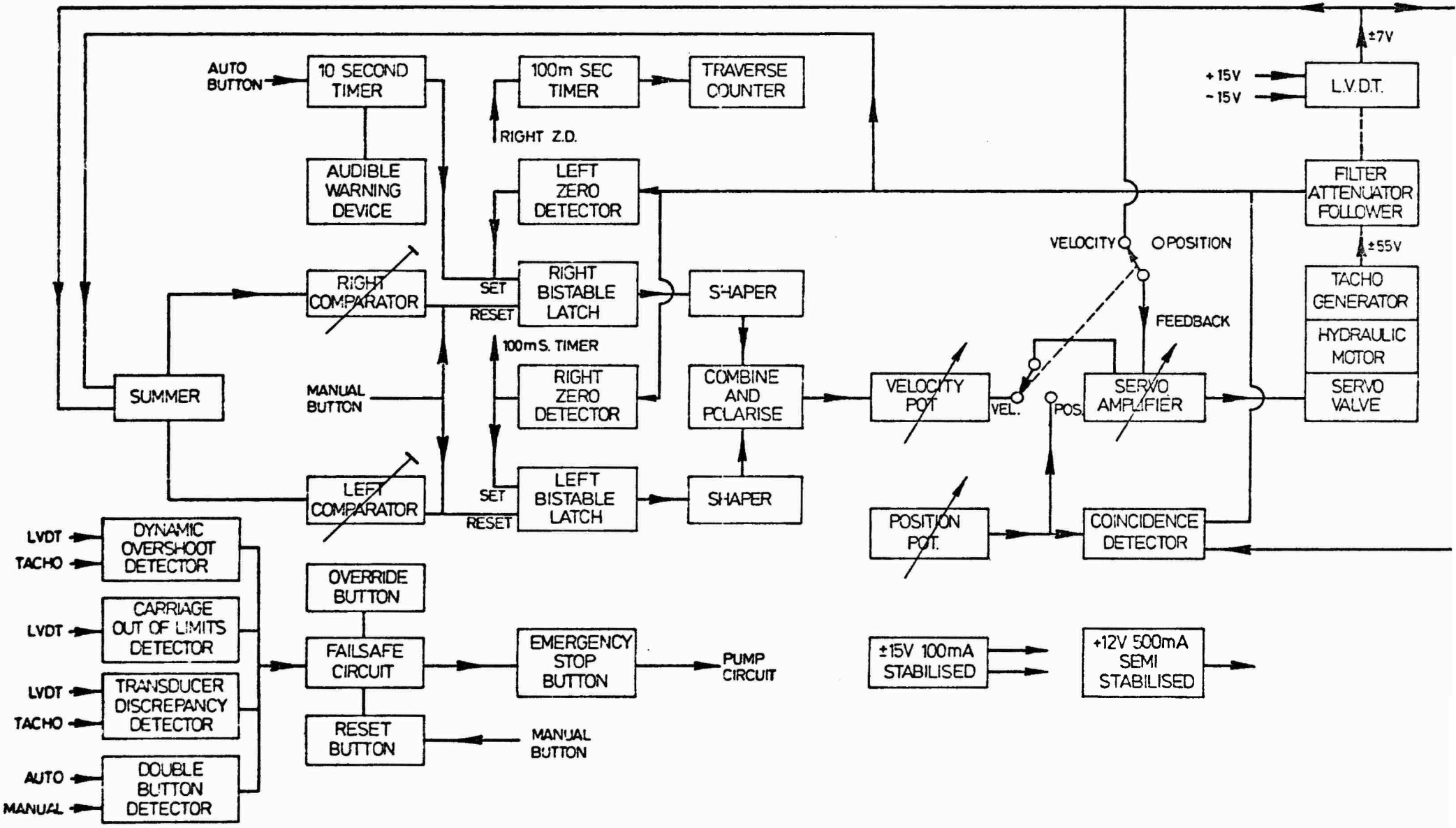

FIG. A1.1 CONTROL CIRCUIT BLOCK DIAGRAM

left comparator operates at the appropriate position and resets the left bistable. The carriage slows down, stops and the cycle is repeated. At higher speeds the tachogenerator signal adds to the LVDT signal causing the comparators to operate earlier to prevent overrun.

The carriage can be stopped by pressing the MANUAL button, which resets both bistables and initiates "ramp down", at any part of the auto cycle. The carriage, however, will not be controlled by the POSITION potentiometer until it is stationary, and the manual latch is set by making the POSITION potentiometer voltage equal to the LVDT output. When this occurs a relay is de-energised and alters the servo mode to the LVDT control, i.e. the command signal is changed from velocity to position and the feedback signal is changed from the tachogenerator to the LVDT. The carriage can now be accurately moved by turning the POSITION potentiometer which "locks" into the LVDT output related to the positional voltage.

The following circuits will stop the main hydraulic pump if activated. A discrepancy detector between the differentiated LVDT signal and tachogenerator output will be operational if the cable snaps, i.e. the two signals become very different if the drum suddenly becomes unloaded. Normally these signals are of the same sign and magnitude. An LVDT "carriage out of limits" detector operates at the extreme ends of the beam and will sense overtravel. A dynamic overshoot detector is activated, if the carriage is running too fast near the end of a pass, by adding the tachogenerator signal to the LVDT signal. Limit switches in series with the electrical supply to the pump will be engaged by the carriage at either end of the loading facility. A detector senses if both AUTO and MANUAL buttons are in or out as it is essential that only one of these modes is operational. Also a relay will operate if the

"electronics" mains supply is accidentally disconnected. Finally, emergency stop (panic) buttons are fitted to the front panel of the control unit and in an accessible position in the test room.

Further circuit features include a tachogenerator signal filter-variable attenuator and voltage follower. This is to maintain a compatible signal with the control system which requires a noise free input of a similar magnitude to the LVDT voltage (± 7 v). The mains input is converted to a d.c. power supply for the LVDT, relays etc., and all linear and logic circuitry are isolated in a screened box to eliminate interference. If the carriage stops beyond an electrical limit it will prevent pump restart, so an override button is provided in the rear panel to allow return of the carriage in the manual mode. However, this facility does not override the emergency stop buttons, limit switches and the pump motor controller stop.

APPENDIX 2

LATERAL POSITION CONTROL SYSTEM

A schematic layout of the electronic control unit is shown in Fig. A2.1. Initially, the positions are set in the order required for traversing. Then the numbers of passes are entered sequentially as selected for each position displayed and the programme will be retained until the control is switched off.

During the "enter" operation, data (number of passes) from the BCD (Binary coded decimal) switches is stored, one complete number at a time in the data register. When the register has the information, the data appears at the output and is available, one complete number at a time, to preset a count-down decade counter during the "run" operation. This loading procedure also clocks a nine position sequence register in step with the data register and this enables the programming progress to be monitored. During "run" the first number entered is counted down by pulses from the pass counter on the loading facility electronic control unit. When this count down reaches zero a pulse is developed which clocks the data register to the second number entered. It also clocks the sequence register to number two, loads the second number in the count-down decade counter, and produces a start pulse. The process is repeated as the number is counted down to zero and eventually for all nine pass-totals entered.

Voltages are developed from the sequence register which are compared with the traverse LVDT voltage. They command the direction of the traversing rams and the length of travel. The voltages developed are in nine discrete steps, one step per sequence register step, and these correspond to the nine traverse positions. To set up the required

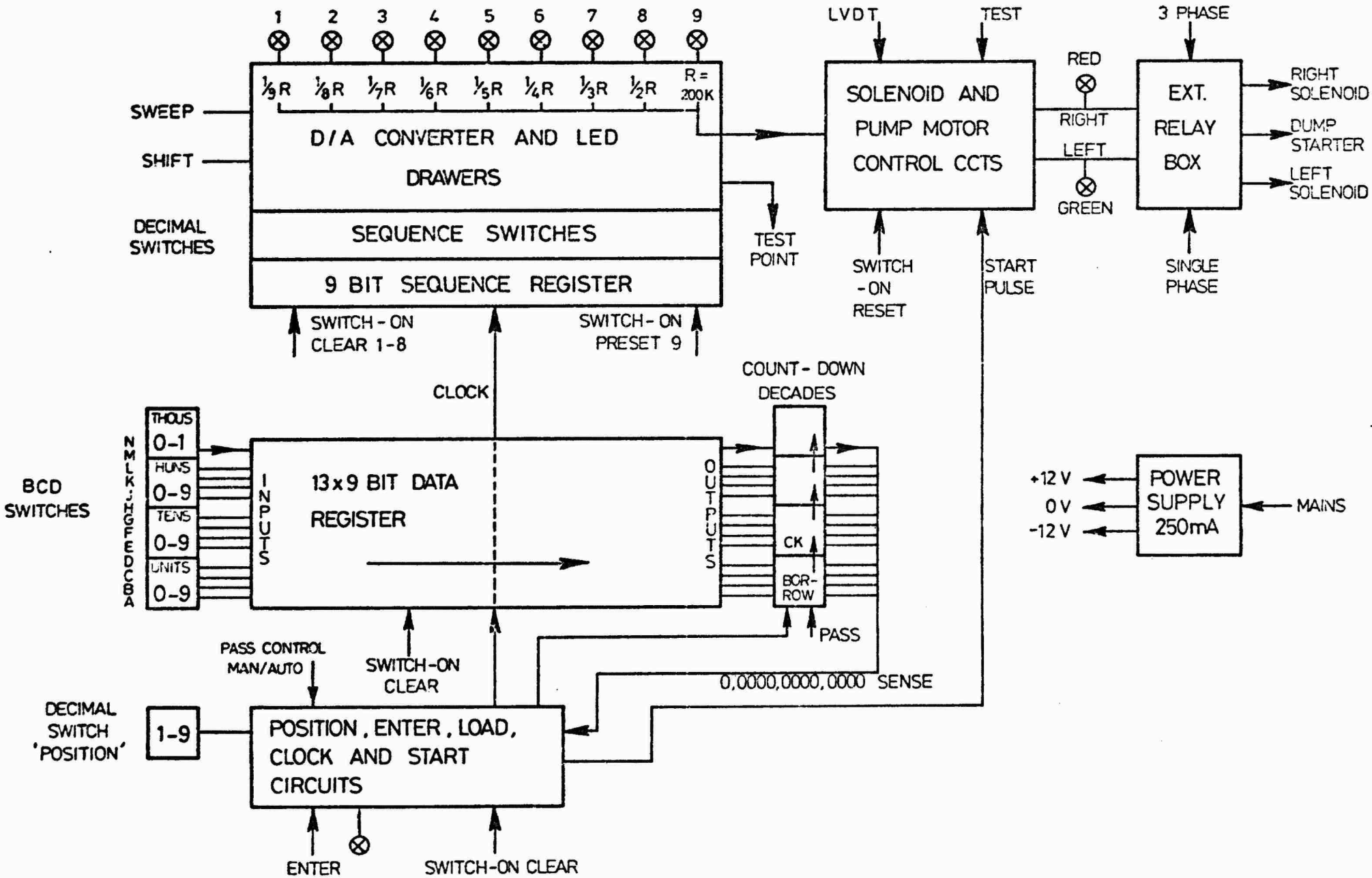

FIG. A2.1 TRAVERSE CONTROL BLOCK DIAGRAM

positions, nine "nine-position" thumbwheel switches enable any of the nine generated voltages to be routed to any of the nine positions. Depending on the state of the voltage comparator at the time of the start pulse, a "run right" or "run left" signal will be produced from the solenoid and pump motor control circuits. As soon as the loading facility reaches the required position one of these signals will be cancelled as depicted by the red and green indicators (Fig. A2.1). The signals are passed to a power relay unit which simulates a momentary "press" on the pump motor start button and closes the appropriate solenoid contact. The pump motor starts and pressure is applied to the rams which operate in the direction dictated by the solenoid valve. When the desired position is reached the motor is switched off. A "manual position" is provided on the relay unit and the circuit has also been designed to allow the pump motor "stop" button to be operational in an emergency even when the unit is in the "auto" position. The normal method of stopping a traverse in progress, is to push the "run" switch to "off".

UNCLASSIFIED

SECURITY CLASSIFICATION OF THIS PAGE (When Data Entered)

REPORT DOCUMENTATION PAGE		READ INSTRUCTIONS BEFORE COMPLETING FORM
1. REPORT NUMBER	2. GOVT ACCESSION NO.	3. RECIPIENT'S CATALOG NUMBER
4. TITLE (and Subtitle) Permanent Deformation of Flexible Pavements.		5. TYPE OF REPORT & PERIOD COVERED Final Technical Report Sep 74 - Mar 77 6. PERFORMING ORG. REPORT NUMBER
7. AUTHOR(s) S. F. Brown B. V. Brodrick C. A. Bell		8. CONTRACT OR GRANT NUMBER(s) DAERO-75-G-023
9. PERFORMING ORGANIZATION NAME AND ADDRESS University of Nottingham Nottingham U.K.		10. PROGRAM ELEMENT, PROJECT, TASK AREA & WORK UNIT NUMBERS 6.11.02A-DM161102B2B-00-427
11. CONTROLLING OFFICE NAME AND ADDRESS		12. REPORT DATE March 77 13. NUMBER OF PAGES 137
14. MONITORING AGENCY NAME & ADDRESS(if different from Controlling Office)		15. SECURITY CLASS. (of this report) UNCLASSIFIED 15a. DECLASSIFICATION/DOWNGRADING SCHEDULE

16. DISTRIBUTION STATEMENT (of this Report)

Approved for Public Release - Distribution Unlimited

17. DISTRIBUTION STATEMENT (of the abstract entered in Block 20, if different from Report)

18. SUPPLEMENTARY NOTES

19. KEY WORDS (Continue on reverse side if necessary and identify by block number)

Flexible pavement; bitumen macadam; pavement deformation;

20. ABSTRACT (Continue on reverse side if necessary and identify by block number)

Report presents details of 2nd and 3rd year's work on Permanent Deformation of Flexible Pavement. A pavement test facility capable of applying realistic wheel loads and speeds to semi-full scale pavements was successfully developed. Progress was made on a limited scale for testing theoretical predictions of performance. Work on this will continue in a follow-up study.

DD FORM 1473 EDITION OF 1 NOV 65 IS OBSOLETE

UNCLASSIFIED

SECURITY CLASSIFICATION OF THIS PAGE (When Data Entered)